Patient-derived neuronal models for pharmacogenetic pain treatment of sodium channelopathies

PATIENT-DERIVED NEURONAL MODELS FOR PHARMACOGENETIC PAIN TREATMENT OF SODIUM CHANNELOPATHIES

Julie I.R. Labau

PATIENT-DERIVED NEURONAL MODELS FOR PHARMACOGENETIC PAIN TREATMENT OF SODIUM CHANNELOPATHIES

Julie I.R Labau

The research described in this thesis was funded by the Marie-Sklowdoska Curie Actions foundation, from the Molecule-to-Man Pain Network, a European Commission Multi-Center Collaborative Projects through the European Union's Horizon 2020 research and innovation program under grant agreement No. 721841. This work was also supported by Center Grant B9253-C from the U.S. Department of Veterans Affairs Rehabilitation Research and Development Service.

ISBN: 9789464237559
Print and production: ProefschriftMaken || www.proefschriftmaken.nl
Cover Illustration: Simone Golob
Layout Illustration: Julie I. R. Labau and Simone Golob

Patient-derived neuronal models for pharmacogenetic pain treatment of sodium channelopathies

To obtain the degree of Doctor at the Maastricht University, on the authority of the Rector Magnificus, Prof. Dr. Pamela Habibović, in accordance with the decision of the Board of Deans, to be defended in public on Thursday April 21st, 2022, at 16:00 hours

by

Julie Isabelle Romane Labau

Promotors:
Prof. dr. H.J.M. Smeets
Prof. dr. C.G. Faber
Prof. dr. S.G. Waxman

Co-promotor:
Dr. S. Dib-Hajj

Assessment committee:
Prof. dr. A. Lampert (chair)
Prof. dr. E.A.J. Joosten
Dr. E. Pishva
Prof. dr. S. Walker, UCL, London
Prof. dr. J.H.M. van Zundert

Je dédie ce livre à mes parents, Sylviane et Philippe,
pour leur soutien et amour pendant toutes ses années.

CONTENTS

APPENDIX


1

INTRODUCTION

Part 1

CHAPTER 1.1

GENERAL INTRODUCTION

INTRODUCTION

CHRONIC NEUROPATHIC PAIN

Neuropathic pain represents a major health burden, affecting 6.9% to 10% of the global population [1, 2], and as a leading cause of disability, is often associated with severe emotional and psychological comorbidities [3].

Neuropathic pain is a form of chronic pain characterized by a lesion or disease of the somatosensory system that persists beyond the expected healing point, or despite treatment targeting the cause of disease [1, 3]. Pain may arise from post-surgical nerve damage, vascular or autoimmune conditions, viral infections, such as HIV or postherpetic neuralgia, neurodegenerative disorders, metabolic diseases (eg. diabetic peripheral neuropathy, DPN), exposure to toxins or chemical irritants, as in chemotherapy-induced peripheral neuropathy (CIPN), genetic variants, or be of unknown etiology (ie. idiopathic neuropathies) [1, 4]. Despite a wide etiological spectrum, the clinical presentation of neuropathic pain is often synonymous with ongoing spontaneous pain, intermittent ectopic pain sensations, and exacerbated evoked pain responses from non-noxious (allodynia) and noxious stimuli (hyperalgesia).

The mechanistic underpinnings of neuropathic pain are complex and their relationship to the underlying pathology remain poorly understood. Furthermore, the depiction and severity of pain symptoms widely varies between neurological conditions and across patients with the same underlying etiology [5], emphasizing the need for better understanding the translation of pathophysiological mechanisms into sensory inputs. Yet, hundreds of genes have reportedly been linked to human pain disorders, including, but not limited to, those encoding transient receptor potential (TRP) channels (ie. TRPV1, TRPA1, TRPM8), voltage-gated sodium channels (VGSCs), GTP cyclohydrolase, purinergic receptors, μ1 opiate receptors and catechol-O-methyl transferase (COMT) [6-11]. Clinical neurophysiological investigations have provided some mechanistic clues, with increasing activity in pain-conducting nerve fibers correlating with disease [1, 12, 13]. However, limited non-invasive procedures and accurate diagnostic tests have restricted pain studies in human subjects, with most of our knowledge pertaining to animal and preclinical studies.

VOLTAGE-GATED SODIUM CHANNELS

Voltage-gated sodium channels (VGSCs) are key contributors to neuronal excitability and are required for the generation, transduction, and propagation of action potentials along axons [14-16]. They are part of the P-loop family that includes potassium and calcium channels [17]. The pore-forming α-subunit of sodium channels folds into four homologous domains (DI-DIV), connected by intracellular peptide linkers (L1-L3). Each domain is composed of six transmembrane helices (S1-S6) [17-20], organized in the voltage-sensing region (S1-S4) and the ion-permeation pathway (S5-S6; *Figure 1*)

[10, 17]. VGSC gating and trafficking are regulated through interactions with channel partners, including sodium channel β subunits [21], fibroblast homologous factors [22], and via post-translational modification [23-25].

Nine genes encode the sodium channel α-subunit proteins ($Na_V1.1$-$Na_V1.9$) in humans [20, 27], with each manifesting diverse patterns of expression and biophysical properties [19, 20]. For instance, $Na_V1.1$ and $Na_V1.2$ have been found to be largely expressed in the brain [28], although increasing levels of $Na_V1.1$ have been detected in lumbar, viscera-innervating dorsal root ganglion (DRG) neurons [29, 30]. Similarly, $Na_V1.3$ is predominantly expressed in embryonic sensory neurons [31], but is upregulated following traumatic or metabolic injury in rodent DRGs [31, 32], although its pattern of expression in humans is less clear. On the other hand, $Na_V1.4$ and $Na_V1.5$ are exclusively expressed in muscles, skeletal and myocardial, respectively [27]. $Na_V1.6$ is primarily expressed in the nodes of Ranvier and has been shown to be involved in both CNS and PNS neuronal excitability [33]. Preferential expression of $Na_V1.7$, $Na_V1.8$ and $Na_V1.9$ in DRG and trigeminal sensory neurons has brought attention to their function as primary drivers of nociception [15, 34]. $Na_V1.7$ is also present in sympathetic ganglion cells and $Na_V1.9$ in myenteric neurons [14, 24, 35, 36]. $Na_V1.7$ and $Na_V1.8$ have generated particular interest due to compiling evidence linking them to human pain disorders [15], with recent findings associating $Na_V1.6$ [37] and $Na_V1.9$ [38-46] to several pathologies.

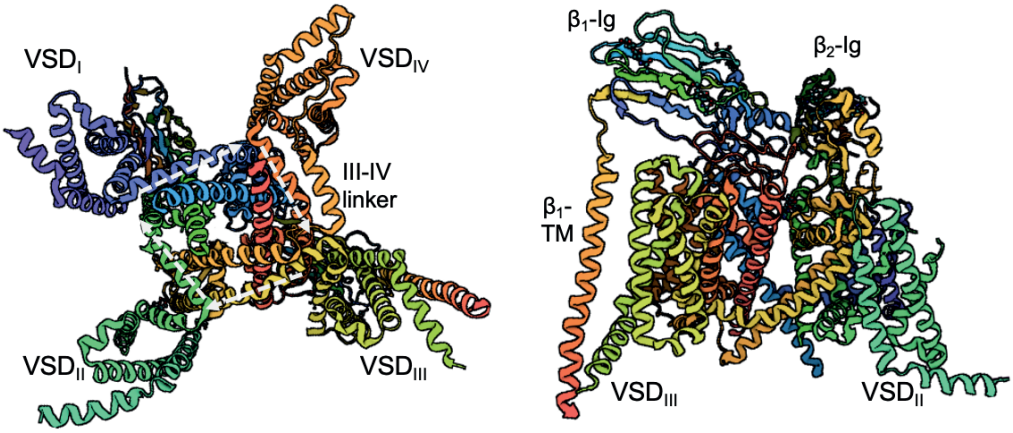

FIGURE 1 – Overall 3D folded structure of human VGSCs. View of the folded structure of the sodium channel α-subunit, in complex with β1 and β2, from the intracellular side of the membrane *(left)* and from its side *(right),* based on the recently published structure of the human $Na_V1.7$ channel by Shen et al. [26]. The channel structure shows the central ion-conducting pore module, colored by repeats; the four peripheral VSDs (S1-S4) are shown in blue (VSD_I), cyan (VSD_{II}), lime green (VSD_{III}) and blood orange (VSD_{IV}). The DIII-DIV linker (L3) carries the fast-inactivation motif and is shown in light orange. VSDs undergo conformational changes in response to membrane depolarization, which are then transmitted to the pore via S4-S5 linkers (indicated by white arrows through helix loops).

The involvement of VGSCs in pain has been demonstrated in lesioned and intact neighboring nociceptive fibers. Following peripheral nerve injury, higher VGSC levels of expression as well as reduced action potential threshold and ectopic activity have been reported [3, 47-49]. The transfection of human channels into heterologous cell systems has been another major step forward in ion channel research [50], allowing the identification of downstream pathways and the functional characterization of VGSC mutations [51-53]. Concomitantly with knock-out (KO) animal models, mutational analysis of sodium channel variants has shed a light on the pathobiological basis of nociceptor excitability, delineating a direct mechanistic link to chronic pain and the contribution of individual channels to the electrogenesis of sensory neurons (SNs) [19, 54, 55]. Animal studies in support of $Na_V1.7$ in pain pathology have described increased levels of expression in DRG neurons after inflammation [56] and in diabetic rats [57]. In contrast, $Na_V1.7$ KO reduced inflammation-induced thermal hyperalgesia in mice [58] and diabetes-induced neuropathy in rats [57], while increasing the action potential threshold in several animal models of pain [59-62].

SODIUM CHANNELOPATHIES

The identification and functional follow-up of rare monoallelic mutants have been instrumental in defining the critical role played by DRG-expressed VGSCs ($Na_V1.7$, $Na_V1.8$, and $Na_V1.9$) in the transmission of pain signals. Numerous genetic variants have been implicated in the pathogenicity of chronic pain. In particular, extensive literature has linked $Na_V1.7$ to a plethora of human pain disorders; gain-of-function (GoF) missense mutations have been found in patients with inherited erythromelalgia (IEM) [52, 53, 63, 64], paroxysmal extreme pain disorder (PEPD) [65], and small fiber neuropathy (SFN) [66, 67]. Whereas, loss-of-function (LoF) mutations in $Na_V1.7$ induce congenital and complete inability to experience pain (CIP) [14, 15, 23, 68-70] and hereditary sensory and autonomic neuropathy (HSAN) [71]. Microneurography analysis in patients carrying the mutant channels validated their contribution to pain pathology, as demonstrated by ectopic increased excitability in afferent nociceptive fibers, without signs of nerve lesions [3, 72-74].

Voltage- and current-clamp assessment of disease-causing mutations parallel the clinical phenotype; sensory neurons showed cellular hyperexcitability, associated with impaired activation (IEM) and fast inactivation (PEPD) in heterologous systems [14, 65, 75]. Recently, *de novo* GoF mutations in $Na_V1.8$ have been linked to SFN in a small group of patients. Functional analysis of the mutations correlated with DRG neuron hyperexcitability [76, 77]. A spectrum of human pain conditions has been associated with dominant GoF mutations in $Na_V1.9$ in both painful and painless channelopathies [35], including SFN [38, 78] and CIP [43, 45]. Extending beyond the α-subunit, mutations in the β2-subunit of sodium channels have been directly linked to the pathogenesis of SFN and DPN [79, 80]. Hence, VGSC inhibition represents a potentially beneficial approach to addressing chronic pain.

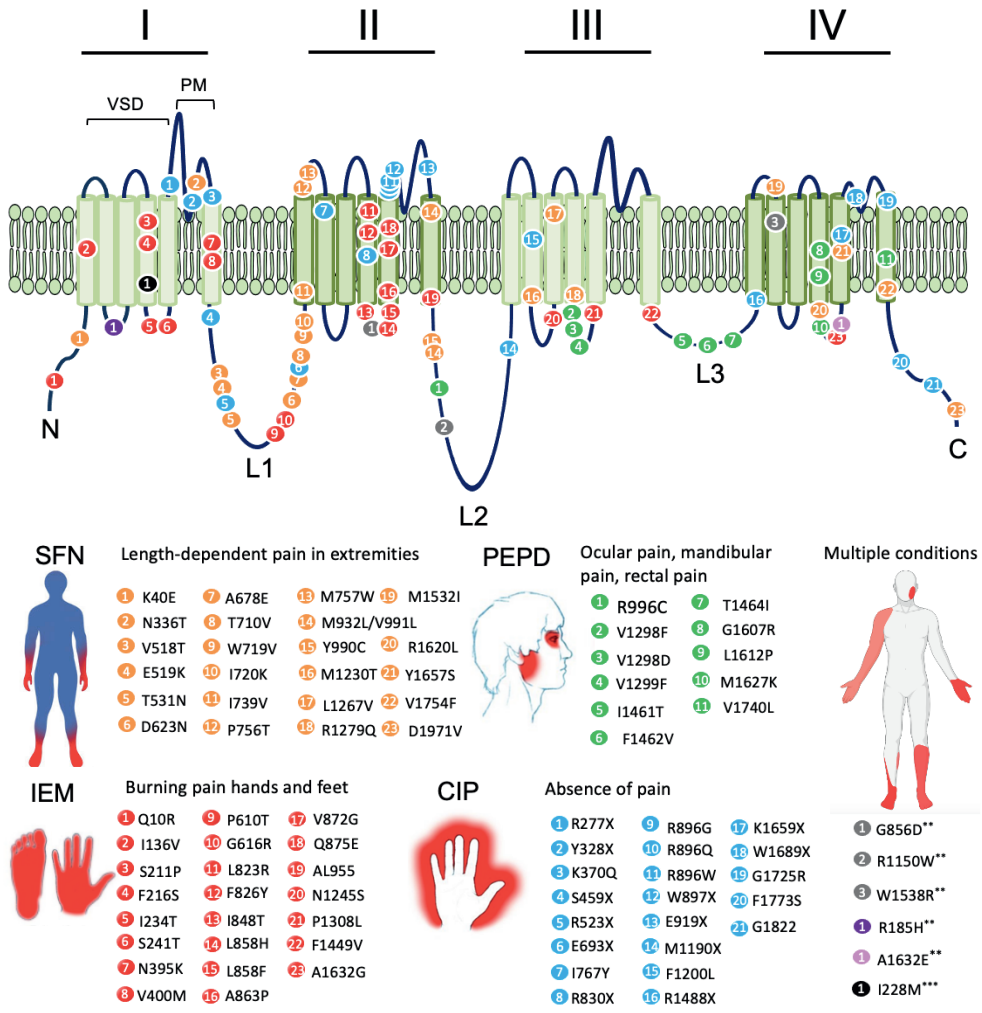

FIGURE 2 – SCN9A mutations result in a wide range of human pain conditions. The linear schematic view of full-length Nav1.7 sodium channel alpha subunit shows its composition of four homologous domains, each consisting of six transmembrane segments (S1-S6) and joined by three intracellular loops (L1-L3). Each domain can be subdivided into the voltage-sensing domain (VSD) formed by the S1-S4 helices, while the pore module (PM) is composed of S5 and S6. The graphic representation of the 'unfolded' channel points to the location of gain-of-function mutations that are linked to small fiber neuropathy (SFN; orange), inherited erythromelalgia (IEM; red) and paroxysmal extreme pain disorder (PEPD; green). Several mutations were described in multiple painful neuropathic conditions or in patients that demonstrated overlapping symptoms with another pain disorder. Variants found in both SFN and IEM (G856D, R1150W, W1538R) are shown in gray; R185H was discovered in both SFN and PEPD and is shown in purple; A1632E was reported in both IEM and PEPD and is shown in light pink; I228M was described in all three pathologies (ie. SFN, IEM and PEPD) and is shown in black. Topology of loss-of-function mutations associated with congenital insensitivity to pain (CIP) are shown in blue. Typical symptoms and clinical presentation of each disease are represented in red and show the painful areas. The position of the mutations on the linear model do not reflect their atomic proximity

in the 3D folded structure. The schematic view of the channel was modified and adapted from references [14, 81, 82].

Rare monoallelic dominant GoF mutations in *SCN9A* have been widely described in patients with IEM [53, 64] and PEPD [65]. These genetic diseases have served as ground for discovery of more common disorders, such as idiopathic SFN [66] (*Figure 2*).

Inherited Erythromelalgia

Inherited Erythromelalgia (IEM) is characterized by excruciating burning pain attacks and redness in the distal extremities (hands and feet), triggered by heat and exercising, and relieved by cooling. Even mild temperatures can trigger painful episodes, and patients often cannot wear warm clothes or closed-toe shoes. Most patients are unresponsive to available pharmacotherapy, with cooling remaining the most effective strategy, which can result in severe tissue damage or gangrene [83]. Functional assessment of heterologous systems transfected with IEM disease-causing mutations with voltage- and current-clamp have shown cellular hyperexcitability in sensory neurons and hyperpolarized activation, paralleling the clinical phenotype [10, 14]

Paroxysmal extreme pain disorder

Paroxysmal extreme pain disorder (PEPD), or severe episodic perirectal pain, is triggered by bowel movement and rectal/perineal stimulation and is most common in infants [65, 75]. Cold- or irritant-triggered ocular and mandibular pain becomes more prominent in older patients. Functional analysis parallels the clinical phenotype and shows impaired fast inactivation in $Na_V1.7$ channels, resulting in a higher number of channels available for activation and increased excitability [65, 84]. Contrary to IEM, PEPD patients respond well to carbamazepine (CBZ) medications [10, 65, 75].

Small Fiber Neuropathy

Small Fiber Neuropathy (SFN) often manifests with an excruciating burning pain sensation in the hands and feet and is generally associated with degeneration of the smaller fibers (ie. A-delta and C fibers) and inappropriate DRG neuronal firing. Interestingly, genetic variants in sodium channels have been described in 16.9% of SFN patients [67], with a higher frequency in *SCN9A* ($Na_V1.7$) [5], highlighting their crucial contribution to the pathogenesis of SFN.

Congenital and complete inability to experience pain (CIP)

Biallelic LoF mutation in *SCN9A* ($Na_V1.7$) results in complete loss of all pain sensations, without autonomic deficits, aside from anosmia [68, 70, 85], providing undisputable evidence for its role in pain biology. Fourteen mutations have been identified thus far. While most have yielded to premature truncation due to a stop codon, missense mutations have also been reported [15].

Taken together, Mendelian co-segregation between VGSC mutations in patients with strong pain phenotypes have provided additional evidence for causality and have validated sodium channels, in particular $Na_V1.7$, as attractive therapeutic targets for next-generation treatment development [14].

TREATMENTS

Pharmacological management of neuropathic pain focuses on the treatment of symptoms, while most drugs treating the etiological cause (eg. cancer or diabetes) have failed to provide pain relief. The therapeutic regimen for all neuropathic pain conditions, recommended by the Neuropathic Pain Special Interest group (NeuPSIG) of the International Association for the Study of Pain (IASP) [86, 87], includes tricyclic antidepressants (eg. amitriptyline) [4, 86, 88-90], selective serotonin-norepinephrine reuptake inhibitors (eg. venlafaxine and duloxetine), and $Ca_V\,\alpha_2\,\delta$ antagonists (eg. gabapentinoids and pregabalin) as first-line strategies. Anti-epileptic drugs (AEDs; eg. carbamazepine (CBZ) and oxcarzepine) are recommended for trigeminal neuralgia (TN) [91]. Second-line treatments include light opioid analgesics (eg. tramadamol and tapentadol), mostly prescribed as second or third-line treatments due to their adverse side effects [90], and topical agents such as lidocaine and capsaicin. Third-line drug applications include stronger opioids, such as morphine and oxycodone, as well as the neurotoxin botulinum toxin-A [4, 86, 88-90, 92]. However, pain management remains a common medical concern. Current treatments are largely ineffective and induce severe side effects, preventing their extensive use at pain-relieving doses [93]. Furthermore, not only less than 50% of patients report symptomatic relief, but within the responders, the degree of pain improvement dramatically varies across this population [94].

This unmet need for therapeutic response might result from heterogenous pain mechanisms and commonly associated emotional and psychological comorbidities. Patients often report coexisting anxiety and depression, with impaired sleep and quality of life, which need to be treated separately and may hinder analgesic efficacy [3]. Up to now, no clear predictors of treatment responsiveness have been identified in neuropathic pain patients. Additionally, the drug actions do not necessarily correlate with the underlying mechanisms, which are yet to be fully understood [3, 87]. Therefore, there is an urgent need to identify the pathological pathways interacting with drug functions to establish the treatments that provide the most pain relief with the fewest adverse effects.

Non-selective sodium channel blockers

Locally administered, non-selective VGSC blockers, including local anesthetics (LAs) and AEDs, have been used to treat neuropathic pain of various etiologies [34]. CBZ is particularly effective in treating TN [95], PEPD [75], and a small subset of IEM patients [51, 96, 97], despite producing mixed outcomes in VGSC mutant carriers [19, 23]. However, due to their lack of selectivity, VGSC blockers also act on central, cardiac, and

peripheral sodium channels, leading to adverse effects, including confusion, somnolence, ataxia, and cardiac arrythmia [34, 98]. Therefore, the development of selective agents targeting peripherally expressed sodium channels (ie. $Na_V1.7$, $Na_V1.8$ and $Na_V1.9$) is highly warranted.

Local anesthetics (LAs)

Local anesthetics, including lidocaine ad mexiletine, are commonly used for treating peripheral neuropathic pain. Classic sodium channel inhibitors have unequivocally been established to share a common binding motif, the 'LA binding site', composed of the phenylalanine and tyrosine residues F1764 and Y1771 [99, 100], located in the inner pore, below the selectivity filter in the S6 segment of domains I, II, and IV [99, 101-105]. They exert their therapeutic effect via stabilization of the fast inactivated state [106-108] and by use-dependent blockade of sodium channels, thereby inhibiting ectopic discharges [109]. Both lidocaine and mexiletine have shown some efficacy in IEM patients [17, 110-113].

Anti-epileptic drugs (AEDs; anticonvulsants)

Originally developed for treating epilepsy and select psychiatric disorders, anticonvulsants like CBZ, lamotrigine, lacosamide, and oxcarbamazepine have been used to treat chronic painful conditions, including postherpetic neuralgia, fibromyalgia, and TN [86]. However, inconsistent results have been described in other neuropathic pain conditions [3, 5, 114]. Typical AEDs are thought to interact with the LA binding site and to selectively bind to the fast inactivated state of sodium channels in a voltage- and use-dependent manner [100, 104, 115, 116]. In recent years, lacosamide (*R*-2-acetamido-*N*-benzyl-3-methoxypropionamide) has received more attention for its unconventional mode of action. First FDA-approved for the treatment of epilepsy, lacosamide has emerged as a promising second-line treatment for DPN [117-119], migraine, postherpetic neuralgia [120], and refractory pain [121]. Although still often unsatisfactory [119], efficacy was recently described in a subgroup of patients with $Na_V1.7$-related SFN [5]. However, the underlying cause for the heterogeneous response remains to be discovered [34]. Contrary to typical AEDs and LAs, lacosamide predominantly acts by enhancing the voltage-dependence of slow inactivation in VGSCs, while having no effect on steady-state fast inactivation [122-126], or by slowly binding to the fast inactivated state [127]. Because of its unique effect on channel biophysics, lacosamide is thought to induce VGSC blockade through a distinct binding site than AEDs and LAs, which is yet to be investigated.

Precision medicine targeting selective sodium channels

The functional validation of $Na_V1.7$, $Na_V1.8$ and $Na_V1.9$ genetic variants as important contributors to human pain, together with problematic side effects of non-selective VGSC blockers, spurred the development of isoform-specific inhibitors. Selective pharmacotherapy is increasingly suggested as a potential solution to treating neuropathic pain without central or cardiac adverse effects [23, 128-130], while

avoiding interactions with the central reward circuitry responsible for opioid-related addiction [34, 131]. Because *SCN9A* LoF mutations result in pain insensitivity, selective blockade of the channel has been under the spotlight for the past decade [82]. Specific inhibitors are shown to increase the firing threshold in human and rat DRGs [132, 133], and to reduce neurotransmitter release from mouse central and peripheral primary afferents [10, 59, 133]. Nevertheless, randomized clinical trials have reported mixed outcomes [87, 134, 135].

Small molecule inhibitors

A new class of aryl sulfonamide isoform-selective, state-dependent, channel blockers has recently been developed [136, 137]. Their mechanisms of action differ from most VGSC inhibitors as they induce use-dependent blockade via binding to the voltage-sensing domain (VSD) of DIV [137], instead of the highly conserved pore residues (ie. 'LA binding site'), reducing undesirable side effects of pore-binding agents and increasing their subtype selectivity. The first orally available, peripherally restricted $Na_V1.7$-selective blocker PF-05089771 [133] has shown some moderate efficacy in dental pain and DPN [138] and has provided some symptomatic relief in a small group of IEM patients in a phase II single-dose, double-blind, placebo-controlled, crossover study [139]. Nonetheless, high variability was detected in subjects carrying the same mutations, and even in the same patient between two sessions [19, 139]. The relatively poor efficacy of the compound may result from limited CNS penetrance, patient stratification and/or pharmacokinetic differences between *in vivo* and in *vitro* drug metabolism. Furthermore, VGSC blockers might be required to act centrally for effective analgesic effects [140], albeit the peripheral restriction of aryl sulfonamides may ultimately hinder drug effects. Another $Na_V1.7$ blocker BIIB074, recently renamed vixotrigine, blocks the channel in an activity-dependent manner [141, 142]. The compound is well tolerated and has reduced the average pain daily scores and the number of painful paroxysms in clinical trials [134]. In parallel, the emerging success of $Na_V1.8$ blockers in animal models [143, 144] have led to clinical testing and provided encouraging results for osteoarthritis and SFN [145].

Toxins

Several neurotoxins derived from venomous invertebrates have been demonstrated to potently block selective VGSC isoforms [146, 147], also via VSD interactions [148, 149]. For example, the tarantula-derived neurotoxin ProTx-II induces a depolarizing shift in the voltage-dependence of activation of $Na_V1.7$ [150-152] while blocking nociceptive C-fiber activity [151]. Current drug development is emerging in clinical trials and may aid reversal of IEM drug-resistance via binding outside the pore, with minimal cross-reactivity with other isoforms [17].

Pharmacogenomics and personalized medicine

The high degree of variation in pain perception and drug responsiveness might be the result of complex nociception processes and the multifactorial influence of genetic and

environmental components [153, 154]. Thus far, recommendations for the management of neuropathic pain have been appointed based on population studies, and clinical rather than genomic criteria, which largely follows a trial-and-error process, leading to years of ineffective pharmacology with debilitating side effects, only to find, if at all, mildly effective strategies. Initial prescription is based on the patient's age and gender, pain description and clinical cause. Pain is a complex trait influenced by ethnicity [155], gender [156], socio-economical context and pain experience [153, 157]. Dosage is adjusted based on the pain experience, which is by nature subjective, and with substantial placebo response, patient-specific precision medicine is desperately needed. Echoing pain research advancement from mutational analysis, the extrapolation of genomic- and genetic-guided strategies can further our knowledge of gene-treatment interactions and substantially impact the clinical field.

Pharmacogenetics and pharmacogenomics aim to unravel how human individual genetic variants and whole genomes, respectively, affect treatment efficacy and toxicity. Genomic-guided approaches can help choose the most appropriate drug and dosage with the fewest unwanted side effects based on individual patients' genetic background [10]. Modern improvements in genetics and genomics have enabled the identification of over 200 candidate pain genes and have revealed pathogenic gene variants that underlie, at least in part, inter-individual differences in analgesic drug response and adverse effects [153]. Thus, their application might predict effective medication choices. Notably, pharmacogenomic-guided treatment of patients carrying variants in the OPRM1 gene, encoding the μ1 opioid receptor, that directly affected their analgesic response and susceptibility to addiction, benefitted from this approach [153, 158].

Pharmacogenomics of AEDs in VGSC mutants

The easily identifiable clinical phenotype and full penetrance of IEM has served as a platform for exploring pharmacogenomic-based treatment approaches to human pain [10, 51, 97, 159]. In contrast to PEPD, the resistance of IEM to CBZ (and most pharmacotherapy) has informed us on its mechanistic basis, whereby the drug is predicted to bind better to channels that are mutated to a persistently open state [10], explaining its success in PEPD and not IEM patients. CBZ is known to exert its analgesic effects via non-selective inhibition of VGSCs in a voltage- and use-dependent fashion [104, 115, 116]. However, recent studies have revealed a novel mode of action of CBZ as an activation modulator in a subset of IEM $Na_V1.7$-mutant channels [96, 97, 159]. Specifically, clinically-relevant concentrations of CBZ induced a depolarizing shift in activation of $Na_V1.7$ mutant channels V400M, S241T and I234T, expressed in HEK293 cells, bringing them to a wild-type (WT) range [96, 97, 159]. Transfected DRG neurons with S241T and V400M showed selective reduction in cellular excitability, without affecting WT or CBZ-unresponsive F1449V mutant channels [23, 51, 97, 159]. Hereby, applied pharmacogenomics unraveled a unique pharmacological signature in selected mutants, suggesting CBZ may have mutant-specific effects based on their atomic proximity, irrespective of WT. Importantly, these findings were the foundation for open-label use of CBZ in IEM patients carrying V400M [96] and S241T [51]

variants, who reported a reduction in the frequency and duration of pain attacks [51, 96] as well as in the number of sleep awakenings [51]. Functional brain imaging of S241T carriers correlated with the clinical phenotype, marked by a shift in the patterns of activity immediately after CBZ administration [51]. Interestingly, CBZ also corrected neuronal hyperexcitability and depolarized activation in the $Na_V1.8$ equivalent of the $Na_V1.7$-S241T mutant channels ($Na_V1.8$-S242T), demonstrating CBZ inter-isoform potential as an activation modulator [160]. Thermodynamic mutant coupling analysis and atomic-level structural modeling of V400M with S241T and I234T demonstrated non-additive, energetic-coupling of the variants during activation as a single unit that predicted common CBZ responsiveness [10, 97]. Hence, atomic proximity of IEM mutations can be used to probe drug responsiveness in novel variants based on the response of already established 'seed' mutations [10].
Pharmacogenetic-guided intervention has also been used to reduce the likelihood of severe adverse effects. Notably, a strong genetic association between the HLA-B*1502 allele and CBZ-induced Stevens–Johnson syndrome and toxic epidermal necrolysis has emerged in a subgroup of pain patients from Asian populations [161-166]. In another study, a $Na_V1.7$ mutation (N395K) has been found to attenuate lidocaine inhibitory effects [167]. Taken together, this collection of studies illustrates the power of pharmacogenomics and atomic modelling in identifying mutation-specific drug mechanisms while supporting a more personalized treatment approach based on the patient's genomic profile [19, 23].

Limitations of current pharmacogenomic models

Despite growing body of knowledge and the rapid progression of technology, current approaches have largely relied on animal and cellular models to study clinical phenotypes and pharmaco-responsiveness. Transfection and functional characterization of human channels into heterologous systems [50-53] is still challenged by the inability to control for physiological levels of expression. Furthermore, transfected HEK293 cells are limited to the sole expression of the channel of interest, which, while advantageous when studying specific gating properties or mutation-induced drug effects, does reduce the model's validity. Thereby, we can assess mutations detected in patients, but we lose the cellular context and influence of other variants.

Ex vivo cellular nucleofection of mutant genes into rodent DRGs provides a more appropriate cell type and has markedly advanced the electrophysiological field. Nonetheless, recordings of human DRGs have underlined important discrepancies in their excitability and biophysical characteristics compared to rat DRGs [168, 169]. Additionally, different functional characteristics of VGSC subtypes in humans and rodents might lead to distinct pathophysiology and pharmacological response. Interspecies differences are a considerable factor for modeling and drug screening. Comparative proteomics have reported only 50-70% of DRG genes expressed in mice [170, 171] and 80% in rats to overlap with humans' [172]. Importantly, differential levels of abundance of pain-regulating proteins, including TRPV1 and $Na_V1.7$, have

been noted between species [172], suggesting a confounding effect on the translation of animal data into the clinical domain. Therefore, a human sensory neuronal model is critical to study human disease mechanisms and develop novel, more effective therapeutic, at both a cellular and molecular level. However, limited access to human native DRGs (especially from pain patients), along with transportation and time-sensitivity concerns, as they rely on streamlined local organ procurement networks, has prevented their use at larger scales and addresses the need for a surrogate model that mimics human DRG properties [173].

PATIENT IPSC TOWARDS PRECISION MEDICINE

Human induced-pluripotent stem cells (iPSC)-derived sensory neurons (iPSC-SNs) have the potential to become the model of choice for personalized, precision medicine. Recent studies have demonstrated that iPSC-SNs can predict the clinical efficacy of analgesics in the patient from which the cells were derived [139].

Human iPSC models

The conversion of adult somatic cells to retrieve their pluripotency and be derived into any desired cell type has revolutionized the field of personalized medicine, providing a more ethical approach to human models than embryonic stem cells [174, 175]. The non-invasive collection of somatic cells from patients has set a cornerstone for generating high numbers of well-characterized human cell lineages in a consistent manner, with a single biopsy or blood sample leading to trillions of stem cells. Furthermore, iPSCs derived from neuropathic pain patients provide animal-free, patient-specific research, enabling the study of rare genetic defects and personalized treatment strategies.

Human iPSCs harbor and preserve the donor's full genetic background and transcriptional machinery throughout differentiation [176], including disease susceptibility and related mutations [154, 177, 178], overcoming genome-editing method challenges, as no alteration is required. Additionally, being patient-specific, the cells already selectively express variants of interest at physiological levels and retain intact endogenous signaling cascades, including the association between accessory protein and auxiliary subunits needed for a more physiologically relevant cellular environment. Their amenability to genome engineering has made them particularly appealing for studying rare mutations that can be introduced or corrected [82, 179-182]. Finally, differentiation from iPSCs to sensory neurons may provide insights into neurogenesis and disease progression, bringing us a step closer to the bed side.

Current state of iPSCs in pain research

The use of iPSC-nociceptors derived from chronic pain patients has been invaluable to the study of ion channels and human nociception, as well as to providing new avenues in personalized medicine and therapeutics development. Demonstrative of their ability to recapitulate the clinical phenotype, iPSCs-SNs have been generated from $Na_V1.7$-related IEM patients, who exhibit severe pain episodes exacerbated by heat.

Electrophysiological assessment showed aberrant ectopic activity, reduced action potential thresholds and hyperexcitability in response to increasing temperatures [139, 154, 183]. Furthermore, the electrogenic profile of IEM iPSC-SNs directly correlated with different levels of pain severity observed in patients [139, 154, 178], where neurons derived from patients with higher pain scores showed heightened spontaneous activity and firing frequency compared to those who scored less [154], highlighting the ability of the model to parallel differential pain manifestations 'in-the-dish'. Expanding to other pain pathologies, iPSC-SNs derived from a patient with idiopathic SFN depicted increased spontaneous activity corresponding to the donor's C-fiber hyperexcitability [184]. Conversely, in an iPSC cellular model of $Na_V1.7$-related CIP, reduced nociceptor excitability and responsiveness to depolarizing stimuli was reported. Their findings paralleled the microneurography evaluation in three CIP patients that lacked functional nociceptors [82], indicative of the potential for iPSCs to recapitulate important aspects of the clinical phenotype.

Human iPSC-SNs have further enabled the discovery of genetic variants and peripheral pathways involved in pain pathology. For instance, analysis of nociceptors derived from patients with hereditary sensory neuropathy type 1 (HSN1) revealed underlying pathological events, whereby altered ganglioside biosynthesis leads to reduced axonal outgrowth and myelin stability [185]. Furthermore, this model allowed the identification of two novel pain resilience genes. Utilizing whole-exome sequencing and dynamic clamp technology, assessment of iPSC-SNs from two separate families of IEM patients, each carrying the same disease-causing $Na_V1.7$ mutation, recapitulated the parent-child differences in pain phenotypes. Also, *in vitro* analysis of the cells pinpointed variants in potassium channels *KCNQ2* [154] and *KCNQ3* [178], that explained at least some of the families' inter-individual differences in pain sensitivity [154, 178].

Moreover, as stem cell-derived nociceptors are assumed to be naïve and uninjured [177, 186], they offer the possibility to study *de novo* injury-induced pain mechanisms and regeneration processes compared to naïve counterparts. In a model of CIPN, healthy iPSC-SNs exposed to chemotherapeutics replicated inter-individual differences in responsiveness to neurotoxic agents from the different healthy donors [187]. Taken together, these studies validate iPSCs as a valuable model to study important cellular mechanisms in patient-specific cells.

iPSCs for individualized treatments

Harvesting somatic cells from neuropathic pain patients with disease-causing mutations has also allowed the identification of personalized treatment strategies. With recent advances in pharmacogenomics focusing on $Na_V1.7$-selective inhibitors, iPSC-SNs provide an ideal humanized *in vitro* platform to assay drug interventions and their application in specific patients [139, 188]. For instance, the $Na_V1.7$ blocker PF-05089771 reduced IEM iPSC-SN hyperexcitability *in vitro* [139, 188]. Critically, this led to a cross-over, randomized, double-bind, placebo-controlled study where patients

reported a decrease in heat-evoked pain, which advanced to phase II trials for IEM and painful diabetic neuropathy [138, 139]. New evidence for effective drug-induced VGSC blockade has been documented in SFN [184]. Patient-specific iPSC-SNs exposed to the AED lacosamide recovered normal electrophysiological behaviors [184], which was successfully extrapolated to the clinic, reducing the patient' pain scores [138, 139] and C-fiber hyperexcitability [184]. Overall, these results demonstrate that patient-specific iPSCs can guide effective therapeutic design, bringing us a step closer to personalized treatments.

Genomic-guided VGSC blockers

The amenability to genome engineering of iPSC-SNs has facilitated drug development and in generating isogenic lines, has provided insights in genetic defects and compound selectivity. Specifically, in a 'proof-of-concept' study, a CRISPR/Cas9-induced $Na_V1.7$ KO line, derived from healthy individuals, paralleled the electrophysiological properties of CIP iPSC-SNs. Interestingly, correcting one deleterious allele in patient-derived CIP cells is sufficient to rescue the physiological phenotype. However, the cells remain less responsive to supra-threshold stimuli than healthy control, indicating the need for two functional copies of alleles to reach their full range of excitability [82]. KO lines also offer the opportunity to assay the selectivity of clinically relevant compounds in a humanized system. The $Na_v1.7$ blocker PF-05089771, for example, was shown to reduce iPSC-SN cellular excitability in healthy controls but not in their isogenic KO lines. BIIB074, on the other hand, while efficacious in TN patients [134], was shown to be non-selective to $Na_V1.7$ after reducing excitability in $Na_V1.7$ KO iPSC-SNs [82], highlighting the use of iPSC KO lines to dissociate excitability from channel activity. These studies confirm our ability to genetically 'correct' mutations to revert to WT sequences, raising new prospects for using genetic engineering in drug discovery [82].

High-throughput screening of drugs and toxins

Development of new treatments that show promising results in rodent models often do not successfully translate to the clinic. Human iPSC-SNs provide the opportunity to interrogate neurotoxicity and inter-species differences in a humanized system. The high scalability of iPSC-SNs enables high-throughput screening against large libraries of neurotoxic agents and chemotherapeutic drugs [187, 189, 190], which has led to the identification of novel disease-modulating therapeutics and target-based mechanisms against relevant phenotypes [191]. Drug-induced changes in iPSC excitability can further be used to predict the clinical outcome in future trials.

Challenges of using iPSC pain models

This novel, exciting iPSC-based pain model is unfortunately not without its own set of challenges. First and foremost, the culture and maintenance of iPSCs is costly, highly technical, time- and labor-intensive. Current protocols consist of multiple induction steps and necessitate weeks to months to reach their nociceptive state, forming random, unorganized clusters that failed to recapitulate DRG cellular diversity and

spatial architectures [192]. The most commonly used method [193], adapted with minor modifications [82, 154, 179, 194, 195], consists in exposing iPSCs to a cocktail of small inhibitory molecules that trigger signaling cascades responsible for achieving a sensory neuronal cell fate [193]. Stem cells are first converted into neural crest progenitor (NCP) cells, before forming a spinal identity and finally reaching their ultimate nociceptor-like state [193]. While very successful in producing neurons depicting the functional profile and markers of nociceptors, this method has also been criticized for its inability to yield heterogenous populations of mature sensory neurons.

Cellular homogeneity

Although homogenous cultures allow us to perform phenotypic and functional analyses of specific cell cohorts, the generation of diverse sensory neuron populations is important to effectively mimic DRG neuronal-neuronal and neuronal-glial interactions in the context of disease. Also, various cell types are involved in the etiology and mechanisms underlying chronic pain, which are lacking in the Chambers protocol; thus, we are as yet still unable to paint a complete picture of the pathology and its range of complexity [196].

Model validity

Most of our molecular and functional knowledge of sensory neuronal circuitry, diversity, development, and disease pertains to animal models, questioning their validity when applied to a humanized system [173]. Notably, differentiation of iPSC-SNs is assessed through their expression of canonical markers identified in rodents. Importantly, inter-species differences in the distribution and co-expression of sensory neuron markers, including NF200, CGRP, P2X3R, TRPM8 and Piezo2 [193, 197-201] lead to a biased view of their functions. For instance, NF200 and CGRP are only expressed in subsets of mouse DRGs [201] while they are both widely detectable in most human sensory neurons [199]. Likewise, iPSC-SNs were found to co-express CGRP/P2X3R [193, 197, 198] and TRPM8/Piezo2 [200]. These proteins co-exist in humans but are non-overlapping in mouse [199], emphasizing the need to define markers in human cells first to then find alternatives to distinguish cell populations.

Imperfect human surrogate

Differential proteomic expression is not limited to rodent markers, along with diverse functional electrogenic profiles, differences between human DRGs and iPSC-SNs represent an ongoing challenge to overcome before their effective use as human cell surrogates. In-depth gene comparative analysis revealed large variations between human DRGs and iPSC-SNs in key pain regulating genes, including *SCN9A*, *SCN10A*, *TRPV1*, *P2X3*, underlying their lack of functional and transcriptional maturity [195]. For instance, $Na_V1.3$ is expressed at relatively high levels in iPSC-SNs, in contrast to uninjured adult DRG neurons where it is undetectable [31, 32], inferring that iPSC-SNs either retain juvenile characteristics, or are 'injured' during RNA isolation [195]. Furthermore, as opposed to human DRG neurons that respond to TRPV1-agonist capsaicin, the majority of TRPV1-expressing iPSC-SNs that are derived from the

Chambers protocol are functionally unresponsive to capsaicin [177, 194, 202], indicating that mRNA transcripts do not necessarily correlate with functional protein expression. Concurrently, functional expression of $Na_V1.8$ and $Na_V1.9$ in iPSC-SNs has long been debated. Most studies supporting their expression are solely based on mRNA expression and the presence of TTX-R currents in iPSC-derived nociceptors [183]. However, Eberhardt et al. have demonstrated that most of iPSC-SN TTX-R current recorded in iPSC-SNs pertains to developmentally regulated $Na_V1.5$, indicative of an immature differentiation state [194], which may also predict altered electro-responsiveness and excitability [173]. The contribution of Nav1.8 and Nav1.9 to the cell resting membrane potential and current density is necessary to pain physiology and further limits the study of patient-specific mutations in the absence of these channels. The utility of the system is dependent on its ability to express the gene of interest. The lack of functional expression of essential pain-related proteins found in mature adult DRG neurons represent a major caveat.

Experimental challenges

Additional experimental challenges have arisen from currently used protocols, including poor replating efficiency and unpracticality for multi-well systems [189, 190]. Furthermore, iPSC-SNs are smaller (even after months in culture) [82, 169] and produce longer neurites compared to human or rodent DRGs, which impair space clamp and hinder current control, ultimately affecting the quality of the recordings [181, 183, 203]. Impaired patch-ability represents a major drawback to their use in pain research considering the necessity of electrophysiological assessment in nociceptors.

Genetic and epigenetic challenges

- *Donor-induced variability*

Inter-individual variability in genetic, epigenetic, and environmental factors, although being the basis of personalized medicine, might account for reduced reproducibility in iPSC-SN models [204-206]. Furthermore, in older individuals, the likelihood of *de novo* somatic mitochondrial DNA mutations increases with the donor's age, leading to metabolic loss functions [207].

- *Culture-induced variability*

Heterogeneity between different iPSC batches has been reported between and within cell lines [180, 204], arising from clonal selection and cell culture environment during reprogramming and differentiation [195, 204]. Small changes in cell media composition, atmospheric conditions, and/or cell density can have a large impact on cell reproducibility and gene expression [195]. Increased genetic and neuronal content variation have been reported in genes involved with neuronal development, as well as in *SCN9A*, upon the choice of medium [204]. Minor modifications of the same Chambers protocol yielded iPSC-SN gene expression profiles that resemble those of pruriceptors [208], proprioceptors [209] and C-low threshold mechanoreceptors [177, 202].

- *Differentiation-induced variability*

Differentiation-induced variability has been shown to affect the neuronal composition of cultures [195] and to contribute to stem cell genetic instability, whereby it increases the risk of *de novo* mutations [204]. Specifically, single cell RNA sequencing has shown that differentiation replicates within the same donor do not always cluster together, meaning that differentiation-induced cell variability is at least as important as those induced by the donor genetic background and iPSC reprogramming together. Furthermore, the composition of the neuronal populations was shown to significantly vary across differentiations [195].

- *Epigenetics-induced variability*

Cell manipulation has been suggested to induce *de novo* epigenetic changes, which constitutes another important bias in pain studies [210]. Specifically, differentiation has been shown to reduce DNA methylation and increase hypomethylated CpG rich regions [211, 212]. While extensive literature suggests that most epigenetic changes occur during differentiation [212], evidence of retention of somatic epigenetic and transcriptomic memory have suggested otherwise [213]. Nevertheless, our current inability to distinguish between differentiation-induced epigenetic modifications and the donor's epigenome still questions the validity of iPSC-derived models.

Rare variants only

Human iPSCs are highly advantageous to study rare genetic diseases; however, the study of common regulatory variants remains limited. In order to achieve significance in 'recall-by-genotype' studies, over 40 samples are required, from 20-80 different donors, which is hardly achievable [195], while culture- and differentiation-induced variability heavily affect their detection. Therefore, better reprogramming and differentiation methods are necessary for disease modelling.

REFERENCES

1. Scholz, J., et al., *The IASP classification of chronic pain for ICD-11: chronic neuropathic pain.* Pain, 2019. **160**(1): p. 53-59.
2. van Hecke, O., et al., *Neuropathic pain in the general population: a systematic review of epidemiological studies.* Pain, 2014. **155**(4): p. 654-662.
3. Baron, R., A. Binder, and G. Wasner, *Neuropathic pain: diagnosis, pathophysiological mechanisms, and treatment.* Lancet Neurol, 2010. **9**(8): p. 807-19.
4. Colloca, L., et al., *Neuropathic pain.* Nat Rev Dis Primers, 2017. **3**: p. 17002.
5. de Greef, B.T.A., et al., *Lacosamide in patients with Nav1.7 mutations-related small fibre neuropathy: a randomized controlled trial.* Brain, 2019. **142**(2): p. 263-275.
6. Lotsch, J., et al., *Functional genomics of pain in analgesic drug development and therapy.* Pharmacol Ther, 2013. **139**(1): p. 60-70.
7. Dib-Hajj, S.D. and S.G. Waxman, *Translational pain research: Lessons from genetics and genomics.* Sci Transl Med, 2014. **6**(249): p. 249sr4.
8. Zorina-Lichtenwalter, K., et al., *Genetic predictors of human chronic pain conditions.* Neuroscience, 2016. **338**: p. 36-62.
9. Mogil, J.S., *Pain genetics: past, present and future.* Trends Genet, 2012. **28**(6): p. 258-66.
10. Yang, Y., et al., *NaV1.7 as a Pharmacogenomic Target for Pain: Moving Toward Precision Medicine.* Trends Pharmacol Sci, 2018. **39**(3): p. 258-275.
11. Julius, D., *TRP channels and pain.* Annu Rev Cell Dev Biol, 2013. **29**: p. 355-84.
12. Gasparotti, R., et al., *New technologies for the assessment of neuropathies.* Nat Rev Neurol, 2017. **13**(4): p. 203-216.
13. Kennedy, D.L., et al., *Reliability of conditioned pain modulation: a systematic review.* Pain, 2016. **157**(11): p. 2410-2419.
14. Dib-Hajj, S.D., et al., *The Na(V)1.7 sodium channel: from molecule to man.* Nat Rev Neurosci, 2013. **14**(1): p. 49-62.
15. Bennett, D.L., et al., *The Role of Voltage-Gated Sodium Channels in Pain Signaling.* Physiol Rev, 2019. **99**(2): p. 1079-1151.
16. Catterall, W.A., *Structure and regulation of voltage-gated Ca2+ channels.* Annu Rev Cell Dev Biol, 2000. **16**: p. 521-55.
17. Lampert, A., et al., *Sodium channelopathies and pain.* Pflugers Arch, 2010. **460**(2): p. 249-63.
18. Catterall, W.A., *From ionic currents to molecular mechanisms: the structure and function of voltage-gated sodium channels.* Neuron, 2000. **26**(1): p. 13-25.
19. Dib-Hajj, S.D., P. Geha, and S.G. Waxman, *Sodium channels in pain disorders: pathophysiology and prospects for treatment.* Pain, 2017. **158 Suppl 1**: p. S97-S107.
20. Catterall, W.A., A.L. Goldin, and S.G. Waxman, *International Union of Pharmacology. XLVII. Nomenclature and structure-function relationships of voltage-gated sodium channels.* Pharmacol Rev, 2005. **57**(4): p. 397-409.
21. Bouza, A.A. and L.L. Isom, *Voltage-gated sodium channel β subunits and their related diseases.* Voltage-Gated Sodium Channels: Structure, Function and Channelopathies, 2017: p. 423-450.
22. Goldfarb, M., *Fibroblast growth factor homologous factors: evolution, structure, and function.* Cytokine Growth Factor Rev, 2005. **16**(2): p. 215-20.
23. Dib-Hajj, S.D. and S.G. Waxman, *Sodium Channels in Human Pain Disorders: Genetics and Pharmacogenomics.* Annu Rev Neurosci, 2019.
24. Dib-Hajj, S.D., et al., *Sodium channels in normal and pathological pain.* Annu Rev Neurosci, 2010. **33**: p. 325-47.
25. Pei, Z., Y. Pan, and T.R. Cummins, *Posttranslational Modification of Sodium Channels.* Handb Exp Pharmacol, 2018. **246**: p. 101-124.
26. Shen, H., et al., *Structures of human Nav1.7 channel in complex with auxiliary subunits and animal toxins.* Science, 2019. **363**(6433): p. 1303-1308.

27. Yu, F.H. and W.A. Catterall, *Overview of the voltage-gated sodium channel family.* Genome Biol, 2003. **4**(3): p. 207.
28. Trimmer, J.S. and K.J. Rhodes, *Localization of voltage-gated ion channels in mammalian brain.* Annu Rev Physiol, 2004. **66**: p. 477-519.
29. Hockley, J.R., et al., *Visceral and somatic pain modalities reveal NaV 1.7-independent visceral nociceptive pathways.* J Physiol, 2017. **595**(8): p. 2661-2679.
30. Osteen, J.D., et al., *Selective spider toxins reveal a role for the Nav1.1 channel in mechanical pain.* Nature, 2016. **534**(7608): p. 494-9.
31. Waxman, S.G., J.D. Kocsis, and J.A. Black, *Type III sodium channel mRNA is expressed in embryonic but not adult spinal sensory neurons, and is reexpressed following axotomy.* J Neurophysiol, 1994. **72**(1): p. 466-70.
32. Dib-Hajj, S., et al., *Down-regulation of transcripts for Na channel alpha-SNS in spinal sensory neurons following axotomy.* Proc Natl Acad Sci U S A, 1996. **93**(25): p. 14950-4.
33. Caldwell, J.H., et al., *Sodium channel Na(v)1.6 is localized at nodes of ranvier, dendrites, and synapses.* Proc Natl Acad Sci U S A, 2000. **97**(10): p. 5616-20.
34. Alsaloum, M., et al., *Status of peripheral sodium channel blockers for non-addictive pain treatment.* Nat Rev Neurol, 2020. **16**(12): p. 689-705.
35. Dib-Hajj, S.D., J.A. Black, and S.G. Waxman, *NaV1.9: a sodium channel linked to human pain.* Nat Rev Neurosci, 2015. **16**(9): p. 511-9.
36. Erickson, A., et al., *Voltage-gated sodium channels: (NaV)igating the field to determine their contribution to visceral nociception.* J Physiol, 2018. **596**(5): p. 785-807.
37. Tanaka, B.S., et al., *A gain-of-function mutation in Nav1.6 in a case of trigeminal neuralgia.* Mol Med, 2016. **22**: p. 338-348.
38. Han, C., et al., *The Domain II S4-S5 Linker in Nav1.9: A Missense Mutation Enhances Activation, Impairs Fast Inactivation, and Produces Human Painful Neuropathy.* Neuromolecular Med, 2015. **17**(2): p. 158-69.
39. Han, C., et al., *Familial gain-of-function Nav1.9 mutation in a painful channelopathy.* J Neurol Neurosurg Psychiatry, 2017. **88**(3): p. 233-240.
40. Huang, J., et al., *A Novel Gain-of-Function Nav1.9 Mutation in a Child With Episodic Pain.* Front Neurosci, 2019. **13**: p. 918.
41. Huang, J., et al., *Sodium channel NaV1.9 mutations associated with insensitivity to pain dampen neuronal excitability.* J Clin Invest, 2017. **127**(7): p. 2805-2814.
42. Leipold, E., et al., *Cold-aggravated pain in humans caused by a hyperactive NaV1.9 channel mutant.* Nat Commun, 2015. **6**: p. 10049.
43. Leipold, E., et al., *A de novo gain-of-function mutation in SCN11A causes loss of pain perception.* Nat Genet, 2013. **45**(11): p. 1399-404.
44. Okuda, H., et al., *Infantile Pain Episodes Associated with Novel Nav1.9 Mutations in Familial Episodic Pain Syndrome in Japanese Families.* PLoS One, 2016. **11**(5): p. e0154827.
45. Woods, C.G., et al., *The phenotype of congenital insensitivity to pain due to the NaV1.9 variant p.L811P.* Eur J Hum Genet, 2015. **23**(10): p. 1434.
46. Zhang, X.Y., et al., *Gain-of-function mutations in SCN11A cause familial episodic pain.* Am J Hum Genet, 2013. **93**(5): p. 957-66.
47. Siqueira, S.R., et al., *Abnormal expression of voltage-gated sodium channels Nav1.7, Nav1.3 and Nav1.8 in trigeminal neuralgia.* Neuroscience, 2009. **164**(2): p. 573-7.
48. Lai, J., J.C. Hunter, and F. Porreca, *The role of voltage-gated sodium channels in neuropathic pain.* Curr Opin Neurobiol, 2003. **13**(3): p. 291-7.
49. Black, J.A., et al., *Multiple sodium channel isoforms and mitogen-activated protein kinases are present in painful human neuromas.* Ann Neurol, 2008. **64**(6): p. 644-53.
50. Dib-Hajj, S.D., et al., *Transfection of rat or mouse neurons by biolistics or electroporation.* Nat Protoc, 2009. **4**(8): p. 1118-26.
51. Geha, P., et al., *Pharmacotherapy for Pain in a Family With Inherited Erythromelalgia Guided by Genomic Analysis and Functional Profiling.* JAMA Neurol, 2016. **73**(6): p. 659-67.

52. Yang, Y., et al., *Nav1.7-A1632G Mutation from a Family with Inherited Erythromelalgia: Enhanced Firing of Dorsal Root Ganglia Neurons Evoked by Thermal Stimuli.* J Neurosci, 2016. **36**(28): p. 7511-22.
53. Dib-Hajj, S.D., et al., *Gain-of-function mutation in Nav1.7 in familial erythromelalgia induces bursting of sensory neurons.* Brain, 2005. **128**(Pt 8): p. 1847-54.
54. Dib-Hajj, S.D. and S.G. Waxman, *Diversity of composition and function of sodium channels in peripheral sensory neurons.* Pain, 2015. **156**(12): p. 2406-7.
55. Eijkelkamp, N., et al., *Neurological perspectives on voltage-gated sodium channels.* Brain, 2012. **135**(Pt 9): p. 2585-612.
56. Black, J.A., et al., *Changes in the expression of tetrodotoxin-sensitive sodium channels within dorsal root ganglia neurons in inflammatory pain.* Pain, 2004. **108**(3): p. 237-247.
57. Chattopadhyay, M., et al., *Reduction of voltage gated sodium channel protein in DRG by vector mediated miRNA reduces pain in rats with painful diabetic neuropathy.* Mol Pain, 2012. **8**: p. 17.
58. Yeomans, D.C., et al., *Decrease in inflammatory hyperalgesia by herpes vector-mediated knockdown of Nav1.7 sodium channels in primary afferents.* Hum Gene Ther, 2005. **16**(2): p. 271-7.
59. Minett, M.S., et al., *Distinct Nav1.7-dependent pain sensations require different sets of sensory and sympathetic neurons.* Nat Commun, 2012. **3**: p. 791.
60. Gingras, J., et al., *Global Nav1.7 knockout mice recapitulate the phenotype of human congenital indifference to pain.* PLoS One, 2014. **9**(9): p. e105895.
61. Nassar, M.A., et al., *Nociceptor-specific gene deletion reveals a major role for Nav1.7 (PN1) in acute and inflammatory pain.* Proc Natl Acad Sci U S A, 2004. **101**(34): p. 12706-11.
62. Shields, S.D., et al., *Sodium channel Na(v)1.7 is essential for lowering heat pain threshold after burn injury.* J Neurosci, 2012. **32**(32): p. 10819-32.
63. Cummins, T.R., S.D. Dib-Hajj, and S.G. Waxman, *Electrophysiological properties of mutant Nav1.7 sodium channels in a painful inherited neuropathy.* J Neurosci, 2004. **24**(38): p. 8232-6.
64. Yang, Y., et al., *Mutations in SCN9A, encoding a sodium channel alpha subunit, in patients with primary erythermalgia.* J Med Genet, 2004. **41**(3): p. 171-4.
65. Fertleman, C.R., et al., *SCN9A mutations in paroxysmal extreme pain disorder: allelic variants underlie distinct channel defects and phenotypes.* Neuron, 2006. **52**(5): p. 767-74.
66. Faber, C.G., et al., *Gain of function Nanu1.7 mutations in idiopathic small fiber neuropathy.* Ann Neurol, 2012. **71**(1): p. 26-39.
67. de Greef, B.T.A., et al., *Associated conditions in small fiber neuropathy - a large cohort study and review of the literature.* Eur J Neurol, 2018. **25**(2): p. 348-355.
68. Cox, J.J., et al., *An SCN9A channelopathy causes congenital inability to experience pain.* Nature, 2006. **444**(7121): p. 894-8.
69. Ahmad, S., et al., *A stop codon mutation in SCN9A causes lack of pain sensation.* Hum Mol Genet, 2007. **16**(17): p. 2114-21.
70. Goldberg, Y.P., et al., *Loss-of-function mutations in the Nav1.7 gene underlie congenital indifference to pain in multiple human populations.* Clin Genet, 2007. **71**(4): p. 311-9.
71. Yuan, J., et al., *Hereditary sensory and autonomic neuropathy type IID caused by an SCN9A mutation.* Neurology, 2013. **80**(18): p. 1641-9.
72. Orstavik, K. and E. Jorum, *Microneurographic findings of relevance to pain in patients with erythromelalgia and patients with diabetic neuropathy.* Neurosci Lett, 2010. **470**(3): p. 180-4.
73. Orstavik, K., et al., *Pathological C-fibres in patients with a chronic painful condition.* Brain, 2003. **126**(Pt 3): p. 567-78.
74. Namer, B., et al., *Specific changes in conduction velocity recovery cycles of single nociceptors in a patient with erythromelalgia with the I848T gain-of-function mutation of Nav1.7.* Pain, 2015. **156**(9): p. 1637-1646.
75. Fertleman, C.R., et al., *Paroxysmal extreme pain disorder (previously familial rectal pain syndrome).* Neurology, 2007. **69**(6): p. 586-95.

76. Brouwer, B.A., et al., *Painful neuropathies: the emerging role of sodium channelopathies.* J Peripher Nerv Syst, 2014. **19**(2): p. 53-65.
77. Han, C., J. Huang, and S.G. Waxman, *Sodium channel Nav1.8: Emerging links to human disease.* Neurology, 2016. **86**(5): p. 473-83.
78. Huang, J., et al., *Gain-of-function mutations in sodium channel Na(v)1.9 in painful neuropathy.* Brain, 2014. **137**(Pt 6): p. 1627-42.
79. Alsaloum, M., et al., *A gain-of-function sodium channel beta2-subunit mutation in painful diabetic neuropathy.* Mol Pain, 2019. **15**: p. 1744806919849802.
80. Alsaloum, M., et al., *A novel gain-of-function sodium channel beta2 subunit mutation in idiopathic small fiber neuropathy.* J Neurophysiol, 2021. **126**(3): p. 827-839.
81. Baker, M.D. and M.A. Nassar, *Painful and painless mutations of SCN9A and SCN11A voltage-gated sodium channels.* Pflugers Arch, 2020. **472**(7): p. 865-880.
82. McDermott, L.A., et al., *Defining the Functional Role of NaV1.7 in Human Nociception.* Neuron, 2019. **101**(5): p. 905-919 e8.
83. Drenth, J.P. and S.G. Waxman, *Mutations in sodium-channel gene SCN9A cause a spectrum of human genetic pain disorders.* J Clin Invest, 2007. **117**(12): p. 3603-9.
84. Dib-Hajj, S.D., et al., *Paroxysmal extreme pain disorder M1627K mutation in human Nav1.7 renders DRG neurons hyperexcitable.* Mol Pain, 2008. **4**: p. 37.
85. Nilsen, K.B., et al., *Two novel SCN9A mutations causing insensitivity to pain.* Pain, 2009. **143**(1-2): p. 155-8.
86. Finnerup, N.B., et al., *Pharmacotherapy for neuropathic pain in adults: a systematic review and meta-analysis.* Lancet Neurol, 2015. **14**(2): p. 162-73.
87. Finnerup, N.B., R. Kuner, and T.S. Jensen, *Neuropathic Pain: From Mechanisms to Treatment.* Physiol Rev, 2021. **101**(1): p. 259-301.
88. Attal, N., et al., *EFNS guidelines on the pharmacological treatment of neuropathic pain: 2010 revision.* Eur J Neurol, 2010. **17**(9): p. 1113-e88.
89. Moulin, D., et al., *Pharmacological management of chronic neuropathic pain: revised consensus statement from the Canadian Pain Society.* Pain Res Manag, 2014. **19**(6): p. 328-35.
90. Cavalli, E., et al., *The neuropathic pain: An overview of the current treatment and future therapeutic approaches.* Int J Immunopathol Pharmacol, 2019. **33**: p. 2058738419838383.
91. Maarbjerg, S., et al., *Trigeminal neuralgia - diagnosis and treatment.* Cephalalgia, 2017. **37**(7): p. 648-657.
92. Szok, D., et al., *Therapeutic Approaches for Peripheral and Central Neuropathic Pain.* Behav Neurol, 2019. **2019**: p. 8685954.
93. Sopacua, M., et al., *Small-fiber neuropathy: Expanding the clinical pain universe.* J Peripher Nerv Syst, 2019. **24**(1): p. 19-33.
94. Sopacua, M., et al., *Small-fiber neuropathy: Expanding the clinical pain universe.* J Peripher Nerv Syst, 2018.
95. Gronseth, G., et al., *Practice parameter: the diagnostic evaluation and treatment of trigeminal neuralgia (an evidence-based review): report of the Quality Standards Subcommittee of the American Academy of Neurology and the European Federation of Neurological Societies.* Neurology, 2008. **71**(15): p. 1183-90.
96. Fischer, T.Z., et al., *A novel Nav1.7 mutation producing carbamazepine-responsive erythromelalgia.* Ann Neurol, 2009. **65**(6): p. 733-41.
97. Yang, Y., et al., *Structural modelling and mutant cycle analysis predict pharmacoresponsiveness of a Na V 1.7 mutant channel.* Nature communications, 2012. **3**: p. 1186.
98. Mao, J. and L.L. Chen, *Systemic lidocaine for neuropathic pain relief.* Pain, 2000. **87**(1): p. 7-17.
99. Ragsdale, D.S., et al., *Common molecular determinants of local anesthetic, antiarrhythmic, and anticonvulsant block of voltage-gated Na+ channels.* Proc Natl Acad Sci U S A, 1996. **93**(17): p. 9270-5.
100. Kuo, C.C., *A common anticonvulsant binding site for phenytoin, carbamazepine, and lamotrigine in neuronal Na+ channels.* Mol Pharmacol, 1998. **54**(4): p. 712-21.

101. Lipkind, G.M. and H.A. Fozzard, *Molecular model of anticonvulsant drug binding to the voltage-gated sodium channel inner pore.* Mol Pharmacol, 2010. **78**(4): p. 631-8.
102. Lipkind, G.M. and H.A. Fozzard, *Molecular modeling of local anesthetic drug binding by voltage-gated sodium channels.* Mol Pharmacol, 2005. **68**(6): p. 1611-22.
103. Liu, G., et al., *Differential interactions of lamotrigine and related drugs with transmembrane segment IVS6 of voltage-gated sodium channels.* Neuropharmacology, 2003. **44**(3): p. 413-22.
104. Yang, Y.C., C.S. Huang, and C.C. Kuo, *Lidocaine, carbamazepine, and imipramine have partially overlapping binding sites and additive inhibitory effect on neuronal Na+ channels.* Anesthesiology, 2010. **113**(1): p. 160-74.
105. Nau, C. and G.K. Wang, *Interactions of local anesthetics with voltage-gated Na+ channels.* J Membr Biol, 2004. **201**(1): p. 1-8.
106. Catterall, W.A., *Common modes of drug action on Na+ channels: local anesthetics, antiarrhythmics and anticonvulsants.* Trends in Pharmacological Sciences, 1987. **8**(2): p. 57-65.
107. Catterall, W.A., *Voltage-gated sodium channels at 60: structure, function and pathophysiology.* J Physiol, 2012. **590**(11): p. 2577-89.
108. Rogawski, M.A. and W. Loscher, *The neurobiology of antiepileptic drugs.* Nat Rev Neurosci, 2004. **5**(7): p. 553-64.
109. Devor, M., P.D. Wall, and N. Catalan, *Systemic lidocaine silences ectopic neuroma and DRG discharge without blocking nerve conduction.* Pain, 1992. **48**(2): p. 261-268.
110. Harty, T.P., et al., *Na(V)1.7 mutant A863P in erythromelalgia: effects of altered activation and steady-state inactivation on excitability of nociceptive dorsal root ganglion neurons.* J Neurosci, 2006. **26**(48): p. 12566-75.
111. Iqbal, J., et al., *Experience with oral mexiletine in primary erythromelalgia in children.* Ann Saudi Med, 2009. **29**(4): p. 316-8.
112. Kuhnert, S.M., W.J. Phillips, and M.D. Davis, *Lidocaine and mexiletine therapy for erythromelalgia.* Arch Dermatol, 1999. **135**(12): p. 1447-9.
113. Nathan, A., et al., *Primary erythromelalgia in a child responding to intravenous lidocaine and oral mexiletine treatment.* Pediatrics, 2005. **115**(4): p. e504-7.
114. Demant, D.T., et al., *Pain relief with lidocaine 5% patch in localized peripheral neuropathic pain in relation to pain phenotype: a randomised, double-blind, and placebo-controlled, phenotype panel study.* Pain, 2015. **156**(11): p. 2234-2244.
115. Kuo, C.C., et al., *Carbamazepine inhibition of neuronal Na+ currents: quantitative distinction from phenytoin and possible therapeutic implications.* Mol Pharmacol, 1997. **51**(6): p. 1077-83.
116. Tanelian, D.L. and W.G. Brose, *Neuropathic pain can be relieved by drugs that are use-dependent sodium channel blockers: lidocaine, carbamazepine, and mexiletine.* Anesthesiology, 1991. **74**(5): p. 949-51.
117. Wymer, J.P., et al., *Efficacy and safety of lacosamide in diabetic neuropathic pain: an 18-week double-blind placebo-controlled trial of fixed-dose regimens.* Clin J Pain, 2009. **25**(5): p. 376-85.
118. Shaibani, A., et al., *Lacosamide in painful diabetic neuropathy: an 18-week double-blind placebo-controlled trial.* J Pain, 2009. **10**(8): p. 818-28.
119. Ziegler, D., et al., *Efficacy and safety of lacosamide in painful diabetic neuropathy.* Diabetes Care, 2010. **33**(4): p. 839-41.
120. Carona, A., et al., *Pharmacology of lacosamide: From its molecular mechanisms and pharmacokinetics to future therapeutic applications.* Life Sci, 2021. **275**: p. 119342.
121. McCleane, G., B. Koch, and C. Rauschkolb, *Does SPM 927 have an analgesic effect in human neuropathic pain? An open label study.* Neurosci Lett, 2003. **352**(2): p. 117-20.
122. Errington, A.C., et al., *The investigational anticonvulsant lacosamide selectively enhances slow inactivation of voltage-gated sodium channels.* Mol Pharmacol, 2008. **73**(1): p. 157-69.
123. Niespodziany, I., et al., *Comparative study of lacosamide and classical sodium channel blocking antiepileptic drugs on sodium channel slow inactivation.* J Neurosci Res, 2013. **91**(3): p. 436-43.

124. Sheets, P.L., et al., *Differential block of sensory neuronal voltage-gated sodium channels by lacosamide [(2R)-2-(acetylamino)-N-benzyl-3-methoxypropanamide], lidocaine, and carbamazepine.* J Pharmacol Exp Ther, 2008. **326**(1): p. 89-99.
125. Wang, Y., et al., *Development and characterization of novel derivatives of the antiepileptic drug lacosamide that exhibit far greater enhancement in slow inactivation of voltage-gated sodium channels.* ACS Chem Neurosci, 2011. **2**(2): p. 90-106.
126. Rogawski, M.A., et al., *Current understanding of the mechanism of action of the antiepileptic drug lacosamide.* Epilepsy Res, 2015. **110**: p. 189-205.
127. Jo, S. and B.P. Bean, *Lacosamide Inhibition of Nav1.7 Voltage-Gated Sodium Channels: Slow Binding to Fast-Inactivated States.* Mol Pharmacol, 2017. **91**(4): p. 277-286.
128. Theile, J.W. and T.R. Cummins, *Recent developments regarding voltage-gated sodium channel blockers for the treatment of inherited and acquired neuropathic pain syndromes.* Front Pharmacol, 2011. **2**: p. 54.
129. Dib-Hajj, S.D., J.A. Black, and S.G. Waxman, *Voltage-gated sodium channels: therapeutic targets for pain.* Pain Med, 2009. **10**(7): p. 1260-9.
130. McKerrall, S.J. and D.P. Sutherlin, *Nav1.7 inhibitors for the treatment of chronic pain.* Bioorg Med Chem Lett, 2018. **28**(19): p. 3141-3149.
131. Le Merrer, J., et al., *Reward processing by the opioid system in the brain.* Physiol Rev, 2009. **89**(4): p. 1379-412.
132. Vasylyev, D.V., et al., *Dynamic-clamp analysis of wild-type human Nav1.7 and erythromelalgia mutant channel L858H.* J Neurophysiol, 2014. **111**(7): p. 1429-43.
133. Alexandrou, A.J., et al., *Subtype-Selective Small Molecule Inhibitors Reveal a Fundamental Role for Nav1.7 in Nociceptor Electrogenesis, Axonal Conduction and Presynaptic Release.* PLoS One, 2016. **11**(4): p. e0152405.
134. Zakrzewska, J.M., et al., *Safety and efficacy of a Nav1.7 selective sodium channel blocker in patients with trigeminal neuralgia: a double-blind, placebo-controlled, randomised withdrawal phase 2a trial.* Lancet Neurol, 2017. **16**(4): p. 291-300.
135. Price, N., et al., *Safety and Efficacy of a Topical Sodium Channel Inhibitor (TV-45070) in Patients With Postherpetic Neuralgia (PHN): A Randomized, Controlled, Proof-of-Concept, Crossover Study, With a Subgroup Analysis of the Nav1.7 R1150W Genotype.* Clin J Pain, 2017. **33**(4): p. 310-318.
136. Bagal, S.K., et al., *Recent progress in sodium channel modulators for pain.* Bioorg Med Chem Lett, 2014. **24**(16): p. 3690-9.
137. McCormack, K., et al., *Voltage sensor interaction site for selective small molecule inhibitors of voltage-gated sodium channels.* Proc Natl Acad Sci U S A, 2013. **110**(29): p. E2724-32.
138. McDonnell, A., et al., *Efficacy of the Nav1.7 blocker PF-05089771 in a randomised, placebo-controlled, double-blind clinical study in subjects with painful diabetic peripheral neuropathy.* Pain, 2018. **159**(8): p. 1465-1476.
139. Cao, L., et al., *Pharmacological reversal of a pain phenotype in iPSC-derived sensory neurons and patients with inherited erythromelalgia.* Sci Transl Med, 2016. **8**(335): p. 335ra56.
140. MacDonald, D.I., et al., *A central mechanism of analgesia in mice and humans lacking the sodium channel NaV1.7.* Neuron, 2021. **109**(9): p. 1497-1512 e6.
141. Deuis, J.R., et al., *Analgesic Effects of GpTx-1, PF-04856264 and CNV1014802 in a Mouse Model of NaV1.7-Mediated Pain.* Toxins (Basel), 2016. **8**(3).
142. Zheng, Y.M., et al., *Enhancing inactivation rather than reducing activation of Nav1.7 channels by a clinically effective analgesic CNV1014802.* Acta Pharmacol Sin, 2018. **39**(4): p. 587-596.
143. Jarvis, M.F., et al., *A-803467, a potent and selective Nav1.8 sodium channel blocker, attenuates neuropathic and inflammatory pain in the rat.* Proc Natl Acad Sci U S A, 2007. **104**(20): p. 8520-5.
144. Payne, C.E., et al., *A novel selective and orally bioavailable Nav 1.8 channel blocker, PF-01247324, attenuates nociception and sensory neuron excitability.* Br J Pharmacol, 2015. **172**(10): p. 2654-70.

145. Dib-Hajj, S.D. and S.G. Waxman, *Sodium Channels in Human Pain Disorders: Genetics and Pharmacogenomics.* Annu Rev Neurosci, 2019. **42**: p. 87-106.
146. Wang, C.G., et al., *Exploration of the functional site of a scorpion alpha-like toxin by site-directed mutagenesis.* Biochemistry, 2003. **42**(16): p. 4699-708.
147. Wang, S.Y. and G.K. Wang, *Voltage-gated sodium channels as primary targets of diverse lipid-soluble neurotoxins.* Cell Signal, 2003. **15**(2): p. 151-9.
148. Xiao, Y., et al., *Tarantula huwentoxin-IV inhibits neuronal sodium channels by binding to receptor site 4 and trapping the domain ii voltage sensor in the closed configuration.* J Biol Chem, 2008. **283**(40): p. 27300-13.
149. Cestele, S., et al., *Structure and function of the voltage sensor of sodium channels probed by a beta-scorpion toxin.* J Biol Chem, 2006. **281**(30): p. 21332-21344.
150. Priest, B.T., et al., *ProTx-I and ProTx-II: gating modifiers of voltage-gated sodium channels.* Toxicon, 2007. **49**(2): p. 194-201.
151. Schmalhofer, W.A., et al., *ProTx-II, a selective inhibitor of NaV1.7 sodium channels, blocks action potential propagation in nociceptors.* Mol Pharmacol, 2008. **74**(5): p. 1476-84.
152. Xiao, Y., et al., *The tarantula toxins ProTx-II and huwentoxin-IV differentially interact with human Nav1.7 voltage sensors to inhibit channel activation and inactivation.* Mol Pharmacol, 2010. **78**(6): p. 1124-34.
153. Cornett, E.M., et al., *Pharmacogenomics of Pain Management: The Impact of Specific Biological Polymorphisms on Drugs and Metabolism.* Curr Oncol Rep, 2020. **22**(2): p. 18.
154. Mis, M.A., et al., *Resilience to Pain: A Peripheral Component Identified Using Induced Pluripotent Stem Cells and Dynamic Clamp.* J Neurosci, 2019. **39**(3): p. 382-392.
155. Faucett, J., N. Gordon, and J. Levine, *Differences in postoperative pain severity among four ethnic groups.* J Pain Symptom Manage, 1994. **9**(6): p. 383-9.
156. Fillingim, R.B., *Sex, gender, and pain: women and men really are different.* Curr Rev Pain, 2000. **4**(1): p. 24-30.
157. Dorner, T.E., et al., *The impact of socio-economic status on pain and the perception of disability due to pain.* Eur J Pain, 2011. **15**(1): p. 103-9.
158. Crist, R.C. and W.H. Berrettini, *Pharmacogenetics of OPRM1.* Pharmacol Biochem Behav, 2014. **123**: p. 25-33.
159. Yang, Y., et al., *Reverse pharmacogenomics: carbamazepine normalizes activation and attenuates thermal hyperexcitability of sensory neurons due to Nav 1.7 mutation I234T.* Br J Pharmacol, 2018. **175**(12): p. 2261-2271.
160. Han, C., et al., *The Novel Activity of Carbamazepine as an Activation Modulator Extends from NaV1.7 Mutations to the NaV1.8-S242T Mutant Channel from a Patient with Painful Diabetic Neuropathy.* Mol Pharmacol, 2018. **94**(5): p. 1256-1269.
161. Ko, T.M., et al., *Pharmacogenomics for personalized pain medicine.* Acta Anaesthesiol Taiwan, 2016. **54**(1): p. 24-30.
162. Locharernkul, C., et al., *Carbamazepine and phenytoin induced Stevens-Johnson syndrome is associated with HLA-B*1502 allele in Thai population.* Epilepsia, 2008. **49**(12): p. 2087-91.
163. Mehta, T.Y., et al., *Association of HLA-B*1502 allele and carbamazepine-induced Stevens-Johnson syndrome among Indians.* Indian J Dermatol Venereol Leprol, 2009. **75**(6): p. 579-82.
164. Nguyen, D.V., et al., *HLA-B*1502 and carbamazepine-induced severe cutaneous adverse drug reactions in Vietnamese.* Asia Pac Allergy, 2015. **5**(2): p. 68-77.
165. Then, S.M., et al., *Frequency of the HLA-B*1502 allele contributing to carbamazepine-induced hypersensitivity reactions in a cohort of Malaysian epilepsy patients.* Asian Pac J Allergy Immunol, 2011. **29**(3): p. 290-3.
166. Kim, S.H., et al., *Carbamazepine-induced severe cutaneous adverse reactions and HLA genotypes in Koreans.* Epilepsy Res, 2011. **97**(1-2): p. 190-7.
167. Sheets, P.L., et al., *A Nav1.7 channel mutation associated with hereditary erythromelalgia contributes to neuronal hyperexcitability and displays reduced lidocaine sensitivity.* J Physiol, 2007. **581**(Pt 3): p. 1019-31.

168. Han, C., et al., *Human Na(v)1.8: enhanced persistent and ramp currents contribute to distinct firing properties of human DRG neurons.* J Neurophysiol, 2015. **113**(9): p. 3172-85.
169. Zhang, X., et al., *Voltage-gated Na(+) currents in human dorsal root ganglion neurons.* Elife, 2017. **6**.
170. Parisien, M., et al., *Effect of Human Genetic Variability on Gene Expression in Dorsal Root Ganglia and Association with Pain Phenotypes.* Cell Rep, 2017. **19**(9): p. 1940-1952.
171. Ray, P., et al., *Comparative transcriptome profiling of the human and mouse dorsal root ganglia: an RNA-seq-based resource for pain and sensory neuroscience research.* Pain, 2018. **159**(7): p. 1325-1345.
172. Schwaid, A.G., et al., *Comparison of the Rat and Human Dorsal Root Ganglion Proteome.* Sci Rep, 2018. **8**(1): p. 13469.
173. Middleton, S.J., et al., *Studying human nociceptors: from fundamentals to clinic.* Brain, 2021. **144**(5): p. 1312-1335.
174. Takahashi, K., et al., *Induction of pluripotent stem cells from adult human fibroblasts by defined factors.* Cell, 2007. **131**(5): p. 861-72.
175. Takahashi, K. and S. Yamanaka, *Induction of pluripotent stem cells from mouse embryonic and adult fibroblast cultures by defined factors.* Cell, 2006. **126**(4): p. 663-76.
176. Inoue, H., et al., *iPS cells: a game changer for future medicine.* EMBO J, 2014. **33**(5): p. 409-17.
177. Chrysostomidou, L., A.H. Cooper, and G.A. Weir, *Cellular models of pain: new technologies and their potential to progress preclinical research.* Neurobiology of Pain, 2021: p. 100063.
178. Yuan, J.H., et al., *KCNQ variants and pain modulation: a missense variant in Kv7.3 contributes to pain resilience.* Brain Commun, 2021. **3**(3): p. fcab212.
179. Pettingill, P., et al., *A causal role for TRESK loss of function in migraine mechanisms.* Brain, 2019. **142**(12): p. 3852-3867.
180. Viventi, S. and M. Dottori, *Modelling the dorsal root ganglia using human pluripotent stem cells: A platform to study peripheral neuropathies.* Int J Biochem Cell Biol, 2018. **100**: p. 61-68.
181. Lampert, A., et al., *Human sensory neurons derived from pluripotent stem cells for disease modelling and personalized medicine.* Neurobiol Pain, 2020. **8**: p. 100055.
182. Hockemeyer, D. and R. Jaenisch, *Induced Pluripotent Stem Cells Meet Genome Editing.* Cell Stem Cell, 2016. **18**(5): p. 573-86.
183. Meents, J.E., et al., *The role of Nav1.7 in human nociceptors: insights from human induced pluripotent stem cell-derived sensory neurons of erythromelalgia patients.* Pain, 2019. **160**(6): p. 1327-1341.
184. Namer, B., et al., *Pain relief in a neuropathy patient by lacosamide: Proof of principle of clinical translation from patient-specific iPS cell-derived nociceptors.* EBioMedicine, 2019. **39**: p. 401-408.
185. Clark, A.J., et al., *An iPSC model of hereditary sensory neuropathy-1 reveals L-serine-responsive deficits in neuronal ganglioside composition and axoglial interactions.* Cell Rep Med, 2021. **2**(7): p. 100345.
186. Jones, I., et al., *Development and validation of an in vitro model system to study peripheral sensory neuron development and injury.* Sci Rep, 2018. **8**(1): p. 15961.
187. Schinke, C., et al., *Modeling chemotherapy induced neurotoxicity with human induced pluripotent stem cell (iPSC) -derived sensory neurons.* Neurobiol Dis, 2021. **155**: p. 105391.
188. Capurro, A., et al., *Nav1. 7 gating in human iPSC derived sensory neurons: an experimental and computational study.* bioRxiv, 2020.
189. Hoelting, L., et al., *Stem Cell-Derived Immature Human Dorsal Root Ganglia Neurons to Identify Peripheral Neurotoxicants.* Stem Cells Transl Med, 2016. **5**(4): p. 476-87.
190. Stacey, P., et al., *Plate-Based Phenotypic Screening for Pain Using Human iPSC-Derived Sensory Neurons.* SLAS Discov, 2018. **23**(6): p. 585-596.
191. Elitt, M.S., L. Barbar, and P.J. Tesar, *Drug screening for human genetic diseases using iPSC models.* Hum Mol Genet, 2018. **27**(R2): p. R89-R98.

192. Mazzara, P.G., et al., *Frataxin gene editing rescues Friedreich's ataxia pathology in dorsal root ganglia organoid-derived sensory neurons.* Nat Commun, 2020. **11**(1): p. 4178.
193. Chambers, S.M., et al., *Combined small-molecule inhibition accelerates developmental timing and converts human pluripotent stem cells into nociceptors.* Nat Biotechnol, 2012. **30**(7): p. 715-20.
194. Eberhardt, E., et al., *Pattern of Functional TTX-Resistant Sodium Channels Reveals a Developmental Stage of Human iPSC- and ESC-Derived Nociceptors.* Stem Cell Reports, 2015. **5**(3): p. 305-13.
195. Schwartzentruber, J., et al., *Molecular and functional variation in iPSC-derived sensory neurons.* Nat Genet, 2018. **50**(1): p. 54-61.
196. Wiegand, C. and I. Banerjee, *Recent advances in the applications of iPSC technology.* Curr Opin Biotechnol, 2019. **60**: p. 250-258.
197. Saito-Diaz, K., et al., *Derivation of Peripheral Nociceptive, Mechanoreceptive, and Proprioceptive Sensory Neurons from the same Culture of Human Pluripotent Stem Cells.* Stem Cell Reports, 2021. **16**(3): p. 446-457.
198. Wainger, B.J., et al., *Modeling pain in vitro using nociceptor neurons reprogrammed from fibroblasts.* Nat Neurosci, 2015. **18**(1): p. 17-24.
199. Shiers, S., et al., *ACE2 and SCARF expression in human dorsal root ganglion nociceptors: implications for SARS-CoV-2 virus neurological effects.* Pain, 2020. **161**(11): p. 2494-2501.
200. Nickolls, A.R., et al., *Transcriptional Programming of Human Mechanosensory Neuron Subtypes from Pluripotent Stem Cells.* Cell Rep, 2020. **30**(3): p. 932-946 e7.
201. Rostock, C., et al., *Human vs. Mouse Nociceptors - Similarities and Differences.* Neuroscience, 2018. **387**: p. 13-27.
202. Guimaraes, M.Z.P., et al., *Generation of iPSC-Derived Human Peripheral Sensory Neurons Releasing Substance P Elicited by TRPV1 Agonists.* Front Mol Neurosci, 2018. **11**: p. 277.
203. Hulme, A.J., et al., *Molecular and Functional Characterization of Neurogenin-2 Induced Human Sensory Neurons.* Front Cell Neurosci, 2020. **14**: p. 600895.
204. Young, G.T., et al., *Characterizing human stem cell-derived sensory neurons at the single-cell level reveals their ion channel expression and utility in pain research.* Mol Ther, 2014. **22**(8): p. 1530-1543.
205. Popp, B., et al., *Need for high-resolution Genetic Analysis in iPSC: Results and Lessons from the ForIPS Consortium.* Sci Rep, 2018. **8**(1): p. 17201.
206. Volpato, V. and C. Webber, *Addressing variability in iPSC-derived models of human disease: guidelines to promote reproducibility.* Dis Model Mech, 2020. **13**(1).
207. Kang, E., et al., *Age-Related Accumulation of Somatic Mitochondrial DNA Mutations in Adult-Derived Human iPSCs.* Cell Stem Cell, 2016. **18**(5): p. 625-36.
208. Umehara, Y., et al., *Robust induction of neural crest cells to derive peripheral sensory neurons from human induced pluripotent stem cells.* Sci Rep, 2020. **10**(1): p. 4360.
209. Dionisi, C., et al., *Primary proprioceptive neurons from human induced pluripotent stem cells: a cell model for afferent ataxias.* Sci Rep, 2020. **10**(1): p. 7752.
210. Thanuthanakhun, N., et al., *The impact of culture dimensionality on behavioral epigenetic memory contributing to pluripotent state of iPS cells.* J Cell Physiol, 2021. **236**(7): p. 4985-4996.
211. Ankam, S., et al., *DNA methylation patterns in human iPSC-derived sensory neuronal differentiation.* Epigenetics, 2019. **14**(9): p. 927-937.
212. Efrat, S., *Epigenetic Memory: Lessons From iPS Cells Derived From Human beta Cells.* Front Endocrinol (Lausanne), 2020. **11**: p. 614234.
213. Khoo, T.S., et al., *Retention of Somatic Memory Associated with Cell Identity, Age and Metabolism in Induced Pluripotent Stem (iPS) Cells Reprogramming.* Stem Cell Rev Rep, 2020. **16**(2): p. 251-261.

CHAPTER 1.2

AIMS AND THESIS OUTLINE

AIMS

The clinical, economical, and psycho-emotional burden of neuropathic pain underlines the urgency to find novel, effective treatment options. Patients consistently report lack of efficacy from available treatments and severe adverse effects, yielding to years of trial-and-error therapies that result in insignificant improvements. With no analgesic development in over a decade, there is a considerable need to focus on personalized and precision medicine. For example, patients can react differently to commonly used analgesics, like lacosamide, requiring a personalized approach to decide upfront who will benefit from the treatment and who will not.

Therefore, the first aim (i) of my project is to delineate the involvement of specific residues in the pharmacology of lacosamide and the effect of associated mutations in patients' responsiveness as a template for using pharmacogenomic-based approaches to treat human pain disorders. As discussed above, current cell and animal models are often poor surrogates for studying human pathologies and mechanisms and studies using these models may not provide an accurate answer. Furthermore, even in humanized systems, such as patient-derived iPSC models, our ability to develop a personalized strategy is affected by culture and differentiation-induced variability. Therefore, developing better models and tools to study pain pathologies is critical for advancing pharmacogenomics and precision medicine research. My second aim (ii) is to develop alternative iPSC systems that express critical proteins and better mimic human DRGs to study neuropathic pain-associated sodium channel mutations. My final aim (iii) is to shed light on iPSC behaviors in transplanted DRGs, which are still unexplored.

THESIS OUTLINE

Clinical assessment of lacosamide in $Na_V1.7$-related small fiber neuropathy (SFN) patients revealed discrepancies in treatment responsiveness, **chapter 2** describes the pharmacogenetic relationship between lacosamide and five different SCN9A variants from responsive and non-responsive SFN patients and reports a biophysical signature in responsive mutants. Furthermore, the study points to a variant that fully abolishes the effect of lacosamide (W1538R) and sets the stage for intrinsic effect of drug-channel interactions underlying unknown binding mechanisms.

Building on these findings, **chapter 3** describes the implication of the mutant channel W1538R in blocking lacosamide functions and identifies W1538 as a pivotal residue in enabling lacosamide binding to the pore. In turn, this chapter describes a novel working model for the mechanisms of action of lacosamide in $Na_V1.7$ channels.

While heterologous systems transfected with $Na_V1.7$ variants have allowed us to identify mutations altering lacosamide responsiveness (**Chapter 2**), and determine lacosamide functions (**Chapter 3**), we were unable to obtain a complete picture for the discrepancies in patient-specific responses to treatments. New evidence supports iPSC-derived nociceptors as a humanized pain model. However, differentiated cells lack maturity and expression of relevant sodium channels. With the goal to advance pharmacogenomics development, **chapter 4** describes a novel microniche-based iPSC model to induce sensory neurogenesis in vivo and ex vivo in rodent DRGs using the native microenvironment to induce differentiation and paramount some of the current in vitro challenges.

Xeno-transplanted iPSCs did not achieve a nociceptor cell fate (**chapter 4**) and hence, did not recover functional expression of missing $Na_V1.8$ and $Na_V1.9$ channels. Instead of forcing expression through microniche interactions, **chapter 5** shows the utilization of dynamic clamp technology to inject missing $Na_V1.8$ and $Na_V1.9$ currents into iPSC-SNs and for the first time, study a SCN10A ($Na_V1.8$) mutation in stem cells.

The findings of the thesis are discussed in **chapter 6**, providing perspectives and future directions. Last, chapter 7 highlights the significance and future implementations the findings detailed in this thesis can have.


2

PHARMACOLOGY OF LACOSAMIDE IN $NA_V1.7$-RELATED PAIN

Part 2

CHAPTER 2

Differential effect of lacosamide on $Na_V1.7$ variants from responsive and non-responsive patients with small fibre neuropathy

Published as:

Julie I. R. Labau, Mark Estacion, Brian S. Tanaka, Bianca T. A. de Greef, Janneke G. J. Hoeijmakers, Margot Geerts, Monique M. Gerrits, Hubert J. M. Smeets, Catharina G. Faber, Ingemar S. J. Merkies, Giuseppe Lauria, Sulayman D. Dib-Hajj, Stephen G. Waxman. Differential effect of lacosamide on Nav1.7 variants from responsive and non-responsive patients with small fibre neuropathy. *Brain.* (2020) 1;143(3):771-782.

doi: 10.1093/brain/awaa016. PMID: 32011655; PMCID: PMC7089662

ABSTRACT

Small fiber neuropathy is a common pain disorder, which in many cases fails to respond to treatment with existing medications. Gain-of-function mutations of voltage-gated sodium channel $Na_v1.7$ underlie dorsal root ganglion neuronal hyperexcitability and pain in a subset of patients with small fiber neuropathy. Recent clinical studies have demonstrated that lacosamide, which blocks sodium channels in a use-dependent manner, attenuates pain in some patients with $Na_v1.7$ mutations; however, only a subgroup of these patients responded to the drug. Here, we used voltage-clamp recordings to evaluate the effects of lacosamide on five $Na_v1.7$ variants from patients who were responsive or non-responsive to treatment. We show that, at the clinically-achievable concentration of 30 μM, lacosamide acts as a potent sodium channel inhibitor of $Na_v1.7$ variants carried by responsive patients, via a hyperpolarizing shift of voltage-dependence of both fast- and slow-inactivation and enhancement of use-dependent inhibition. By contrast, the effects of lacosamide on slow-inactivation and use-dependence in $Na_v1.7$ variants from non-responsive patients were less robust. Importantly, we found that lacosamide selectively enhances fast-inactivation only in variants from responders. Taken together, these findings begin to unravel biophysical underpinnings that contribute to responsiveness to lacosamide in patients with small fiber neuropathy carrying select $Na_v1.7$ variants.

INTRODUCTION

Painful peripheral neuropathy represents a major health burden and a globally unmet clinical need. Current first-line therapeutic strategies for the management of chronic pain associated with painful neuropathy, including tricyclic antidepressants, pregabalin, gabapentin or serotonin-noradrenaline reuptake inhibitors, are in many cases reported as unsatisfactory, in part due to adverse effects [1, 2]. Furthermore, the degree of pain improvement dramatically varies across the population [3]. More effective pharmacological management of neuropathic pain represents a high priority.

Genetic studies have provided compelling evidence regarding the contribution of altered voltage-gated sodium channel (VGSC) expression and function in neuropathic pain. The $Na_v1.7$ sodium channel has drawn particular interest because it is preferentially expressed in peripheral sensory and sympathetic neurons and has directly been linked to multiple human pain conditions: gain-of-function (GoF) missense mutations in *SCN9A* (encoding the $Na_v1.7$ protein) have been reported in patients with inherited erythromelalgia (IEM), paroxysmal extreme pain disorder, and some forms of small fiber neuropathy (SFN). Conversely, loss-of-function mutations in $Na_v1.7$ have been identified in individuals with congenital complete insensitivity to pain [4-6].

SFN is morphologically characterized by injury to the small intraepidermal nerve fibers, specifically the unmyelinated C and thinly myelinated Aδ-fibers, and

functionally by dorsal root ganglion (DRG) neuronal and axonal hyperexcitability. Prominent burning pain in the distal extremities, often accompanied with autonomic dysfunction, tend to dominate the clinical picture [3, 7, 8]. Sodium channel variants have been described in about 15% of SFN patients, with a higher frequency in missense mutants of *SCN9A* [9, 10]. Many of these variants have been functionally profiled and shown to confer GoF attributes on the channel and render DRG neurons hyperexcitable [4-6]. The GoF attributes of these variants increase confidence in their pathogenicity [11], suggesting that carriers of these variants might benefit from treatments using sodium channel blockers.

Lacosamide (LCM), an FDA-approved anti-epileptic drug (AED), has been reported to preferentially enhance slow-inactivation of VGSC, including $Na_v1.7$ [12-14]. However, a recent study has alternatively suggested that LCM binds to the fast-inactivated state of $Na_v1.7$, but at a slower rate [15]. There is also evidence that lacosamide may alter the effect of CRMP2 (collapsin-response mediator protein-2) on $Na_v1.7$ channel trafficking [16, 17]. Furthermore, lacosamide has been found to have a higher affinity for tetrodotoxin-sensitive sodium channels over other ion channels and central receptors [16, 18] that are targeted by traditional AEDs [12], conferring increased selectivity. A retrospective study of patients with seizures who had switched from other AED drugs to lacosamide, due to deleterious effects from their original AED treatment, has shown successful conversion in many of these patients [19], suggesting lacosamide to have improved tolerability. Lacosamide has also been tested in small clinical trials as a potential therapy for painful diabetic neuropathy where the majority of patients reported significant pain improvement with less than 10% reporting adverse effects [20-23]. However, until recently, the clinical effects of LCM on patients with $Na_v1.7$-related pain disorders had yet to be investigated.

A recent randomized, placebo-controlled, double-blind, crossover trial (de Greef, *et al.*,2019) assessed the effect of lacosamide treatment in twenty-four SFN patients carrying multiple $Na_v1.7$ variants. Fifteen different mutations were identified in this cohort, of which five were carried by several patients. Different subjects in this trial exhibited a spectrum of responses to treatment, with some patients reporting substantial pain relief while others did not show any improvement (*Figure 1*). In a different study, lacosamide has been shown to produce pain relief in one patient with SFN [24]. However, the factors responsible for variable LCM responsiveness in the de Greef, *et al.* (2019) study are not known. In the present study, we report the $Na_v1.7$ variants in these patients and assess the pharmacogenomic correlation between the $Na_v1.7$ genetic variants and the response to lacosamide in this series of patients. Using voltage-clamp recordings of HEK293 (human embryonic kidney) cells expressing variants from both responsive and non-responsive patients, we characterized the effect of lacosamide on the biophysical properties of the $Na_v1.7$ channel, at a clinically-achievable concentration, and identified for the first time a hyperpolarizing effect on fast-inactivation, which reduces the fraction of the channels that are available to open, as a distinguishing property of variants that correlates with lacosamide responsiveness in patients with SFN.

MATERIALS & METHODS

PATIENTS

Twenty-four participants (18-80 years old) were recruited at the Maastricht University Medical Center+ (UMC+) for the Lacosamide Efficacy-N'-Safety Study (LENSS) [25]. Subjects were selected based on diagnosis of pure SFN with no associated conditions (except for Diabetes Mellitus), with a mutation in the *SCN9A* gene ($Na_v1.7$ channel) of class III, IV or V (variants of uncertain pathogenicity, likely to be or clearly pathogenic, respectively), using genetic classification criteria, as described [26].

The clinical study design and results were published previously [25, 27]. Briefly, the participants either received 200 mg of lacosamide or placebo twice daily for eight weeks, preceded by a titration period and followed by a tapering period, and a two-week washout period before receiving the alternative compound. They were asked to rate their pain twice daily using the daily pain intensity numerical rating scale (PI-NRS) ranging from 0 to 10. The patients were considered responsive to treatment when at least a 1-point reduction was reported from the individual baseline pain scores.

PLASMIDS AND HEK293 CELL TRANSFECTION

The construct of the human $Na_v1.7$ wild-type (WT) isoform was rendered tetrodotoxin-resistant (TTX-R) and fused to an eGFP-2A linker, as previously described [28]. The construct produces a green fluorescent protein with the $Na_v1.7$ channel as independent proteins from the same transcript, which enables the visual identification of transfected cells based on their fluorescence. $Na_v1.7$-related SFN mutations identified in participants in this study (I739V, I228M, L1267V, W719C and W1538R) were introduced into the constructs using QuickChange XL site-directed mutagenesis (Stratagene, La Jolla, CA). HEK293 cells, grown under standard culture conditions (5% CO_2, 37°C) in Dulbecco's modified Eagle's medium supplemented with 10% fetal bovine serum, were transiently transfected by electroporation with a $Na_v1.7$ variant using Lipojet (SignaGen Laboratories, Rockville, MD). The transfected cells were resuspended and plated onto coverslips the next day and patch-clamp recordings were performed over the following 48 hours.

ELECTROPHYSIOLOGY

Whole-cell voltage-clamp recordings were obtained at room temperature on isolated HEK293 cells showing green fluorescence. Recordings were alternatively performed on coverslips of HEK293 cells expressing WT or a $Na_v1.7$ variant, either treated with vehicle (extracellular solution) or lacosamide. Electrodes were pulled from 1.65 mm O.D. borosilicate glass micropipettes (WPI, Sarasota, FL) and had a resistance of 0.8-2.0 MΩ when filled with intracellular pipette solution, which contained (in mM): 140 CsF, 10 NaCl, 10 HEPES, 1 EGTA (pH 7.3 with CsOH, adjusted to 320 mOsm with dextrose). The extracellular solution contained (in mM): 140 NaCl, 3 KCl, 1 $MgCl_2$, 1 $CaCl_2$, 10 HEPES (pH 7.3 with NaOH, adjusted to 320 mOsm with dextrose). Voltage-clamp protocols for the biophysical characterization of VGSCs were initiated 5 min after

establishing whole-cell configuration on an EPC-10 USB amplifier (HEKA Electronics) and acquired using PatchMaster software (HEKA Electronics) at an acquisition rate of 50 kHz with a lowpass Bessel filter setting of 2.9 kHz. Voltage errors were minimized with 60-90% series resistance compensation, and only cells with <4 mV voltage error after compensation were included for analysis. When appropriate, linear leak currents and capacitance artifacts were corrected by P/6 subtraction.

To examine the current-voltage (I-V) relationship a series of step depolarizations from -80 mV to +50 mV in 5 mV increments were applied from a holding potential of -120 mV at 5 second interpulse intervals. To evaluate the effect of lacosamide on steady-state fast-inactivation, the membrane potential was held at conditioning potentials that varied from -140 mV to 10 mV for 500 ms, and cells were then given a 20 ms test pulse to 0 mV to elicit current from remaining available channels.

For the slow-inactivation protocol, the cell was held at conditioning potentials that varied from -130 mV to 10 mV for 30 sec; the membrane potential was then pulsed to -120 mV for 100 ms to allow channels not in the slow-inactivated state to recover from fast-inactivation, and then given a 20 ms test pulse to 0 mV to elicit current from available channels.

To measure the use-dependence of inhibition of lacosamide at 20 Hz stimulation, series of 20 ms pulses were applied at -10 mV. Peak inward currents were measured and normalized to the maximum current amplitude.

IN VITRO PHARMACOLOGY

A bi-daily 200 mg lacosamide dose results in a maximum plasma concentration of 30 μM [29]. The patients assessed in this study received lacosamide at this bi-daily dose during the trial [25]; thus 30 μM of lacosamide was used for the studies described here.

Lacosamide (or Vimpat®, UCB, obtained from the West Haven VA Medical Center pharmacy), with a concentration of 10 mg/ml (39.9 mM) in aqueous saline (pH=4), was diluted in the extracellular bath solution (vehicle; described above) to achieve the final working concentration of 30 μM. Working solutions were prepared fresh daily.
The extracellular bath solution was continuously perfused at a consistent flow rate of 1 mL/min through a 250 μm perfusion pipette, using a pressure-regulated system (AutoMate Scientific). Complete bath exchange was enabled via aspiration from the opposite end of the cell chamber from the perfusion pipette. To control for time-dependent changes in channel properties, independent cell cohorts were exposed to only one test concentration of lacosamide or vehicle at a consistent time after initiation of whole-cell recording. Specifically, the solution was exchanged for two minutes, corresponding to an absolute bath exchange of 2 mL, starting two minutes following breakage of the cell membrane.

STATISTICAL ANALYSIS

Whole-cell voltage-clamp data were analysed using Fitmaster (HEKA Electronics), Excel (Microsoft) and Origin (OriginLab Corporation, Microcal Software, Northhampton, MA). Data are expressed as means ± standard error (SEM). Statistical significance was determined by unpaired Student's t-test and was reached when $p < 0.05$.

RESULTS

Clinical characterization

Whole-exome sequencing of the patients' genomes identified fifteen different *SCN9A* mutations, including five recurrent variants (*Supplementary Table 1*). Patients carrying different $Na_v1.7$ variants displayed a range of response to lacosamide. We selected variants that were most representative of the range of clinical responsiveness for biophysical analysis. Specifically, we selected two variants from responsive patients (≥ 1 point on the PI-NRS scale) and three variants from non-responsive patients (≤ 1 point on the PI-NRS scale), based upon the pain scores plot in the clinical trial study [25], shown in *Figure 1*.

We considered the W719C (2157G>C; p.Trp719Cys) and the I739V (c.2215A>G; p.Ile739Val) variants to be associated with responders. W719C showed the largest response to lacosamide compared to the other variants, with a 3.65 point decrease from the baseline average score. I739V, which has been functionally profiled in detail previously [30, 31], was found in five different patients. While four I739V carriers displayed decreases (1.1 to 2.8-points) in their pain scores, one carrier did not exhibit any significant improvement while treated with lacosamide (*Figure 1D*).
By contrast, I228M (c.684C>G; p.Ile228Met), L1267V (c.3799C>G; p.Leu1267Val) and W1538R (c.4612T>C; p.Trp1538Arg) variants were associated with non-responders. L1267V was selected because it was carried by four patients. Three did not respond to lacosamide, while one carrier of this variant responded to both lacosamide and placebo; there was a 3.0 point reduction in the baseline pain score following the lacosamide phase compared to the placebo phase (*Figure 1E*). I228M is a well-studied variant with a clearly defined pathogenicity [32, 33] (*Figure 1B*), and W1538R, previously characterized as a GoF variant altering cellular excitability [34], was identified in two carriers with compound mutations in $Na_v1.7$, both of whom were non-responders (*Figure 1F*). The two patients carrying the W1538R variation were both found to also carry a M932L/V991L (c.2794A>C and c.2971G>T ; p.Met932Leu/Val991Leu) double mutation, with one of them further carrying I739V, in addition to the M932L/V991L mutation. Notably, patients who only carry M932L/V991L or I739V variants alone have been responsive to lacosamide treatment (*Supplementary Table 1*). The pain scores are presented in *Figure 1*.

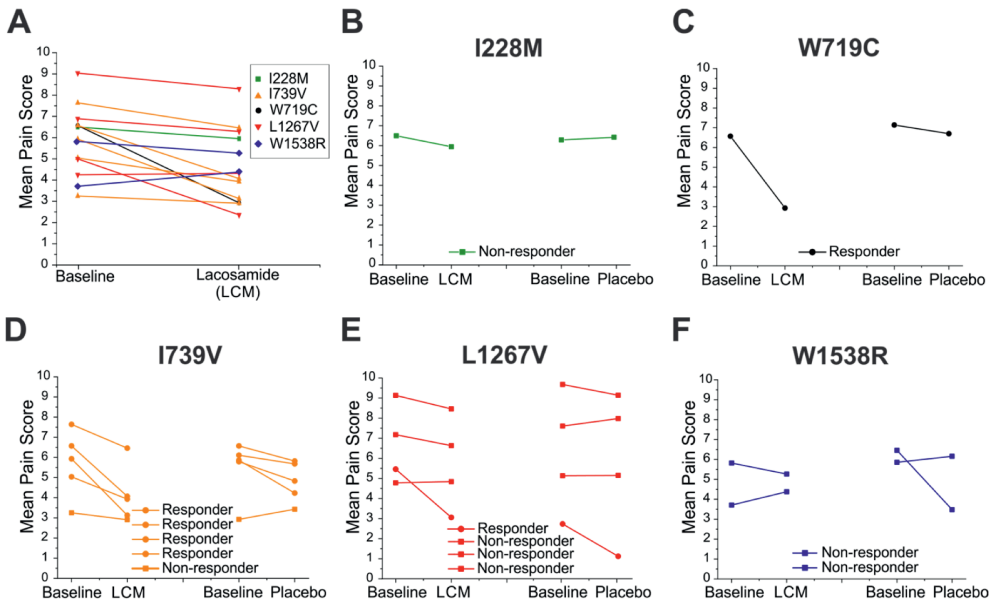

FIGURE 1 – Clinical response of patients carrying specific Nav1.7 variants. (A) The changes in pain scores in response to either lacosamide or placebo are plotted for all subjects carrying Nav1.7 variants assessed in this study. Black and orange colors, adapted from *de Greef, et al. 2019*, represent results from mostly responsive patients, whereas green, red and blue represent the results of mostly unresponsive patients. **(B-F)** show the clinical responses for each variant. **(B)** The responses from a non-responder carrying variant I228M. **(C)** The responses from a patient with a large clinical response carrying variant W719C. **(D)** The responses from the patients carrying the I739V variant (five patients, four responders). **(E)** The responses from patients carrying the L1267V variant (four patients, three non-responders). **(F)** The responses from patients carrying the W1538R variant (two patients, both non-responders).

The locations of the variants within the Nav1.7 backbone are shown in *Figure 2*. Both responder variants are located in the second domain (DII): I739V is located within the first transmembrane segment of the voltage-sensing domain (VSD; DII/S1) [8], while W719C is found twenty amino acids upstream, at the end of the first intracellular loop linking DI/S6 to DII/S1 (Linker 1). The non-responder variants are spread across the three other domains within the VSD (S1-S4) of the channel: I228M is located in DI/S4 [8], L1267V in DIII/S3 [7] and W1538R in DIV/S2 [34, 35].

Lacosamide fails to alter the voltage-dependence of activation in responsive and non-responsive Nav1.7 variants

Representative Nav1.7 sodium currents recorded after perfusion with 30 µM lacosamide or vehicle control are shown in *Figure 3*. Consistent with previous data [12, 13], the voltage-dependence of activation, represented as the Boltzmann fit of

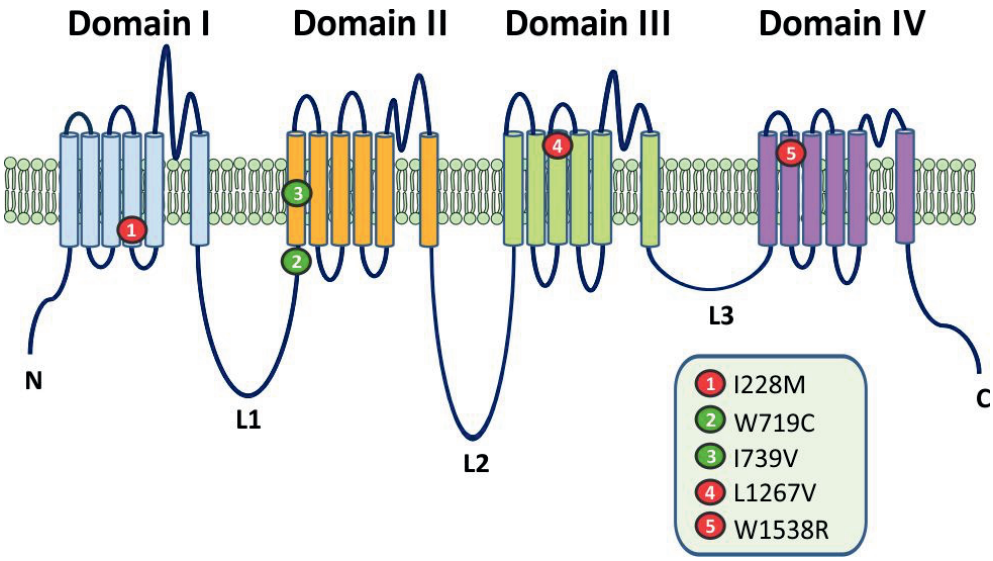

FIGURE 2 – Topology of the human $Na_v1.7$ sodium channel, with the location of I228M, W719C, I739V, L1267V and W1538R. All but one mutation (W719C) are located in the voltage-sensing domains (VSD) of the channel. The two lacosamide-responsive mutations are shown in green. Both are located within the vicinity of domain II: W719C is located at the end of Linker 1 and I739V in VSD II). Non-responsive mutations are indicated in red. All three variants (I228M, L1267V and W1538R) map to the VSD in domain I, III and IV, respectively.

normalized conductance, was unaffected by the clinically-achievable concentration of 30 μM lacosamide in both the mutant and WT cells (*Figure 3*).

Lacosamide evokes a hyperpolarizing shift in slow-inactivation in most of the $Na_v1.7$ variants

Lacosamide has previously been reported to have large effects on sodium channel slow-inactivation [12-14]. To assess the potential impact of the variants on the lacosamide-mediated shift in slow-inactivation, we compared the normalized slow-inactivation curves from each of the variants examined in the presence of 30 μM lacosamide or vehicle control, as shown in *Figure 4*. As expected, lacosamide shifted the voltage-dependence of slow- inactivation of the WT channel to more hyperpolarized potentials (i.e. enhancing slow-inactivation, thus reducing the number of $Na_v1.7$ channels that are available to open at physiological membrane potentials; *Figure 4A*). The half-inactivation voltage ($V_{1/2}$) of slow-inactivation Boltzmann fits from each variant are shown in *Table 1*. The variants from patients that were scored as responders showed substantially enhanced slow-inactivation in response to lacosamide: W719C demonstrated a - 20 mV hyperpolarized shift (*Figure 4C, p = 0.02*), while I739V channels showed a - 12.2 mV shift to more hyperpolarized potentials *(Figure 4D*, $p < 0.01$). The shifts in voltage-dependence of slow-inactivation for the non-responsive variants (L1267V, W1538R, and I228M) were - 9.3 mV, + 1.4 mV, and - 12.1 mV,

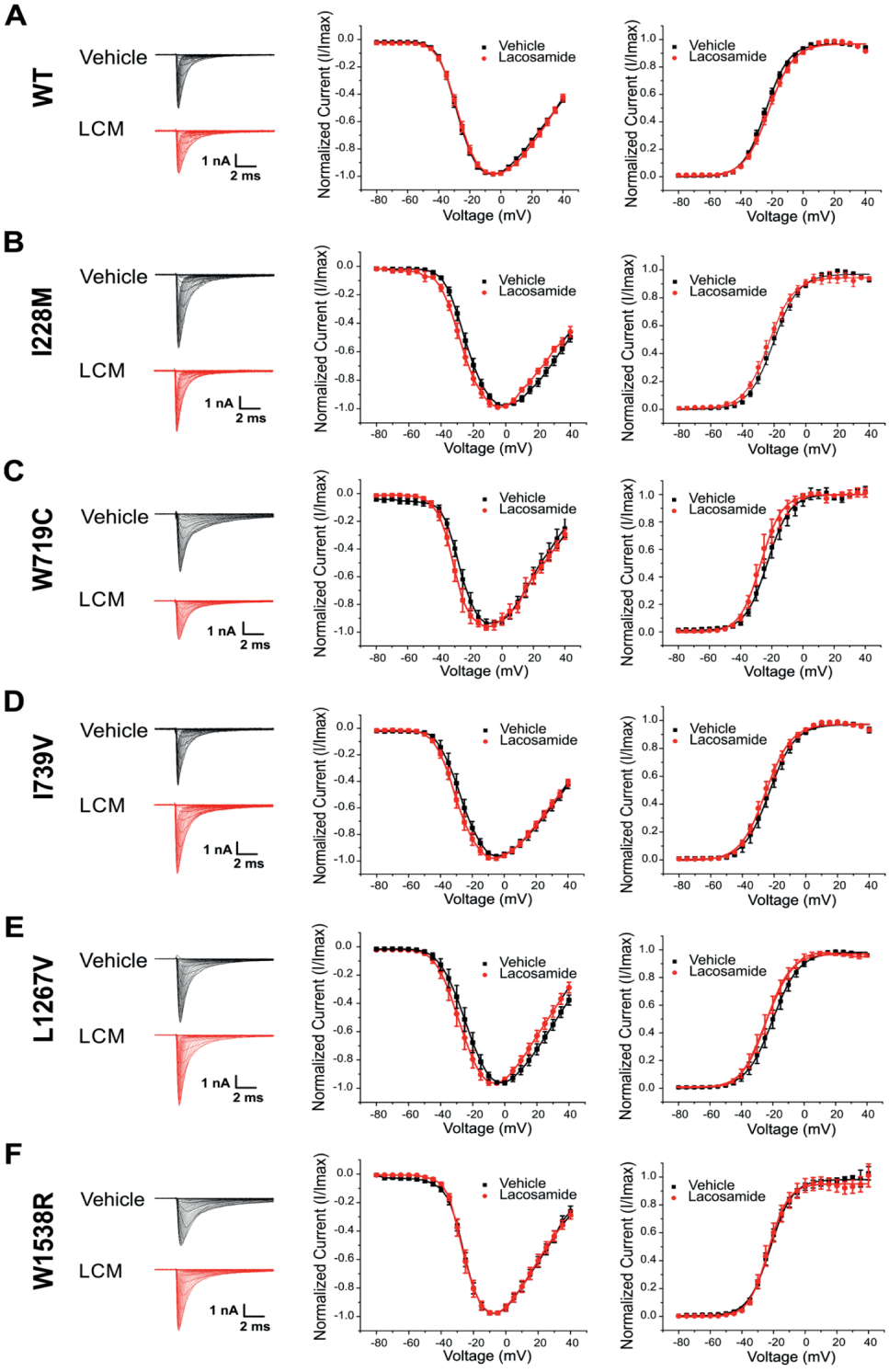
A
WT
Vehicle
LCM
1 nA
2 ms
Normalized Current (I/Imax)
Voltage (mV)
Vehicle
Lacosamide
B
I228M
C
W719C
D
I739V
E
L1267V
F
W1538R

FIGURE 3 – Lacosamide effects on voltage-dependence of activation for each $Na_v1.7$ variant. (A) Sodium current traces elicited by the activation protocol from different cells exposed to either lacosamide or vehicle control. Sodium inward currents were elicited from a holding potential of -120 mV to various depolarizing steps ranging from -80 to +40 mV in 5 mV increments. **(B)** Normalized current-voltage relationship obtained by measuring the peak inward current elicited as a function of the stimulus voltage. **(C)** Voltage-dependence of activation for cells treated with lacosamide or vehicle control. The peak inward currents were transformed to normalized conductance from current-voltage plot.

respectively (*Figure 4B, E, F*). Except for W1538R, lacosamide induced a significant hyperpolarizing shift in voltage-dependence of slow inactivation in all variants.

Lacosamide produces a variable effect on use-dependent block in non-responders

We also examined the development of use-dependent block at 20 Hz for each of the variants upon exposure to 30 μM lacosamide or vehicle control (*Figure 6*). lacosamide enhanced use-dependent inhibition in WT channels (*Figure 6A*) and in variants from patients who were scored as responders (*Figure 6C, D*). Interestingly, lacosamide did not increase use-dependent blockade in two of the variants identified in non-responsive patients (L1267V and W1538R; *Figure 6E, F*), while it did in the non-responsive I228M variant (*Figure 6B, Table 1*). The degree of use-dependent block from each $Na_v1.7$ mutation is shown in *Table 1*.

DISCUSSION

Pharmacotherapy for the treatment of pain in SFN is limited, with many patients reporting inadequate pain relief from currently available medications, including sodium channel blockers.

However, while mutations in peripheral sodium channels have been linked to pathological pain, there have only been a few studies documenting treatment outcomes in patients with specific $Na_v1.7$ mutations. We have recently described pharmacogenomically-guided targeting of rare but drug-responsive $Na_v1.7$ mutations with CBZ in patients with IEM [38-41]. However, thus far there has not been a pharmacogenomic study of patients with more common pain disorders who carry $Na_v1.7$ channel mutations. In this study, we build on the findings of the LENSS trial [25] which investigated the efficacy of lacosamide for the treatment of patients with $Na_v1.7$-related SFN, and provide biophysical data that may explicate why a subset of $Na_v1.7$ variants differentially responded to lacosamide treatment.

Lacosamide has been shown to operate via different mechanisms of action compared to classical sodium channel blockers. Using standard recording protocols, AEDs have been found to enhance both fast- and slow-inactivation, while lacosamide has been reported to selectively enhance voltage-dependence of slow-inactivation. According to this model, lacosamide has been proposed to either bind to a different site, or at

	Variant	Slow Inactivation ($V_{1/2}$)		Fast Inactivation ($V_{1/2}$)		Use-dependence	
		Vehicle	LCM	Vehicle	LCM	Vehicle	LCM
	WT	-70.6 ± 1.4 (n=16)	-79.5 ± 2.1** (n=9)	-86.8 ± 1.4 (n=19)	-88.0 ± 1.9 (n=8)	0.82 ± 0.02 (n=20)	0.75 ± 0.02* (n=9)
Responders	W719C	-56.9 ± 4.4 (n=8)	-77.1 ± 5.3* (n=4)	-78.7 ± 0.8 (n=11)	-88.4 ± 1.3** (n=5)	0.96 ± 0.01 (n=10)	0.87 ± 0.04** (n=4)
Responders	I739V	-67.1 ± 1.6 (n=12)	-79.3 ± 2.1** (n=5)	-85.2 ± 1.0 (n=11)	-99.8 ± 1.1** (n=6)	0.82 ± 0.01 (n=16)	0.73 ± 0.03** (n=5)
Non-responders	L1267V	-74.4 ± 2.1 (n=9)	-83.7 ± 2.7* (n=8)	-82.5 ± 2.4 (n=7)	-87.1 ± 1.6 (n=11)	0.89 ± 0.02 (n=12)	0.87 ± 0.02 (n=10)
Non-responders	W1538 R	-69.4 ± 4.0 (n=10)	-68.0 ± 2.8 (n=8)	-79.5 ± 3.0 (n=10)	-73.9 ± 1.2 (n=8)	0.91 ± 0.02 (n=11)	0.93 ± 0.01 (n=8)
Non-responders	I228M	-66.0 ± 2.9 (n=7)	-78.1 ± 2.5** (n=7)	-87.1 ± 1.6 (n=11)	-88.9 ± 2.8 (n=6)	0.82 ± 0.03 (n=6)	0.75 ± 0.01 * (n=7)

TABLE 1 – Half-inactivation voltage ($V_{1/2}$) and use-dependence of inhibition for the $Na_V1.7$ mutations to lacosamide (LCM). Lacosamide significantly enhanced slow-inactivation in wild-type (WT) and all mutant channels, except for W1538R; while fast-inactivation was only affected by lacosamide in W719C and I739V channels. Use-dependence of inhibition at 20 Hz was changed in the two responder variants as well as in WT and I228M. Data are shown as means ± SEMs. Significant values are represented by the following symbol (*); *p<0.05, **p<0.01

significantly slower binding rates than other anticonvulsants [13, 18]. However, using a different recording protocol and a concentration of 100 μM, lacosamide has been reported to effectively enhance steady-state fast-inactivation when exposed for long depolarizations, possibly due to binding to the fast-inactivated state but at a very slow rate [15]. In the present study, we observed that, at clinically-achievable concentration of 30 μM, lacosamide does not affect fast-inactivation in $Na_V1.7$ WT channels when standard recording protocols were used (*Figure 5A*). Lacosamide failure to alter fast-inactivation in WT channels in our study is likely due to the different lacosamide concentration and recording conditions, compared to those used by Jo and Bean [15].

Lacosamide binding activity is known to share several properties with well-established sodium channel inhibitors. For instance, lacosamide has been found to compete with CBZ and lidocaine for channel inhibition *in vitro*, suggesting that they likely bind at the same site, but with different pharmacodynamics [15]. Classical sodium channel blockers have been shown to share the same binding site located in the pore forming region of the channel, within S6 of DI, DIII and DIV [42-45]. Genetic alterations at these sites have been shown to fully abolish both voltage- and use-dependent block [46], highlighting the importance of maintaining the integrity of these regions for

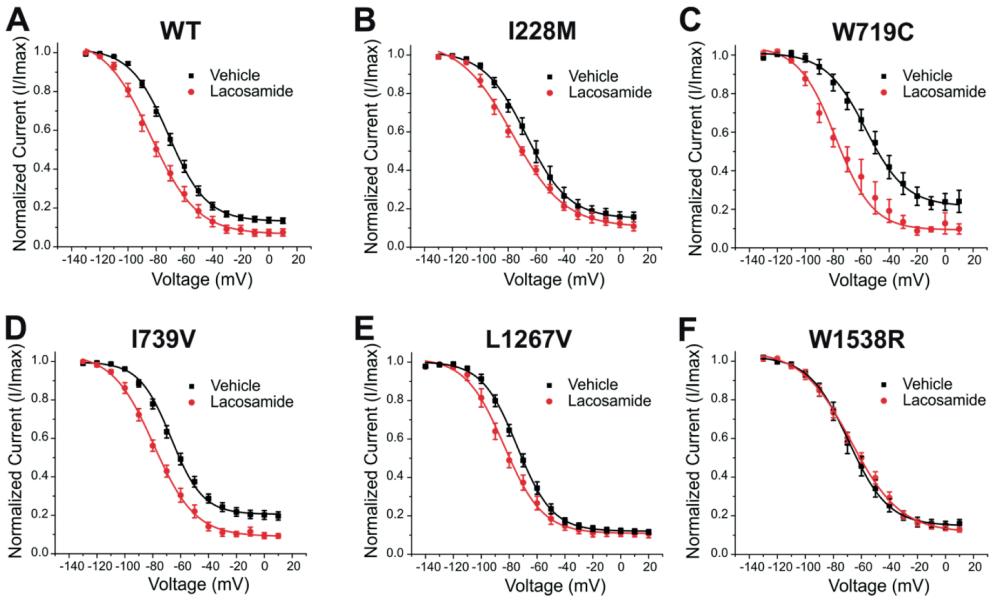

FIGURE 4 – Lacosamide effects on slow-inactivation for each $Na_v1.7$ variant. The averaged voltage-dependence of slow-inactivation curves in the presence (red) or absence (black) of lacosamide are shown for **(A)** WT, **(B)** I228M, **(C)** W719C, **(D)** I739V, **(E)** L1267V and **(F)** W1538R. The average $V_{1/2}$s calculated from of the Boltzmann fits are listed in *Table 1*.

potent inhibition. Topological mapping shows that none of the five variants described in this study map to the pore domain itself, but instead they map to the VSD (*Figure 2*). Therefore, the variants might not directly interfere with the drug binding site in the ion conduction pathway.

While lacosamide did not affect fast-inactivation in WT channels (*Figure 5A*) or any of the three non-responder variants (*Figure 5B, E, F*), it caused a significant and substantial hyperpolarizing shift in the two variants identified in responsive patients (W719C and I739V; Figu*re 5C, D*). These differences in response to lacosamide may result from a novel emerging mechanism of action, conferred by these specific variants. This type of phenomenon has previously been reported in IEM, where multiple examples of $Na_v1.7$ variants underlying IEM pathogenicity have been shown to be treatment responsive to CBZ in a disorder in which most patients are treatment-resistant. Three IEM-causing variants mapping to Domain I (I234T, S241T and V400M) have been shown to respond to CBZ via a depolarizing (corrective) shift in activation [41, 47, 48]. Importantly, none of the mutations described above are located near the CBZ/local anesthetic binding site. These findings together with the present results indicate that mutations outside the pore domain
can alter the response of the mutant channel to drugs traditionally considered to be pore-binding, and suggests that functional testing of these variants *in vitro* may predict treatment responsiveness.

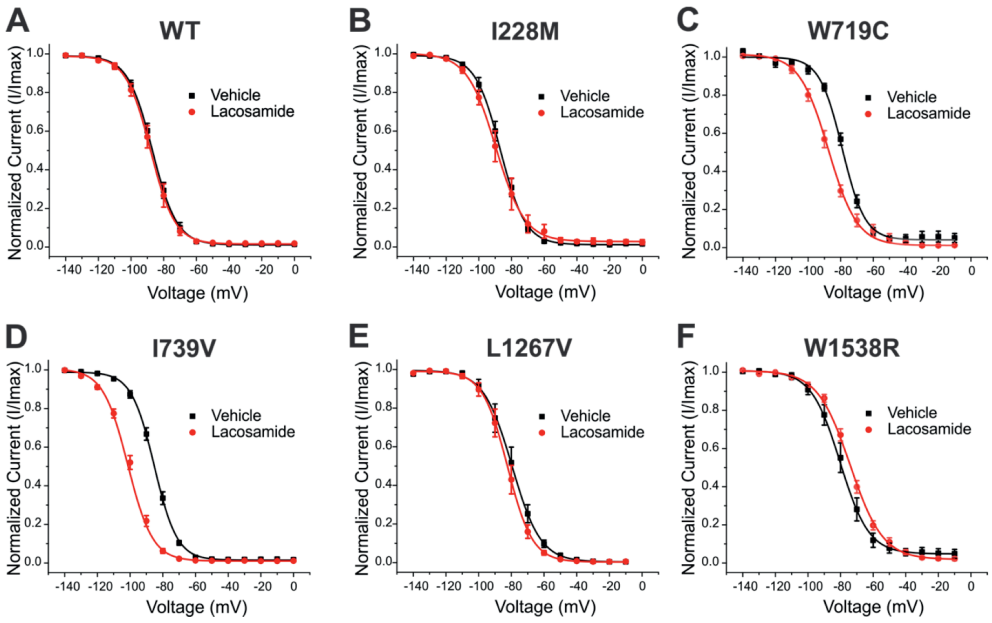

FIGURE 5 – Lacosamide effects on steady-state fast-inactivation for each Nav1.7 variant. The averaged fast-inactivation curves in the presence or absence of lacosamide are shown for **(A)** WT, **(B)** I228M, **(C)** W719C, **(D)** I739V, **(E)** L1267V and **(F)** W1538R. The average $V_{1/2}$s calculated from of the Boltzmann fits are listed in *Table 1*.

Whereas fast-inactivation seems to be the parameter that discriminates the responders from the non-responders, effects of lacosamide on slow-inactivation and use-dependence might also be required for complete and sustained pain relief. In agreement with the known effects of lacosamide on slow-inactivation, the WT channel as well as all but one mutant channel (W1538R) underwent a significant hyperpolarizing shift in the voltage-dependence of slow-inactivation (*Figure 4*). Interestingly, the W1538R variant was also found to be the strongest non-responder, with one carrier reporting better pain improvement from placebo than from treatment itself (*Figure 1*). This variant specifically has been mapped to the VSD of DIV, and is part of the binding site of the new class of aryl sulfonamide $Na_v1.7$ blockers, such as PF-05089771, which targets both the fast- and slow-inactivated states of $Na_v1.7$ with high selectivity [49-51]. This observation raises the possibility of a potential common mechanism of action between the two drugs and suggests that a disruption at this site might alter lacosamide function.

Whole-exome sequencing (WES) of the two patients carrying the W1538R variant identified additional $Na_v1.7$ mutations in both of these subjects. Both individuals carried the M932L/V991L variant, which has been associated with DRG neuron hyperexcitability [8], and one of these subjects also carried the I739V mutation (which also has been shown to produce DRG neuron hyperexcitability [8, 52]. WES analysis,

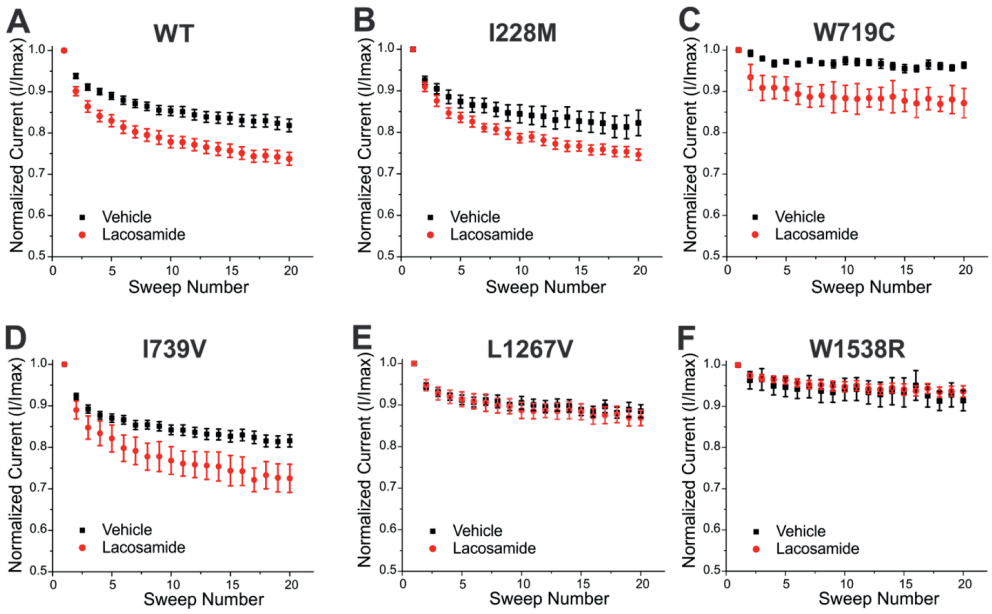

FIGURE 6 – Lacosamide effects on use-dependent block for each $Na_v1.7$ variant. The averaged use-dependent block to a train of twenty pulses at twenty hertz in the presence or absence of lacosamide are shown for **(A)** WT, **(B)** I228M, **(C)** W719C, **(D)** I739V, **(E)** L1267V and **(F)** W1538R. The averages of the normalized responses are shown in *Table 1*.

as carried out in this study, does not allow the identification of the distribution of these mutations between the two $Na_v1.7$ alleles, which requires analysis of DRG-specific RNA sequences from these patients. Such analysis is beyond the scope of this study because it requires access to sensory tissues from these patients or the development of induced pluripotent stem cells that can then be differentiated into nociceptors *in vitro*. Nonetheless, as other subjects in this cohort carrying either the I739V alone or the M932L/V991L compound variants responded to lacosamide (*Table S1*), and fast-inactivation of I739V mutant channels was hyperpolarized by exposure to lacosamide (*Figure 5*), the W1538R mutation potentially acts as a dominant contributor to the poor efficacy of lacosamide in these subjects carrying the compound genotypes. Future clinical studies on patients carrying only the W1538R mutation will be needed to provide a more definitive conclusion that carriers of this mutation will not respond to treatment with lacosamide.

Interestingly, one of the patients carrying solely the I739V variant was unresponsive to lacosamide, while the four other patients were previously reported to respond well to lacosamide (*Figure 1*) [25]. Furthermore, in the current study we demonstrated lacosamide to significantly shift all three gating parameters of I739V channels (*Table 1*). Thus, the cause for the lack of response of one carrier with the I739V mutation is

not channel intrinsic, but is likely to be affected by additional genetic, epigenetic or environmental

factors. Notably, the non-responder carrier had a relatively low level of pain severity, which may have limited the detection of lacosamide efficacy. Many factors can impact on an individual's response to a drug. While focusing on the interaction between drug and target molecule, our data suggest that *in vitro* pharmacological and biophysical analysis of $Na_v1.7$ mutations may predict the likelihood of specific carriers to be responsive to treatment, which could be important in the future as an approach to personalized treatment based on the patient's genetic background. Building on the first clinical trial of lacosamide for treatment of patients with SFN and carriers of $Na_v1.7$ variants (LENSS) [25], the present results suggest that, at least for strong positive responders and non-responders, pharmacogenomic analysis *in vitro* may correlate with clinical responsiveness. The relatively small number of variants that were studied here, two responders and three non-responders, necessitates caution in generalizing this data to suggest that SFN patients who carry Nav1.7 variants that enhance fast-inactivation upon exposure to lacosamide will necessarily be responsive to treatment. If supported by studies in larger numbers of patients tested with lacosamide and if extended to other potential medications, the pharmacogenomic approach described in this paper might contribute to the development of selective, individualized pain treatment strategies.

REFERENCES

1. Nishikawa, N. and M. Nomoto, *Management of neuropathic pain.* J Gen Fam Med, 2017. **18**(2): p. 56-60.
2. Finnerup, N.B., et al., *Pharmacotherapy for neuropathic pain in adults: a systematic review and meta-analysis.* Lancet Neurol, 2015. **14**(2): p. 162-73.
3. Sopacua, M., et al., *Small-fiber neuropathy: Expanding the clinical pain universe.* J Peripher Nerv Syst, 2019. **24**(1): p. 19-33.
4. Bennett, D.L., et al., *The Role of Voltage-Gated Sodium Channels in Pain Signaling.* Physiol Rev, 2019. **99**(2): p. 1079-1151.
5. Dib-Hajj, S.D. and S.G. Waxman, *Sodium Channels in Human Pain Disorders: Genetics and Pharmacogenomics.* Annu Rev Neurosci, 2019.
6. Dib-Hajj, S.D., et al., *The Na(V)1.7 sodium channel: from molecule to man.* Nat Rev Neurosci, 2013. **14**(1): p. 49-62.
7. Brouwer, B.A., et al., *Painful neuropathies: the emerging role of sodium channelopathies.* J Peripher Nerv Syst, 2014. **19**(2): p. 53-65.
8. Faber, C.G., et al., *Gain of function Nanu1.7 mutations in idiopathic small fiber neuropathy.* Ann Neurol, 2012. **71**(1): p. 26-39.
9. de Greef, B.T.A., et al., *Associated conditions in small fiber neuropathy - a large cohort study and review of the literature.* Eur J Neurol, 2018. **25**(2): p. 348-355.
10. Eijkenboom, I., et al., *Yield of peripheral sodium channels gene screening in pure small fibre neuropathy.* J Neurol Neurosurg Psychiatry, 2019. **90**(3): p. 342-352.
11. Waxman, S.G., et al., *Sodium channel genes in pain-related disorders: phenotype-genotype associations and recommendations for clinical use.* Lancet Neurol, 2014. **13**(11): p. 1152-1160.
12. Errington, A.C., et al., *Seeking a mechanism of action for the novel anticonvulsant lacosamide.* Neuropharmacology, 2006. **50**(8): p. 1016-29.
13. Errington, A.C., et al., *The investigational anticonvulsant lacosamide selectively enhances slow inactivation of voltage-gated sodium channels.* Mol Pharmacol, 2008. **73**(1): p. 157-69.
14. Niespodziany, I., et al., *Comparative study of lacosamide and classical sodium channel blocking antiepileptic drugs on sodium channel slow inactivation.* J Neurosci Res, 2013. **91**(3): p. 436-43.
15. Jo, S. and B.P. Bean, *Lacosamide Inhibition of Nav1.7 Voltage-Gated Sodium Channels: Slow Binding to Fast-Inactivated States.* Mol Pharmacol, 2017. **91**(4): p. 277-286.
16. Moutal, A., et al., *CRISPR/Cas9 editing of Nf1 gene identifies CRMP2 as a therapeutic target in neurofibromatosis type 1-related pain that is reversed by (S)-Lacosamide.* Pain, 2017. **158**(12): p. 2301-2319.
17. Wilson, S.M. and R. Khanna, *Specific binding of lacosamide to collapsin response mediator protein 2 (CRMP2) and direct impairment of its canonical function: implications for the therapeutic potential of lacosamide.* Mol Neurobiol, 2015. **51**(2): p. 599-609.
18. Sheets, P.L., et al., *Differential block of sensory neuronal voltage-gated sodium channels by lacosamide [(2R)-2-(acetylamino)-N-benzyl-3-methoxypropanamide], lidocaine, and carbamazepine.* J Pharmacol Exp Ther, 2008. **326**(1): p. 89-99.
19. Kim, D.W., H.K. Kim, and E.K. Bae, *Switching from traditional sodium channel blockers to lacosamide in patients with epilepsy.* Seizure, 2019. **65**: p. 172-175.
20. Rauck, R.L., et al., *Lacosamide in painful diabetic peripheral neuropathy: a phase 2 double-blind placebo-controlled study.* Clin J Pain, 2007. **23**(2): p. 150-8.
21. Shaibani, A., et al., *Long-term oral lacosamide in painful diabetic neuropathy: a two-year open-label extension trial.* Eur J Pain, 2009. **13**(5): p. 458-63.
22. Shaibani, A., et al., *Lacosamide in painful diabetic neuropathy: an 18-week double-blind placebo-controlled trial.* J Pain, 2009. **10**(8): p. 818-28.
23. Wymer, J.P., et al., *Efficacy and safety of lacosamide in diabetic neuropathic pain: an 18-week double-blind placebo-controlled trial of fixed-dose regimens.* Clin J Pain, 2009. **25**(5): p. 376-85.

24. Namer, B., et al., *Pain relief in a neuropathy patient by lacosamide: Proof of principle of clinical translation from patient-specific iPS cell-derived nociceptors.* EBioMedicine, 2019. **39**: p. 401-408.
25. de Greef, B.T.A., et al., *Lacosamide in patients with Nav1.7 mutations-related small fibre neuropathy: a randomized controlled trial.* Brain, 2019. **142**(2): p. 263-275.
26. Wallis, Y., Payne, S., McAnulty, C., Bodmer, D., Sistermans, E., Robertson, K. et al., *Practical guidelines for the evaluation of pathogenicity and the reporting of sequence variants in clinical molecular genetics.* The Association for Clinical Genomic Science (ACGS), 2013: p. 1-16.
27. de Greef, B.T., et al., *Efficacy, safety, and tolerability of lacosamide in patients with gain-of-function Nav1.7 mutation-related small fiber neuropathy: study protocol of a randomized controlled trial-the LENSS study.* Trials, 2016. **17**(1): p. 306.
28. Yang, Y., et al., *Nav1.7-A1632G Mutation from a Family with Inherited Erythromelalgia: Enhanced Firing of Dorsal Root Ganglia Neurons Evoked by Thermal Stimuli.* J Neurosci, 2016. **36**(28): p. 7511-22.
29. Cawello, W., *Clinical pharmacokinetic and pharmacodynamic profile of lacosamide.* Clin Pharmacokinet, 2015. **54**(9): p. 901-14.
30. Han, C., et al., *Nav1.7-related small fiber neuropathy: impaired slow-inactivation and DRG neuron hyperexcitability.* Neurology, 2012. **78**(21): p. 1635-43.
31. Fu, W., et al., *Residual undifferentiated cells during differentiation of induced pluripotent stem cells in vitro and in vivo.* Stem Cells Dev, 2012. **21**(4): p. 521-9.
32. Estacion, M., et al., *Intra- and interfamily phenotypic diversity in pain syndromes associated with a gain-of-function variant of NaV1.7.* Mol Pain, 2011. **7**: p. 92.
33. Persson, A.K., et al., *Neuropathy-associated Nav1.7 variant I228M impairs integrity of dorsal root ganglion neuron axons.* Ann Neurol, 2013. **73**(1): p. 140-5.
34. Cregg, R., et al., *Novel mutations mapping to the fourth sodium channel domain of Nav1.7 result in variable clinical manifestations of primary erythromelalgia.* Neuromolecular Med, 2013. **15**(2): p. 265-78.
35. Kapetis, D., et al., *Network topology of NaV1.7 mutations in sodium channel-related painful disorders.* BMC Syst Biol, 2017. **11**(1): p. 28.
36. Mantegazza, M., et al., *Voltage-gated sodium channels as therapeutic targets in epilepsy and other neurological disorders.* Lancet Neurol, 2010. **9**(4): p. 413-24.
37. Kuo, C.C. and L. Lu, *Characterization of lamotrigine inhibition of Na+ channels in rat hippocampal neurones.* Br J Pharmacol, 1997. **121**(6): p. 1231-8.
38. Han, C., et al., *The Novel Activity of Carbamazepine as an Activation Modulator Extends from NaV1.7 Mutations to the NaV1.8-S242T Mutant Channel from a Patient with Painful Diabetic Neuropathy.* Mol Pharmacol, 2018. **94**(5): p. 1256-1269.
39. Yang, Y., et al., *Structural modelling and mutant cycle analysis predict pharmacoresponsiveness of a Na(V)1.7 mutant channel.* Nat Commun, 2012. **3**: p. 1186.
40. Yang, Y., et al., *Reverse pharmacogenomics: carbamazepine normalizes activation and attenuates thermal hyperexcitability of sensory neurons due to Nav 1.7 mutation I234T.* Br J Pharmacol, 2018. **175**(12): p. 2261-2271.
41. Geha, P., et al., *Pharmacotherapy for Pain in a Family With Inherited Erythromelalgia Guided by Genomic Analysis and Functional Profiling.* JAMA Neurol, 2016. **73**(6): p. 659-67.
42. Catterall, W.A. and T.M. Swanson, *Structural Basis for Pharmacology of Voltage-Gated Sodium and Calcium Channels.* Mol Pharmacol, 2015. **88**(1): p. 141-50.
43. Ragsdale, D.S., et al., *Molecular determinants of state-dependent block of Na+ channels by local anesthetics.* Science, 1994. **265**(5179): p. 1724-8.
44. Yarov-Yarovoy, V., et al., *Molecular determinants of voltage-dependent gating and binding of pore-blocking drugs in transmembrane segment IIIS6 of the Na(+) channel alpha subunit.* J Biol Chem, 2001. **276**(1): p. 20-7.

45. Yarov-Yarovoy, V., et al., *Role of amino acid residues in transmembrane segments IS6 and IIS6 of the Na+ channel alpha subunit in voltage-dependent gating and drug block.* J Biol Chem, 2002. **277**(38): p. 35393-401.
46. Fozzard, H.A., M.F. Sheets, and D.A. Hanck, *The sodium channel as a target for local anesthetic drugs.* Front Pharmacol, 2011. **2**: p. 68.
47. Fischer, T.Z., et al., *A novel Nav1.7 mutation producing carbamazepine-responsive erythromelalgia.* Ann Neurol, 2009. **65**(6): p. 733-41.
48. Meijer, I.A., et al., *An atypical case of SCN9A mutation presenting with global motor delay and a severe pain disorder.* Muscle Nerve, 2014. **49**(1): p. 134-8.
49. Focken, T., et al., *Discovery of Aryl Sulfonamides as Isoform-Selective Inhibitors of NaV1.7 with Efficacy in Rodent Pain Models.* ACS Med Chem Lett, 2016. **7**(3): p. 277-82.
50. McCormack, K., et al., *Voltage sensor interaction site for selective small molecule inhibitors of voltage-gated sodium channels.* Proc Natl Acad Sci U S A, 2013. **110**(29): p. E2724-32.
51. Theile, J.W., M.D. Fuller, and M.L. Chapman, *The Selective Nav1.7 Inhibitor, PF-05089771, Interacts Equivalently with Fast and Slow Inactivated Nav1.7 Channels.* Mol Pharmacol, 2016. **90**(5): p. 540-548.
52. Han, C., et al., *Functional profiles of SCN9A variants in dorsal root ganglion neurons and superior cervical ganglion neurons correlate with autonomic symptoms in small fibre neuropathy.* Brain, 2012. **135**(Pt 9): p. 2613-28.

SUPPLEMENTARY MATERIALS

Nº of patients	Nucleotide change	Amino acid change	GoF	Allele Freq (GnomAD)	Allele count (GnomAD)	Type of variation	Classification ACGS guidelines	Overall LCM response	References
1	c.684C>G	p.Ile228Met	YES	8.58e-4	241/281046	missense	Pathogenic	-	[1] [2] [3]
1	c.1552G>T	p.Val518Phe	UK	4.02e-6	1/249054	missense	Unknown significance	+	[4]
1	c.1592A>C	p.Thr531Asn	UK	-	0	missense	Unknown significance	+	[4]
1	c.1691T>C	p.Ile564Thr	UK	1.21e-5	1/248986	missense	Unknown significance	-	Unpublished data
2	c.1964A>G	p.Lys655Arg	UK	1.90e-3	592/279028	missense	Unlikely to be pathogenic	-	[5] [6] [7]
1	c.2157G>C	p.Trp719Cys	UK	9.81e-4	293/243602	missense	Unknown significance	+	[4]
6*	c.2215A>G	p.Ile739Val	YES	2.47e-3	597/241656	missense	Pathogenic risk factor	+	[8] [1] [9]
1	c.2266C>A	p.Pro756Thr	UK	2.85e-5	7/245266	missense	Uncertain significance	-	[4]
1	c.3734A>G	p.Asn1245Ser	NO	4.4e-3	1224/278244	missense	Unlikely to be pathogenic	+	[7]
4	c.3799C>G	p.Leu1267Val	YES	1.31e-3	321/245832	missense	Unknown significance (data available upon request)	-	[10] [11] [12]
1	c.5260G>T	p.Val1754Phe	UK	-	0	-	Uncertain significance	+	[4]
3*	c.2794A>C and c.2971G>T	p.Met932Leu and p.Val991Leu	YES	3.38e-2 and 3.01e-2	9571/282670 and 7160/237770	missense and missense	Pathogenic	+	[1] [13]
2*	c.4612T>C	p.Trp1538Arg	YES	2.02e-3	565/279548	missense	Pathogenic	-	[14]
1	c.3595-11T>G	-	UK	-	0	splice	Uncertain significance	+	Unpublished data
1	c.2842-6_2842-5delinsG	-	UK	-	0	splice	Uncertain significance -	-	Unpublished data

SUPPLEMENTARY TABLE 1 – Summary of SCN9A variants reported in the cohort from the *de Greef et al. (2019)* study. All participants were diagnosed with pure (or with Diabetes Mellitus) painful SFN, with an associated Na$_V$1.7 variant. Variants were classified and reported according the Practice Guidelines of the Association for Clinical Genetic Science (ACGS), Wallis, et al. (2013). Whenever the variant has functionally been assessed, the classification is reported accordingly, with appropriate referencing.

The star sign (*) next to the patient number indicates that one or more patients carried at least one additional variant: One out of the six patients carrying the I739V variant also carries M932L/V991L and W1538R.
Two out of the three patients carrying the M932L/V991L double mutation carry additional variants: one patient carries the W1538R, and the other patient, both W1538R and I739V (same as above).
Both patients carrying the W1538R carry additional variants (as described above, the M932L/V991L variant, and the M932L/V991L + I739V variants)
Abbreviations: GoF (Gain-of-function), UK (unknown).

REFERENCES

1. Faber, C.G., et al., *Gain of function Nanu1.7 mutations in idiopathic small fiber neuropathy.* Ann Neurol, 2012. **71**(1): p. 26-39.
2. Persson, A.K., et al., *Neuropathy-associated Nav1.7 variant I228M impairs integrity of dorsal root ganglion neuron axons.* Ann Neurol, 2013. **73**(1): p. 140-5.
3. Estacion, M., et al., *Intra- and interfamily phenotypic diversity in pain syndromes associated with a gain-of-function variant of NaV1.7.* Mol Pain, 2011. **7**: p. 92.
4. Eijkenboom, I., et al., *Yield of peripheral sodium channels gene screening in pure small fibre neuropathy.* J Neurol Neurosurg Psychiatry, 2019. **90**(3): p. 342-352.
5. Singh, N.A., et al., *A role of SCN9A in human epilepsies, as a cause of febrile seizures and as a potential modifier of Dravet syndrome.* PLoS Genet, 2009. **5**(9): p. e1000649.
6. Klein, C.J., M. Sinnreich, and P.J. Dyck, *Indifference rather than insensitivity to pain.* Ann Neurol, 2003. **53**(3): p. 417-8; author reply 418-9.
7. Brouwer, B.A., et al., *Painful neuropathies: the emerging role of sodium channelopathies.* J Peripher Nerv Syst, 2014. **19**(2): p. 53-65.
8. Han, C., et al., *Functional profiles of SCN9A variants in dorsal root ganglion neurons and superior cervical ganglion neurons correlate with autonomic symptoms in small fibre neuropathy.* Brain, 2012. **135**(Pt 9): p. 2613-28.
9. Devigili, G., et al., *Paroxysmal itch caused by gain-of-function Nav1.7 mutation.* Pain, 2014. **155**(9): p. 1702-7.
10. Huang, J., et al., *Gain-of-function mutations in sodium channel Na(v)1.9 in painful neuropathy.* Brain, 2014. **137**(Pt 6): p. 1627-42.
11. Della Mina, E., et al., *Improving molecular diagnosis in epilepsy by a dedicated high-throughput sequencing platform.* Eur J Hum Genet, 2015. **23**(3): p. 354-62.
12. Wadhawan, S., et al., *NaV channel variants in patients with painful and nonpainful peripheral neuropathy.* Neurol Genet, 2017. **3**(6): p. e207.
13. Li, Q.S., et al., *SCN9A Variants May be Implicated in Neuropathic Pain Associated With Diabetic Peripheral Neuropathy and Pain Severity.* Clin J Pain, 2015. **31**(11): p. 976-82.
14. Cregg, R., et al., *Novel mutations mapping to the fourth sodium channel domain of Nav1.7 result in variable clinical manifestations of primary erythromelalgia.* Neuromolecular Med, 2013. **15**(2): p. 265-78.

CHAPTER 3

Lacosamide inhibition of $Na_V1.7$ channels depends on its interaction with the voltage sensor domain and the channel pore

Published as:

Julie I. R. Labau, Matthew Alsaloum, Mark Estacion, Brian Tanaka, Fadia B. Dib-hajj, Giuseppe Lauria, Hubert J. M. Smeets, Sulayman Dib-Hajj, Stephen G. Waxman. Lacosamide inhibition of NaV1.7 channels depends on its interaction with the voltage sensing domain and the channel pore.
Frontiers Pharmacology. (2021) 12:791740.

doi: 10.3389/fphar.2021.791740

ABSTRACT

Lacosamide, developed as an anti-epileptic drug, has been used for the treatment of pain. Unlike typical anticonvulsants and local anesthetics which enhance fast-inactivation and bind within the pore of sodium channels, lacosamide enhances slow-inactivation of these channels, suggesting different binding mechanisms and mode of action. It has been reported that lacosamide's effect on $Na_V1.5$ is sensitive to a mutation in the local anesthetic binding site, and that it binds with slow kinetics to the fast-inactivated state of $Na_V1.7$. We recently showed that the $Na_V1.7$-W1538R mutation in the voltage-sensing domain 4 completely abolishes $Na_V1.7$ inhibition by clinically-achievable concentration of lacosamide. Our molecular docking analysis suggests a role for W1538 and pore residues as high affinity binding sites for lacosamide. Aryl sulfonamide sodium channel blockers are also sensitive to substitutions of the W1538 residue but not of pore residues. To elucidate the mechanism by which lacosamide exerts its effects, we used voltage-clamp recordings and show that lacosamide requires an intact local anesthetic binding site to inhibit $Na_V1.7$ channels. Additionally, the W1538R mutation does not abrogate local anesthetic lidocaine-induced blockade. We also show that the naturally occurring arginine in $Na_V1.3$ ($Na_V1.3$-R1560), which corresponds to $Na_V1.7$-W1538R, is not sufficient to explain the resistance of $Na_V1.3$ to clinically-relevant concentrations of lacosamide. However, the $Na_V1.7$-W1538R mutation conferred sensitivity to the $Na_V1.3$-selective aryl-sulfonamide blocker ICA-121431. Together, the W1538 residue and an intact local anesthetic site are required for lacosamide's block of $Na_V1.7$ at a clinically-achievable concentration. Moreover, the contribution of W1538 to lacosamide inhibitory effects appears to be isoform-specific.

INTRODUCTION

Chronic pain affects 20-25% of the global population [1-3] and is commonly associated with impaired quality of life, opioid addiction, and psychiatric comorbidities [1, 4-8]. Existing treatments are often limited by inadequate pain relief and severe side effects [9, 10]. Pharmacotherapy targeting voltage-gated sodium channels (VGSCs) has been used with some success for the treatment of neuropathic pain [11-15]. The anticonvulsant lacosamide (*R*-2-acetamido-*N*-benzyl-3-methoxypropionamide), which is FDA-approved for the treatment of epilepsy, has been investigated as a potential treatment for diabetic neuropathic pain [16-18], refractory pain [19], and recently, $Na_V1.7$-related painful small fiber neuropathy [20], among others [21]. The clinical effects of lacosamide are thought to be due to its function as a sodium channel blocker [22].

Unlike typical antiepileptic drugs (AEDs) such as carbamazepine, phenytoin, and lamotrigine, as well as local anesthetics (LAs), such as lidocaine and benzocaine, lacosamide enhances the voltage-dependence of slow inactivation but not steady-state fast inactivation, and increases use-dependent inhibition of sodium channels [23-27]. This suggested that lacosamide exerts its effect on VGSCs by a different mechanism

than AEDs and LAs and Jo and Bean reported slow binding of lacosamide to the fast-inactivated state [28]. Also, LAs and conventional AEDs are pore-blockers that share a common binding motif, the "LA binding site", composed of residues in the S6 segment of domains DI, DII, and DIV [29-34], which include the critical residues phenylalanine (F1764, Na$_V$1.7 numbering) and tyrosine (Y1771) [31, 35]. Previous studies have posited that lacosamide's binding site is within the permeation pathway, overlapping with the binding site for batrachotoxins and LAs in the S6 helix [28, 36, 37]; however, radio-ligands essays have failed to assign a specific residue to lacosamide binding against hundreds of known receptors and binding sites [22]. These data suggest a complex mechanism for lacosamide binding and inhibition of VGSC.

The Na$_V$1.7-W1538R mutation, located in the S2 helix of the voltage sensing domain of the channel's domain IV (VSD4), causes a hyperpolarizing shift in the voltage-dependence of activation of Na$_V$1.7 channels and has been implicated in the pathology of both inherited erythromelalgia [38] and small fiber neuropathy [39]. Furthermore, the mutation has been shown to abolish the effect of lacosamide on slow-inactivation and use-dependent inhibition of the channel at clinically-achievable concentrations [40]**.** Interestingly, an arginine residue is a natural variant at the corresponding position to W1538 in Na$_V$1.1 and Na$_V$1.3 channels (R1560 in human Na$_V$1.3), and Na$_V$1.3 has been shown to be less sensitive to lacosamide, compared to Na$_V$1.7 [25]. Importantly, the W1538 residue is one of three residues required for selective blockade of Na$_V$1.7 by aryl sulfonamide small molecules [41, 42]. Aryl sulfonamides are nanomolar potent sodium channel inhibitors, which exhibit up to 1000-fold selectivity for specific channel subtypes. Similar to lacosamide, they show a slow onset of block [43]. Moreover, these compounds exhibit binding to the extracellular surface of the VSD4, independently of an intact LA binding site in the pore [41, 42]. These data suggest that lacosamide inhibition of Na$_V$1.7 may share mechanistic features with AEDs/LAs and aryl-sulfonamides.

In this study, we show using voltage-clamp analysis that lacosamide requires both an intact LA binding site in the pore and the W1538 residue in VSD4 for effective Na$_V$1.7 inhibition by a therapeutic concentration of lacosamide. Using molecular docking analysis of human Na$_V$1.7 channels, we propose that W1538 is a putative high affinity site, which possibly guides lacosamide to the pore. In support of this view, high doses of lacosamide block Na$_V$1.7-W1538R mutant channels. Additionally, we demonstrate that the W1538R mutation is sufficient to render Na$_V$1.7 channels sensitive to the Na$_V$1.3-selective aryl sulfonamide blocker ICA-121431. We also show that the reciprocal mutation (R1560W) in Na$_V$1.3 was insufficient to render Na$_V$1.3 channels sensitive to lacosamide at clinically-achievable concentrations, suggesting that the effect of the tryptophan residue in VSD4 on lacosamide block is isoform-dependent.

METHODS

PLASMIDS AND CELL CULTURE

The constructs for wild-type (WT) carrying the adult-long (AL) splicing isoforms of the human $Na_V1.7$ and $Na_V1.3$ channels were made tetrodotoxin-resistant (TTX-R) by Y362S and Y384S substitutions, respectively. A green fluorescent protein (GFP)-2A linker was then fused in-frame at the N-terminus of the channel, as previously described [44]. The GFP-2A-Na_V construct allows the production of separate GFP and Na_V proteins from the same transcript, thus enabling the visual identification of the channel-expressing cells by green fluorescence labeling. Mutations in these WT channels were introduced by site-directed mutagenesis using QuickChange XL (Stratagene, La Jolla, CA, USA), and identity of the inserts was confirmed by Sanger sequencing. The following mutations were introduced into the $Na_V1.7$ and $Na_V1.3$ WT channels: $Na_V1.7$-F1737A/Y1744A mutant (established to prevent the binding of LAs and AEDs in the pore [31, 32, 41, 45], h$Na_V1.7$ -W1538R; and h$Na_V1.3$ 2A-R1560W. Constructs were transfected into human embryonic kidney (HEK293) cells (1 μg/μL) using Lipojet (SignaGen Laboratories) for transient expression together with β1 and β2 subunits: pCD8-IRES-hB1 (0.5 μg/μL) and pCDNA3-hB2 (0.5 μg/μL).
HEK293 cells were grown in DMEM/F12 (Dulbecco's modified Eagle's medium), supplemented with 10% fetal bovine serum and 1% penicillin/streptomycin, and incubated at 5% CO2 and 37°C. The cells were passaged 1-2 times per week and media was replaced one hour before transfection. Transfected cells were resuspended in TryplE Express (ThermoFischer) and either replated onto laminin/PDL-coated coverslips for manual voltage patch-clamp recordings or resuspended in Sophion extracellular bath solution for automated voltage-clamp recordings on the Qube 384 (Sophion Bioscience, Inc)[46].

IN VITRO PHARMACOLOGY – Reagents

The effect of lacosamide, obtained from either Adooq (Adooq Biosciences, A10510) or UCB (Vimpat®, West Haven VA Medical Center pharmacy), was assessed both at a clinically-achievable concentration (30 μM), based on the maximum plasma concentration of patients receiving a daily dose of 200 mg [20, 47], and at 300 μM. At a concentration of 10 mg/ml (39.9 mM) in saline (pH 4), Vimpat was diluted in extracellular bath solution to achieve a final concentration of either 30 μM or 300 μM. The formulation was used to evaluate the effect of therapeutic lacosamide concentration (30 μM) and 10-fold that dose (300 μM) on $Na_V1.7$-W1538R and $Na_V1.3$-R1560W mutant channel properties.

Lacosamide from Adooq Bioscience was used to test the drug on the $Na_V1.7$-F1737A/Y1744A channels. The compound was diluted in dimethyl sulfoxide (DMSO; Tocris Bioscience, Cat. No. 3176) at 100 mg/1.33 ml to give a 300 mM stock solution. Further dilutions were performed to a working solution of 30 μM in 0.1% DMSO in extracellular bath solution.

Lidocaine (lidocaine hydrochloride monohydrate, Sigma Aldrich, L5647) was diluted in Sophion extracellular bath solution, as described [46], to make a stock solution of 80 mM, and then diluted 1000x to a working concentration of 80 μM in extracellular bath solution.
The aryl sulfonamide $Na_V1.3$-selective blocker ICA-121431 was obtained from Adooq Bioscience (A13773). ICA-121431 was first solubilized in DMSO to make a stock solution of 50 mM. The stock was diluted with DMSO to a 0.1 mM concentration, before further dilution to a final concentration of 0.1 μM in 0.1% DMSO in Sophion working extracellular solution [46]. Dosage was selected based on prior publication [41] and preliminary dose-response assay using 0.01, 0.1, and 1 μM (*data not shown*).

The stock solutions were kept in the freezer at – 20°C; working solutions were prepared fresh daily and kept at room temperature (RT).

ELECTROPHYSIOLOGY

Manual voltage-clamp recordings

Biophysical responses of $Na_V1.7$ sodium channels to different treatments were evaluated by whole-cell voltage-clamp analysis. The recordings were performed at RT on isolated GFP-positive HEK293 cells, alternating between cells expressing a mutant and its corresponding WT channel on the same day. Furthermore, each pair recorded was assessed with either vehicle or treatment on one given day. As such, the $Na_V1.7$-WT and W1538R pair were recorded with either 30 μM or 300 μM lacosamide and vehicle (extracellular bath) on the same day, and the alternative concentration, on a separate day. For each coverslip, a single cell was recorded, either exposed to treatment or vehicle.

Solutions

The vehicle, or extracellular bath solution, contained (in mM): 140 NaCl, 3 KCl, 1 MgCl2, 1 CaCl2, 10 HEPES. The pH was adjusted to 7.3 with NaOH, and the solution was brought to 320-330 mOsm using dextrose. The intracellular solution contained (in mM): 140 CsF, 10 NaCl, 10 HEPES, 1 EGTA. The pH was adjusted to 7.3 with CsOH. The solution was brought to 310-320 mOsm with dextrose, before being used to fill borosilicate glass micropipettes (WPI; 1.65-mm outer diameter) containing the recording electrode. The pipettes were pulled to a 0.7-1.5 MΩ resistance to maintain a series resistance under 4 MΩ.

Protocols

Initiation of the voltage-clamp protocols was set at 5 min following breakage of the cell membrane. All recordings were obtained with whole-cell configuration using an EPC-10 USB amplifier (HEKA Electronics), with the software PatchMaster (HEKA Electronics). Data was acquired at a rate of 50 kHz, with a low-pass 2.9 kHz Bessel filter. To minimize voltage errors, the series resistance was compensated to 40%-90%, and only cells that could maintain a voltage error below 3.5 mV were analyzed. Linear

leak currents, along with capacitance artefacts were corrected, whenever appropriate, using a P/6 subtraction.
The voltage-clamp protocols were systematically applied in the following order to reduce the risk for time-dependent variation in treatment effects:
Activation was evaluated by applying a 5 mV series of depolarizing increments for 100 ms, starting from -80 mV to + 50 mV, every 5 seconds, from a -120 mV holding potential.
Steady-state fast-inactivation was measured by holding the membrane potential for 500 ms at conditioning potentials, varying from -140 mV to 10 mV, with 10 mV depolarizing increments.
Use-dependent block of $Na_V1.7$ channels with lacosamide was measured at 20 Hz using a series of 20 ms pulses applied at -10 mV and following a -120 mV holding potential. The peak inward currents were normalized to their maximum current amplitude.
Slow-inactivation was evaluated by holding the cell for 30 seconds at conditioning potentials ranging from -130 mV to 10 mV (with 10 mV increments), after which a -120 mV pulse was applied to the membrane potential for 100 ms to enable any channel not in the slow-inactivated state to recover from fast-inactivation. After both (fast and slow) inactivation protocols, an additional 20 ms test pulse at 0 mV was used to elicit current from any remaining available channels.

Perfusion

Vehicle and lacosamide were perfused at a continuous flow rate of 1 ml/min, 2 min after establishing whole-cell configuration and for two uninterrupted minutes. Alternatively, cells recorded in larger chambers were perfused at a continuous flow rate of 0.3 ml/min, 2 min after break-in and for 8-9 uninterrupted minutes or until the initiation of the slow-inactivation protocol. Complete bath exchange was ensured by using a pressure-regulated system which allowed consistent solution distribution on one end of the chamber (AutoMate Scientific), through a 250 μm perfusion pipette, and by slowly aspirating it from the opposite end, as previously described [40]. To control for time-dependent and perfusion-related pressure-dependent alterations in channel properties, each cell was exposed consistently to only one solution at a time and for each recording.

Automated high-throughput Patch-clamping: Qube 384

The Qube automated electrophysiology instrument from Sophion Bioscience was utilized to perform higher throughput assessment of the effects of lidocaine, lacosamide and ICA-121431. A detailed description of the capabilities and the setting up of modules to perform voltage-step protocols for the Qube instrument has previously been published [46]. In general, the pulse protocols were configured to match as closely as possible those used in the manual patch-clamp experiments. There were two notable differences when performing our experiments on the Qube compared to manual patch-clamp. The first was that the Qube performs a solution exchange by utilizing a pipetting step which dispenses 7 μL per well. The volume of the part of the well that contains the recorded cell is approximately 1 μL, so a solution change results in a seven-fold volume

exchange. The second difference was the implementation of leak subtraction and series resistance compensation. The Sophion instrument does not implement P/n pulses but instead performs an analysis of the transient response to small test pulses which are then scaled to match the applied pulses resulting in leak-subtracted trace data. For series resistance compensation, Sophion has implemented a method developed by Alembic [48], which is less prone to positive feedback oscillations and can reach 100% compensation. For the data presented here, the series resistance compensation level was set to 90%.

Solutions

The solutions used when performing experiments with the Qube are as recommended by Sophion [46]. Briefly, the standard extracellular solution contained (in mM): NaCl (145), KCl (4), CaCl2·(2H_2O; 2), MgCl2·(6H_2O; 1), HEPES (10) titrated to pH 7.4 with NaOH and osmolarity was adjusted to 305 mOsm with glucose.

The standard intracellular solution contained (in mM): CsF (140), EGTA (1), HEPES (10), NaCl (10), titrated to pH 7.3 with CsOH and osmolarity was adjusted to 310 mOsm with glucose. Compounds or vehicle were diluted from stock solutions into Sophion standard extracellular solution and placed into compound plates of various formats, where we tested vehicle against up to two different compounds at different dilutions (or a minimum of one solution in 32 wells per genotype per plate), and with each cell exposed to a different compound. For lidocaine, however, we implemented a 'before-and-after recording' system, where each cell was first exposed to vehicle (extracellular solution) and then to 80 μM lidocaine.

Protocols

The voltage-clamp pulse protocols were implemented on the Qube instrument so as to replicate the ones used for manual patch-clamp. Shortly after establishing the whole-cell configuration, the cells were pulsed from a holding potential of -120 mV to a 0 mV stepping voltage for 50 msec, after which, the voltage was returned to the holding potential and the step was repeated with a 10 second interval. The whole protocol was repeated for one minute, after which, the pipetting solution exchange was initiated. Three complete solution exchanges were implemented at one min intervals during the recurring pulses. Following each well equilibration with its designated compound and concentration, the biophysical characterization was performed. Similar to manual patch-clamp experiments, protocols were applied in a specific order to prevent time-dependent bias, as follows:

Voltage-dependence of activation consisted of 100 ms duration pulses, from a holding potential of -120 mV, that were stepped from -80 mV, then returned to the original holding potential. Step depolarization was applied in 5 mV increments and looping at 5 seconds intervals until the last pulse to 10 mV.

Voltage-dependence of fast-inactivation was measured by holding the cell at -120 mV, after which conditioning pulses of 500 ms were applied from -120 mV to 20 mV in 10 mV increments. Following the conditioning pulse, a test pulse to 0 mV was applied for 50 ms to determine the fraction of sodium channels still available for opening. The

potential is then returned to the holding potential of -120 mV until the next loop occurring at 5 seconds intervals.
Use-dependence of inhibition consisted of a train of 20 ms 20 Hz depolarizing pulses to 0 mV, starting from a holding potential of -120 mV.
Voltage-dependence of slow-inactivation consisted of 20 seconds long pulses starting at -140 mV and stepping with 10 mV increments until the last loop at 20 mV. Each loop was spaced by 30 seconds. Following the conditioning pulse, a brief 100 ms pulse to -120 mV was used to recover the remaining channels from the fast-inactivated state, which was then stimulated by a 100 ms pulse to 0 mV prior to returning to the initial holding potential of -120 mV. The peak inward currents were normalized to their maximum current amplitude. Cells that were selected for analysis were those that had a peak series resistance < 20 MΩ, average membrane resistance > 200 MΩ, a peak current > 1 nA, and a fit quality (as determined by the Sophion Boltzmann fit of the data) < 0.15 for activation and 0.05 for fast-inactivation and slow-inactivation, as well as minimal leak (< 10% of the peak sodium current).

STRUCTURAL MODELING & MOLECULAR DOCKING

The Protein Data Bank (PDB) structure of the $Na_V1.7$ channel (PDB ID: 6J8I) from [49] was edited to remove all toxins and auxiliary subunits. Blind docking analysis utilizing the Achilles Blind Docking server was subsequently performed for lacosamide (ZINC structure ZINC7673) [50] on the $Na_V1.7$ α-subunit. The channel was visualized using PyMol (Schrödinger, LLC).

STATISTICAL ANALYSES

Manual electrophysiology data were obtained with FitMaster (HEKA Electronics) and automated electrophysiology data were obtained with Sophion Analyzer v6.5.76 (Sophion Instruments).
All datasets were analyzed in Excel (Microsoft), OriginLab (OriginLab Corporation, Microcal Software, Northhampton, MA) and/or GraphPad Prism 8.4.3.

Data are expressed as means ± standard error of the mean (SEM). Statistical significance was determined by *P < 0.05 and **P < 0.01 using either unpaired Student's t-tests or One-way ANOVA. When ANOVA was used, Dunnett's multiple comparison analysis was run for the means to assess significant differences between the treatment groups and control.

Voltage-dependent activation was analyzed as the conductance (G), calculated using the following equation: $G = I/(V-V_{rev})$, where I is the peak current at each voltage (V) measured, and V_{rev} is the reversal voltage calculated by extrapolating peak currents with depolarizing potentials ranging from 10 to 40 mV. Conductance was normalized to the maximal sodium conductance (G_{max}) for a given cell, and curves were fitted using the Boltzmann equation: $G/G_{max} = 1/(1+\exp((V_{1/2}-V)/k))$, where $V_{1/2}$ is half the maximal activation voltage, and k the slope factor. Steady-state fast and slow inactivation residual currents were also normalized to the maximal sodium current

(I_{max}), plotted against the voltage of incremental conditioning pulses. The inactivation curves were fitted with the Boltzmann equation, as follows: $I/I_{max} = 1/(1+\exp((V_{1/2}-V)/k))$, when appropriate. Alternatively, when the curves had two distinct components, a double Boltzmann equation was applied: $I/Imax=1/\{F[1+\exp(V-V1_{1/2})/k_1]\}+\{1-F[1+\exp(V-V2_{1/2})/k_2]\}$, where F is the first component's fraction and 1-F is the second component's fraction. For use-dependence of inhibition, the peak current of each evoked pulse was normalized to the first pulse of the series and significance was evaluated by comparing the control's last pulse mean to those of the drug groups.

RESULTS

The W1538 region is predicted as the most energetically favorable binding site for lacosamide

Neither the binding characteristics of lacosamide to $Na_V1.7$ nor the underlying mechanisms of action by which it blocks the channel are well understood. To address this gap in knowledge and assess possible allosteric effect of lacosamide on the pore and determine potential structural mechanisms underpinning lacosamide's mode of action, we performed unbiased docking analysis for lacosamide on the $Na_V1.7$ α-subunit (*Figure 1*). This method allows us to predict the preferred binding sites for the compound with no bias towards particular local structures of the channel. This analysis identified 1139 possible poses, which could be grouped into 62 distinct clusters with non-overlapping coordinates. The top 10 most energetically favorable clusters had binding energies more negative than -6.2 kcal/mol. The most energetically favorable cluster for lacosamide binding docked the compound near the W1538 residue, with the most energetically favorable pose in this cluster approximately 8.8 Å away, although it shared no discernible interactions directly with the W1538 residue (*Figure 1C*). The binding energy for lacosamide at this site was approximately -7.3 kcal/mol. Interestingly, the second, fourth, and eighth most energetically favorable clusters for lacosamide docking were found near the F1737 and Y1744 residues (*Figure 1D*). Thus, while the most energetically favorable site for lacosamide binding is near to W1538, lacosamide also readily binds in many positions around the LA binding site.

Lacosamide fails to exert its inhibitory effects on the $Na_V1.7$-F1737A/Y1744A mutant

Having shown that lacosamide exhibits high affinity binding near both the W1538 residue and the LA binding site, we next sought to investigate whether lacosamide does indeed require active binding to the pore to block VGSCs. We introduced the F1737A/Y1744A mutation into $Na_V1.7$ channels using site-directed mutagenesis, abolishing the LA binding site [41, 45]. Mutated constructs were transfected into HEK293 cells for transient expression. Whereas lacosamide readily inhibits $Na_V1.7$-WT channels at the therapeutic dose of 30 μM [23, 40], it did not cause a hyperpolarizing shift in the voltage-dependence of slow-inactivation in the F1737A/Y1744A mutant channels (*Figure 2*). Using unpaired Student's t-tests, the voltage of half maximal slow

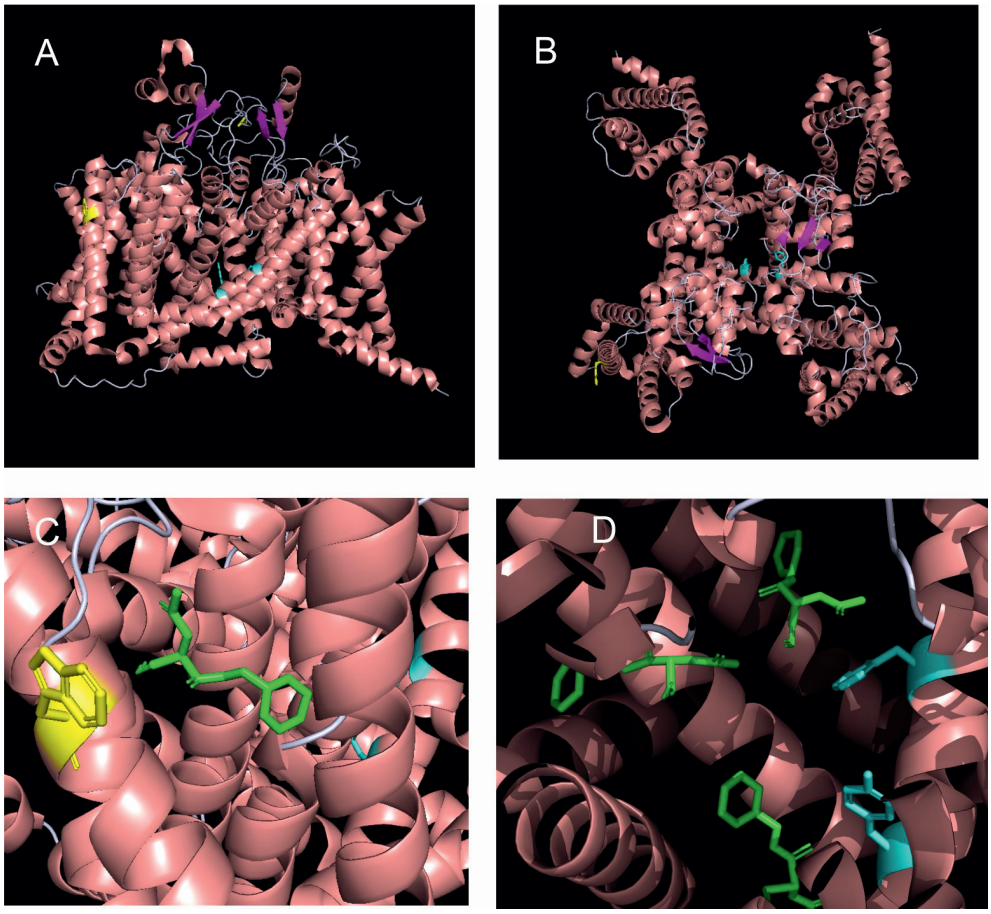

FIGURE 1 – Structural modeling and unbiased docking simulations suggest binding sites of lacosamide on Nav1.7 channels. (A-B) Structural analysis of sodium channels allows the visualization of the W1538 residue in the VSD of DIV, as shown in yellow. The local anesthetic (LA) site F1737 and Y1744 residues locate in the pore of the channel and are both shown in cyan. Structure of the $Na_V1.7$ voltage-gated sodium channel is based on Shen et al [49] and is represented **(A)** from the side and **(B)** from the top. **(C-D)** In silico docking identifies the LA site (F1737/Y1744) and the W1538 as putative binding sites of lacosamide on $Na_V1.7$ sodium channels. **(C)** Lacosamide (green) docked in its most favorable position is predicted by blind docking. The W1538 side chain is shown in yellow. **(D)** Lacosamide (green) docked in its second, fourth, and eighth most favorable positions, predicted by blind docking, near the LA binding site.

inactivation ($V_{1/2}$; *Figure 2B*) of the mutant channel after treatment with lacosamide was statistically comparable to channels treated with vehicle (0.1% DMSO; *Table 1*). Furthermore, lacosamide's known enhancement of use-dependent block of the $Na_V1.7$-WT channel [40], measured by a series of twenty 20 Hz pulses, was lost in $Na_V1.7$-F1737A/Y1744A mutant channels (*Figure 2C, Table 1*), indicating that, at clinically-

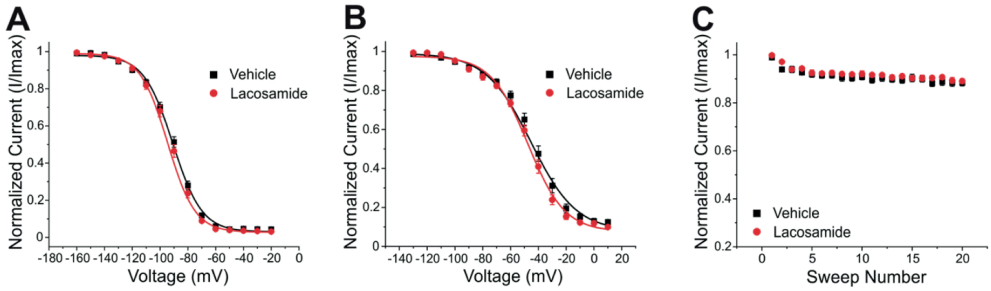

FIGURE 2 – The local anesthetic binding site (F1737/Y1744) in the channel pore is necessary for inhibition of Nav1.7 by lacosamide. The clinically-achievable concentration (30 μM) of lacosamide does not block Nav1.7 channels with a disabled LA binding site (F1737A/Y1744A). **(A)** No difference in the voltage-dependence of steady-state fast-inactivation was observed with the application of 30 μM lacosamide in mutant Nav1.7 channels lacking a functional LA binding site. **(B)** Similarly, the voltage-dependence of slow-inactivation was unchanged. **(C)** Abolishing the LA binding site resulted in no appreciable effects of lacosamide on Nav1.7 use-dependent inhibition at 20 Hz.

achievable concentrations, lacosamide requires a functional LA binding site to affect Nav1.7 function. Finally, lacosamide did not alter the $V_{1/2}$ of steady-state fast-inactivation in F1737A/Y1744A-expressing cells (-92.5 ± 1.5 mV, n=12, *Figure 2A*), compared to vehicle (-91.3 ± 1.3 mV, n=13, p=0.51).

The W1538 residue is not critical for lidocaine binding to Nav1.7 channels

The W1538R mutation, which maps to the VSD4, has been shown to completely abolish the effect of lacosamide on Nav1.7 gating mechanisms at therapeutic concentrations [40]. Whether this mutation exerts an allosteric effect on the LA site in the pore to reduce the effect of lacosamide remains unclear. To test whether W1538R impairs the LA binding site in Nav1.7, we assessed the blocking effect of lidocaine on Nav1.7-W1538R channels (*Figure 3*) using the Qube automated electrophysiology platform and analyzed the data with unpaired Student's t-tests. In response to 80 μM lidocaine, and in line with previous studies [51], lidocaine did not evoke a shift in the voltage-dependence of activation of Nav1.7-WT channels (*Figure 3A*). Likewise, W1538R channel activation was unaffected by the presence of the drug (*Figure 3B*). As expected from past reports [51-53], lidocaine significantly hyperpolarized the WT channel voltage-dependence of both fast-inactivation (*Figure 3C*) and slow inactivation (*Figure 3E*). Similar results were observed in the mutant channels where lidocaine significantly hyperpolarized the $V_{1/2}$ of fast-inactivation (*Figure 3D*) and slow-inactivation of W1538R channels (*Figure 3F*). Lidocaine induced a two-component slow inactivation shift in both variants, and was fitted to a double Boltzmann. Finally, lidocaine significantly enhanced the use-dependence of inhibition in both WT (*Figure 3G*) and W1538R channels (*Figure 3H*), indicating that the effect of lidocaine was not affected by the presence of the W1538R mutation. The activation and inactivation $V_{1/2}$s as well as the degree of block of both variants are listed in *Table 2*.

			Nav1.7-WT	Nav1.7-W1538R	Nav1.7-F1737A/Y1744A	Nav1.3-WT	Nav1.3-R1560W
Lacosamide	*Slow inactivation $V_{1/2}$ (mV)*	Vh.1	-63.47 ± 1.75, n=13	-71.24 ± 2.68, n=6	-43.1 ± 2.2, n=13	-51.45 ± 0.92, n=27	-52.17 ± 1.08, n=27
		LCM 30μM	-71.12 ± 1.86, n=11, p=0.007	-74.61 ± 2.22, n=8, p=0.35	-47.1 ± 1.6, n=12, p=0.16	-54.78 ± 1.87, n=17, p=0.4	54.50 ± 1.41, n=32, p=0.47
		Vh.2	-77.56 ± 2.5, n=5	-79.36 ± 2.04, n=5		= Vehicle 1	= Vehicle 1
		LCM 300μM	-113.71 ± 0.22 N=6 P=1.25e^{-6}	-117.32 ± 1.99 N=6 P= 7.05e^{-5}		-62.95 ± 2.9, n=21, p<0.0001	-58.32 ± 1.94, n=32, p=0.014
	Use-dependent block	Vh.1	0.9 ± 0.01, n=10	0.91± 0.01, n=6	0.88 ± 0.01, n=13	0.88 ± 0.01, n=21	0.87 ± 0.05 n=27
		LCM 30μM	0.86 ± 0.02, n=7, p=0.04	0.88 ± 0.02, n=8, p= 0.30	0.89 ± 0.01, n=13, p=0.68	0.87 ± 0.01, n=18, p=0.5	0.88 ± 0.05, n=27, p=0.61
		Vh.2	0.8 ± 0.03, n=5	0.85 ± 0.02, n=5		= Vehicle 1	= Vehicle 1
		LCM 300μM	0.69 ± 0.02, n=6, p=0.0083	0.67 ± 0.06, n=6, p=0.033		0.85 ± 0.01, n=29, p=0.056	0.83 ± 0.08, n=32, p=0.07

TABLE 1 – Effects of lacosamide at the clinically-achievable concentration of 30μM and at 300μM on Nav1.7 and Nav1.3 wild-type and mutant channels. Lacosamide (LCM) significantly enhanced slow inactivation and use-dependence of inhibition in Nav1.7-WT channels at both 30 μM and 300 μM compared to vehicle, Vh.1 for 30 μM and Vh.2 for 300 μM (Vehicle; extracellular solution), as per different recording days for manual patch clamp analysis. Clinically-achievable concentrations (30 μM) of lacosamide had no effect on any of the mutant channels (ie. Nav1.7-W1538R, Nav1.7-F1737A/Y1744A and Nav1.3-R1560W) or Nav1.3-WT channels. However, at the higher dose of 300 μM, lacosamide evoked a significant hyperpolarizing shift in slow inactivation of Nav1.3-WT, Nav1.3-R1560W and Nav1.7-W1538R mutant channels. In both Nav1.7-WT and W1538R channels, 300 μM lacosamide-induced slow inactivation hyperpolarizing shift was best fitted by a double Boltzmann, therefore yielding two half-inactivation ($V_{1/2}$) voltages. Here, we only report the $V_{1/2}$ of the first component occurring during the first drug response phase and corresponding to the $V_{1/2}$ of most inactivated channels. Nav1.3-WT and R1560W channels were fitted with a single Boltzmann. A 10-fold increase in the lacosamide therapeutic dose also significantly enhanced use-dependent block in Nav1.7-W1538R mutant channels, but not in any of the Nav1.3 variants. The effect of 300μM lacosamide was not tested in Nav1.7- F1737A/Y1744A channels. The Qube allowed the same vehicle group to be tested against Nav1.3 variants, where data from vehicle 1 = vehicle 2. Data are presented as Means ± SEM

At 10-fold the clinical dose, lacosamide recovers its inhibitory properties of W1538R mutant channels

Lacosamide's poor efficacy in blocking W1538R mutant channels, whether in heterologous cell models [40] or in human carriers [20], has thus far exclusively been studied at the clinically-achievable dose of 30 μM. To further evaluate the affinity profile of the W1538 residue as a binding site for lacosamide, we investigated whether a 10-fold increase in lacosamide (300 μM) restores the drug-induced block of $Na_V1.7$-W1538R channels. As expected, lacosamide had no effect on the voltage-dependence of activation or steady-state fast-inactivation in either $Na_V1.7$-WT or W1538R channels at either 30 or 300 μM (*Data not shown*), using unpaired Student's t-tests. In an attempt to directly compare our past results using 30 μM lacosamide [40] to the gating outcomes from a 10-fold increase in lacosamide concentration, we first reproduced the significant hyperpolarizing shift observed in the $V_{1/2}$ of slow-inactivation of $Na_V1.7$-WT channels exposed to 30 μM lacosamide (*Figure 4A*) as well as the enhanced use-dependence of inhibition at 20 Hz (*Figure 4E*). In WT channels, 300 μM lacosamide induced a two-component slow inactivation shift and increased use-dependent block (*Figure 4C,G*). We also reproduced the lack of effect of 30 μM lacosamide on W1538R channel's $V_{1/2}$ of slow-inactivation (*Figure 4B*) and use-dependence of inhibition (*Figure 4F*). However, a 10-fold increase in the concentration of lacosamide significantly blocked W1538R channels by hyperpolarizing the $V_{1/2}$ of the first phase of two-component slow-inactivation (*Figure 4D*) and increased the use-dependence of inhibition of the mutant channel (*Figure 4H*), indicating that higher concentrations rescue the inhibitory action of lacosamide on the $Na_V1.7$-W1538R mutant channels. Furthermore, the two-phase slow inactivation shift is suggested to be evoked by higher concentrations of lacosamide (*Figure 4E,F*) and lidocaine (*Figure 3E,F*), where the effect of the compounds are primarily on the more hyperpolarized component. We speculate that while a fraction of channels does not change in the presence of the compound, the majority does. Therefore, the resulting shift in slow inactivation whether fitted to a single or double-Boltzmann remains significant compared to vehicle. Also, the large hyperpolarization of slow-inactivation of WT and W1538R subjected to 300 μM lacosamide, initiated at voltages as low as -130 mV, and in the absence of a preceding plateau phase, might suggest that the magnitude of the shift may be even larger than calculated in *Figure 4C,D*. The datasets are summarized in *Table 1*.

The mutant W1538R arginine residue confers $Na_V1.7$ channels responsiveness to ICA-121431

The arginine (R1538) residue in the mutant $Na_V1.7$-W1538R channel has been shown to contribute to $Na_V1.7$ aryl sulfonamide inhibitor selectivity and is the naturally occurring residue present in $Na_V1.3$ (R1560) channels [41], which may contribute to the resistance of $Na_V1.3$ to lacosamide inhibition, compared to $Na_V1.7$ channels [25]. Here, we first tested whether the W1538R mutation alone is sufficient to confer $Na_V1.7$ channels responsiveness to ICA-121431, using the Qube and unpaired Student's t-test

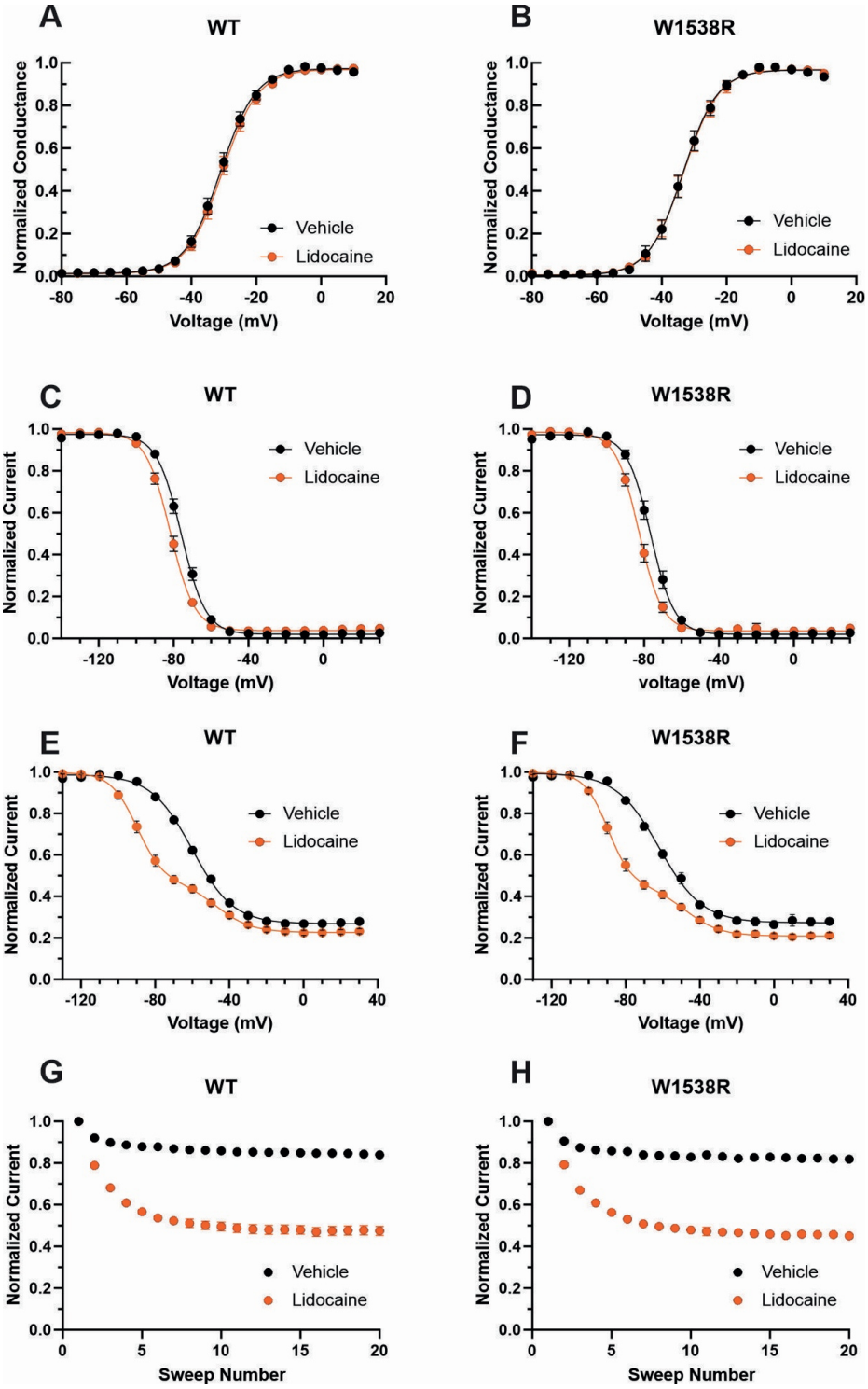
A
WT
Normalized Conductance
Voltage (mV)
Vehicle
Lidocaine
B
W1538R
Normalized Conductance
Voltage (mV)
Vehicle
Lidocaine
C
WT
Normalized Current
Voltage (mV)
Vehicle
Lidocaine
D
W1538R
Normalized Current
voltage (mV)
Vehicle
Lidocaine
E
WT
Normalized Current
Voltage (mV)
Vehicle
Lidocaine
F
W1538R
Normalized Current
Voltage (mV)
Vehicle
Lidocaine
G
WT
Normalized Current
Sweep Number
Vehicle
Lidocaine
H
W1538R
Normalized Current
Sweep Number
Vehicle
Lidocaine

FIGURE 3 – Lidocaine inhibits $Na_V1.7$-W1538R mutant channels. The effect of 80 μM lidocaine on the voltage-dependence of activation, shown with single (vehicle) and double (lidocaine) Boltzmann fits of normalized conductance transformed from the current-voltage plot peak inward currents, of **(A)** $Na_V1.7$-WT was indiscernible from **(B)** $Na_V1.7$-W1538R channels. **(C, D)** Relative to vehicle (extracellular bath solution, black), lidocaine (orange) hyperpolarizes the voltage-dependence of fast-inactivation of both $Na_V1.7$-WT and $Na_V1.7$-W1538R. **(E, F)** Lidocaine additionally hyperpolarizes the voltage-dependence of slow-inactivation of both $Na_V1.7$-WT and $Na_V1.7$-W1538R. **(G, H)** Lidocaine also enhances the use-dependent inhibition of $Na_V1.7$-WT and $Na_V1.7$-W1538R.

analysis. The selectivity of 0.1 μM ICA-121431 was confirmed by the absence of effect on $Na_V1.7$-WT channels for any of the studied parameters (*Figure 5A,C,E,G,I*). The compound had also no effect on the voltage-dependence of activation, measured as the conductance $V_{1/2}$, of W1538R channels (*Figure 5D*) in comparison to vehicle (0.1% DMSO). However, it did significantly shift W1538R fast-inactivation (*Figure 5F*) as well as hyperpolarized the slow-inactivation $V_{1/2}$ by nearly 10 mV (*Figure 5H*), compared to vehicle. Furthermore, ICA-121431 significantly enhanced the W1538R channel use-dependence of inhibition (*Figure 5J*), indicating that the arginine residue found in the W1538R mutant confers sensitivity to ICA-121431 blocker on $Na_V1.7$ channels. The respective $V_{1/2}$s and degree of block of each $Na_V1.3$ variant in response to ICA-121431 are reported in *Table 2*.

The $Na_V1.3$-R1560W mutation does not confer lacosamide sensitivity to the channel

Since the W1538R mutation abolishes the effect of 30 μM lacosamide on $Na_V1.7$, we investigated whether the naturally occurring $Na_V1.7$-W1538 tryptophan residue contributes to differences in lacosamide's subtype selectivity. Using automated patch-clamping on the Qube and One-Way ANOVA with Dunnett's multiple comparison analysis, we tested the effect of 30 μM and 300 μM lacosamide on mutant $Na_V1.3$ channels in which the arginine residue (R1560) is substituted with a tryptophan, R1560W, to determine whether the presence of a tryptophan residue in $Na_V1.3$ can confer sensitivity to lacosamide.

At 30 μM, lacosamide failed to shift the voltage-dependence of slow-inactivation in both $Na_V1.3$-WT (*Figure 6C*) and $Na_V1.3$-R1560W channels (*Figure 6F*) compared to vehicle. Likewise, use-dependence of inhibition at 20 Hz was unaltered by the presence of 30 μM lacosamide in either variant (*Figure 6D,G*), demonstrating that a single amino acid substitution in $Na_V1.3$ channels cannot bestow pharmacological responsiveness to this therapeutic concentration of lacosamide. However, at a 10-fold increase in lacosamide concentration, the voltage-dependence of slow-inactivation of $Na_V1.3$-WT channels was hyperpolarized by 11.5 mV (*Figure 6C*), in the same range as $Na_V1.7$-WT at 30 μM (*Figure 4A*), and by 6.2 mV in the R1560W channels (*Figure 6F*) compared to vehicle. However, use-dependence of inhibition was not increased at 300 μM for either $Na_V1.3$-WT (*Figure 6E*) or R1560W (*Figure 6H*) channels from control, which is in contrast to our finding that 300 μM lacosamide significantly increased

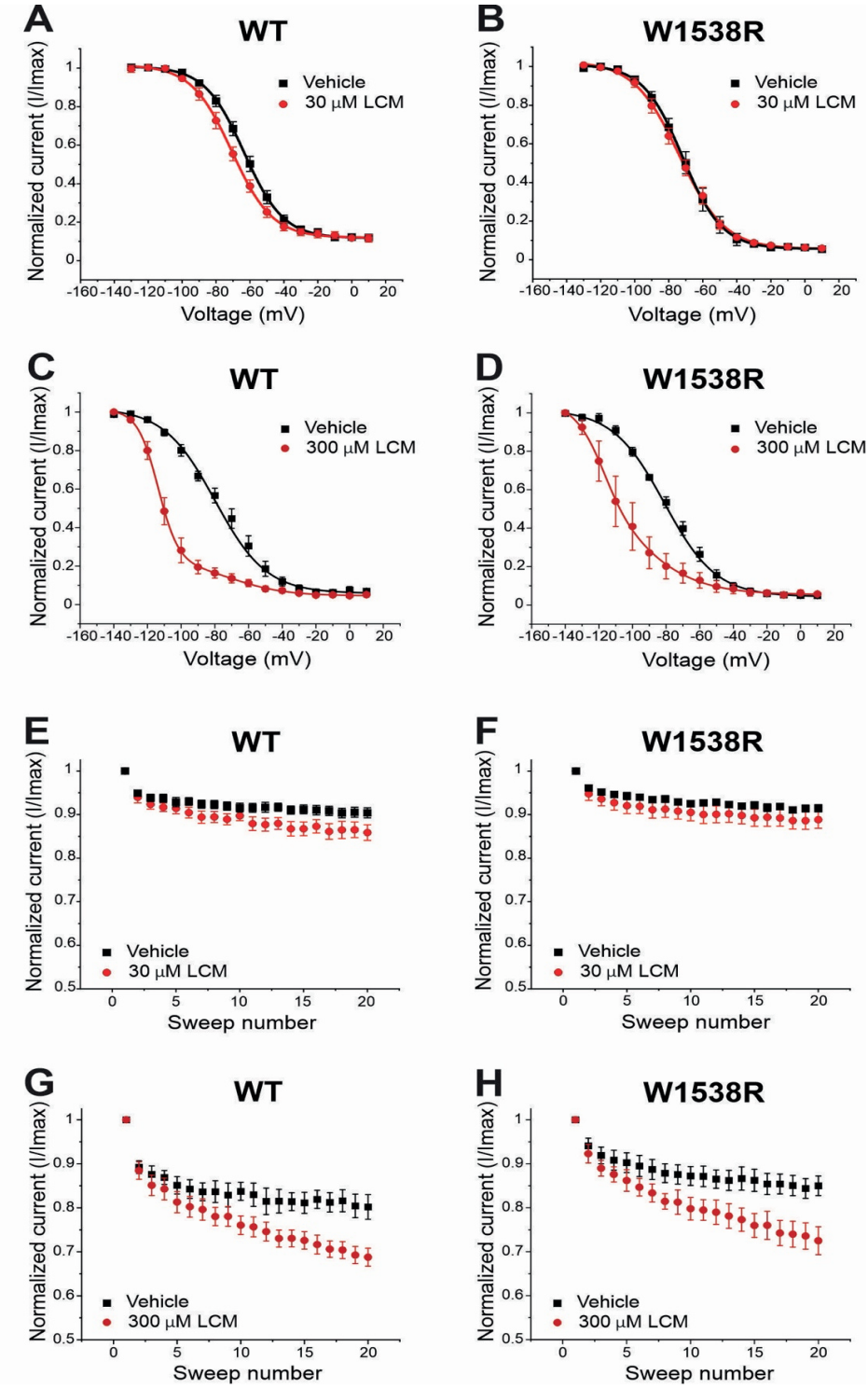
A
WT
Vehicle
30 μM LCM
Normalized current (I/Imax)
Voltage (mV)
B
W1538R
Vehicle
30 μM LCM
Normalized current (I/Imax)
Voltage (mV)
C
WT
Vehicle
300 μM LCM
Normalized current (I/Imax)
Voltage (mV)
D
W1538R
Vehicle
300 μM LCM
Normalized current (I/Imax)
Voltage (mV)
E
WT
Vehicle
30 μM LCM
Normalized current (I/Imax)
Sweep number
F
W1538R
Vehicle
30 μM LCM
Normalized current (I/Imax)
Sweep number
G
WT
Vehicle
300 μM LCM
Normalized current (I/Imax)
Sweep number
H
W1538R
Vehicle
300 μM LCM
Normalized current (I/Imax)
Sweep number

FIGURE 4 – Nav1.7-W1538R channels are inhibited after a 10-fold increase in the lacosamide therapeutic concentration. The effect of lacosamide on Nav1.7 voltage-gating properties were evaluated for **(A-D)** Voltage-dependence of slow inactivation and **(E-H)** use-dependence of inhibition at 20 Hz. The slow inactivation curves were fitted to a single Boltzmann for vehicle and 30 μM lacosamide, and to a double Boltzmann equation for 300 μM lacosamide. Cells expressing Nav1.7-WT or Nav1.7-W1538R were either treated with lacosamide at the clinically-achievable dose of 30 μM (shown in red, A, B, E, G), its 10-fold increase of 300 μM (shown in dark red, C, D, F, H), or vehicle (black; extracellular bath solution).

Nav1.7-W1538R use-dependence of inhibition (*Figure 4H*). These results suggest that the R1560 residue in Nav1.3 may contribute to the sodium channel isoform sensitivity to lacosamide, but that it is not sufficient to explain the subtype differences in lacosamide responsiveness. The slow inactivation and use-dependence values are reported in *Table 1*.

DISCUSSION

The mechanisms by which lacosamide inhibits sodium channels at clinically-achievable concentrations in an isoform-dependent manner, compared to other inhibitors in the pharmacopoeia, have long been debated and are not well understood. Existing data suggest that residues outside the pore can affect channel sensitivity to lacosamide and raise the possibility that lacosamide's effect may also be dependent on interactions with both the VSD4 and the LA binding

site in the pore-forming region of VGSCs. In the present study, we describe a new pathway for lacosamide's mechanism of action, where lacosamide requires the W1538 residue in VSD4 and an intact LA binding site to block Nav1.7 at the clinically-achievable concentration of 30 μM. The presence of an arginine residue in Nav1.7-W1538R channels does not abolish LA pore access and confers sensitivity to aryl-sulfonamide blocker ICA-121431. Conversely, the W1538 tryptophan residue does not explain lacosamide's resistance in other isoforms, specifically in Nav1.3 channels. Taken together, our results highlight the importance of the W1538 residue combined with pore accessibility in allowing 30 μM lacosamide's inhibitory effects, and suggest the contribution of W1538 for VGSC isoform-specificity.

In silico docking analysis in human Nav1.7 channels predicted a pocket that includes W1538 as the most energetically-favorable binding site to lacosamide, closely followed by the LA site in the pore (*Figure 1)*, suggesting a novel mechanism for the drug to access the pore. Previous molecular docking studies that have described lacosamide as a pore-binding ligand only studied the compound in the homotetramer bacterial VGSCs [54]. Here, we provide a new hypothesis in which both W1538 and F1737/Y1744 are necessary for lacosamide's inhibitory effect of the mammalian Nav1.7 channel, consistent with the prediction that lacosamide efficiently binds at both sites (*Figure 1C-D*). Furthermore, the structural distance between the two regions indicate that W1538R

			Nav1.7-WT	Nav1.7-W1538R
Lidocaine	Conductance $V_{1/2}$ (mV)	Vehicle	-30.83 ± 0.98, n=24	-33.08 ± 1.19, n=18
		LDC 80 μM	-30.02 ± 0.98, n=24, p=0.44	-32.6 ± 1.16, n=18, p=0.55
	Fast inactivation $V_{1/2}$ (mV)	Vehicle	-75.93 ± 0.92, n=38	-76.54 ± 1.28, n=19
		LDC 80 μM	-81.73 ± 0.94, n=38, $p=6.71e^{-13}$	-82.59 ± 1.13, n=19, $p=1.03e^{-9}$
	Slow inactivation $V_{1/2}$ (mV)	Vehicle	-60.20 ± 0.87, n=35	-61.48 ± 1.08, n=19
		LDC 80 μM	-89.92 ± 0.49, n=35 $p=6.82e^{-26}$	-89.63 ± 0.34, n=19 $p=5.73e^{-19}$
	Use-dependence of inhibition	Vehicle	0.84 ± 0.008, n=23	0.82 ± 0.01, n=14
		LDC 80 μM	0.48 ± 0.02, n = 23, $p=1.16e^{-7}$	0.45 ± 0.02, n = 14, $p=3.70e^{-5}$
ICA-121431	Activation $V_{1/2}$ (mV)	Vehicle (0.1% DMSO)	-30.35 ± 1.74, n=13	-31.48 ± 1.72, n=11
		ICA (0.1 μM)	-32.32 ± 1.90, n=9, p=0.46	-31.64 ± 1.1, n=14, p=0.94
	Fast inactivation $V_{1/2}$ (mV)	Vehicle (0.1% DMSO)	-74.13 ± 1.89, n=12	-72.99 ± 0.95, n=27
		ICA (0.1 μM)	-74.83 ± 2.07, n=12, p=0.81	-77.02 ± 0.99, n=22, p=0.0054
	Slow inactivation $V_{1/2}$ (mV)	Vehicle (0.1% DMSO)	-57.66 ±1.8, n=12	-57.25 ± 1.2, n=26
		ICA (0.1 μM)	-55.34 ± 2.3, n=9, p=0.81	-66.37 ± 1.5, n=24, p<0.0001
	Use-dependence of inhibition	Vehicle (0.1% DMSO)	0.88 ± 0.01, n=19	0.92 ± 0.009, n=30
		ICA (0.1 μM)	0.88 ± 0.01, n=19, p=0.92	0.7 ± 0.03, n=38, p<0.0001

TABLE 2 – Inhibitory effects of sodium channel blockers Lidocaine and ICA-121431 on $Na_V1.7$-WT and W1538R mutant channels. Lidocaine (LDC) blocked both $Na_V1.7$ WT and W1538R channels, by hyperpolarizing fast and slow inactivation as well as increasing use-dependence inhibition. $Na_V1.3$-selective blocker ICA-121431 (ICA) potently inhibited $Na_V1.7$-W1538R mutant channels while having no effect on $Na_V1.7$-WT channels. Treatment with ICA-121431 caused a hyperpolarizing shift in both fast and slow inactivation and increased use-dependent block of W1538R mutant channels. Like for 300 μM lacosamide, 80 μM lidocaine-induced shift in slow inactivation of both $Na_V1.7$-WT and W1538R channels was best fitted by a double Boltzmann, hence the first $V_{1/2}$ of the fit is reported in the table below, while vehicle was best fitted to a single Boltzmann. Data are presented as Means ± SEM.

is unlikely to mechanically interfere with pore binding (*Figure 1A-B*), but might impact the ability of lacosamide to utilize the nearby fenestration to reach the pore. While this in silico docking method neither allows the application of atomic forces nor considers interactions with β subunits, the model points to W1538 as a strong putative binding site for lacosamide and, combined with our previous findings [40], indicates that the W1538 residue is necessary to enable lacosamide's inhibition of $Na_V1.7$ channels. Consistent with previous studies [28, 36], we demonstrate that lacosamide interacts with the LA site, or at least requires the F1737 and Y1744 residues to exert its inhibitory effect on $Na_V1.7$ channels (*Figure 2*). These results suggest that lacosamide's mechanism of action aligns with the hypothesis that binding to the LA site may correlate with preferential binding to the fast-inactivated state but with very slow kinetics [28]. However, while an intact LA site in the pore is necessary for lacosamide's effect, it is not sufficient to explain the striking differences in gating induced by lacosamide compared to other pore-binding agents that modulate fast inactivation, nor the lack of drug sensitivity observed in Nav1.7-W1538R channels [40].The requirement for an interaction of lacosamide with W1538 in VSD4 before reaching the pore might underlie the slow kinetics of binding to the fast-inactivated state of $Na_V1.7$ channels that have been previously reported [28].

The W1538R mutation might block pore access to lacosamide or cause an allosteric effect that prevents conformational changes exposing the LA binding site in the pore where the drug needs to bind to cause its inhibitory effect. During activation, the DIV S6 segment undergoes a spatial re-arrangement from a closed to an open configuration that exposes the previously hidden F1737 residue of the LA site via asynchronous voltage sensor movements [55, 56]. However, the W1538R mutation did not prevent pore binding of lidocaine and inhibition of $Na_V1.7$ channels (80 μM, *Figure 3*). This finding aligns with a previous report showing that W1538R, together with $Na_V1.7$-Y1537S and $Na_V1.7$-D1586E, had no effect on the LA tetracaine-induced $Na_V1.7$ channel inhibition [41]. Therefore, W1538R is unlikely to prevent a conformational shift in the pore that is needed for lacosamide's inhibitory effect on VGSCs. Nonetheless, since 30 μM lacosamide does not inhibit Nav1.7-W1538R channels [40] (*Figure 4A-B, E-F*), this residue might selectively regulate the access of lacosamide but not LAs to the pore.

We further explored the role of W1538 in lacosamide inhibition of $Na_V1.7$ channels and tested the effect of a 10-fold increase in lacosamide concentration (*Figure 4*). We show that, at 300 μM, the W1538R-induced lacosamide block can be overcome, suggesting that the likelihood of lacosamide access to the pore is increased and is sufficient to rescue the inhibitory effect on the channel. This phenomenon may be explained by an allosteric W1538R-induced change in binding affinity at the pore, whereby higher concentrations of lacosamide can circumvent the need for W1538 facilitation and bind to the pore. Otherwise, the W1538 residue (alone or together with other sites) might be viewed as an initial binding site of lacosamide which may impose the slow phase of the drug's interaction with the channel, allowing an increase in the local effective concentration of the drug in the vicinity of the pore. The next phase may correspond to

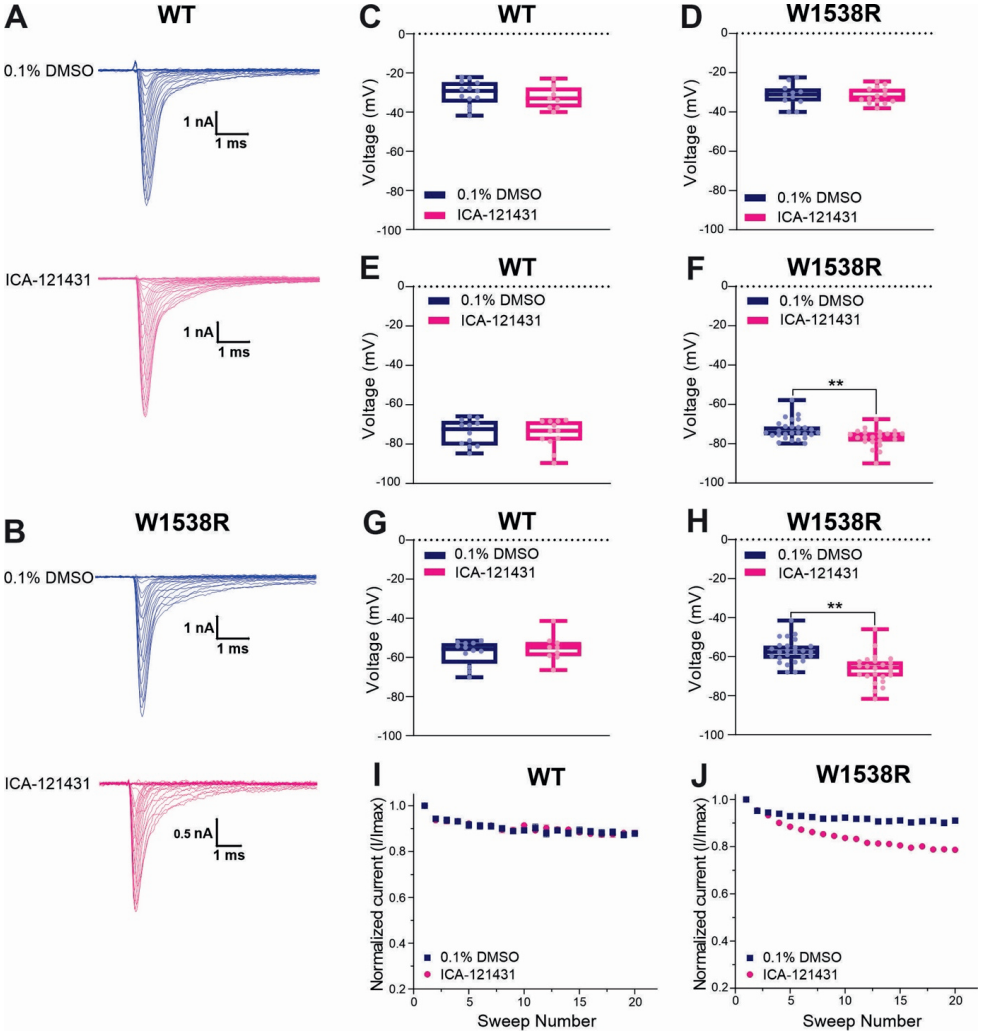

FIGURE 5 – Aryl-sulfonamide Nav1.3-selective inhibitor ICA-121431 blocks Nav1.7-W1538R mutant channels. The sodium current traces were produced using the activation protocol from $Na_V1.7$ **(A)** WT and **(B)** W1538R-expressing cells. The half-inactivation voltage ($V_{1/2}$) of **(C-D)** Activation, **(E-F)** Fast-inactivation and **(G-H)** Slow-inactivation was calculated from the Boltzmann fits and averaged for each genotype in response to 0.1 μM ICA-121431 (pink) or vehicle (0.1% DMSO in extracellular bath solution; blue). Data are shown as scatter plots and boxes at the 25 and 75th percentile of the data with medians ± min/max. P* < 0.05, P** < 0.01 The use-dependence of inhibition of **(I)** WT and the **(J)** W1538R channels in response to treatment with 0.1 μM ICA-121431 or vehicle was normalized to the first pulse and averaged across a series of twenty 20 Hz pulses. Data are shown means ± SEM. P* < 0.05, P** < 0.01

lacosamide's fast binding phase, which has been suggested to correlate with binding to partially open channels, with rapid access to the non-obstructed inner pore [28]. These

data support a role for W1538 in the slow phase at a clinically-achievable concentration. However, at 10x higher concentrations, alternative pathways may be used, where lacosamide no longer requires the integrity of W1538 to reach the pore and exert its functions.

Lacosamide's inhibition shares features of AED/LA pore-blocking drugs and the novel aryl sulfonamide blockers. The high state-dependence, the ultra-slow on-rate binding and the role of the W1538 residue in this process are features in common between VSD4 blockers (ie. ICA-121431, PF-05089771) and lacosamide, and the dependence of lacosamide's inhibition on the LA site in the pore is common with AEDs and LAs [15]. VSD4-blockers have been suggested to undergo reorientation steps and to use transitional sites, including pockets that are proximal to the S6 segment, en-route to their final position on VSD4 where they interact with the gating charges in the S4 to effect their inhibitory action, which presumably contribute to their slow rate of channel inhibition [57]. Our results suggest a working model in which lacosamide may first bind with high affinity to the W1538 residue in a pre-open state, before transiting to the LA binding site upon channel opening where it blocks the pore. Alternatively, the W1538 motif might act as an allosteric site modulating the binding affinity of lacosamide at the LA/AED pore sites F1737 and Y1444 (*Figure 7*). It is not clear whether lacosamide's first interaction with the W1538 residue or its transit to the pore causes the slow on-rate of the drug. Irrespective of this, it appears that lacosamide's effect on $Na_V1.7$ channels follows a hybrid model of interaction with VSD4 and the pore which makes it distinct from both VSD4-binders and pore-blocker inhibitors of VGSCs. Of note, $Na_V1.7$ blockers have recently been suggested to have a higher analgesic potential when acting centrally (MacDonald, et al., 2021), a proposal that contradicts efforts to develop selective compounds, such aryl sulfonamides, that are relatively CNS-impermeant. Nevertheless, while lacosamide shares features with VSD4 blockers, it is not a peripherally-restricted drug.

To further understand the similarity between lacosamide and VSD4 blockers, we assessed the role of W1538 in the response of $Na_V1.7$ channels to these blockers. We demonstrate that the W1538R mutation is sufficient to render $Na_V1.7$ channels responsive to selective $Na_V1.1$/$Na_V1.3$ blocker ICA-121431 (*Figure 5*). Our results align with previous studies showing that the W1538 residue is critical in determining VGSC sensitivity to aryl sulfonamide-based blockers [41] and show that this substitution alone leads to a significant ICA-121431-induced block. However, we did not observe that the corresponding substitution in $Na_V1.3$ (R1650W) renders these channels sensitive to lacosamide at therapeutic concentrations (*Figure 6*). These data suggest that the role of this tryptophan residue in lacosamide-induced inhibition at low concentrations appears to be isoform-dependent.

Importantly, W1538, as a moderately conserved residue, is unlikely to be the sole contributor to lacosamide's VGSC isoform selectivity. $Na_V1.1$, $Na_V1.3$, $Na_V1.5$ and $Na_V1.8$ channels might be expected to be less sensitive to lacosamide because they carry different residues at this position [57]. Evidence of lacosamide's weak inhibition of

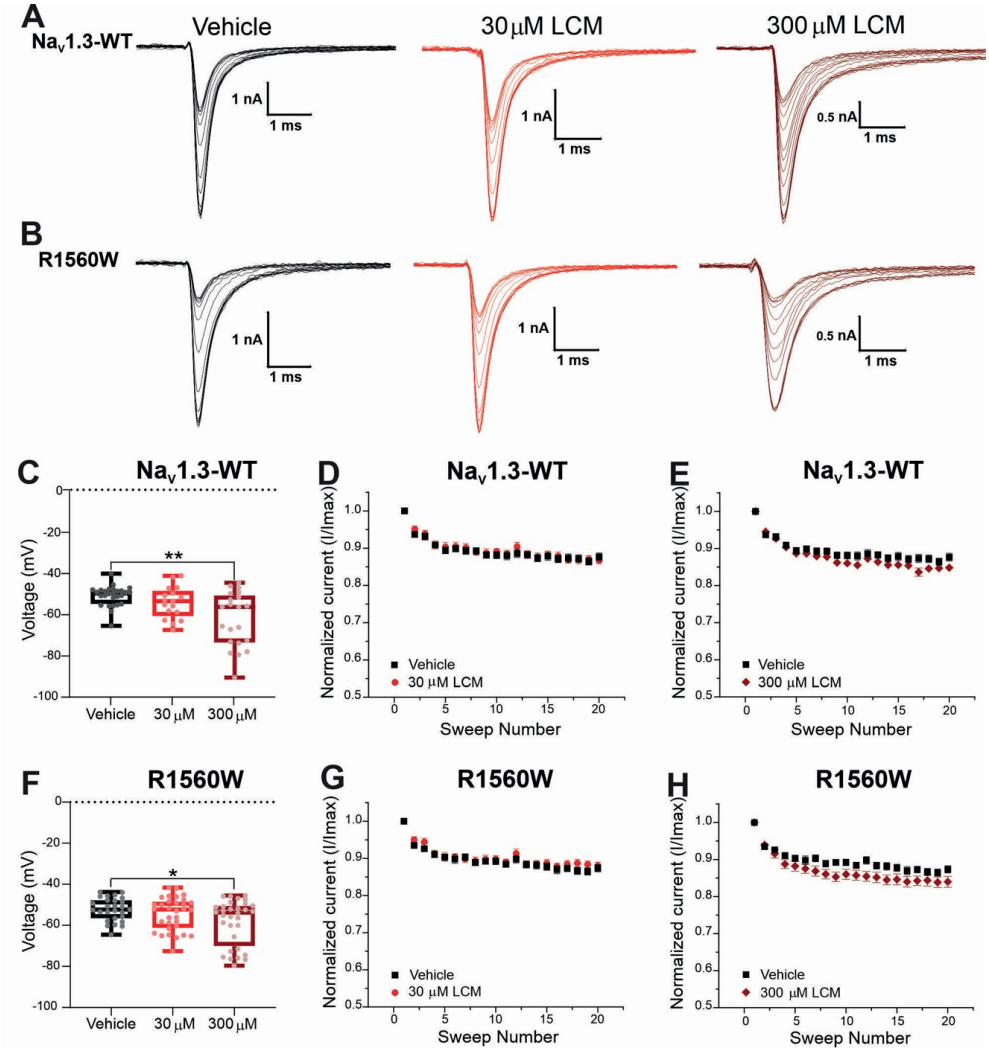

FIGURE 6 – The Nav1.3-R1560W mutation is not sufficient to confer lacosamide sensitivity to Nav1.3 channels. The R1560 residue in Nav1.3, which corresponds to the W1538R mutation in Nav1.7, was mutated from an arginine (R) to a tryptophan (W) to match the sequence of Nav1.7 WT at this site, and the responsiveness of the Nav1.3-R1560W to lacosamide was determined. **(A-B)** Representative sodium current traces were generated from the activation protocol and show Nav1.3-WT **(A)** and Nav1.3-R1560W **(B)** currents in response to vehicle (black), 30 μM (red) and 300 μM (dark red) lacosamide. Dose-dependent effects of 30 μM and 300 μM lacosamide were measured for **(C,F)** slow-inactivation and **(D-E,G-H)** use-dependence of inhibition at 20 Hz for human Nav1.3-WT and Nav1.3-R1560W channels using an automated electrophysiology platform (Qube 384, Sophion Bioscience). **(C,F)** Data are shown as individual scattered points and boxes at the 25 and 75th percentile of the data with medians ± min/max. Significance was evaluated with One-way ANOVA. P* < 0.05, P** < 0.01. **(C-F)** Data are shown as the averaged current normalized to the first pulse.

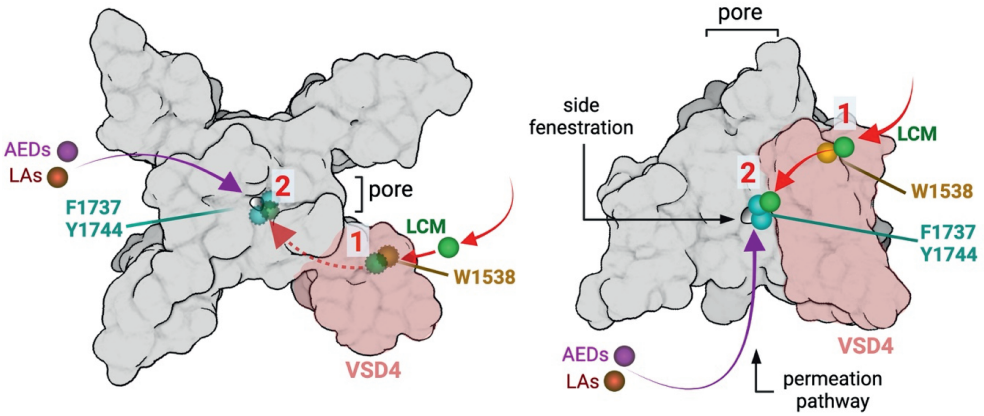

FIGURE 7 – Working hypotheses of lacosamide binding mechanisms. Schematic representation of the Nav1.7 channel showing lacosamide (LCM; green) binding residues W1538 (shown in gold) and LA binding pore residues F1737 and Y1444 (shown in cyan). The left panel shows the Nav1.7 channel visualized from the top, where, in order to reach the pore, lacosamide may first bind to the W1538 region in VSD4 (shaded in pink), before accessing the pore through the side fenestration where it exerts its inhibitory effects (not visible from the top, visualizable with dotted lines). This process would differ from typical AEDs (magenta) and LAs (red) that can reach the pore without an interaction with the W1538 residue. Alternatively, the W1538 residue might represent an allosteric site modulating lacosamide binding affinity to F1737 and Y1444 in the pore. After coming into contact with the VSD4, in the W1538 vicinity, lacosamide is able to access the pore and tightly bind to LA-binding residues. The right panel represents the Nav1.7 channel from the side, top down, and shows the suggested path lacosamide may take through the pore's side fenestration via the W1538 residue or directly to the pore after some molecules become W1538-bound.

Nav1.3 and Nav1.5 is well-documented [25, 36]. Interestingly, the fact that Nav1.3-R1650W channels are not inhibited by 30 μM lacosamide, and the ability to rescue lacosamide inhibition of resistant channels at 300 μM of Nav1.7-W1538R (*Figure 4*), and both Nav1.3 (*Figure 6*) and Nav1.5 channels [25, 36], suggests a different pathway for lacosamide to access the pore in the more resistant channel isoforms.

In conclusion, this study presents the W1538 residue as necessary for the initial binding of lacosamide to the Nav1.7 channel, facilitating its access to the channel's pore at therapeutic concentrations. The mechanistic differences between lacosamide, LAs, and conventional AEDs may be explained by the W1538 residue's participation in lacosamide's slow binding. Furthermore, our results suggest that while the W1538 residue is necessary to confer lacosamide sensitivity on Nav1.7 channels, it is not sufficient to explain the molecular basis for lacosamide-resistant isoforms, suggesting the presence of additional molecular determinants for the drug sensitivity. A better understanding of the hybrid mechanism of inhibition of Nav1.7 by therapeutically-achievable concentrations of lacosamide might lead to more selective and effective VGSC blockers.

REFERENCES

1. Reid, K.J., et al., *Epidemiology of chronic non-cancer pain in Europe: narrative review of prevalence, pain treatments and pain impact.* Curr Med Res Opin, 2011. **27**(2): p. 449-62.
2. Kennedy, J., et al., *Prevalence of persistent pain in the U.S. adult population: new data from the 2010 national health interview survey.* J Pain, 2014. **15**(10): p. 979-84.
3. McCarberg, B.H. and R. Billington, *Consequences of neuropathic pain: quality-of-life issues and associated costs.* Am J Manag Care, 2006. **12**(9 Suppl): p. S263-8.
4. Ballantyne, J.C. and S.K. LaForge, *Opioid dependence and addiction during opioid treatment of chronic pain.* Pain, 2007. **129**(3): p. 235-255.
5. Menefee, L.A., et al., *Self-reported sleep quality and quality of life for individuals with chronic pain conditions.* Clin J Pain, 2000. **16**(4): p. 290-7.
6. Breivik, H., et al., *Survey of chronic pain in Europe: prevalence, impact on daily life, and treatment.* Eur J Pain, 2006. **10**(4): p. 287-333.
7. Hojsted, J. and P. Sjogren, *Addiction to opioids in chronic pain patients: a literature review.* Eur J Pain, 2007. **11**(5): p. 490-518.
8. Tunks, E.R., J. Crook, and R. Weir, *Epidemiology of chronic pain with psychological comorbidity: prevalence, risk, course, and prognosis.* Can J Psychiatry, 2008. **53**(4): p. 224-34.
9. Nishikawa, N. and M. Nomoto, *Management of neuropathic pain.* J Gen Fam Med, 2017. **18**(2): p. 56-60.
10. Finnerup, N.B., et al., *Pharmacotherapy for neuropathic pain in adults: a systematic review and meta-analysis.* Lancet Neurol, 2015. **14**(2): p. 162-73.
11. Theile, J.W. and T.R. Cummins, *Recent developments regarding voltage-gated sodium channel blockers for the treatment of inherited and acquired neuropathic pain syndromes.* Front Pharmacol, 2011. **2**: p. 54.
12. Dib-Hajj, S.D., et al., *Voltage-gated sodium channels in pain states: role in pathophysiology and targets for treatment.* Brain Res Rev, 2009. **60**(1): p. 65-83.
13. Dib-Hajj, S.D. and S.G. Waxman, *Sodium Channels in Human Pain Disorders: Genetics and Pharmacogenomics.* Annu Rev Neurosci, 2019.
14. Alsaloum, M., et al., *Status of peripheral sodium channel blockers for non-addictive pain treatment.* Nat Rev Neurol, 2020. **16**(12): p. 689-705.
15. McKerrall, S.J. and D.P. Sutherlin, *Nav1.7 inhibitors for the treatment of chronic pain.* Bioorg Med Chem Lett, 2018. **28**(19): p. 3141-3149.
16. Wymer, J.P., et al., *Efficacy and safety of lacosamide in diabetic neuropathic pain: an 18-week double-blind placebo-controlled trial of fixed-dose regimens.* Clin J Pain, 2009. **25**(5): p. 376-85.
17. Shaibani, A., et al., *Lacosamide in painful diabetic neuropathy: an 18-week double-blind placebo-controlled trial.* J Pain, 2009. **10**(8): p. 818-28.
18. Ziegler, D., et al., *Efficacy and safety of lacosamide in painful diabetic neuropathy.* Diabetes Care, 2010. **33**(4): p. 839-41.
19. McCleane, G., B. Koch, and C. Rauschkolb, *Does SPM 927 have an analgesic effect in human neuropathic pain? An open label study.* Neurosci Lett, 2003. **352**(2): p. 117-20.
20. de Greef, B.T.A., et al., *Lacosamide in patients with Nav1.7 mutations-related small fibre neuropathy: a randomized controlled trial.* Brain, 2019. **142**(2): p. 263-275.
21. Carona, A., et al., *Pharmacology of lacosamide: From its molecular mechanisms and pharmacokinetics to future therapeutic applications.* Life Sci, 2021. **275**: p. 119342.
22. Errington, A.C., et al., *Seeking a mechanism of action for the novel anticonvulsant lacosamide.* Neuropharmacology, 2006. **50**(8): p. 1016-29.
23. Errington, A.C., et al., *The investigational anticonvulsant lacosamide selectively enhances slow inactivation of voltage-gated sodium channels.* Mol Pharmacol, 2008. **73**(1): p. 157-69.
24. Niespodziany, I., et al., *Comparative study of lacosamide and classical sodium channel blocking antiepileptic drugs on sodium channel slow inactivation.* J Neurosci Res, 2013. **91**(3): p. 436-43.

25. Sheets, P.L., et al., *Differential block of sensory neuronal voltage-gated sodium channels by lacosamide [(2R)-2-(acetylamino)-N-benzyl-3-methoxypropanamide], lidocaine, and carbamazepine.* J Pharmacol Exp Ther, 2008. **326**(1): p. 89-99.
26. Wang, Y., et al., *Development and characterization of novel derivatives of the antiepileptic drug lacosamide that exhibit far greater enhancement in slow inactivation of voltage-gated sodium channels.* ACS Chem Neurosci, 2011. **2**(2): p. 90-106.
27. Rogawski, M.A., et al., *Current understanding of the mechanism of action of the antiepileptic drug lacosamide.* Epilepsy Res, 2015. **110**: p. 189-205.
28. Jo, S. and B.P. Bean, *Lacosamide Inhibition of Nav1.7 Voltage-Gated Sodium Channels: Slow Binding to Fast-Inactivated States.* Mol Pharmacol, 2017. **91**(4): p. 277-286.
29. Lipkind, G.M. and H.A. Fozzard, *Molecular model of anticonvulsant drug binding to the voltage-gated sodium channel inner pore.* Mol Pharmacol, 2010. **78**(4): p. 631-8.
30. Lipkind, G.M. and H.A. Fozzard, *Molecular modeling of local anesthetic drug binding by voltage-gated sodium channels.* Mol Pharmacol, 2005. **68**(6): p. 1611-22.
31. Ragsdale, D.S., et al., *Common molecular determinants of local anesthetic, antiarrhythmic, and anticonvulsant block of voltage-gated Na+ channels.* Proc Natl Acad Sci U S A, 1996. **93**(17): p. 9270-5.
32. Liu, H., et al., *Mutations in cardiac sodium channels: clinical implications.* Am J Pharmacogenomics, 2003. **3**(3): p. 173-9.
33. Yang, Y.C., C.S. Huang, and C.C. Kuo, *Lidocaine, carbamazepine, and imipramine have partially overlapping binding sites and additive inhibitory effect on neuronal Na+ channels.* Anesthesiology, 2010. **113**(1): p. 160-74.
34. Nau, C. and G.K. Wang, *Interactions of local anesthetics with voltage-gated Na+ channels.* J Membr Biol, 2004. **201**(1): p. 1-8.
35. Kuo, C.C., *A common anticonvulsant binding site for phenytoin, carbamazepine, and lamotrigine in neuronal Na+ channels.* Mol Pharmacol, 1998. **54**(4): p. 712-21.
36. Wang, G.K. and S.Y. Wang, *Block of human cardiac sodium channels by lacosamide: evidence for slow drug binding along the activation pathway.* Mol Pharmacol, 2014. **85**(5): p. 692-702.
37. Stevens, M., S. Peigneur, and J. Tytgat, *Neurotoxins and their binding areas on voltage-gated sodium channels.* Front Pharmacol, 2011. **2**: p. 71.
38. Cregg, R., et al., *Novel mutations mapping to the fourth sodium channel domain of Nav1.7 result in variable clinical manifestations of primary erythromelalgia.* Neuromolecular Med, 2013. **15**(2): p. 265-78.
39. Eijkenboom, I., et al., *Yield of peripheral sodium channels gene screening in pure small fibre neuropathy.* J Neurol Neurosurg Psychiatry, 2019. **90**(3): p. 342-352.
40. Labau, J.I.R., et al., *Differential effect of lacosamide on Nav1.7 variants from responsive and non-responsive patients with small fibre neuropathy.* Brain, 2020. **143**(3): p. 771-782.
41. McCormack, K., et al., *Voltage sensor interaction site for selective small molecule inhibitors of voltage-gated sodium channels.* Proc Natl Acad Sci U S A, 2013. **110**(29): p. E2724-32.
42. Jo, S. and B.P. Bean, *Lidocaine Binding Enhances Inhibition of Nav1.7 Channels by the Sulfonamide PF-05089771.* Mol Pharmacol, 2020. **97**(6): p. 377-383.
43. Theile, J.W., M.D. Fuller, and M.L. Chapman, *The Selective Nav1.7 Inhibitor, PF-05089771, Interacts Equivalently with Fast and Slow Inactivated Nav1.7 Channels.* Mol Pharmacol, 2016. **90**(5): p. 540-548.
44. Yang, Y., et al., *Nav1.7-A1632G Mutation from a Family with Inherited Erythromelalgia: Enhanced Firing of Dorsal Root Ganglia Neurons Evoked by Thermal Stimuli.* J Neurosci, 2016. **36**(28): p. 7511-22.
45. Panigel, J. and S.P. Cook, *A point mutation at F1737 of the human Nav1.7 sodium channel decreases inhibition by local anesthetics.* J Neurogenet, 2011. **25**(4): p. 134-9.
46. Qian, B., S.H. Park, and W. Yu, *Screening Assay Protocols Targeting the Nav1.7 Channel Using Qube High-Throughput Automated Patch-Clamp System.* Curr Protoc Pharmacol, 2020. **89**(1): p. e74.

47. Cawello, W., *Clinical pharmacokinetic and pharmacodynamic profile of lacosamide.* Clin Pharmacokinet, 2015. **54**(9): p. 901-14.
48. Sherman, A.J., A. Shrier, and E. Cooper, *Series resistance compensation for whole-cell patch-clamp studies using a membrane state estimator.* Biophys J, 1999. **77**(5): p. 2590-601.
49. Shen, H., et al., *Structures of human Nav1.7 channel in complex with auxiliary subunits and animal toxins.* Science, 2019. **363**(6433): p. 1303-1308.
50. Sterling, T. and J.J. Irwin, *ZINC 15--Ligand Discovery for Everyone.* J Chem Inf Model, 2015. **55**(11): p. 2324-37.
51. Chevrier, P., K. Vijayaragavan, and M. Chahine, *Differential modulation of Nav1.7 and Nav1.8 peripheral nerve sodium channels by the local anesthetic lidocaine.* Br J Pharmacol, 2004. **142**(3): p. 576-84.
52. Sheets, P.L., B.W. Jarecki, and T.R. Cummins, *Lidocaine reduces the transition to slow inactivation in Na(v)1.7 voltage-gated sodium channels.* Br J Pharmacol, 2011. **164**(2b): p. 719-30.
53. Wang, Y., et al., *Comparison of Gating Properties and Use-Dependent Block of Nav1.5 and Nav1.7 Channels by Anti-Arrhythmics Mexiletine and Lidocaine.* PLoS One, 2015. **10**(6): p. e0128653.
54. Tikhonov, D.B. and B.S. Zhorov, *Mechanism of sodium channel block by local anesthetics, antiarrhythmics, and anticonvulsants.* J Gen Physiol, 2017. **149**(4): p. 465-481.
55. Goldschen-Ohm, M.P., et al., *Multiple pore conformations driven by asynchronous movements of voltage sensors in a eukaryotic sodium channel.* Nat Commun, 2013. **4**: p. 1350.
56. Pless, S.A., et al., *Molecular basis for class Ib anti-arrhythmic inhibition of cardiac sodium channels.* Nat Commun, 2011. **2**: p. 351.
57. Corry, B., *Physical basis of specificity and delayed binding of a subtype selective sodium channel inhibitor.* Sci Rep, 2018. **8**(1): p. 1356.


3

NOVEL STRATEGIES FOR DERIVING FUNCTIONAL IPSC-NOCICEPTORS

Part 3

CHAPTER 4

Targeted *in vivo* and *ex vivo* differentiation of human iPSCs in rat dorsal root ganglions

In preparation:

Labau, J. I. R; Carrara, J; Zhao, P; Zwinger, P. J; Liu, S; Alsaloum, M., Smeets, H. J. M, Dib-Hajj, S., Waxman, SG. Targeted *in vivo* and *ex vivo* differentiation of human iPSCs in rat dorsal root ganglions

ABSTRACT

Neuropathic pain affects a wide range of the global population and is confronted by largely unmet therapeutic needs. Developing models that can accurately recapitulate the clinical phenotype is crucial to better understand underlying pathophysiological mechanisms and find adapted treatments. Current heterologous cell and animal models have been limited and criticized for their inability to reproduce the core composition and functions of human organs. However, the limited availability of post-mortem tissue, in particular dorsal root ganglions, has prevented further research in human cells. Human induced-pluripotent stem cells (iPSC) have emerged as an exciting platform to study patient-specific diseases. Stem cell-derived sensory neurons have provided new avenues into elucidating unknown peripheral mechanisms and identifying both personalized treatments and novel compounds via high-throughput screening. Nevertheless, reprogramming and differentiation protocols to obtain nociceptors have mostly yielded immature, homogenous cell populations. To close the gap between native human tissue and iPSCs, we developed a model based on the influence of the dorsal root ganglia microniche to induce cellular differentiation and provide cells with the full spatiotemporal context and nutrients needed for acquiring a mature phenotype. Using two different approaches, we grafted undifferentiated iPSCs tagged with green fluorescence into immunosuppressed juvenile rats and allowed the cells to mature *in vivo* for up to 4 weeks. Concomitantly, we injected iPSCs, pre-differentiated into neural precursors, *in vivo* and in the excavated ganglions of neonatal rats *ex vivo* while optimizing DRG growth conditions via different culture strategies. In both studies, we reported limited cell survival and differentiation into neuronal-like cells. Furthermore, xeno-transplanted undifferentiated iPSCs showed high proliferative potential that segregated into the formation of a large growth, suggesting tumorigenesis. These results demonstrated the capacity of cells with undetermined fate to maintain pluripotency *in vivo*. Nevertheless, in both models, we observed clusters of GFP-expressing cells with a neuronal morphology. However, the lack of immunoreactivity with canonical neuronal markers underlined their insufficient maturity and their need for further differentiation to improve their surrogacy as human neurons.

INTRODUCTION

Painful neuropathy affects a large part of the world population and is often associated with unclear etiology and limited symptomatic relief to currently available treatments [1-3]. Furthermore, important inter-individual variation in pain perception and drug response makes the search for a cure cumbersome [4, 5]. The pathological mechanisms are commonly associated with dysfunctional dorsal root ganglia (DRG)-expressing voltage-gated sodium channels (VGSC) and cellular hyperexcitability [6-8]. However, current *in vitro* and *in vivo* models have failed to accurately portray the full phenotype, which hinders analgesic development, underscoring the need for better tools to solve clinical pain. In general, creating models for mendelian genetic diseases has been a particularly tedious task, due for instance to off-target effects, even using state-of-the-

art gene editing technologies, or to unmatched cellular or tissue phenotypes from those observed in patients. Hence, there is still an unmet need for developing cellular systems mimicking those in physiological conditions.

Ex vivo cellular nucleofection of mutant sodium channels into heterologous expression systems including Human Embryonic Kidney (HEK293) cells and DRG neurons has helped establish the pathogenic potential of these mutations and suggested a genotype-phenotype correlation for VGSC variants [9-14]. However, transfected cells are limited to the sole expression of the channel and genetic variant of interest, of which physiological levels of expression cannot be controlled. Furthermore, recordings of human DRGs have demonstrated significant differences in their excitability and biophysical characteristics compared to rat DRGs [15, 16], which prevents the extrapolation of data from animal cells to humans and thus, their translation to the clinic.

The development of a cell-based system that overcomes these limitations can markedly advance the field. Human induced-pluripotent stem cells (iPSCs) have the capacity to preserve the donor's genetic background and transcriptional machinery throughout differentiation [17]. Additionally, being patient-specific, the cells already selectively express the genetic variant of interest, at physiological levels. Recently, utilizing whole-exome sequencing and dynamic clamp technology, *in vitro* analysis of iPSC-derived sensory neurons (iPSC-SNs) from two families with inherited erythromelalgia (IEM), carrying the same disease-causing $Na_V1.7$ mutation, but with different pain profiles, not only recapitulated the parent-child differences in pain phenotypes, but also pinpointed variants in potassium channels that explained at least some of the families' inter-individual differences in pain sensitivity [5, 18]. These findings have highlighted the ability to model pain resiliency "in-a-dish" using patient-specific iPSC-SNs and to recapitulate important aspects of the clinical phenotypes.

Nonetheless, several challenges for using iPSC-SNs *in vitro* remain to be overcome. Current *in vitro* differentiation protocols induce neurons that lack expression of the full complement of VGSCs that are found in mature adult DRG [19-21]. As a result, the overall electro-responsiveness and excitability are predicted to be altered when other ion channels are missing [22]. Furthermore, differentiated cells lack essential proteins required for sensory neurogenesis [23]. This incomplete differentiation might result from the lack of ligands in the media to activate appropriate signaling cascades and the absence of cell-to-cell interaction with normal constituents of the native DRG tissue [24], which can only be provided by the organ's microniche [25, 26]. Indeed, nociception requires neurons to act in concert with various cell types for physiological pain functions. As such, providing the endogenous spatiotemporal context, including critical nutrients and cellular
interactions, lacking from *in vitro* cultures, may provide signaling cues necessary for sensory neurons to reach their final mature state and express the full protein range. Interactions within the microenvironment have been demonstrated to have substantial effects on transplanted iPSCs' maturation [25]. For instance, *in vivo* differentiated

iPSC-derived cardiac cells, grafted in rodents, have been shown to acquire expression of additional proteins specific to adult cardiomyocytes, compared to *in vitro*-differentiated iPSCs and at similar levels to native cells [26]. Therefore, organ-directed injection of human iPSCs could resolve a major limitation of *in vitro* models that lack expression of crucial proteins and allow the formation of neurons delineating a complete phenotype.

Targeting the DRG has provided promising therapeutic avenues in degenerative diseases such as Friedreich's Ataxia (FRDA) [27] and has been highly informative on the cells' capacity to expand, survive and differentiate *in vivo*. Viventi et al. and Xiao et al. are amongst the first to ever attempt DRG injection of human GFP-labelled iPSC-SNs in rodents [27, 28]. In both studies, *ex vivo* [28] and *in vivo* [27] transplanted cells showed high survival and yielded heterogenous neuron populations. Nonetheless, functional electrogenic profile and heterogeneity within-nociceptive subtypes was not reported. Furthermore, expression of missing VGSC and other critical proteins were not retrieved in these studies, as cells may require interactions from an earlier developmental stage. Injection of undifferentiated iPSCs have been highlighted to promote neuronal differentiation in the mouse brain in region-specific patterns [25]. Hence, targeted DRG graft of undifferentiated cells may bridge the gap towards mature neurons by providing the necessary nutrients and cellular interactions, prior to cell fate determination.

In this study, we investigated the behavior of transplanted human iPSCs in the rat DRG *in vivo* and *ex vivo* and assessed the potential of undifferentiated and pre-differentiated neural precursors cells (NPCs) to survive, differentiate and recover full protein expression. Using GFP-expressing iPSCs, we showed the ability of the cells to proliferate *in vivo* at different stages post-graft. Furthermore, undifferentiated iPSCs maintained their pluripotency *in vivo* and likely induced teratogenesis. However, the cells did not differentiate into sensory cells of either neuronal or glial lineage. Nevertheless, evoked differentiation into NPCs prevented tumor formation and promoted neuronal morphology *in vivo* and *ex vivo*.

METHODS

MATERIALS

GFP-iPSC line

A green fluorescent protein (GFP)-tagged iPSC cell line, *WTC-mEGFP-AAVS1-cl6 (monoallelic tag),* from the Allen Institute for Cell Science (Coriell, AICS-0036-006) was used to evaluate iPSC *in vivo* differentiation into functional sensory neurons. The line was derived from the WTC parental line AICS-0 at passage 33 (Coriell, GM25256), obtained from fibroblasts and reprogrammed using episomal vectors (OCT3/4, shp53, SOX2, KLF4, LMYC, and LIN28), as described [29]. To minimize the risk of GFP silencing, the cell line was selected to incorporate GFP expression within the adeno-associated virus integration site 1 (AAVS1) safe-harbor locus, demonstrated to have

robust and stable expression for at least 7 weeks *in vivo* and *in vitro* [30]. Briefly, a fluorescent reporter cassette was inserted into AAVS1, within the PPP1R12C intron, using transcription activator-like effector nucleases (TALENs). The TALENs generated a double-stranded DNA break, allowing initiation of homologous repair machinery. The GFP vector, comporting a splicing-acceptor, 2A self-cleaving peptide restricted puromycin gene expression to the targeted-integration site, while a chicken β-actin globin (CAG) promoter in targeted cells drove fluorescence expression (*Figure S1A*). Puromycin-resistant iPSC showing persistent transgene expression were selected [30].

Cyclosporine A

To prevent graft rejection following human cell xenotransplantation, animals received 15mg/kg/day of cyclosporin A, USP (50 mg/mL; Perrigo) diluted in saline solution (0.9% NaCl), starting 24h before surgery until the day they were euthanized for tissue collection [31, 32]. Compound delivery was either carried out via daily subcutaneous injection or consistently perfused through an osmotic pump (2ML4, Alzet®), inserted under the skin, below the neck, and performed at the same time as DRG injections to minimize stress. The pumps were weighted before insertion and after euthanasia to ensure functioning of the pump. The pumps were pre-filled 24h prior surgery and placed at 37°C overnight to initiate drug release, as per manufacturer's instructions.

Antibodies

The antibodies used for immunohistochemistry and immunocytochemistry were as follows, primary antibodies: mouse monoclonal anti-human nuclear antigen (hNu) antibody [235-1] (Abcam, ab191181), mouse monoclonal anti-NeuN (Abcam, ab104224), chicken polyclonal anti-peripherin (PER7857983, Aves Labs), mouse monoclonal anti-S100 (Invitrogen, MA5-12969), and rabbit monoclonal anti-glial fibrillary acidic protein (GFAP) [SP78] (ThermoFisher, MA5-16367); the fluorescent labeled-secondary antibodies used were: donkey anti-chicken 594-conjugated (Jackson ImmunoResearch, lot 86803), donkey anti-rabbit Alexa Fluor 594 (Life Technologies, A21207) and donkey anti-mouse Alexa Fluor 647 (Jackson ImmunoResearch, 715-606-150).

HUMAN INDUCED - PLURIPOTENT STEM CELLS (iPSCs)

Cell maintenance

Human iPS cells *(Allen Institute for Cell Science, Coriell, AICS-0036-006)* were screened for pluripotent markers and human nucleus (*Figure S1B*). Karyotyping was performed by the manufacturer. iPSCs were passaged once a week and mTesR Plus medium (05827, StemCell Technologies, Canada) was replaced every other day, as described [5, 18]. The cells were cultured for at least 5 generations prior to being injected in rat DRGs.

iPSC differentiation

Differentiation into neural precursor cells (iPSC-NPCs) was initiated as previously described [5, 18]. Using a modified Chambers protocol [33-35], cells were exposed to

LSB and 3i inhibitors for 9-12 days, by which time neural cell fate is established [36], and maintained in KnockOut Serum Replacement (KSR) and Neurobasal Medium (NB), supplemented with N2/B27 GlutaMAX (Thermo Fisher Scientific). iPSC-NPCs that carried on to fully differentiated neurons were maintained in N2 media with four growth factors (N2+4GF) [recombinant human β nerve growth factor (NGF), brain-derived neurotrophic factor (BDNF), glial cell line-derived neurotrophic factor (GDNF), and neurotrophin-3 (NT-3; 25 μg/ml; PeproTech)] for up to 8 weeks.

ANIMALS

Animals were group-housed at an Association for Assessment and Accreditation of Laboratory Animal Committee–accredited facility, at the Veterans Administration Connecticut Healthcare System (New Haven, USA) in solid bottom polycarbonate cages with corn-cob bedding, which was removed and replenished at least once a week. Animals were maintained on a 12:12 hour light:dark cycle, at humidity 50 ± 20 % and temperature 21 ± 3˚C, and had access to an enriched environment with pelleted food (Teklad 2018; Envigo, Madison, WI) and water *ad libitum*. Cyclosporin A-induced immunodeficiency was initiated one day prior to surgery and adult rats were placed in sterile housing (2-3/cage), whereby cages, water bottles, food and bedding were autoclaved at 134°C. All animal procedures were approved by the Institutional Animal Care and Use Committee (IACUC) of the Veterans Administration Connecticut Healthcare System. Animal groups were identified by using a permanent marker, applied daily. Sham animals were kept separately from iPSC animals. Male and female Juvenile Sprague-Dawley (SD) rats (5 to 7 weeks old, 144-257g), obtained from Envigo, were used for undifferentiated and pre-differentiated iPSC *in vivo* differentiation. Neonatal SD rats (1-5 days post-partum) of both sexes were used for iPSC-NPC *ex vivo* differentiation in DRG explants.

DRG INJECTION

In accordance with compiled *in vivo* stem cell research [25, 37-41], approximately 3-5μL of 1,000-30,000 cells/μL, or an average of ~100,000 undifferentiated iPSCs and ~20,000 iPSC-NPCs were injected into the L4 DRG of juvenile SD rats (*Supplementary methods*). iPSCs were diluted in DMEM/F12 or mTeSR Plus at RT, and iPSC-NPCs in N2 + 4GF, filtered through a 70 μM nylon mesh strainer (Becton Dickinson), centrifuged at 500 RPM and resuspended 5 min prior to each injection. The cells were kept on ice before administration. Non-injected cells were immediately counted and replated in Matrigel-coated plates to assess survival.

Pre-operative care

Complete aseptic conditions were used throughout the surgery. All surgical instruments, gloves, and cotton buds were autoclaved at 134°C; the operation table and microscope were cleaned with 70% ethanol, prior to each surgical intervention. Animals were deeply anesthetized with 0.1ml/100g (80/5 mg/kg, i.p.) ketamine/xylazine, supplemented with 3% isoflurane, 0.5-1.5% oxygen and 300 air flow, as needed, to complete the surgery. Concentration was adjusted based on the

animal breathing pattern to avoid over- or under-dosing. Animals were placed on top of a heating pad at 37 °C to prevent hypothermia, and ophthalmologic ointment was applied to both eyes to avoid corneal drying. Pre-operative weight was registered, and the back shaved. The shaved area was disinfected with Betadine (Povidone-iodine) and 70% ethanol.

Surgery and injection

Partial laminectomy to expose the right L4 DRG was performed as described [42]. Before incising the skin, T12 was located by feeling the spinous processes over the skin, corresponding to the end of the thoracic cavity. From there, the L4 DRG locates between L4 and L5, five vertebrae prominences down from T12. A skin incision was made between L2 and S1 with a n. 10 scalpel blade. A similar sized incision was performed on the superficial layer of muscle, along the white midline. An additional cut was made immediately left to the vertebrae on the deeper, second layer of muscle. Using bent forceps (curettes), the muscle was gently removed from the bone of the vertebrae until the vertebrae ailerons were fully exposed. A hemi-laminectomy was performed on the L4-S1 vertebrae using a pair of rongeurs. Once the L4 DRG was appropriately exposed, the iPSC solution was added to a syringe fitted with a 33-gauge blunt needle. The needle was left in for one minute after perforation of the DRG, before slowly injecting the solution. The needle was withdrawn after an additional 60 seconds. The deeper and artificial layers of muscle were loosely closed by interrupted sutures using absorbable 6.0 suture material (polypropylene), starting with the deep layer, and followed by the more artificial layer. The skin was sutured with absorbable 4-0 suture material. In case of hemorrhage, bleeding was stopped using sterilized cotton buds, and subcutaneously injected with an additional 1-2 mL of saline to compensate the loss of fluid.

Post-operative care

Animals were placed on a heating pad, in a clean autoclaved cage with soft cotton bedding, food and water *ad libitum*, and were regularly monitored for at least 1h post-surgery before returning to the animal facility. To promote recovery, the animals were placed at maximal capacity of two per cage for at least a week following surgery. Animal health state was monitored daily and checked for abnormal growth formation and/or pain behaviors (i.e. hunched back, grimacing, reduced grooming). Animals showing signs of infection, severe discomfort, distress, aberrant weight loss or visible tumors were subsequently euthanized. Due to the current study targeting chronic pain research, no post-operative analgesics were administrated. Signs of post-operative pain-related symptoms persisting for longer than one week also resulted in euthanasia. Animals that died or were euthanized prematurely without tissue collection are not described in this study.

EUTHANASIA & TISSUE COLLECTION

Transplanted animals were anesthetized with (80/5 mg/kg, i.p.) ketamine/xylazine and euthanized by cardiac perfusion using 0.01M phosphate-buffered saline (PBS) followed by ice-cold 4% paraformaldehyde (PFA) in 0.1M phosphate buffer (ddH_2O,

1L; sodium phosphate, 2.96g; anhydrous disodium phosphate, 11.5g; pH 7.4), as described [43]. Spinal cord, ipsilateral and contralateral L3, L4, L5 and L6 DRGs were collected at 24h, 72h, two-, four- and six-weeks post-transplant. After removal, tissues were immersed in 4% PFA for 20 min and cryo-preserved in 30% sucrose in PBS at 4°C overnight. DRGs were examined under the (two-photon) fluorescent microscope to evaluate changes in DRG size, presence of cancerous lesions, and GFP expression. They were then molted into OCT (ThermoFisher Scientific, Pittsburg, PA), snap-frozen in 70% ethanol in melting dry ice and stored at -80°C for at least 24h prior to cryostat sectioning. Embedded tissue blocks were cut at 10 μm, mounted on slides (Fisher Scientific, Pittsburgh, PA), and either immediately processed for immunohistochemistry or stored at -20°C. For simple euthanasia without tissue harvest, animals were euthanized with carbon dioxide narcosis and decapitated using a rat-sized guillotine. For DRG explant collection, neonatal rats (P1-P5) were injected with ketamine/xylazine i.p. and decapitated.

DRG EXPLANT CULTURE

DRG injection explants

Quickly after euthanasia, an incision was made along the animal's back and vertebrae. A laminectomy was performed and exposed lumbar L3-L6 DRGs from both sides of the vertebrae were each injected with 1 μL of ~1,000-10,000 iPSC-NPCs in N2 + 4GFs medium. Immediately, injected lumbar DRGs were carefully dissected out and placed in cold DMEM/F12 and cleaned of meninges, blood, and roots.

Explant culture

The DRGs from the same animal were individually (max 3 per dish) planted on 35-mm glass bottom dishes (MatTek), pre-coated 2h prior with either Matrigel (in serum-free Dulbecco's modified Eagle's medium (DMEM)/F12 (1:1), Gibco™), rat-tail collagen COL IV in DMEM/F12 on poly-D-lysine/laminin (PDL/LAM) pre-coated coverslips (BD Biosciences), or PDL/LAM coverslips only, and maintained at 37°C. Explants were immersed in a 30-50 μL drop of media for 24h to prevent detachment, before slowly adding the complement 2 mL media. The medium used for explant growth were either DRG media (DMEM/F12 with penicillin (100 U/ml), streptomycin (0.1 mg/ml; Gibco), 2 mM L-glutamine (Gibco), and 10% fetal bovine serum (SH30088, Hyclone, Logan, UT), supplemented with NGF/GDNF 1:1000); Neurobasal-A (NB) media supplemented with 2% B27, 0.37% L-glutamate/ 0.25% L-glutamine, with or without NGF and/or GDNF; and serum-free DMEM/F12 media. The different culture conditions are listed in *Table 1*. The media was replaced every 48-72h for up to 4 weeks.

IMMUNOHISTOCHEMISTRY

Cryostat 10 μm tissue sections were mounted on glass microscope slides (Fisher Scientific, Pittsburgh, PA), air dried for 2h and either immediately processed for antigen detection or stored at 4°C overnight. Alternatively, sections were stored at -20°C for later use. The sectioned tissues were rehydrated using 0.01M PBS for 10 min, then incubated in blocking solution (4% normal donkey serum, 2% BSA, 0.1% Triton

X-100 in 0.01M PBS) for 1h at RT. The sections were subsequently incubated with the primary antibodies of interest in blocking solution, as follows: mouse anti-hNu (1:200), mouse anti-NeuN (1:200), chicken anti-hGFAP (1:250), mouse anti-S100 (1:100), and chicken anti-peripherin (1:1000) overnight at 4°C or 2h at RT. Sections were rinsed 3 times for 5 min with 0.01 M PBS, before incubation with the appropriate secondary antibodies (1:1000) in blocking solution for 1h at RT. The sections were further washed 3 x 5min in 0.01M PBS, stained with 4', 6-diamidino-2-phenylindole (DAPI, ThermoFisher (1:1000) in PBS) for 10 min, rinsed 3 x 5 min in PBS, then mounted on glass coverslips with mounting medium and left to dry at RT for 2h, then ON at 4°C.

IMAGING

Inverted optical microscope

Injected neonatal whole-DRG explants in culture were assessed bi-weekly under optical microscopy.

Two-photon confocal

Images from *in vivo* transplanted iPSCs and iPSC-NPCs in juvenile animals were acquired using a two-photon Nikon C1 confocal microscope. Tissue sections were imaged with a 20x air objective or a 40x water immersive objective, using the confocal acquisition settings. Collected whole DRG explant from transplanted adult rats with undifferentiated iPSCs were immersed in an optically transparent gel (GENTEAL®, lubricant eye gel) to immobilize them without altering the tissue and placed between two glue-bound coverslips. An A1RMP+ (Nikon) equipped with gallium arsenide phosphide detectors and a Chameleon Vision II (Coherent) two-photon laser, tuned to excite GFP, was used to acquire z-stack image slices in 0.5-µm steps of the whole explant, through a 25x/1.1 water immersion objective (Nikon). Stacked images with detected GFP fluorescence were pre-selected and compiled into a single plane with maximum intensity. Injected DRGs were compared to contralateral, non-injected DRGs, after adjusting threshold and subtracting background, as described [44, 45].

Spinning disk

Images of DRG explants from adult rats transplanted with iPSC-NPCs were acquired using an Andor Dragonfly spinning disk confocal microscope built on a Nikon Eclipse Ti fluorescence microscope, as described [46, 47]. Whole explants were mechanically detached by gently scraping grown extensions 3-4 weeks post-graft. DRGs (n=12) were then either enzymatically dissociated for culture (Supplementary material) or prepared for microscopy (n=7). Tissues were fixed in 4% PFA for 20 min and cryopreserved in 30% sucrose at 4°C. After at least 45 min in sucrose, the explants were placed on PDL/LAM-coated glass-bottom 35 mm dish in a clear gel (GENTEAL®, lubricant eye gel), mounted to a coverslip for imaging. Images were collected with an Andor iXon Ultra 888 EMCCD camera through a Plan Apo Lambda 60× (NA1.4) oil objective.

STATISTICAL ANALYSIS

All the acquired images were processed using FIJI (ImageJ)

RESULTS

Undifferentiated iPSCs in adult rat DRGs survived and proliferated *in vivo*

Current *in vitro* iPSC differentiation protocols are limited to homogenous, immature cultures. Recently, targeted DRG injection of iPSC-SNs for *in vivo* development has provided promising avenues, yet this methodology has failed to show a mature electrogenic profile [27]. In an effort to recapitulate *in vivo* developmental conditions from an early stage, we introduced undifferentiated iPSCs into the lumbar L4 DRG of immunosuppressed juvenile rats (n=13; *Figure 1*). Building on past findings that iPSCs in the adult mouse brain require at least four weeks to reach their fully differentiated, mature phenotype [25], we assessed the progress of transplanted cells until one-month post-graft. Human iPSCs were provided by the Allen Institute, where they were transduced to express GFP in the safe harbor locus AAVS1 of the PPP1R12C gene, allowing iPSCs to be distinguished from naive rat cells. Endogenous GFP expression was achieved in over 99% of cells and maintained throughout differentiation *in vitro* (*Figure S1, S2*), indicative of robust fluorescence without silencing. *In vitro* differentiated iPSC-SNs depicted normal biophysical properties and cellular electrophysiology (*Figure S2*).

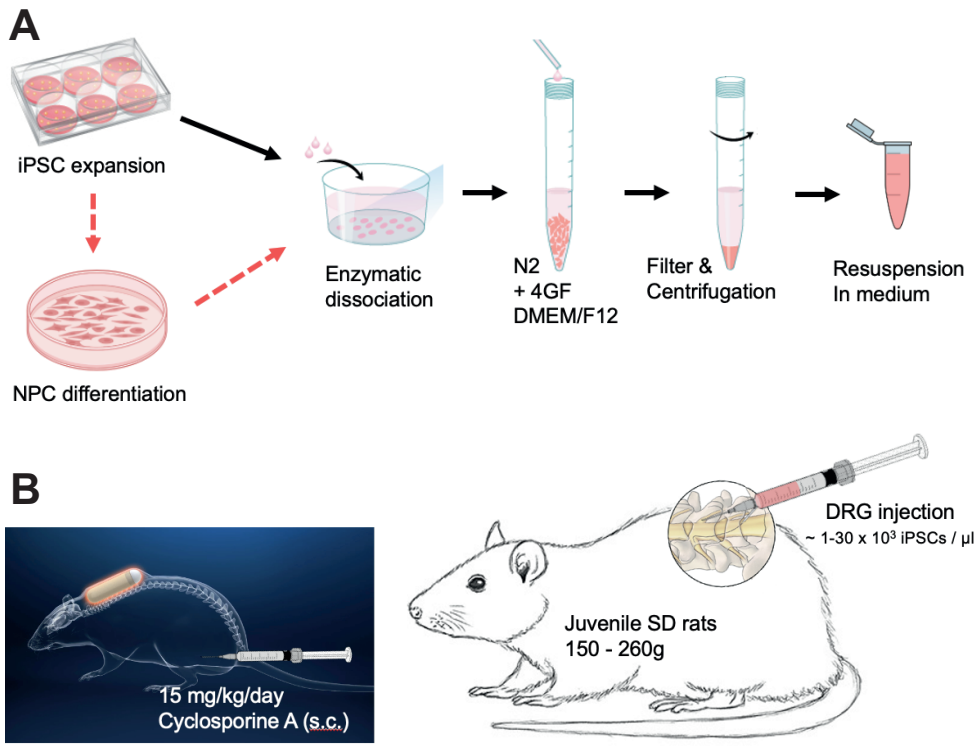

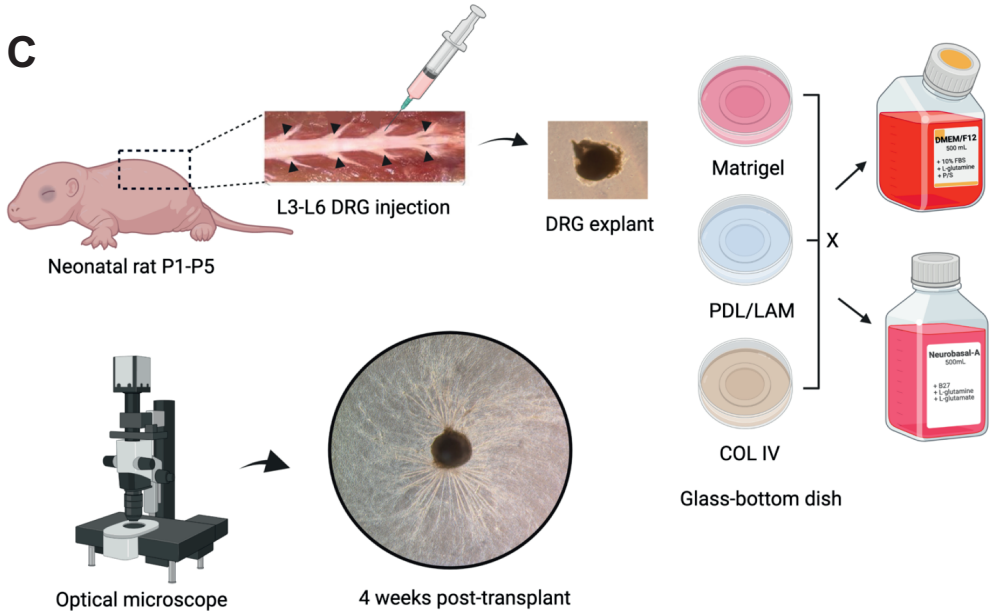

FIGURE 1 – Targeted *In vivo* and *ex vivo* differentiation of human iPSCs in rat dorsal root ganglions (DRG). (A) WTC-mEGFP-AAVS1-cl6 iPSCs were maintained as described (Methods). Undifferentiated cells were either directly prepared for DRG transplant or differentiated into NPCs. Prior to DRG injection, iPSCs were enzymatically detached with Dispase (iPSC) or TryplE (iPSC-NPC) and further mechanically dissociated into DMEM/F12 (iPSC) or N2 + 4GF (iPSC-NPCs). The cells were filtered through a 70 μM nylon mesh strainer and centrifuged. The pellet was resuspended into 1mL of the appropriate medium, counted and placed on ice until injection. **(B)** The cells were transplanted into juvenile rats, made immune-deficient by daily dosing of 15mg/kg of cyclosporine A, either subcutaneously (s.c.) injected, or perfused through an osmotic pump, inserted immediately post-transplant. A partial laminectomy was performed under sterile conditions to expose the L4 DRG, and 5μL of cells were injected. The animals were sutured, and the pump was inserted, when appropriate. iPSC and iPSC-NPC were left to differentiate for up to 6 weeks. **(C)** Neonatal rats were euthanized, and the L3 through L6 DRGs from both sides of the vertebrae were exposed. 1μL of iPSC-NPC were injected in each of the six DRGs. The explants were dissected out, cleaned in DMEM/F12 and plated onto pre-coated 35mm glass bottom dishes with either Matrigel, poly-D-lysine/laminin (PDL), and fed with neurobasal A or DRG medium for up to 4 weeks. Whole DRG explants were regularly monitored under an optical microscope to observe changes in morphology and neurite development.

Transplanted DRGs were examined under two-photon confocal microscopy to evaluate changes in DRG size, presence of cancerous lesions, as well observe endogenous GFP patterns of expression underlying iPSC survival and differentiation. Fluorescent cells were shown to cluster within the injection site after one week (*Figure 2A*), and to expand over time, forming a large GFP-positive growth within two weeks post-graft between the ganglia and its dorsal root (*Figure 2C, D*). After one month, GFP-expressing iPSCs segregated and proliferated within the bulb-shaped mass, which had at least doubled in size (*Figure 2E*) since the two-week end point (*Figure 2D*). Additionally, iPSCs developed a more cell-like shape with elongations, forming a

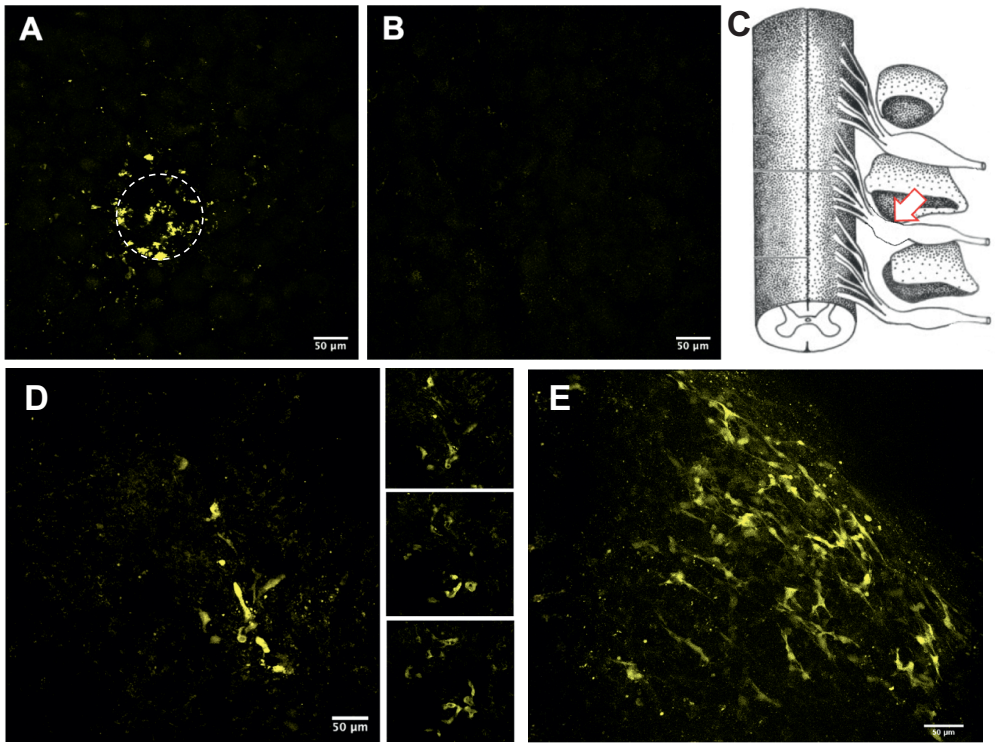

FIGURE 2 – Two-photon imaging of juvenile SD rat DRGs following injection of undifferentiated iPSCs. Xeno-transplanted DRGs were collected **(A-B)** one-, **(D)** two-, and **(E)** four-weeks after surgery. Images were obtained by compiling Z optical sections, selected for the maximal intensity at 510 nm wavelength to excite endogenous GFP fluorescence [48]. **(A)** After one week, imaging of the injected L4 DRG (z-section 20 to 32) shows the syringe needle tract (encircled with white dots), where GFP-expressing cells were found to cluster; **(B)** while in the contralateral, un-injected L4 DRG, no fluorescence was observed. **(C-E)** After two-four weeks, a GFP-positive mass was visible at the dorsal root of the injected DRGs, which enlarged over time. **(C)** Cartoon representation of the size and morphology of the mass after is shown one-month post-graft. **(D)** Two-photon analysis of the mass revealed elevated fluorescence of cellular bodies, indicating the presence of iPSCs. Selected stacked z frames 18/64, 29/64, 36/64 (top to bottom) show diverse cell shapes developing in deep layers of the mass (z-section 1 to 20). **(E)** One-month post-transplant, the mass almost doubled in size and depicted a complex cellular network with increased fluorescence and higher cell numbers. The cells segregated in an organized fashion and formed elongated cellular extensions. Scale bars 50 µM.

complex cellular network (*Figure 2E, 3C*). To verify the exclusive expression of GFP in human iPSC-derived cells and not in rat endogenous cells, DRGs sections were stained against the human nuclear antigen (hNu). Immunostaining of endogenously expressing GFP (eGFP$^+$) cells demonstrated selective hNu expression in iPSCs, which co-localized outside the ganglia (*Figure 3*). GFP$^+$/hNu$^+$ DRG sections showed elevated iPSC proliferation surrounding the dorsal root and part of the DRG, as early as two weeks post-graft (*Figure 3B, D*). However, iPSCs remained in the DRG vicinity and did not migrate to the spinal cord (*Figure S3*).

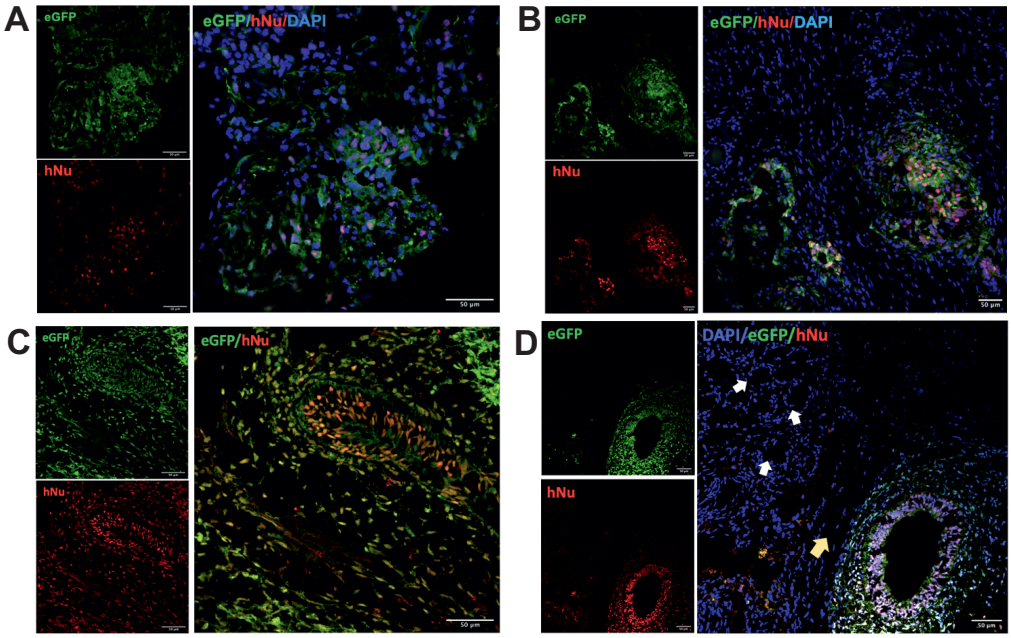

FIGURE 3 – GFP-expressing cells in xeno-transplanted DRG sections are immunoreactive to the human nuclear antigen. (A-D) Following injection of undifferentiated iPSCs into the DRG of juvenile rats, all GFP-expressing cells were found to co-localize with the human nucleus (hNu; red) antibody. hNu-labeled iPSC-derived cells proliferated and segregated into diverse shapes. DRG sections were visualized using confocal microscopy **(A-B)** two weeks and **(C-D)** one-month post-transplant. **(A-C)** The cells present in the GFP-positive mass, adjacent to the DRG, stained positively against hNu-647. **(B-D)** The mass grew exponentially within the DRG tissue without co-localizing with endogenous DRG neurons in either the ganglia or the root. **(D)** DRG neurons are indicated by white arrow, the dorsal root is indicated by a yellow arrow. Scale bars 50 μM.

Enlargement of the mass was reported between two and four weeks, within which the cells further differentiated and formed cellular connections with one another, but not with naive rat DRG neurons (*Figure 3A, C*).

In vivo derived iPSCs failed to differentiate into DRG cells of neuronal or glial lineages

With the goal to induce sensory neurogenesis *in vivo* through microniche endogenous interactions, we immunolabelled iPSC-transplanted DRG sections with canonical markers of neurons and sensory neurons (*Figure 4*). Immunohistochemistry was performed to determine the percentage of neuronal versus non-neuronal cells expressing GFP, as well as to evaluate the different cell types into which the iPSCs differentiated. GFP-expressing cells were located exclusively outside the ganglion and along the root and did not co-localize with animal neurons (*Figure 4A, C, E*). However, NeuN$^+$ and peripherin$^+$ cells were detected within the iPSC mass, suggesting that rodent neuronal derivatives developed post-graft (*Figure 4B, D, F*). Nevertheless, the

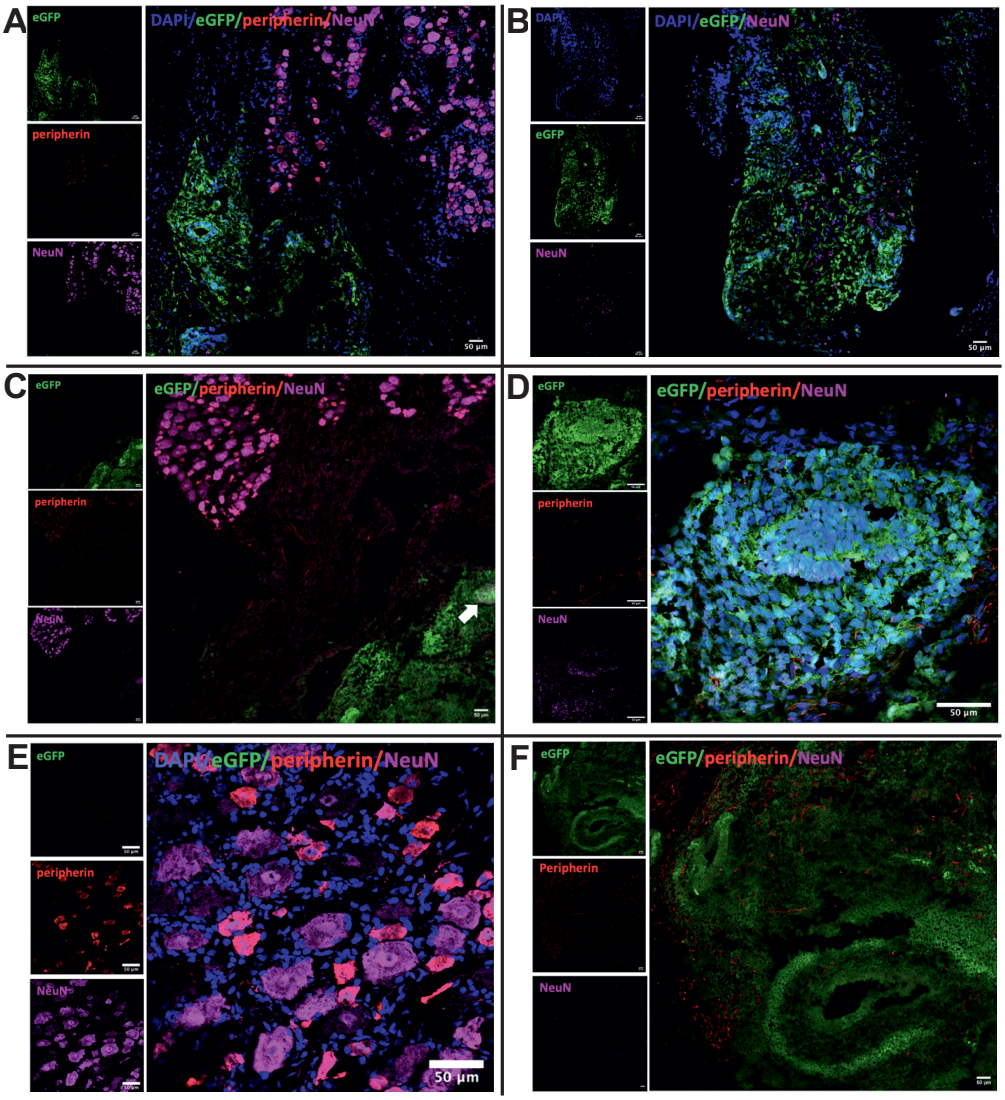

FIGURE 4 – iPSC-derived cells do not show clear co-localization with neuronal markers. (A-F) DRG-injected undifferentiated iPSCs were immunostained against neuronal marker NeuN (magenta) and sensory neuronal marker peripherin (red). Images were obtained using confocal microscopy **(A-B)** two weeks and **(C-F)** one-month post-transplant. **(A-B, D-F)** Endogenous GFP (eGFP) expression was detected throughout the mass layers; however, **(A,C,D)** No green fluorescence was detected within the neuronal core of the ganglia. **(C)** Immunoreactivity to NeuN was observed in a small fraction of the eGFP^{+} iPS mass, pointed out with a white arrow. **(D)** Magnification of the eGFP+/NeuN+ mass shown in (C); and **(E)** the eGFP^{+} iPS mass zoomed in, indicating possible co-localization and/or depth-related autofluorescence. **(B,F)** Immuno-labelled NeuN and peripherin cells were found within the eGFP^{+} mass without GFP co-expression. iPSCs 'co-habit' with endogenous neurons but do not express neuronal markers. Scale bars 50 µM.

morphology and size of NeuN$^+$/peripherin$^+$ cells in the eGFP mass may indicate immaturity of the derivatives. Alternatively, the presence of impurities within the sections or the heightened 3D structure of the mass may have resulted in unspecific binding. Furthermore, the neuronal cells detected in the growth did not express GFP, demonstrative that iPSCs did not differentiate into neurons. Beyond sensory neurons, the DRG is composed of numerous other cell types, including glial cells, which represent a large portion of the ganglia network. To assess whether iPSCs differentiated into non-neuronal cell types, specifically glia, DRG sections were stained against the glial GFAP and S100 markers (*Figure 5)*. Like for neuronal cells, eGFP$^+$ iPSCs did not positively stain for either marker (*Figure 5A, C*), but immunoreactivity to glial cell antibodies was observed in the iPSC mass (*Figure 5B, D*). In particular, GFAP$^+$ cells grew long extensions throughout the iPSC environment (*Figure 5B, D*), in a similar fashion to those located in the DRG root (*Figure 5A, C*), suggesting plasticity of animal DRG glial cells, whereby endogenous cells can grow outside of the DRG and 'co-habit' with iPSCs without directly co-localizing.

Transplantation of undifferentiated iPSCs into immunosuppressed animals induced cellular proliferation into a tumor-like growth

Xenotransplantation of iPSCs remains limited for its elevated risk of tumorigenicity, as a result of iPSCs' pluripotent nature and the need for compromising immunity to prevent graft rejection [25, 37]. Morphological analysis of the eGFP$^+$/hNu$^+$ iPSC mass suggests trilineage differentiation into the embryonic germ layers, demonstrating the ability of injected iPSCs to maintain their pluripotent potential *in vivo* (*Figure 6, S4*). After four weeks, GFP-expressing cells within the mass formed extensive cellular networks of repetitive patterns. Direct comparison with a published histological staining of a teratoma [49] and embryonic germ layers [25] showed ectoderm morphology in iPSC-formed open clusters (*Figure 6B, left*), the mesoderm in iPSC closed clusters (*Figure 6B, middle*), while luminal cell-like conformation corresponded to the endoderm layer (*Figure 6B, right*), suggesting teratoma formation. In an attempt to reduce the risk of teratogenesis, we transplanted undifferentiated iPSCs into the DRG of immunocompetent animals (n=6). Tissue collection was performed 72h and one-week post-graft and revealed inflammation at the site of injection and in the DRG. Two-photon imaging showed some dimer fluorescence in both injected and some non-injected DRGs, which may result from immune cell infiltration, possibly of macrophage-ingested iPSCs. While the animals did not show cancerous lesions, no GFP or immunoreactivity to hNu was detected in the DRG sections, suggesting iPSC graft rejection (*Data not shown*).

Additionally, to circumvent limitations related to undifferentiated iPSC-induced teratoma, iPSCs were pre-differentiated to NPCs. iPSCs were exposed to a cocktail of inhibitory molecules for 9-16 days, by which time the neural fate was achieved but sensory neuron differentiation had not been initiated [36]. Targeted DRG injection of iPSC-NPCs into immunodeficient rats (n=6) resulted in iPSC differentiation into

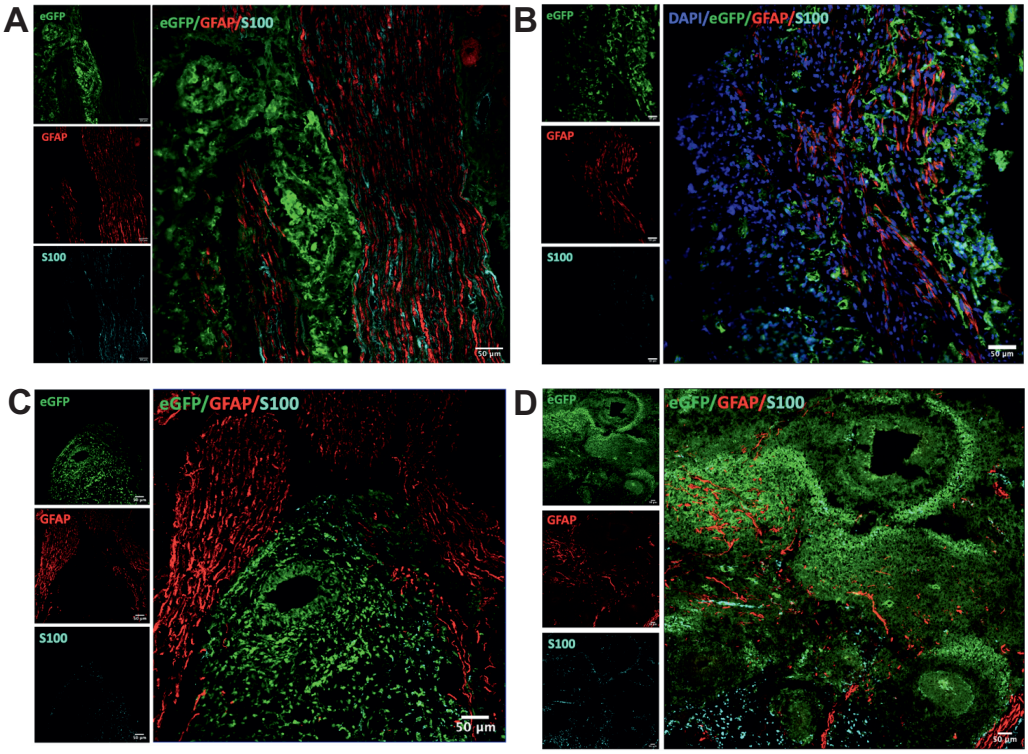

FIGURE 5 – GFP-expressing cells do not express glial markers. **(A-D)** *In vivo* transplanted undifferentiated iPSCs were labeled for glial marker GFAP (red) and non-myelinating Schwann cell marker S100 (cyan). Images were obtained under confocal microscopy **(A-B)** two weeks and **(C-D)** four weeks post-transplant. **(A,C)** eGFP^{+} iPSCs did not co-localize with endogenous glial or Schwann cells. **(B,D)** However, immunoreactivity to GFAP and S100 cell markers was observed within the iPSC mass. Scale bars 50 µM.

neuronal-like cells when DRGs were dissociated in culture. (*Supplementary methods*, *Figure S5*). Furthermore, animals showed no sign of tumor formation for up to 6 weeks post-graft. However, we were unable to functionally assess GFP-expressing cells using patch clamp technology due to their limited numbers and location on the edge of the coverslip. In turn, we were unable to perform immunostaining to establish their lineage identity.

Long-term culture of whole DRG explant relies on selective extracellular matrices and medium

Over the past decade, several DRG explant protocols have been developed without a gold-standard method being established. In this study, we exposed neonatal DRGs injected with iPSC-NPCs to different combinations of extracellular matrices (ECM), medium, and growth factors for up to four weeks post-graft (*Figure 1, 7, Table 1, Figure S1*). DRG explants from neonatal rats have been shown to have a higher capacity to

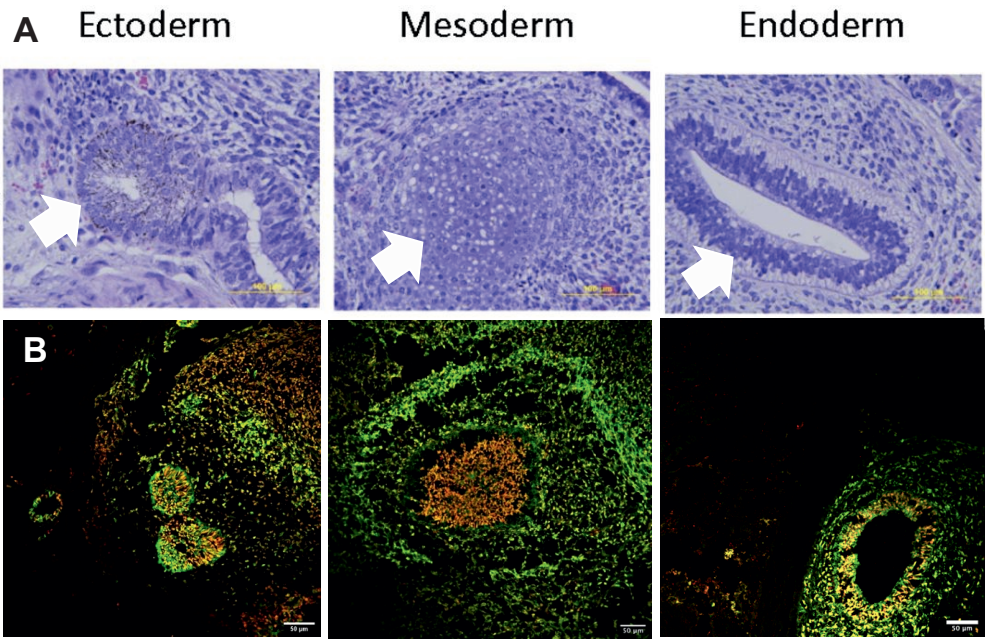

FIGURE 6 – Transplanted IPSCs differentiated into the three embryonic germ layers *In vivo*. (A) The three embryonic germ layers are canonical markers of iPSC pluripotency and teratogenicity. The staining shows the representative structures (indicated by arrows) of the ectoderm, mesoderm, and endoderm. **(B)** DRG sections of the iPSC mass, under confocal microscopy show eGFP+ (green) repetitive patterns, such as luminal cell-like conformation and web-like networks, which are co-labeled with hNu (red). The diverse shapes adopted by transplanted iPSCs one-month post-graft demonstrate close similarity to tumor-like clusters. Histological staining of teratoma formation with hematoxylin and eosin was published by Iovino et al [49]. Scale bars 50 μM.

grow compared to adult neurons [50] and to depict enhanced neurogenesis. Cells from explants cultured on Matrigel attached strongly to the ECM and depicted a healthy morphology (*Figure 7, Table 1*). Additionally, cells started migrating from the DRG rapidly and expanded, completely covering the 35mm dish by week 3-4. On the other hand, explants grown on PDL-coated dishes developed limited neurite extension and showed reduced cell migration. Cell migration, clustering, and neurite growth were improved when the cells were exposed to NB media, rather than DRG media. Nonetheless, the DRG still maintained strong attachment to the matrix in either medium. Both NB and DRG media were successful in providing the nutrients necessary for long-term cultures. However, explants grown in DRG media required less replating and maintained their integrity better, while NB media increased neurite length and fasciculation. Furthermore, addition of both NGF and GDNF growth factors always improved the culture conditions. Collagen matrix and serum-free DMEM/F12 media showed the least success (*data not shown*).

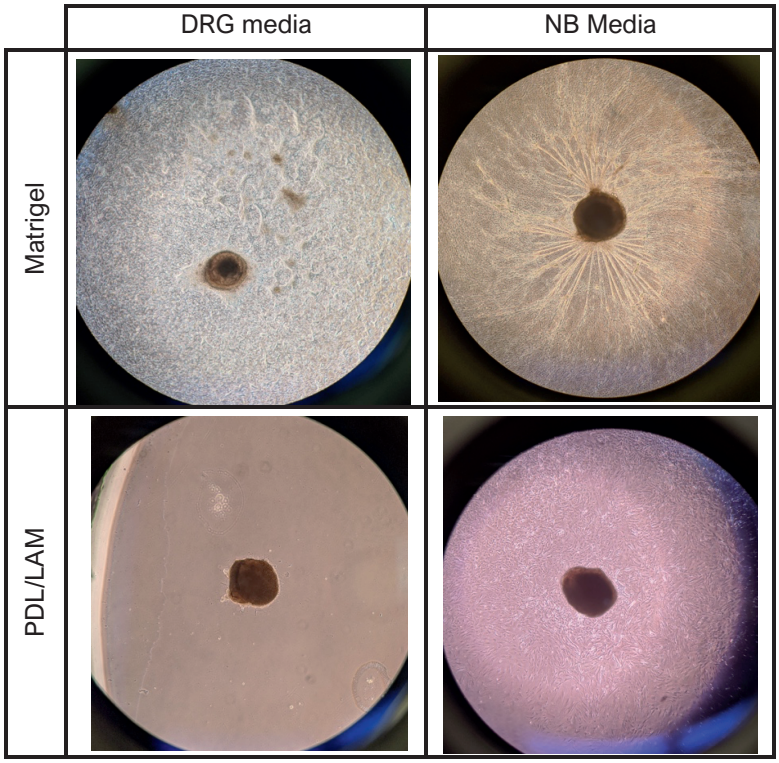

FIGURE 7 – Representative cultures of whole DRG explants, 4-week post-iPSC-NPC injection. Neonatal DRGs were injected with iPSC-NPCs post-mortem and plated on Matrigel- or PDL/LAM-coated 35 mm glass-bottom dishes for 3.5 - 4 weeks. Explants were supplied with DRG media or Neurobasal-A (NB) media with NGF and GDNF. DRG explants plated on Matrigel-coated dishes developed extensive neurite outgrowth with either medium. In PDL-coated dishes, DRGs maintained their integrity but showed limited neurite development. The cultures were imaged using optical microscopy at 10x and 20x magnification.

iPSC-NPCs survived and maintained GFP fluorescence *ex vivo* in whole neonatal DRG explant cultures

Targeted DRG explant injection of iPSC-NPCs provides the advantage and limitation of being independent from complex body interactions. Hence, iPSCs are only subjected to direct microniche interactions without risk of graft rejection. Injected pre-differentiated cells were able to survive *ex vivo* for up to 4 weeks and were detected in three out of seven explants under spinning disk confocal microscopy (*Figure 8A, B, S6*). Culture conditions did not appear to impact cell survival, as GFP fluorescence was observed in DRG explants grown in Matrigel-coated plates with NB media, and in PDL/LAM-coated plates with either DRG or NB media (*Table 1, S1*). Z optical planes were performed throughout the whole explants yielding 60-125 individual sections that were stacked together and selected for maximal intensity. Obtained images revealed

selective endogenous GFP expression in cells depicting a neuronal morphology with ramifications that extended to form a cellular network within the DRG (*Figure 8A*). eGFP$^+$ iPSC-derived cells further formed clusters independently from endogenous neurons (*Figure 8B)* and segregated in the outer edge of the DRG, in the superficial layer (*Figure 8C, D*). Subsequent immunolabeling of the iPSC cluster in DRG sections showed that the *ex vivo* derived cells did not co-localize with the neuronal marker NeuN, indicating a non-neuronal identity (*Figure 8D*). Other explants (n=12), including two DRGs with endogenous cellular GFP expression were enzymatically dissociated for functional assessment. However, elevated cell debris in culture prevented the detection of eGFP$^+$ cells.

DISCUSSION

The influence of the native DRG microenvironment on the fate and behavior of iPSCs is still poorly understood. Most iPSC xenotransplantation studies in sensory systems have focused on spinal cord injury for regenerative medicine. Injection of iPSCs into the DRG is still relatively novel, with limited research available. To the best of our knowledge, this is the first study to attempt DRG transplantation of undifferentiated iPSCs. The native niche exposes iPSCs to signaling cues necessary for maturation and full protein expression [25, 26]. By tagging the cells with green fluorescence, we were able to assess the behavior of the donor cells *in vivo* and *ex vivo*. We show that xenotransplantation of undifferentiated human stem cells into rat DRGs *in vivo* induces cells to proliferate uncontrollably overtime and to segregate into a large mass, suggesting tumorigenesis. We also found that the pluripotency of grafted cells impacted their ability to differentiate into sensory neurons and glial cells. Forced neural induction in stem cells, by pre-differentiating them into neural precursors, prevented teratoma formation and allowed the cells to form neuronal-like connective structures. Likewise, iPSC-NPCs were found to differentiate *ex vivo* and to form neurite-like extensions when injected into neonatal DRG explants. Although the donor cells did not stain for mature neuronal markers, these findings are promising for developing safe DRG transplantation strategies and establishing *in/ex vivo* differentiation protocols.

A major concern that has restricted the use of transplanted undifferentiated iPSCs in current research lays in their elevated tumorigenic potential, due to their pluripotent nature [37]. In line with compiled studies that have shown tumorigenesis to occur in immune-depressed recipients of iPSCs [25], we show that transplanting undifferentiated iPSCs into the DRG of immunocompromised animals results in exponential cellular proliferation outside the ganglia and around the dorsal root (*Figure 2,3*). Specifically, we demonstrate that grafted undifferentiated iPSCs segregate into a large mass and cluster into organized networks that resemble those described in the embryonic germ layers and teratomas [25, 49], suggesting tumor formation (*Figure 2, 6, S4*). Yet, immunolabeling of the donor cells located in the mass with pluripotent cell markers is needed to confirm tumor composition. Targeted transplantation of

ECM	Media	Growth factors	Time (weeks)	DRG explant growth	Presence GFP-tagged cells
Matrigel	DRG	NGF + GDNF (n=6)	3 - 4	Grew extensions and cellular development on ECM	-
	NB	NGF + GDNF (n=2)	3.5 - 4	Optimal for explant extension growth	Yes
		NGF only (n=1)	4	Poor growth	-
	DMEM	No GFs (n=1)	4	Replating required.	-
Collagen COL IV	DRG	NGF only (n=1)	4	DRG planted outside the coverslip	-
	NB	NGF only (n=1)	4	Lifted, not good	-
PDL/LAM	DRG	NGF + GDNF (n=8)	3 - 4	One lifted, others good. Most explant showed no growth in-dish	Yes
	NB	NGF + GDNF (n=4)	3 - 4	One lifted, others good. Better in-dish growth	Yes
		NGF only (n=1)	4	Not good, replated	-

TABLE 1 – DRG explant culture conditions. Whole DRG explants injected with iPSC-NPCs were grown on 35 mm glass-bottom dishes pre-coated with Matrigel, Collagen IV, or poly-D-lysin/laminin (PDL/LAM). The explants were provided with either DRG medium, Neurobasal-A (NB) medium or serum-free DMEM/F12, supplemented with NGF, NGF/GDNF or no growth factors. Optimal DRG growth conditions were observed when planted on Matrigel plates with either medium, supplemented with both NGF/GDNF. Second, DRG explants showed effective attachment and growth when planted on PDL/LAM coverslips in both medium, supplemented with NGF and GDNF. Poor culture conditions were reported when DRG explants were grown on collagen-coated dishes, and in all ECM, when fed with serum-free media or in NB/DRG medium without the full complement of growth factors. GFP endogenous fluorescence was detected in explants grown in Matrigel-coated plates, supplemented with NB medium and NGF/GDNF and in PDL/LAM-coated dishes, supplemented with either DRG or NB medium with NGF/GDNF.

undifferentiated iPSCs into the brain of immunocompetent animals has been shown to promote cell survival and differentiation into mature neurons, without tumor or precancerous lesions for a year post-graft [25].

However, when transplanting iPSCs into the DRG of immunocompetent animals, grafted cell survival was dramatically impacted. While we did not observe teratoma formation, marked inflammation at the site of incision and in the DRG suggests graft-versus-host rejection. Successful cell engraftment in the brain of immunocompetent mice rather than in rat DRGs may be explained by differences in the organ context for induced-iPSC differentiation. With active neurogenesis, the brain has been shown to promote substantial nuclear fusion between injected and recipient cells, while different brain regions have been demonstrated to have distinct properties in their influence on transplanted iPSCs [25]. Hence, the DRG might simply be less permissive to cell engraftment and survival than other organs. Moreover, the number of injectable cells in the DRG is significantly smaller compared to the rodent brain, which may have participated in reducing our rates of engraftment. Also, its anatomical location and

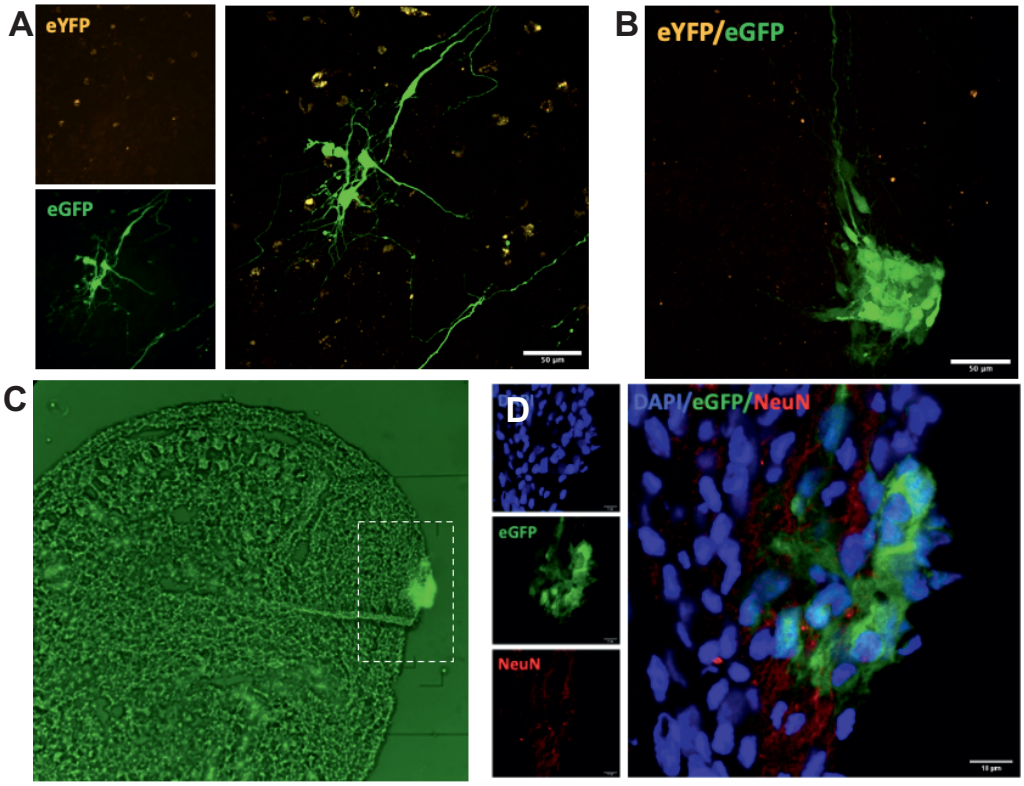

FIGURE 8 – *Ex vivo* transplanted iPSC-NPCs survive and develop neurite-like extensions but do not differentiate into mature neurons. (A-B) Whole DRG explants were imaged using spinning disk confocal microscopy. Z optical sections were stacked and selected for maximum intensity. eGFP^{+} iPSC-NPCs were visualized by applying a 510 nm excitatory wavelength. Specific GFP fluorescence was demarked by exciting endogenous yellow fluorescence (eYFP) and demonstrated iPSC-selective GFP expression. GFP-expressing cells segregated and formed neuronal-like bodies with long extensions. Scale bars 50 μM. **(C)** Subsequent cryostat sections of the DRG explant (B) were visualized under a fluorescent optical microscope, which recapitulated endogenous GFP expression. **(D)** The sections were immunolabeled with neuronal marker NeuN (red). eGFP+ iPSC-NPCs did not express neuronal antigens, indicating that the cells did not differentiate into neurons. Scale bar 10 μM.

small structure make injections more difficult to perform [27]; as such, we might have induced sufficient damage to evoke an immune response. Conversely, incurred damages to the DRG may have contributed to teratoma growth, as increased tumorigenic potential has been reported in immunocompromised animals with lesioned and diseased tissues [32, 38]. Opting for an automated injection system mounted on a stereotaxic apparatus may limit unnecessary perforations during surgery.

Alternatively, pre-differentiation into a specific lineage before graft has been reported to reduce the risk of teratogenesis in immunodeficient animals. By forcing neural fate

expression, the cells lose their pluripotent potential and their capacity to proliferate uncontrollably [25, 51-53]. Although not guaranteeing their safe utilization, differentiation into neural precursors for DRG injection has highlighted protective effects in a recently published study [27]. Pre-differentiated iPSC-neurospheres, transplanted into immunodeficient rat DRGs, demonstrated effective survival and differentiation *in vivo* for up to eight weeks post-graft. Furthermore, injected cells showed markers of all three sensory neuron subtypes, indicative of their ability to produce heterogeneous populations, with neuronal projections that extended into the spinal cord and along the neuronal tracts [27]. Here, the inability of transplanted iPSCs to differentiate into DRG neuronal and glial cells (*Figure 4,5*), or migrate to the spinal cord (*Figure S3*), might result from clustered iPSCs spontaneously differentiating into embryonic germ layers. From our experience with *in vitro* iPSC maintenance, cell-to-cell interactions between undifferentiated and differentiated iPSCs promotes aggravated, widespread spontaneous differentiation. In turn, it can be expected that grafted cells differentiated uncontrollably and were unable to achieve a neuronal identity. Furthermore, cellular segregation outside the DRG may have filtered out the signaling cues necessary to initiate their derivation into sensory neurons. Nonetheless, transplanted iPSC-NPCs residing outside the DRG have been shown to retain expression of neuronal and glial markers [27], suggesting that failure to differentiate into DRG cell lineages pertained to the cells' pluripotency. Otherwise, as it is generally well-accepted that iPSC-converted somatic cells retain an epigenetic memory [54-56], due to incomplete silencing of the specific expression patterns of the donor cells [54, 57]. As such, the cell type of origin may bias the differentiation propensity of iPSCs [58, 59]. Perhaps here, the use of fibroblast-derived iPSCs compromised their capacity to differentiate *in vivo*.

Neural induction was instead elicited pre-graft by exposing iPSCs to the same inhibitory cocktail as for *in vitro* sensory neuron differentiation, for nine to sixteen days instead of eight weeks [5]. Transplanted iPSC-NPCs appear to have differentiated into neuronal-like cells six weeks post-graft after DRGs were dissociated in culture (*Figure S5*), indicating that depleting cells of their pluripotency may promote their differentiation into sensory neurons, while preventing teratoma development. However, functional characterization of the donor cells was not possible due to their limited numbers, perhaps caused by substantial cell loss during the culture process. In the future, DRG injection of Ca^{2+} reporter iPSCs might circumvent culture-related challenges and allow *in vivo* electrophysiological assessment. Selecting iPSCs with a pre-differentiated NPC lineage [27] and thorough screening for pluripotent markers prior to grafting [60] might provide the means for sensory neuron differentiation, without tumorigenesis, and should be extrapolated in future experiments.

Ex vivo iPSC graft of DRG explants has provided interesting avenues to combat both the tumorigenic potential of stem cells and the risk of graft rejection. Recently, fibroblast derived-organoids injected into rat DRG explants showed high survival rate while maintaining nociceptive, proprioceptive and mechanosensitive identity two

weeks post-graft. Furthermore, transplanted cells were shown to aggregate with endogenous neurons and to form interconnected structures [28]. Importantly, as the injected donor cells were already fully differentiated into DRG organoids, their ability to differentiate and mature *ex vivo* cannot be accurately measured. After developing a DRG explant model for iPSC differentiation (*Figure 7*), we show that GFP-expressing iPSC-NPCs survived and portrayed a neuronal-like morphology (*Figure 8, S6*). However, immunostaining of one of the explants with verified endogenous GFP expression failed to show expression of neuronal markers (*Figure 8D*). Nonetheless, these results should be carefully interpreted due to the particularly small sample size of DRG explants with detectable iPSC levels. Furthermore, NeuN is a marker of mature, differentiated neurons, and as explant sections were imaged after only four weeks, longer allocated timeframes may have yielded mature neurons. Immunolabeling with markers of early neuronal development, such as Brn3A and Islet1 might allow us to better assess cellular identity and stages of differentiation. Finally, an important drawback of *ex vivo* generation of sensory neurons lays in the lack of complex, integrated organ network interactions as the DRGs are isolated from the whole body, which might hinder their derivation.

CONCLUSIONS

The current gap in knowledge on sensory neurogenesis and maturation *in vivo* has hindered our ability to model human DRGs using iPSCs. In this study, we attempted to bring iPSC-derived cells closer to mature native cells by providing the microenvironmental context lacking from *in vitro* cultures. Our findings show the necessity of adopting a neural fate for *in vivo* differentiation in the DRG and to prevent tumorigenesis. Nevertheless, premature neural induction remains challenging due to cells lacking the nutrients and signaling cues required pre-differentiation to reach functional maturity. Solutions are currently being developed for eliminating the teratogenic potential of iPSCs, such as bee venom [61], allowing future studies to reinvestigate the potential prospects of transplanting early-stage iPSCs. Advances in xenotransplantation research can propel our knowledge of critical key components of the DRG microniche influencing cell behaviors and foster the development of *in vitro* enrichment strategies [62].

REFERENCES

1. Nishikawa, N. and M. Nomoto, *Management of neuropathic pain.* J Gen Fam Med, 2017. **18**(2): p. 56-60.
2. Finnerup, N.B., et al., *Pharmacotherapy for neuropathic pain in adults: a systematic review and meta-analysis.* Lancet Neurol, 2015. **14**(2): p. 162-73.
3. Bouhassira, D., *Neuropathic pain: Definition, assessment and epidemiology.* Rev Neurol (Paris), 2019. **175**(1-2): p. 16-25.
4. Sopacua, M., et al., *Small-fiber neuropathy: Expanding the clinical pain universe.* J Peripher Nerv Syst, 2019. **24**(1): p. 19-33.
5. Mis, M.A., et al., *Resilience to Pain: A Peripheral Component Identified Using Induced Pluripotent Stem Cells and Dynamic Clamp.* J Neurosci, 2019. **39**(3): p. 382-392.
6. Bennett, D.L., et al., *The Role of Voltage-Gated Sodium Channels in Pain Signaling.* Physiol Rev, 2019. **99**(2): p. 1079-1151.
7. Dib-Hajj, S.D. and S.G. Waxman, *Sodium Channels in Human Pain Disorders: Genetics and Pharmacogenomics.* Annu Rev Neurosci, 2019.
8. Dib-Hajj, S.D., et al., *The Na(V)1.7 sodium channel: from molecule to man.* Nat Rev Neurosci, 2013. **14**(1): p. 49-62.
9. Geha, P., et al., *Pharmacotherapy for Pain in a Family With Inherited Erythromelalgia Guided by Genomic Analysis and Functional Profiling.* JAMA Neurol, 2016. **73**(6): p. 659-67.
10. Yang, Y., et al., *Nav1.7-A1632G Mutation from a Family with Inherited Erythromelalgia: Enhanced Firing of Dorsal Root Ganglia Neurons Evoked by Thermal Stimuli.* J Neurosci, 2016. **36**(28): p. 7511-22.
11. Dib-Hajj, S.D., et al., *Gain-of-function mutation in Nav1.7 in familial erythromelalgia induces bursting of sensory neurons.* Brain, 2005. **128**(Pt 8): p. 1847-54.
12. Han, C., et al., *Early- and late-onset inherited erythromelalgia: genotype-phenotype correlation.* Brain, 2009. **132**(Pt 7): p. 1711-22.
13. Dib-Hajj, S.D., et al., *Voltage-gated sodium channels in pain states: role in pathophysiology and targets for treatment.* Brain Res Rev, 2009. **60**(1): p. 65-83.
14. Dib-Hajj, S.D., et al., *Transfection of rat or mouse neurons by biolistics or electroporation.* Nat Protoc, 2009. **4**(8): p. 1118-26.
15. Han, C., et al., *Human Na(v)1.8: enhanced persistent and ramp currents contribute to distinct firing properties of human DRG neurons.* J Neurophysiol, 2015. **113**(9): p. 3172-85.
16. Zhang, X., et al., *Voltage-gated Na(+) currents in human dorsal root ganglion neurons.* Elife, 2017. **6**.
17. Inoue, H., et al., *iPS cells: a game changer for future medicine.* EMBO J, 2014. **33**(5): p. 409-17.
18. Yuan, J.H., et al., *KCNQ variants and pain modulation: a missense variant in Kv7.3 contributes to pain resilience.* Brain Commun, 2021. **3**(3): p. fcab212.
19. Schwartzentruber, J., et al., *Molecular and functional variation in iPSC-derived sensory neurons.* Nat Genet, 2018. **50**(1): p. 54-61.
20. Eberhardt, E., et al., *Pattern of Functional TTX-Resistant Sodium Channels Reveals a Developmental Stage of Human iPSC- and ESC-Derived Nociceptors.* Stem Cell Reports, 2015. **5**(3): p. 305-13.
21. Namer, B., et al., *Pain relief in a neuropathy patient by lacosamide: Proof of principle of clinical translation from patient-specific iPS cell-derived nociceptors.* EBioMedicine, 2019. **39**: p. 401-408.
22. Middleton, S.J., et al., *Studying human nociceptors: from fundamentals to clinic.* Brain, 2021. **144**(5): p. 1312-1335.
23. Wiegand, C. and I. Banerjee, *Recent advances in the applications of iPSC technology.* Curr Opin Biotechnol, 2019. **60**: p. 250-258.

24. Iyer, N.R., T.S. Wilems, and S.E. Sakiyama-Elbert, *Stem cells for spinal cord injury: Strategies to inform differentiation and transplantation.* Biotechnol Bioeng, 2017. **114**(2): p. 245-259.
25. Martinez-Cerdeno, V., et al., *Behavior of Xeno-Transplanted Undifferentiated Human Induced Pluripotent Stem Cells Is Impacted by Microenvironment Without Evidence of Tumors.* Stem Cells Dev, 2017. **26**(19): p. 1409-1423.
26. Yu, T., et al., *In vivo differentiation of induced pluripotent stem cell-derived cardiomyocytes.* Circ J, 2013. **77**(5): p. 1297-306.
27. Viventi, S., et al., *In vivo survival and differentiation of Friedreich ataxia iPSC-derived sensory neurons transplanted in the adult dorsal root ganglia.* Stem Cells Transl Med, 2021. **10**(8): p. 1157-1169.
28. Xiao, D., et al., *Generation of self-organized sensory ganglion organoids and retinal ganglion cells from fibroblasts.* Sci Adv, 2020. **6**(22): p. eaaz5858.
29. Kreitzer, F.R., et al., *A robust method to derive functional neural crest cells from human pluripotent stem cells.* Am J Stem Cells, 2013. **2**(2): p. 119-31.
30. Luo, Y., et al., *Stable enhanced green fluorescent protein expression after differentiation and transplantation of reporter human induced pluripotent stem cells generated by AAVS1 transcription activator-like effector nucleases.* Stem Cells Transl Med, 2014. **3**(7): p. 821-35.
31. Jensen, M.B., et al., *Injected Versus Oral Cyclosporine for Human Neural Progenitor Grafting in Rats.* J Stem Cell Res Ther, 2012. **Suppl 10**: p. 003.
32. Rhee, Y.H., et al., *Protein-based human iPS cells efficiently generate functional dopamine neurons and can treat a rat model of Parkinson disease.* J Clin Invest, 2011. **121**(6): p. 2326-35.
33. Chambers, S.M., et al., *Combined small-molecule inhibition accelerates developmental timing and converts human pluripotent stem cells into nociceptors.* Nat Biotechnol, 2012. **30**(7): p. 715-20.
34. Young, G.T., et al., *Characterizing human stem cell-derived sensory neurons at the single-cell level reveals their ion channel expression and utility in pain research.* Mol Ther, 2014. **22**(8): p. 1530-1543.
35. Cao, L., et al., *Pharmacological reversal of a pain phenotype in iPSC-derived sensory neurons and patients with inherited erythromelalgia.* Sci Transl Med, 2016. **8**(335): p. 335ra56.
36. Guimaraes, M.Z.P., et al., *Generation of iPSC-Derived Human Peripheral Sensory Neurons Releasing Substance P Elicited by TRPV1 Agonists.* Front Mol Neurosci, 2018. **11**: p. 277.
37. Fu, W., et al., *Residual undifferentiated cells during differentiation of induced pluripotent stem cells in vitro and in vivo.* Stem Cells Dev, 2012. **21**(4): p. 521-9.
38. Yamashita, T., et al., *Tumorigenic development of induced pluripotent stem cells in ischemic mouse brain.* Cell Transplant, 2011. **20**(6): p. 883-91.
39. Lamba, D.A., et al., *Generation, purification and transplantation of photoreceptors derived from human induced pluripotent stem cells.* PLoS One, 2010. **5**(1): p. e8763.
40. Zhang, J., et al., *Human Neural Stem Cells with GDNF Site-Specific Integration at AAVS1 by Using AAV Vectors Retained Their Stemness.* Neurochem Res, 2018. **43**(4): p. 930-937.
41. Oki, K., et al., *Human-induced pluripotent stem cells form functional neurons and improve recovery after grafting in stroke-damaged brain.* Stem Cells, 2012. **30**(6): p. 1120-33.
42. Cheah, M., J.W. Fawcett, and M.R. Andrews, *Dorsal Root Ganglion Injection and Dorsal Root Crush Injury as a Model for Sensory Axon Regeneration.* J Vis Exp, 2017(123).
43. Grubinska, B., et al., *Rat NaV1.7 loss-of-function genetic model: Deficient nociceptive and neuropathic pain behavior with retained olfactory function and intra-epidermal nerve fibers.* Mol Pain, 2019. **15**: p. 1744806919881846.
44. Chen, L., et al., *Sodium channel Nav1.6 in sensory neurons contributes to vincristine-induced allodynia.* Brain, 2020. **143**(8): p. 2421-2436.
45. Benson, C.A., et al., *Conditional RAC1 knockout in motor neurons restores H-reflex rate-dependent depression after spinal cord injury.* Sci Rep, 2021. **11**(1): p. 7838.
46. Akin, E.J., et al., *Paclitaxel increases axonal localization and vesicular trafficking of Nav1.7.* Brain, 2021. **144**(6): p. 1727-1737.

47. Akin, E.J., et al., *Building sensory axons: Delivery and distribution of NaV1.7 channels and effects of inflammatory mediators.* Sci Adv, 2019. **5**(10): p. eaax4755.
48. Drobizhev, M., et al., *Two-photon absorption properties of fluorescent proteins.* Nat Methods, 2011. **8**(5): p. 393-9.
49. Iovino, S., et al., *Myotubes derived from human-induced pluripotent stem cells mirror in vivo insulin resistance.* Proc Natl Acad Sci U S A, 2016. **113**(7): p. 1889-94.
50. Gonzalez-Perez, F., et al., *Substratum preferences of motor and sensory neurons in postnatal and adult rats.* Eur J Neurosci, 2016. **43**(3): p. 431-42.
51. Cai, J., et al., *Dopaminergic neurons derived from human induced pluripotent stem cells survive and integrate into 6-OHDA-lesioned rats.* Stem Cells Dev, 2010. **19**(7): p. 1017-23.
52. Kawabata, S., et al., *Grafted Human iPS Cell-Derived Oligodendrocyte Precursor Cells Contribute to Robust Remyelination of Demyelinated Axons after Spinal Cord Injury.* Stem Cell Reports, 2016. **6**(1): p. 1-8.
53. Sun, J., et al., *Protective Effects of Human iPS-Derived Retinal Pigmented Epithelial Cells in Comparison with Human Mesenchymal Stromal Cells and Human Neural Stem Cells on the Degenerating Retina in rd1 mice.* Stem Cells, 2015. **33**(5): p. 1543-53.
54. Kim, K., et al., *Epigenetic memory in induced pluripotent stem cells.* Nature, 2010. **467**(7313): p. 285-90.
55. Bar-Nur, O., et al., *Epigenetic memory and preferential lineage-specific differentiation in induced pluripotent stem cells derived from human pancreatic islet beta cells.* Cell Stem Cell, 2011. **9**(1): p. 17-23.
56. Kim, K., et al., *Donor cell type can influence the epigenome and differentiation potential of human induced pluripotent stem cells.* Nat Biotechnol, 2011. **29**(12): p. 1117-9.
57. Ohi, Y., et al., *Incomplete DNA methylation underlies a transcriptional memory of somatic cells in human iPS cells.* Nat Cell Biol, 2011. **13**(5): p. 541-9.
58. Efrat, S., *Epigenetic Memory: Lessons From iPS Cells Derived From Human beta Cells.* Front Endocrinol (Lausanne), 2020. **11**: p. 614234.
59. Boland, M.J., K.L. Nazor, and J.F. Loring, *Epigenetic regulation of pluripotency and differentiation.* Circ Res, 2014. **115**(2): p. 311-24.
60. Peterson, S.E. and J.F. Loring, *Genomic instability in pluripotent stem cells: implications for clinical applications.* J Biol Chem, 2014. **289**(8): p. 4578-84.
61. Kim, A., et al., *Elimination of Teratogenic Human Induced Pluripotent Stem Cells by Bee Venom via Calcium-Calpain Pathway.* Int J Mol Sci, 2020. **21**(9).
62. Nickolls, A.R., et al., *Transcriptional Programming of Human Mechanosensory Neuron Subtypes from Pluripotent Stem Cells.* Cell Rep, 2020. **30**(3): p. 932-946 e7.

SUPPLEMENTARY MATERIALS

SELECTION OF INJECTABLE NUMBERS OF IPSCS

Juvenile, rather than adult, rats were selected to improve dissociated DRG recording conditions and for their amenability to surgical intervention. The lumbar DRGs were selectively transplanted, as they not only contain the cell bodies of the nociceptive fibers, but as the largest, they enabled higher cell numbers to be injected. The number of injected iPSCs was estimated based on relative organ size/volume, animal species and strain, and based on whether the cells were pre- or un-differentiated at the time of transplant [1-6]. Additional calculations were based on the average number of neurons contained by a lumbar rat DRG (15,000) [7]. Previous studies have showed 200,000-250,000 undifferentiated iPSCs to be injectable in the mouse striatum [2]. The adult rat striatum itself contains roughly 1.5 million neurons, or 100 times more [8]. Furthermore, the CNS offers a much larger surface for the cells to migrate. While considering elevated cell death from the dish to the DRG, an average of ~100,000 undifferentiated and iPSCs was injected into a single DRG per animal.

DRG CULTURE

DRGs were enzymatically dissociated into single neurons, as described [9, 10]. Briefly, DRG neurons were isolated from Sprague-Dawley (SD) adult rats (240-310g; n=6) and 1- to 5-days old rat pups (n=4) injected with iPSC-NPCs. Dissected DRGs (4-6weeks post-graft) and neonatal DRG explants (3-4 weeks post-graft; n=12) were incubated 20 min at 37°C in complete saline solution (CSS; 137 mM NaCl, 5.3 mM KCl, 1 mM $MgCl_2$, 25 mM sorbitol, 3 mM $CaCl_2$, and 10 mM Hepes (pH 7.2), adjusted with NaOH), supplemented with collagenase A and 0.6 mM EDTA (1.5 mg/ml; Roche). Adult and neonatal DRGs were then incubated in CSS, supplemented with Collagenase D (1.5 mg/ml; Roche), papain (30 U/ml; Worthington Biochemical) and 0.6 mM EDTA at 37°C for 17 min and 20 min, respectively. The tissues were centrifuged at 100g and triturated with 1 mL of BSA/TI (1:1) bovine serum albumin (Sigma-Aldrich) and trypsin inhibitor (Sigma-Aldrich) solution. For adult rat neurons, the cell suspension was filtered through a 70-µm cell strainer (Becton Dickinson). The cells were seeded onto PDL-coated coverslips and fed after 45 min with 1 mL/well DRG medium (*see Methods*).

CURRENT - AND VOLTAGE - CLAMP ANALYSIS

Whole-cell patch clamp experiments were performed as described [11]. Recordings were acquired using an EPC-10 amplifier and the PATCHMASTER program (HEKA Elektronik, Holliston, MA). Current-clamp recordings were obtained at 50 kHz and filtered at 10 Khz. Recording electrodes had a resistance <1.5 MΩ and were filled with the internal solution, consisting of: KCl 140 mM; HEPES, 5 mM; EGTA, 0.5 mM; Dextrose 20 mM; pH 7.3, 295–300 mOsm. The external solution contained: NaCl, 140 mM; KCl, 3 mM; HEPES-NaOH, 10 mM; $MgCl_2$, 2 mM; $CaCl_2$, 2 mM; Dextrose, 15 mM; pH 7.3, ~320 mOsm. The current threshold was assessed as the minimum amount of current necessary to induce an action potential. The firing rate was established by measuring the number of action potentials generated in response to incremental 500 ms depolarizing stimuli.

For voltage-clamp experiments, patch pipette electrodes were filled with intracellular solution, consisting of (in mM): 140 CsF, 10 NaCl, 1.1 EGTA, 10 HEPES, and 20

dextrose, pH 7.3, ~320 mOsm. The external solution contained (in mM): 140 NaCl, 20 tetraethylammonium (TEA), 3 KCl, 1 CaCl2, 1 MgCl2, 10 HEPES, 0.1 CdCl, pH 7.3, ~320 mOsm. Total sodium current was measured by holding iPSC-SNs at -100 mV, before inducing 5 mV incremental depolarizing potentials, lasting 100 ms, ranging from -80 mV to +40 mV.

IMMUNOCYTOCHEMISTRY

Immunostaining of iPSCs and iPSC-SNs was performed as described [11]. Briefly, undifferentiated or *in vitro* differentiated GFP-tagged iPSCs were fixed in 4% PFA for 10 min in 0.01M PBS. Primary antibodies against markers for sensory neuron peripherin (1:900) and human nucleus hNu (1:300) were incubated overnight at 4°C, or 2h at RT, in phosphate buffered saline-tween (PBS-T; 0.1% Triton X-100, 2% BSA, 4% donkey serum in PBS). Secondary antibodies (1:1000) donkey anti-chicken Alexa Fluor 594 and anti-mouse Alexa Fluor 647 were incubated 2h at RT in PBS-T.

SUPPLEMENTARY FIGURES

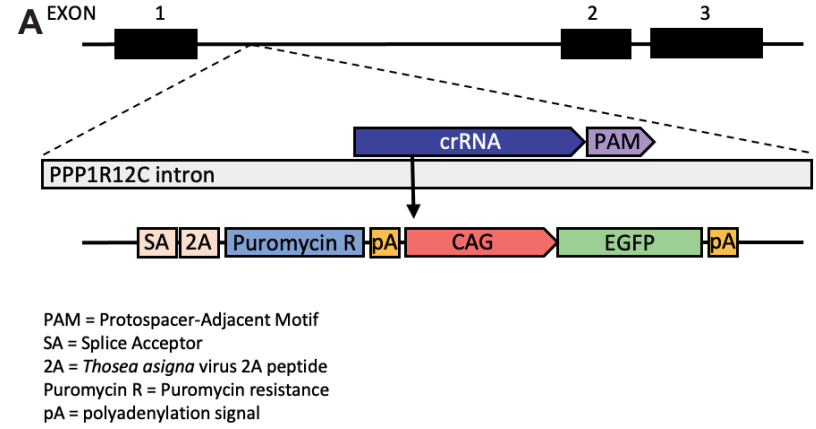

FIGURE S1 – CRISPR-Cas9 methodology was used to insert mEGFP at the AAVS1 safe harbor locus of the PPP1R12C gene intron. (A) Top: Insertion site of mEGFP, bottom: Zoomed insertion sequence at AAVS1. Adapted from the Allen Institute certificate of analysis for generating the AICS-0036-006:WTC-mEGFP-Safe harbor locus (AAVS1)-cl6 (mono-allelic tag). **(B)** Endogenous GFP (eGFP) expression was confirmed in undifferentiated iPSC colonies under fluorescent light. Immunoreactivity to the human nuclear antibody (hNu), tagged with Alexa Fluor 549, was detected. The antibody showed selective binding to human cells only and co-localized with eGFP. Conversely, the anti-hNu antibody did not detect rat cell nuclei, showcasing its validity (not shown). Scale bar 50 µM.

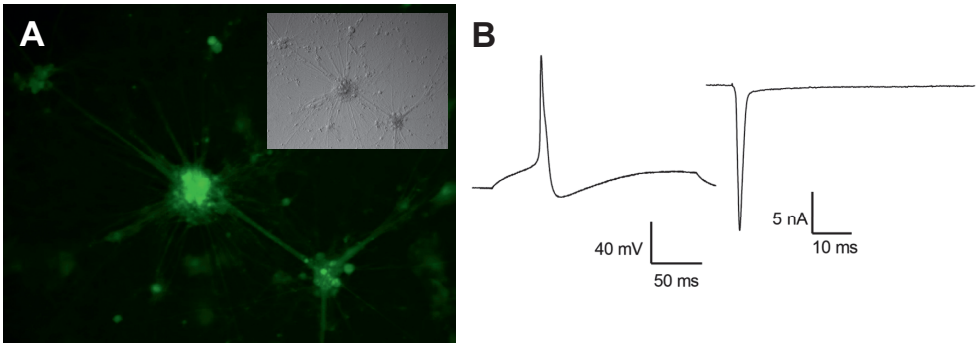

FIGURE S2 – *In vitro* differentiated iPSCs are functional and retain GFP expression throughout differentiation. (A) GFP-expressing iPSCs were differentiated using our standard protocol [11], modified from Chambers [12]. After 8 weeks, iPSC-derived sensory neurons were exposed to fluorescent light at exciting wavelength 510 nm and showed consistent GFP expression across cultures. **(B)** iPSC-nociceptors were functionally tested using current-clamp (left) and voltage-clamp (right) analysis. The cells were responsive to applied current stimuli, inducing action potentials, and displayed typical wild-type biophysical properties.

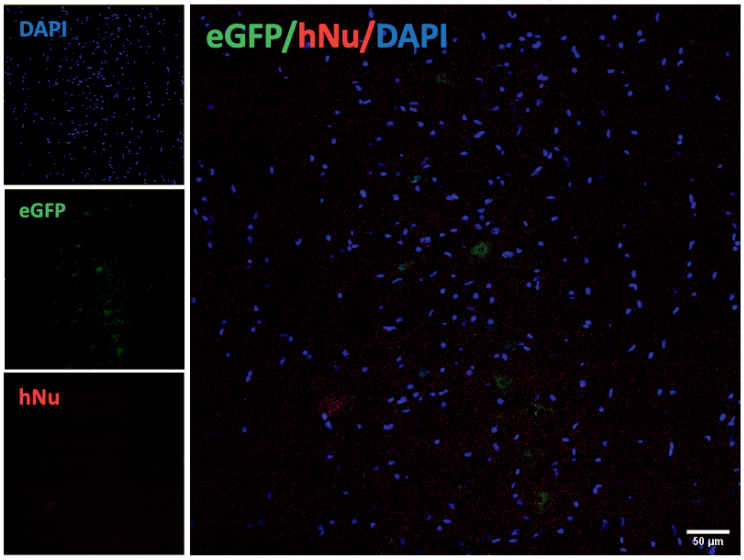

FIGURE S3 – Undifferentiated iPSCs did not migrate to the spinal cord following transplant. Longitudinal section of the spinal cord from injected animals 4 weeks post-transplant of undifferentiated GFP-iPSCs. The tissue was visualized under confocal microscopy and was stained against the human nuclear antigen (hNu) and nuclear antigen DAPI. The section shows no specific fluorescence. Scale bar 50 μM

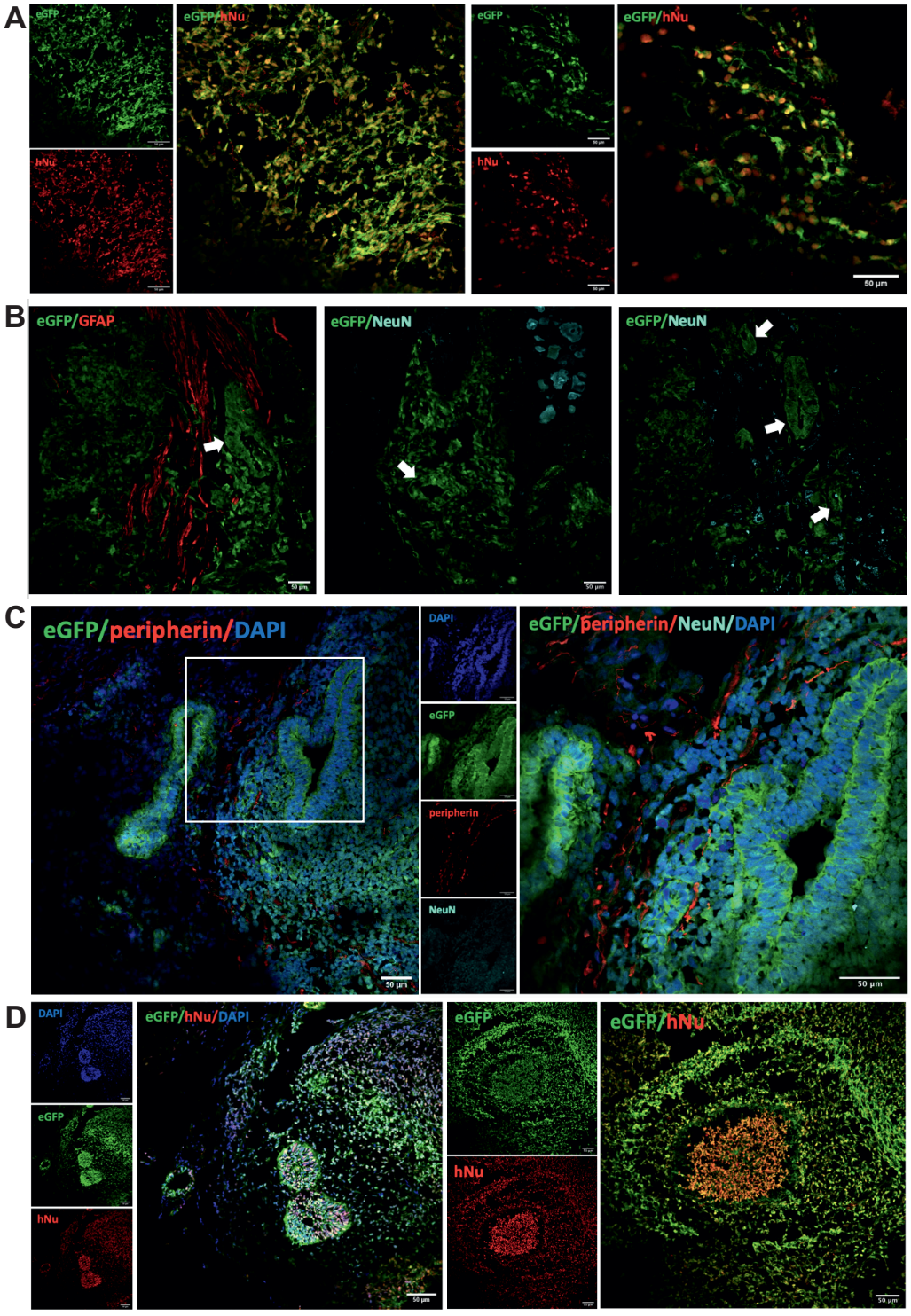
A
eGFP
eGFP/hNu
hNu
eGFP
eGFP/hNu
hNu
50 µm
B
eGFP/GFAP
eGFP/NeuN
eGFP/NeuN
C
eGFP/peripherin/DAPI
DAPI
eGFP
peripherin
NeuN
50 µm
eGFP/peripherin/NeuN/DAPI
50 µm
D
DAPI
eGFP
hNu
eGFP/hNu/DAPI
eGFP
hNu
eGFP/hNu
50 µm

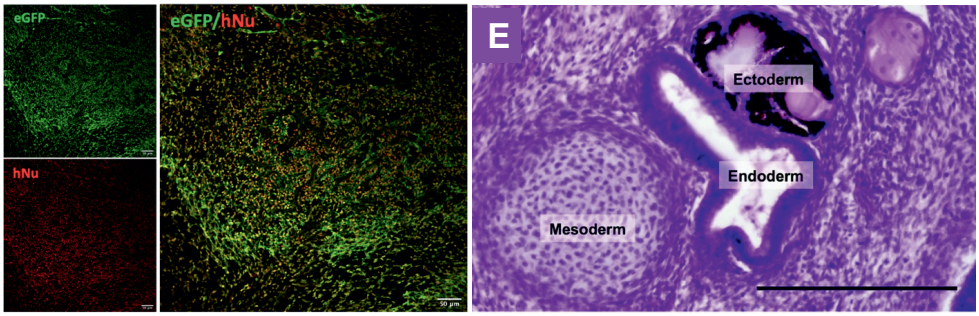

FIGURE S4 – *In vivo* derived IPSCs differentiated into the three embryonic germ layers. (A-D) DRG sections were visualized under confocal microscopy one-month post-graft. eGFP+/hNu+ cells organized in diverse complex morphologies found in teratomas. **(A)** Co-expressing GFP (green) and hNu (red) cells clustered into an enlarged mass in an organized fashion (left, scale bar 10 μM; right, scale bar 50 μM). **(B-C)** iPS-derived cells formed luminal-like organizations, relating to endoderm-like structures, which stained for **(B)** glial GFAP (red), and **(B-C)** neuronal markers NeuN (cyan) and peripherin (red), without clear co-localization. **(C)** left, 20x magnification; **(C)** right 40x. **(D)** eGFP+/hNu+ iPSC-differentiated cells also formed closed or semi-closed clusters, relating to mesoderm and ectoderm-like structures. **(E)** Histological staining of the three embryonic germ layers, from Martinez-Cerdeno [2].

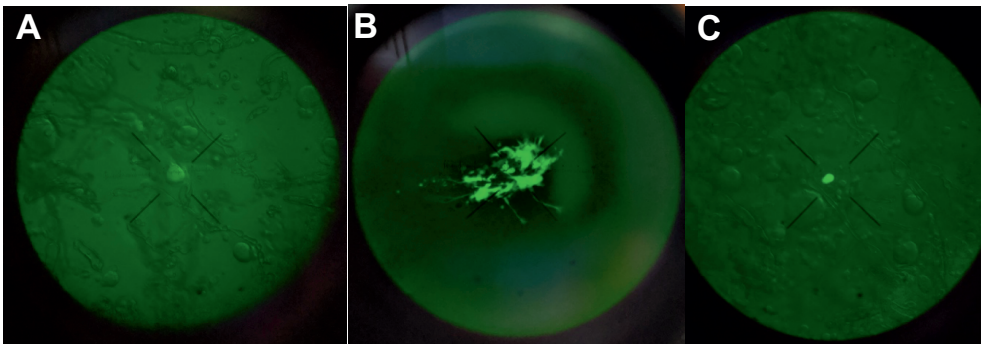

FIGURE S5 – Cultured IPSC-derived NPCs from transplanted DRG neurons. The DRGs from adult SD rats, injected with iPSC-NPCs (pre-differentiated for 10-15 days, and matured *in vivo* for 4-6 weeks), were dissociated and cultured, as described [10]. The neurons were visualized under optical microscopy prior to attempting current-clamp recordings. However, the location and limited numbers of GFP-expressing cells prevented their use for patch clamping. **(A)** A single eGFP+ cells adopted a neuronal-like shape closely resembling that of native rat DRG neurons. Magnification 40x. **(B)** Another eGFP+ cell also adopted a neuronal-like shape, but its small size suggests it to be immature. Magnification 40x **(C)** Cluster of iPSC-NPCs distinguished from the rest of the culture by their GFP expression. Their shape and size suggest that they did not further differentiate. Magnification 20x.

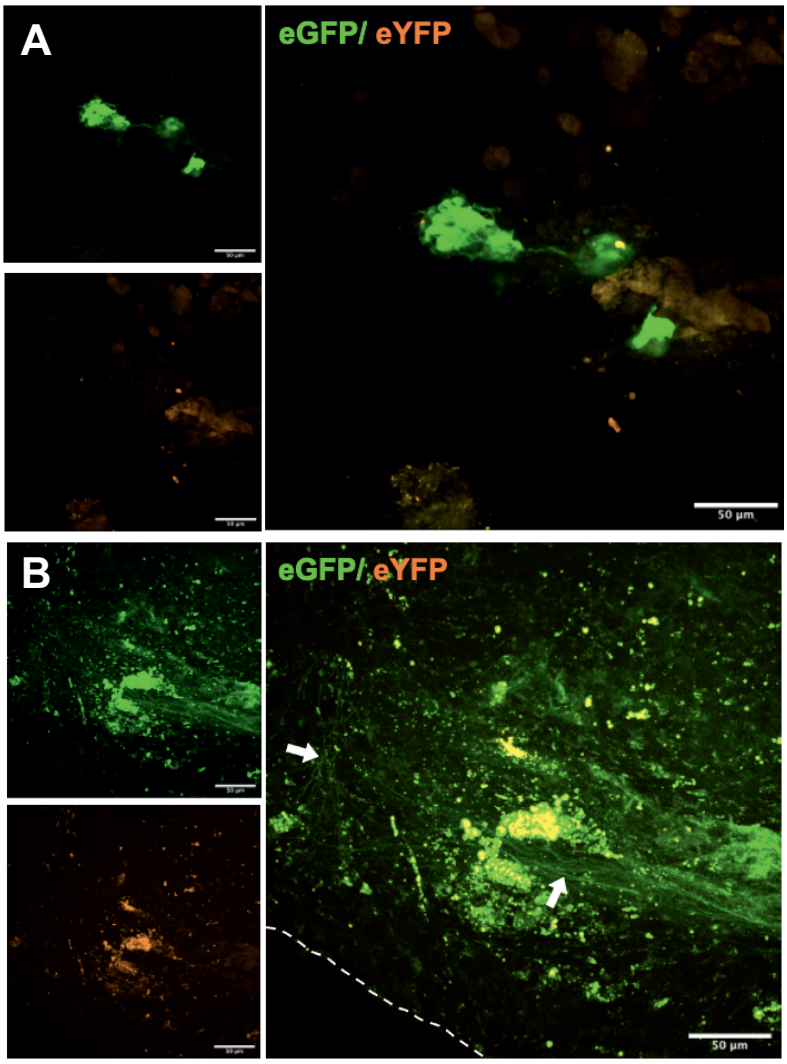

FIGURE S6 – Additional GFP-expressing cell clusters detected in neonatal DRG explants. Cell bodies with long extensions were detected through Z optical sections using spinning disk confocal microscopy throughout whole explants. eGFP fluorescent cells were imaged at 4 weeks post-injection of iPSC-NPCs in post-mortem neonatal rat DRGs, grown in Matrigel- or PDL/LAM-coated plates in DRG media. The Z-sections were stacked together and selected for maximal intensity and showed endogenous yellow fluorescent protein (eYFP) autofluorescence and eGFP fluorescence. Scale bars 50 µM. **(A)** eGFP+ cells with neuronal-like bodies and few extensions are clustered against the eYFP background, indicative of iPSC-specific fluorescence **(B)** eGFP+ fluorescence was detected exclusively in cellular extensions. The white arrows point to GFP+ extensions that did not show under yellow fluorescence, indicating that these soma-free elongations are not the result of autofluorescence, but are instead derived from iPSCs. The cell-like bodies however were excited at both frequencies and are less likely to be iPSC derivatives. The dotted line marks what appears to be the end of the sheath layer outside of the main ganglia.

Explant	ECM	Media	Growth factors	Time (weeks)	#injected NPC	Growth conditions	Exp type	GFP-fluor
1.1	Matrigel	DRG	NGF + GDNF	4	d12 10k	+	IHC	
1.2	Matrigel	NB	NGF	4	d12 10k	-	-	
1.3	Matrigel	DMEM/F12→ DRG replated	NGF → NGF+GDNF	4	d12 10k	+	Culture	
1.4	PDL/LAM	DRG	NGF + GDNF	4	d12 10k	Detached, replated	IHC	
1.5	PDL/LAM	NB	NGF + GDNF	4	d12 10k	detached	-	
1.6	COLIV, replated PDL/LAM	NB	NGF → NGF + GDNF	4	d12 10k	detached	-	
1.7	COL IV	DRG	NGF	4	d12 10k	detached	Culture	
1.8	Matrigel, PDL/LAM	NB → DRG	NGF + GDNF	4	d12 10k	Detached, replated	Culture	Yes
2.1	Matrigel	DRG	NGF + GDNF	3.5	d9 1k	+	Culture	
2.2	Matrigel	NB	NGF + GDNF	3.5	d9 1k	+	Culture	
2.3	Matrigel	DRG	NGF + GDNF	3.5	d16, 10k	+	Culture	
2.4	Matrigel	NB	NGF + GDNF	3.5	d16, 10k	+	IHC	Yes
2.5	PDL/LAM	DRG	NGF + GDNF	3.5	d9 1k	+	Culture	
2.6	PDL/LAM	NB	NGF + GDNF	3.5	d9 1k	+	IHC	Yes
2.7	PDL/LAM	DRG	NGF + GDNF	3.5	d16, 10k	+	IHC	Yes
2.8	PDL/LAM	NB	NGF + GDNF	3.5	d16, 10k	+	Culture	
3.1	Matrigel	DRG	NGF + GDNF	3	d12, 200	+	IHC	
3.2	Matrigel	DRG	NGF + GDNF	3	d12, 200	+	Culture	
3.3	Matrigel	DRG	NGF + GDNF	3	d12, 200	+	Culture	
3.4	PDL/LAM	DRG	NGF + GDNF	3	d12, 200	+	IHC	
3.5	PDL/LAM	DRG	NGF + GDNF	3	d12, 200	+	Culture	
3.6	PDL/LAM	DRG	NGF + GDNF	3	d12, 200	-	-	

TABLE S1 – Descriptive table of individual DRG explant culture conditions. The iPSC-NPCs transplanted into neonatal DRG explants were grown in one of three extracellular matrices (ECMs) and fed with one of three medium, supplemented with NGF, NGF/GDNF or no growth factors. The explants were extracted from four different rat pups and injected with iPSC-NPCs from four colonies, after 9, 12 or 16 days following the initiation of sensory neuronal differentiation. The number of cells injected in each DRG explant is indicated per colony. Explants that detached from their ECM were replated in PDL/LAM-coated dishes. The growth conditions and overall health of the explants is indicated as follows: (+) good, (-) bad. The explants that were maintained throughout the 3-4 weeks of culture were utilized for imaging analysis, with spinning disk microscopy of the whole DRG and immunohistochemistry of DRG sections, or for DRG culture, where explants were dissociated for patch clamp analysis. Endogenous GFP fluorescence was detected in four explants.

REFERENCES

1. Fu, W., et al., *Residual undifferentiated cells during differentiation of induced pluripotent stem cells in vitro and in vivo.* Stem Cells Dev, 2012. **21**(4): p. 521-9.
2. Martinez-Cerdeno, V., et al., *Behavior of Xeno-Transplanted Undifferentiated Human Induced Pluripotent Stem Cells Is Impacted by Microenvironment Without Evidence of Tumors.* Stem Cells Dev, 2017. **26**(19): p. 1409-1423.
3. Yamashita, T., et al., *Tumorigenic development of induced pluripotent stem cells in ischemic mouse brain.* Cell Transplant, 2011. **20**(6): p. 883-91.
4. Lamba, D.A., et al., *Generation, purification and transplantation of photoreceptors derived from human induced pluripotent stem cells.* PLoS One, 2010. **5**(1): p. e8763.
5. Zhang, J., et al., *Human Neural Stem Cells with GDNF Site-Specific Integration at AAVS1 by Using AAV Vectors Retained Their Stemness.* Neurochem Res, 2018. **43**(4): p. 930-937.
6. Oki, K., et al., *Human-induced pluripotent stem cells form functional neurons and improve recovery after grafting in stroke-damaged brain.* Stem Cells, 2012. **30**(6): p. 1120-33.
7. Schmalbruch, H., *The number of neurons in dorsal root ganglia L4-L6 of the rat.* Anat Rec, 1987. **219**(3): p. 315-22.
8. Fentress, J.C., B.B. Stanfield, and W.M. Cowan, *Observation on the development of the striatum in mice and rats.* Anat Embryol (Berl), 1981. **163**(3): p. 275-98.
9. Akin, E.J., et al., *Building sensory axons: Delivery and distribution of NaV1.7 channels and effects of inflammatory mediators.* Sci Adv, 2019. **5**(10): p. eaax4755.
10. Dib-Hajj, S.D., et al., *Transfection of rat or mouse neurons by biolistics or electroporation.* Nat Protoc, 2009. **4**(8): p. 1118-26.
11. Mis, M.A., et al., *Resilience to Pain: A Peripheral Component Identified Using Induced Pluripotent Stem Cells and Dynamic Clamp.* J Neurosci, 2019. **39**(3): p. 382-392.
12. Chambers, S.M., et al., *Combined small-molecule inhibition accelerates developmental timing and converts human pluripotent stem cells into nociceptors.* Nat Biotechnol, 2012. **30**(7): p. 715-20.

CHAPTER 5

Contributions of $Na_V1.8$ and $Na_V1.9$ to excitability in human iPSC-derived somatosensory neurons

Published as:

Matthew Alsaloum, **Julie I. R. Labau**, Shujun Liu, Mark Estacion, Peng Zhao, Fadia Dib-Hajj, Stephen G. Waxman. Contributions of $Na_V1.8$ and $Na_V1.9$ to excitability in human induced pluripotent stem-cell derived somatosensory neurons. Nature Scientific Reports (2021). **11**, 24283

https://doi-org.mu.idm.oclc.org/10.1038/s41598-021-03608-x

ABSTRACT

The inhibition of voltage-gated sodium channels (VGSCs) in somatosensory neurons presents a promising novel modality for the treatment of pain. However, the precise contribution of these channels to neuronal excitability, the cellular correlate of pain, is unknown; previous studies using genetic knockout models or pharmacologic block of VGSCs have identified general roles for distinct sodium channel isoforms, but have never quantified their exact contributions to these processes. To address this deficit, we have utilized dynamic clamp electrophysiology to precisely tune in varying levels of $Na_V1.8$ and $Na_V1.9$ currents into induced pluripotent stem cell-derived sensory neurons (iPSC-SNs), allowing us to quantify how graded changes in these currents affect different parameters of neuronal excitability and electrogenesis. We quantify and report direct relationships between $Na_V1.8$ current density and action potential half-width, overshoot, and repetitive firing. We additionally quantify the effect varying $Na_V1.9$ current densities have on neuronal membrane potential and rheobase. Furthermore, we examined the simultaneous interplay between $Na_V1.8$ and $Na_V1.9$ on neuronal excitability. Finally, we show that minor biophysical changes in the gating of $Na_V1.8$ can render human iPSC-SNs hyperexcitable, in a first-of-its-kind investigation of a gain-of-function $Na_V1.8$ mutation in a human neuronal background.

INTRODUCTION

Chronic pain affects approximately 100 million American adults[1] and similarly high proportions of adults globally[2-7], underscoring the importance of adequate pain management. Unfortunately, current mainstays of pain management are often only partially effective[8, 9], addictive[10], or are associated with serious adverse effects[11]. There is an urgent need for more effective, specific, and well-tolerated treatments for pain.

Voltage-gated sodium channels (VGSCs) have recently emerged as promising therapeutic targets in the treatment of pain. There are nine VGSC isoforms ($Na_V1.1$-$Na_V1.9$)[12, 13], three of which ($Na_V1.7$, $Na_V1.8$, and $Na_V1.9$)[14] are preferentially expressed in dorsal root ganglion (DRG) neurons, the primary afferents of the peripheral nervous system whose hyperexcitability has been shown to result in pain [15-18]. Additionally, all three of these sodium channels have been genetically and functionally linked to pain disorders in humans [19-26]. Consequently, clinical trials investigating the efficacy of VGSC blockers in multiple painful disease states have been conducted, although progress has been mixed and no $Na_V1.7$, $Na_V1.8$, or $Na_V1.9$-specific channel blocker has yet been approved for clinical use [27].

While the functional consequence of VGSC isoform mutations is well-understood, knowledge of the precise role of these channels is also helpful in designing channel blockers. Currently, most knowledge concerning the roles of $Na_V1.8$ and $Na_V1.9$ is based on biophysical studies in heterologous expression systems or derived from knock-out

or pharmacologic block studies. For example, Nav1.8 is known to contribute to the overshoot and width of DRG neuron action potentials through an all-or-none knockout study[28]. Similarly, Nav1.9 displays extensive window current[29] (i.e., overlap of activation and fast-inactivation) that has been theorized to contribute to the depolarized resting membrane potentials of rodent DRG neurons expressing a gain-of-function Nav1.9 variant[30]. However, no study has yet been able to quantify the relationship between varying levels of these currents and their effect on neuronal excitability, the cellular correlate of pain[31]. Moreover, there is a pressing need for these studies to be carried out in human DRG neurons.

Dynamic clamp is an electrophysiological technique that allows for modeled currents, derived from real recordings, to be added to or subtracted in precisely calibrated aliquots from cellular systems with high temporal and voltage fidelity[32]. Previous work has shown that adding Nav1.7 conductance to rodent DRG neurons results in a linear reduction in current threshold to action potential firing, whereas subtracting Nav1.7 conductance linearly increases the threshold to action potential firing[33]. However, there exist many differences between rodent and human DRG neurons, including in the level of expression of Nav1.8- and Nav1.9-positive nociceptors[34]. Fortunately, the development of induced pluripotent stem cell (iPSC) technology and the ability to differentiate iPSCs into somatosensory neurons (iPSC-SNs) that recapitulate human pain phenotypes[35, 36] has allowed for the interrogation of VGSCs in human cell backgrounds.

In this study, we capitalize on methodology that permits differentiation of peripheral somatosensory neurons from human IPSCs, and utilize dynamic clamp electrophysiology to confirm roles for the currents passed by Nav1.8 and Nav1.9 in these human cells. Using before-and-after recordings in the same human sensory neuron, we quantify the contribution of Nav1.8 to the action potential half-width and the sensory neuron's ability to repetitively fire action potentials. Similarly, we quantify a positive relationship between Nav1.9 currents and neuronal resting membrane potential. Moreover, we investigated the interplay between Nav1.8 and Nav1.9 on neuronal excitability, showing that there exists a range of maximal excitability that tapers off with excessive depolarization. Finally, in a first-of-its-kind analysis, we utilized dynamic clamp electrophysiology to simulate Nav1.8 gain-of-function in human sensory neurons, showing that even minor alterations in channel gating result in significant alterations in neuronal excitability.

METHODS

DIFFERENTIATION OF IPSCS INTO IPSC-SNS

We have previously identified a subject who underwent sequencing of the *SCN9A* gene, encoding Nav1.7, and was found to carry no pathogenic Nav1.7 mutations[36]. iPSCs were generated from this phenotypically normal subject (no abnormal pain) as previously described[36]. Differentiation of iPSCs into iPSC-SNs used an eight-week

modified Chambers protocol[35, 37, 38] (*Supplementary table 1*). Medium was changed twice weekly after day 12 through day 56 of differentiation and beyond for electrophysiology experiments; electrophysiological recordings were conducted within 7-14 days after completion of differentiation.

IMMUNOCYTOCHEMISTRY

Eight-week-old differentiated iPSCs-SNs were stained with sensory neuronal markers. The cells were grown on PDL/laminin- and matrigel-coated glass coverslips and were fixed for 10 minutes in 4% paraformaldehyde. Following a 30 minute incubation in 4% donkey serum, 2% BSA, and 0.1% Triton X-100 in PBS (PBS-T), iPSC-SNs were incubated with primary antibodies in PBS-T overnight at 4°C (Rabbit polyclonal anti-NeuN, 1:200, ab104225, Abcam; chicken polyclonal anti-Peripherin, 1:200, Aves Labs, Tigard, OR; rabbit polyclonal anti-BRN3A, 1:200, AB5945, Millipore; and mouse monoclonal anti-$Na_V1.7$, 1:250, 75-103, Neuromab). The cells were washed in 0.01 M PBS and incubated with secondary antibodies (Jackson ImmunoResearch Labs) in PBS-T (1:1000) for 2 hours at room temperature (Donkey anti-chicken-594, AB_2340375, donkey anti-mouse-647, AB_2340863; and donkey anti-rabbit-488, AB_2313584). Coverslips were mounted on microscope glass slides with Aqua Poly/Mount (Cat#18606, Polysciences). Images were acquired 24 hours later using a Nikon Confocal TiE inverted microscope with a Plan Fluor 10x and an Apo LWD 40x/1.5 WI λS, 0.15-0.19 DIC N2 (Nikon, Melville, NY).

DIGITAL DROPLET POLYMERASE CHAIN REACTION (ddPCR)

Human iPSC-SNs were processed for RNA extraction using an RNeasy kit (Qiagen, Germantown, MD) according to the manufacturer's protocol. iPSC-SNs were gently enzymatically detached from the vial they were differentiated in and centrifuged immediately for ddPCR analysis, limiting the time possible for gene expression changes. A total of 135 ng of RNA was reverse transcribed using iScript™ Reverse Transcription Supermix (Bio-Rad, Hercules, CA) according to the manufacturer's instructions. All reagents and equipment used for ddPCR were from Bio-Rad. Twenty-five µl reactions consisted of 1X ddPCR™ Supermix for probes, 1X target primers/probe mix/FAM, 1X reference primers/probe mix/HEX, which correspond to a final concentration of 900 nM primers and 250 nM probe. All the primers/probe mix were from either Bio-Rad or ThermoFisher Scientific (see supplementary table 2 for details). The samples were partitioned into 20,000 nanoliter-sized droplets using a Droplet Generator. The emulsion of droplets was transferred into a 96-well plate, heat-sealed with pierceable foil, and amplified in a C1000 Touch Thermal Cycler (Bio-Rad). The cycling protocol starts with a 95 °C enzyme activation step for 10 minutes, followed by 40 cycles of a two-step cycling protocol (94 °C for 30 seconds and 60 °C for 1 minute). The cycling protocol was followed by an enzyme deactivation step of 98 °C for 10 minutes. A ramp rate of 2 °C per second was required for each step in the PCR. When cycling was complete, the plate was loaded into the QX200 Droplet Reader (Bio-Rad) and data was analyzed using QuantaSoft™ Software (version 1.6.6, Bio-Rad).

WHOLE – CELL VOLTAGE – CLAMP RECORDINGS FROM IPSC-SNS

All patch clamp recordings were obtained using an EPC-10 amplifier and the PATCHMASTER program (HEKA Elektronik, Holliston, MA) at room temperature (22-25 °C). Patch pipettes were pulled from borosilicate glass (1.65/1.1 mm, outside diameter/inside diameter, World Precision Instruments, Sarasota, FL) using a Sutter Instruments P-97 puller and had a resistance of 0.7-1.5 MΩ. Extracellular bath solution contained (in mM): 140 NaCl, 20 tetraethylammonium (TEA), 3 KCl, 1 $CaCl_2$, 1 $MgCl_2$, 10 HEPES, 0.1 CdCl (± 0.001 TTX). The extracellular bath solution was titrated to a pH of 7.3 and the osmolarity was titrated to approximately 320 mOsm with sucrose. Intracellular pipette solution consisted of (in mM): 140 CsF, 10 NaCl, 1.1 EGTA, 10 HEPES, and 20 dextrose. The pH was titrated to 7.3 with CsOH and the osmolarity was also titrated to approximately 320 mOsm.

Total sodium current was recorded in TTX-free extracellular solution. iPSC-SNs were held at -100 mV and subsequently stepped to potentials between -80 and + 40 mV in 5 mV increments for 100 ms duration. To measure total TTX-R currents, the same protocol was applied in a nearly identical bath solution, differing only in the presence of 1 μM TTX. To measure $Na_V1.8$ currents, iPSC-SNs were held at -50 mV to inactivate all non-$Na_V1.8$ channels[39-43] and then stepped to potentials, for 100 ms, between -80 and +40 mV. $Na_V1.9$ currents were considered present if a persistent current with peak current amplitude around -50 mV was observed after reference series subtraction of the current evoked by holding neurons at -50 mV from total TTX-R current. No $Na_V1.9$ currents were appreciated using this paradigm.

ISOLATION AND VOLTAGE – CLAMP RECORDINGS OF PRIMARY HUMAN AUTOPSY – DERIVED DRG NEURONS

Human DRG tissues [lumbar 4 (L4) or thoracic 12 (T12)] were received as anonymized samples from the National Disease Research Interchange. Studies with human tissues were approved by the human investigation committee at Yale University and all methods were performed in accordance with the relevant guidelines and regulations. DRGs were recovered from multiple adult (ages 18-70) human donors, of both sexes, with no history of diabetes, neuropathies, cancer, chemotherapy, or radiation. Previous use of antiepileptic, antiarrhythmic, or local anesthetic medications were also exclusion criteria, as well as any history of trauma to the lower limbs or a history of lumbosacral injury or pain. Human DRGs were obtained from organ donors with full legal consent for use of tissue for research. Informed consent was acquired prior to all tissue donation. DRG neurons were harvested and dissociated within 30 hours of clamping the aorta.

Human DRG neurons were cultured as previously described [44]. In brief, nerve roots and connective tissue were removed, DRGs were sliced into small pieces in complete saline solution (CSS) [in mM: 137 NaCl, 5.3 KCl, 1 MgCl2, 25 sorbitol, 3 CaCl2, and 10 HEPES, adjusted to pH 7.2 with NaOH], and then incubated on a rotating shaker at 37°C for 40-60 minutes in CSS containing 0.5 U/mL Liberase TM (Roche) and 0.6 mM EDTA. This was followed by a 25-40 minute (L4 DRG) or 40-60 minute (T12 DRG)

incubation at 37°C in CSS containing 0.5 U/mL Liberase TL (Roche), 0.6 mM EDTA, and 30 U/mL papain (Worthington Biochemical). DRGs were then triturated in DRG media [DMEM/F12 (Invitrogen) with 100 U/ml penicillin, 0.1 mg/ml streptomycin (Invitrogen), and 10% fetal bovine serum (Hyclone)] containing 1.5 mg/mL BSA (low endotoxin) and 1.5 mg/mL trypsin inhibitor (Sigma). After filtering with a 100 μm nylon mesh cell strainer (BD Biosciences), the cell suspension was centrifuged and the cell pellet was resuspended in DRG media. 100 μl of cell suspension were plated onto each poly-D-lysine/laminin-coated coverslip (BD Biosciences). Plated DRG neurons were incubated at 37°C in a 95% air/5% CO2 (vol/vol) incubator for 60-90 minutes to allow neurons to adhere. 900 μL of DRG media supplemented with nerve growth factor (50 ng/mL) and glial cell line-derived neurotrophic factor (50 ng/mL) were added into each well. DRG neurons were maintained at 37°C in a 95% air-5% CO_2 (vol/vol) incubator and recorded by whole cell patch clamp between 1- and 4-days post-culture. $Na_V1.8$ currents were recorded from human DRG neurons in a bath solution containing (in mM): 70 NaCl, 70 N-methyl-d-glucamine (NMDG), 20 TEA, 3 KCl, 1 $CaCl_2$, 1 $MgCl_2$, 10 HEPES, 0.1 CdCl, and 0.001 TTX. The pH was titrated to 7.3 with HCl and the osmolarity was titrated to approximately 320 mOsm with sucrose. Intracellular pipette solution consisted of (in mM): 140 CsF, 10 NaCl, 1.1 EGTA, 10 HEPES, and 20 dextrose. The pH was titrated to 7.3 with CsOH and the osmolarity was also titrated to approximately 320 mOsm. $Na_V1.8$ currents were recorded from human DRG neurons by first holding the cells to -60 mV to inactivate $Na_V1.9$ channels. Cells were then stepped to a range of potentials, from -80 to +40 mV in 5 mV increments, for 200 ms to record $Na_V1.8$ currents. Data were sampled every 20 μs and P/6 leak subtraction was implemented.

CURRENT – CLAMP AND DYNAMIC – CLAMP RECORDINGS OF IPSC-SNS

iPSC-SNs were recorded from within 7-14 days after the completion of the eight-week differentiation protocol, with medium changes twice per week. Extracellular bath solution contained (in mM): 140 NaCl, 3 KCl, 2 $CaCl_2$, 2 $MgCl_2$, 15 dextrose, and 10 HEPES. Osmolarity was brought to approximately 320 mOsm with sucrose and the pH was titrated to 7.3 with NaOH. Intracellular pipette solution contained (in mM): 140 KCl, 3 Mg-ATP, 0.5 EGTA, 5 HEPES, and 20 dextrose. Osmolarity was similarly adjusted to approximately 320 mOsm and the pH was adjusted to 7.3 using KOH. Current-clamp recordings were sampled at 50 KHz and filtered using two Bessel filters at 10 and 2.9 KHz.

iPSC-SNs with an input resistance lower than 200 MΩ were excluded from analysis. Input resistance was determined by the slope of a linear fit to hyperpolarizing responses to current steps from −5 pA to −40 pA in −5 pA increments. Additionally, neurons with an action potential overshoot below +40 mV were excluded. Multiple recordings, before and after the addition of currents by dynamic clamp, were taken from each neuron, contingent upon the input resistance remaining above 200 MΩ. Dynamic clamp models of $Na_V1.8$ and $Na_V1.9$ were derived from published literature; see Han *et al.*[44] and Huang *et al.[26]* for further information regarding the kinetic

models of these channels. iPSC-SNs were dynamically clamped using the Cybercyte DC1 dynamic clamp system (Cytocybernetics, Buffalo, NY)[45, 46].

In brief, the Nav1.8 channel model was based on Hodgkin-Huxley equations $\frac{dm}{dt} = \alpha_m(1-m) - \beta_m m$ and $\frac{dh}{dt} = \alpha_h(1-h) - \beta_h h$, where m and h represent channel activation and inactivation gates, and α and β are forward and backward rate constants, respectively. These rate constants were voltage-dependent and defined by the following equations:

$$\alpha_m = 7.35 - \frac{7.35}{1 + e^{\frac{V+1.38}{10.9}}}$$

$$\beta_m = \frac{5.97}{1 + e^{\frac{V+56.43}{18.26}}}$$

$$\alpha_h = 0.011 + \frac{1.39}{1 + e^{\frac{V+78.04}{11.32}}}$$

$$\beta_h = 0.56 - \frac{0.56}{1 + e^{\frac{V-21.82}{20.03}}}$$

Similarly, Nav1.9 was modeled with the following equations:

$$\alpha_m = \frac{0.751}{1 + e^{\frac{-(V+32.26)}{13.71}}}$$

$$\beta_m = \frac{5.68}{1 + e^{\frac{V+123.71}{13.94}}}$$

$$\alpha_h = \frac{0.082}{1 + e^{\frac{V+113.69}{17.4}}}$$

$$\beta_h = \frac{0.24}{1 + e^{\frac{-(V-10.1)}{17.2}}}$$

$$\alpha_s = \frac{0.019}{1 + e^{\frac{V+154.51}{11.46}}}$$

$$\beta_s = \frac{0.000376}{1 + e^{\frac{-(V+60.92)}{15.79}}}$$

In the case of the Nav1.9 channel, a slow-inactivation gate (s variable) was included and modeled using the $\frac{ds}{dt} = \alpha_s(1-s) - \beta_s s$. Nav1.8 current was described by $I_{Na} = g_{max} * m^3 * h * (V_m - E_{Na})$. Nav1.9 current was described by the equation $I_{Na} = g_{max} * m * h * s * (V_m - E_{Na})$, where g_{max} is the maximal conductance and E_{Na} is the reversal potential, which was set to +65 mV.

Current threshold was defined as the first current injection step that resulted in action potential firing without subsequent failure and was determined by a series of depolarizing current injections (200 ms) that increased incrementally by 5 pA. For the

calculation of threshold, action potentials were defined as rapid increases in membrane potential to >40 mV with a total amplitude >80 mV. However, as neurons often attenuate firing with repetitive action potential spiking, when examining repetitive firing, action potentials were counted if the membrane potential rapidly crossed 0 mV, regardless of overshoot or total amplitude. Action potential repetitive firing was determined by summing the total number of action potentials that a neuron fired after a 500 ms current injection.

DATA ANALYSIS AND VISUALIZATION

Data were analyzed and visualized in GraphPad Prism and Matlab (for three-dimensional surface fitting). Significance in figures is noted as * ($p \leq 0.05$), ** ($p \leq 0.01$), or *** ($p \leq 0.001$). Paired Student's t-tests were conducted when comparing before-and-after recordings from the same neurons. Best-fit equations are graphed with a solid line. Individual points on graphs represent individual recordings, although multiple recordings were conducted in cells that continued to meet inclusion criteria (input resistance at least 200 MΩ and an action potential amplitude, measured from resting potential to peak, of > 80 mV). Hashed lines on graphs represent the 95% confidence interval for fitted equations.

RESULTS

Generation and characterization of iPSC-SNs

All iPSCs were differentiated from a previously identified subject with no abnormal pain and no $Na_V1.7$ channel mutations[36] into iPSC-SNs using a modified Chambers protocol that produces pain-sensing sensory-like neurons[35, 37, 47] (*Supplementary table 1*). The differentiated cells were validated as peripheral somatosensory neurons by immunocytochemistry (*Figure 1A*). iPSC-SNs stained positively for peripherin (a marker of peripheral neurons), Brn3a (a marker of sensory neurons[48]), NeuN (a marker of neuronal nuclei), and $Na_V1.7$. Unpublished work from our lab and others in this field has questioned whether current iPSC-SN differentiation protocols are able to express the TTX-R VGSCs, $Na_V1.8$ and $Na_V1.9$, seen in human DRG neurons. In line with these previous observations, we were unable to show any $Na_V1.8$ or $Na_V1.9$ RNA by ddPCR (*Figure 1B*) or current by whole-cell voltage-clamp electrophysiology (*Figure 1C*); conversely, the iPSC-SNs expressed very high levels of $Na_V1.7$, as would be expected from somatosensory neurons. TTX-R currents observed in iPSC-SNs exhibited a very hyperpolarized $V_{1/2}$ of activation (-38.17 ± 1.80 mV, n = 8) and fast-inactivation (-87.79 ± 2.93 mV, n = 5, *Figure 1D*), consistent with previous characterizations of iPSC-SNs and closer to values for $Na_V1.5$ than for $Na_V1.8$ [49], suggesting that these cells displayed some characteristics of immature somatosensory-like neurons. Evaluation of iPSC-SNs baseline characteristics by current-clamp displayed largely normal properties with an average cell capacitance of 27.09 ± 1.25 pF, an average input resistance of 320.07 ± 16.2 MΩ, and an average resting membrane potential of -57.25 ± 0.41 mV (n = 71).

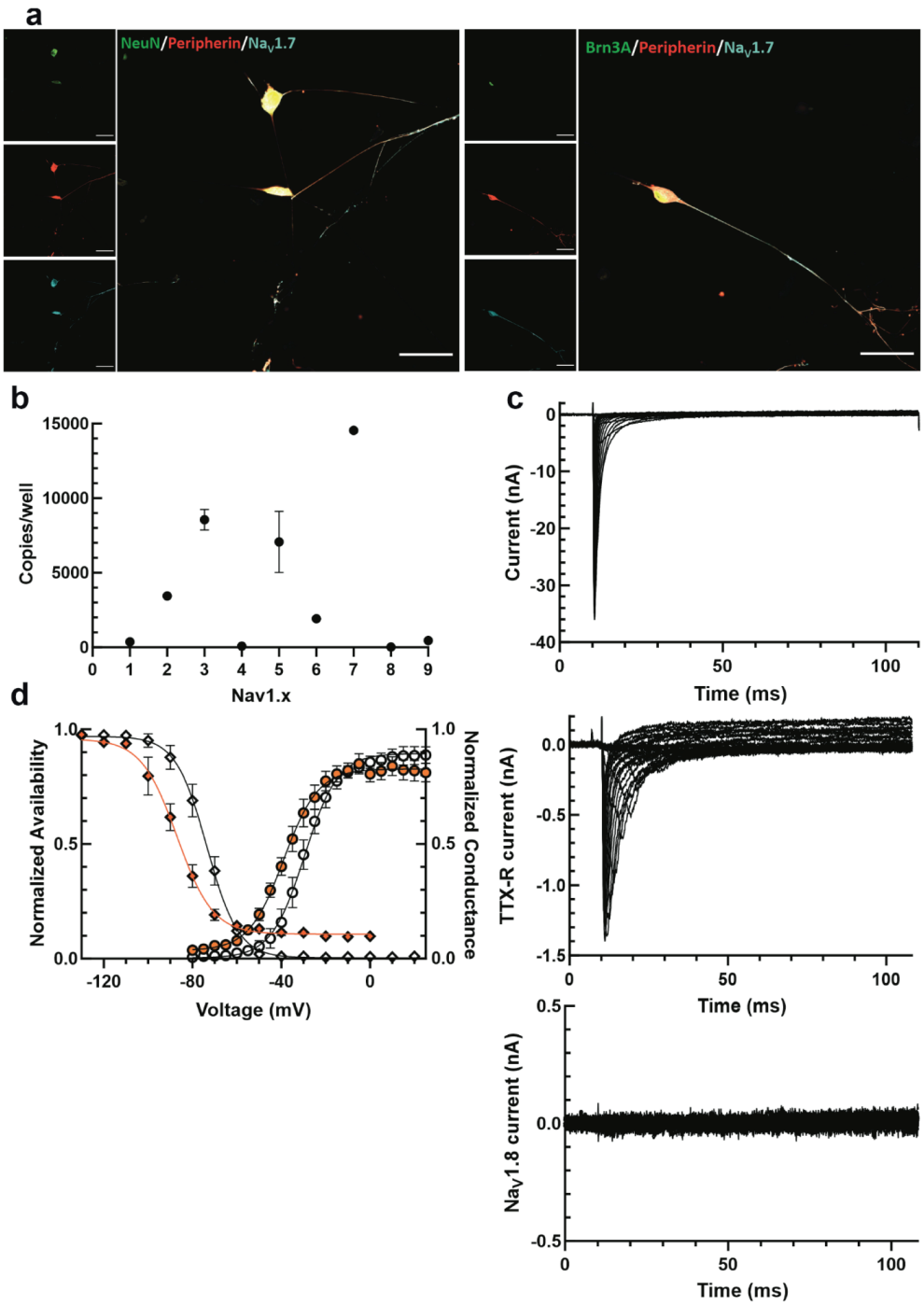

FIGURE 1 – Generation and characterization of IPSC-SNs. (A) iPSC-SNs express canonical sensory neuronal markers. 50 µm scale bar for reference. **(B)** iPSC-SNs express very high levels of Nav1.7 mRNA, but virtually no levels of Nav1.8 and Nav1.9 mRNA, as determined by droplet digital PCR. **(C)** Representative current traces recorded from iPSC-SNs confirm large total sodium currents (top).

However, application of 1 μM tetrodotoxin reveals very little tetrodotoxin-resistant current, which behaves like $Na_V1.5$ and not $Na_V1.8$ or $Na_V1.9$ (middle). Consistent with the lack of $Na_V1.8$ expression by PCR analysis, there is also no $Na_V1.8$ current when cells are clamped at a holding potential of -50 mV to inactivate all other sodium channels besides $Na_V1.8$ (bottom). (D) The $V_{1/2}$ of activation (open circles) and fast-inactivation (open diamonds) of total sodium current in iPSC-SNs was -29.83 ± 2.43 mV and -74.08 ± 2.55 mV, respectively. The $V_{1/2}$ of activation (orange circles) and fast-inactivation (orange diamonds) of TTX-R sodium currents in iPSC-SNs was -38.17 ± 1.80 mV and -87.79 ± 2.93 mV, respectively.

The interesting absence of $Na_V1.8$ and $Na_V1.9$ from the differentiated iPSC-SNs allows for introduction of precisely calibrated levels of these currents by dynamic clamp. Rather than first voltage-clamping neurons to measure the current levels (which may run up or down during experimentation [50-53]), and then subtracting out the measured—and adding back in the modeled—TTX-R currents, we are able to know precisely how much $Na_V1.8$ and $Na_V1.9$ current the neurons are conducting since the amplitude of current is precisely controlled by dynamic clamp.

$Na_V1.8$ contributes to action potential overshoot, half-width, and repetitive firing

To investigate the effects of $Na_V1.8$ currents on parameters of cellular excitability, we tuned in varying levels of $Na_V1.8$ current density using a previously published kinetic model of the human $Na_V1.8$ channel[44] and the CytoCybernetics Cybercyte dynamic clamp system. The peak $Na_V1.8$ current density injected was determined by normalizing the peak modeled current (determined by a series of 100 ms pulses from a holding potential of -100 mV to + 40 mV) to the cell capacitance of the patched iPSC-SN. Representative traces of iPSC-SNs with various levels of modeled $Na_V1.8$ current visualize an effect of increasing this current density on neuronal action potentials (*Figure 2A*).

As we controlled the precise amount of $Na_V1.8$-like current passing through the cell, we next sought to quantify the effect of this conductance on neuronal excitability and electrogenesis properties. First, as Renganathan *et al.* showed, $Na_V1.8$ plays an important role in contributing to the overshoot of the action potential[28], likely due to this channel's depolarized voltage-dependences of activation and inactivation[54]. We observed this visually, but quantifying this parameter proved to be difficult as the action potential overshoot cannot exceed the Nernst potential of approximately +67 mV[55]. Indeed, the absolute maximum overshoot observed in our study was +68 mV. We attempted to best quantify the change in action potential overshoot by stimulating neurons with 200 ms long square pulses of increasing current amplitude (from 5 pA) in 5 pA increments, until the current threshold was reached. We then measured the action potential overshoot at threshold before and after injection of $Na_V1.8$ current by dynamic clamp (*Figure 2B*). As the ability for the action potential overshoot to increase is diminished as the initial overshoot nears the Nernst potential for sodium, we have binned the data in 5 mV increments, based on the overshoot amplitude prior to

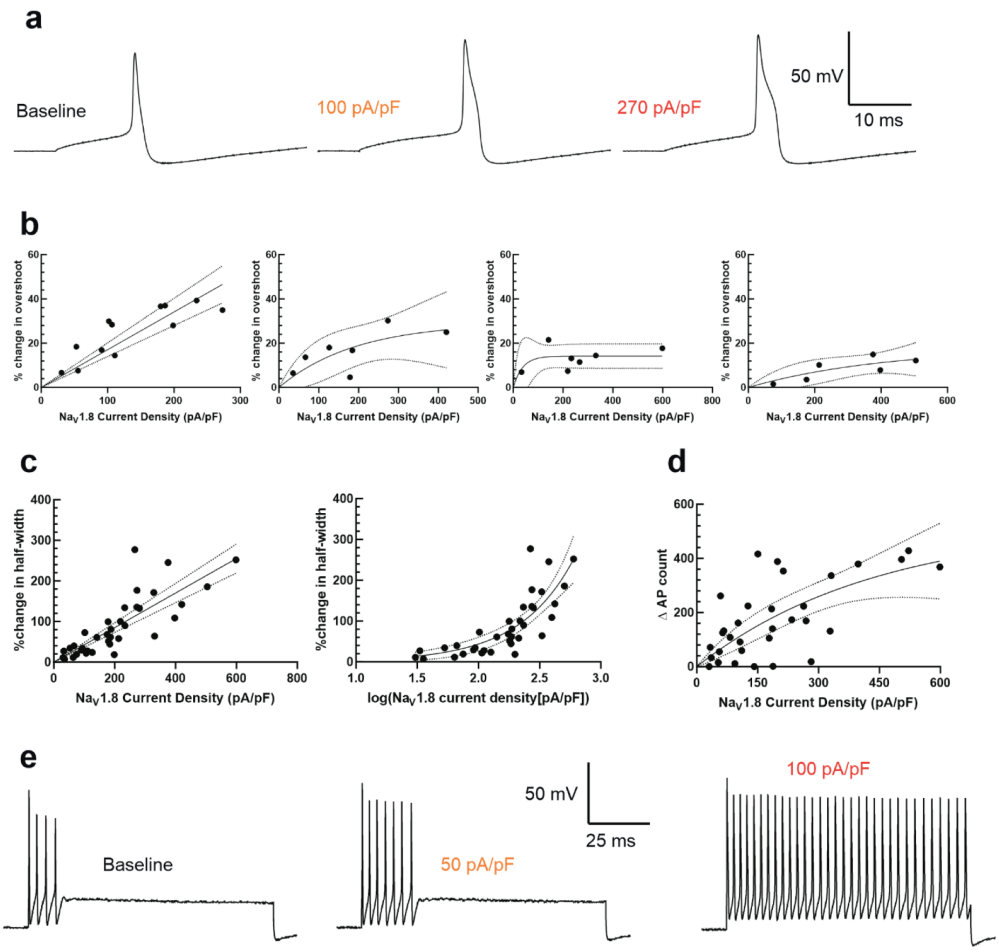

FIGURE 2 – $Na_V1.8$ contributes to action potential overshoot, half-width, and repetitive firing. (A) Representative traces from the same iPSC-SN illustrating the action potential waveform in the setting of varying levels of $Na_V1.8$ current density. **(B)** Increasing $Na_V1.8$ current density increases the overshoot of iPSC-SNs, although the effect is more robust at lower initial overshoot amplitudes. For neurons with an initial overshoot amplitude between 40-45 mV (far left), the change in overshoot is best fit with a linear model with slope 0.1706 and an r^2 of 0.5093. For neurons with an initial overshoot between 45-50 mV (center-left), 50-55 mV (center-right), and 55-60 mV (far right), the change in overshoot amplitudes are best fit with exponential association equations. **(C)** Increasing $Na_V1.8$ current density directly increases the action potential half-width of iPSC-SNs linearly (% change in half-width = 0.4254*current density) with an r^2 of 0.65. An equivalent transformation of the data into base-10 logarithmic form illustrates a similarly robust relationship (% change in half-width = $0.4816*e^{2.253(\log[\text{current density}])}$) with an r^2 of 0.6502. **(D)** Increasing $Na_V1.8$ current density enhances iPSC-SN repetitive firing following (Δ action potential count = $524.9*(1-e^{-0.002266(\text{current density})})$ with an r^2 of 0.4164. **(E)** Representative traces depicting the response of the same iPSC-SN to a 1 second duration 500 pA suprathreshold stimulus with no $Na_V1.8$ currents injected via dynamic clamp (left), approximately 50 pA/pF $Na_V1.8$ current density (middle), and 100 pA/pF current density (right).

dynamic clamp injection. There is a clear linear relationship (slope = 0.1706, r^2 = 0.59) between $Na_V1.8$ current density and action potential overshoot in neurons whose

baseline overshoot was between +40 and +44.99 mV (*Figure 2B*, left), which represented a plurality of the recordings (n=12). This relationship becomes less obvious as the baseline overshoot is increased.

To quantify the observed effect of $Na_V1.8$ currents on action potential half-width, a similar paradigm was implemented as above. The half-width was determined as the duration of time between the rising phase and falling phase of the action potential at the point midway between the overshoot and the undershoot. We observed a linear relationship between $Na_V1.8$ current density and action potential half-width (*Figure 2C*, left), with a slope of 0.4254 and an r^2 of 0.65. This relationship was similarly strong when current density was transformed into the base-10 logarithmic form (*Figure 2C*, right). Additionally, $Na_V1.8$ exhibits rapid recovery from inactivation[56], which has been thought to contribute to repetitive action potential firing in DRG neurons. To quantify this contribution, we stimulated DRG neurons with square pulses of 500 ms duration that increased in amplitude between 25 pA and 500 pA in 25 pA increments. We summed up the total number of action potentials fired under this protocol before and after injection of $Na_V1.8$ modeled currents by dynamic clamp (*Figure 2D*). We noted a direct relationship between $Na_V1.8$ current density and action potential repetitive firing, with r^2 of 0.4164. Representative traces (*Figure 2E*) illustrate the effect of varying the $Na_V1.8$ peak current density injected via dynamic clamp on the same iPSC-SN when stimulated by a 500 pA suprathreshold stimulus. We also recorded $Na_V1.8$ currents from human DRG neurons (*Figures 5B-C*). If iPSC-SNs lacking endogenous $Na_V1.8$ currents expressed a similar level as autopsy-derived human DRG neurons (~290 pA/pF), we would expect that these iPSC-SNs would fire approximately 250 more action potentials across our range of stimuli and would have a half-width approximately 120% as wide.

Increasing $Na_V1.9$ currents depolarize the resting membrane and reduce the threshold to action potential firing

We then investigated the role of $Na_V1.9$ in neuronal excitability. Our primary focus was on the $Na_V1.9$'s ability to set and depolarize the neuronal membrane potential. Because of extensive overlap between the activation and inactivation curves of the channel, $Na_V1.9$ passes significant amounts of "window current," and gain-of-function mutations have been linked to depolarized resting potentials in DRG neurons[26]. To quantify the ability of $Na_V1.9$ currents to set the resting membrane potential, we averaged 30 seconds of passive membrane potential with no stimulus before addition of any modeled $Na_V1.9$ current density and compared that average membrane potential, in the same neuron, after addition of modeled $Na_V1.9$ currents by dynamic clamp (*Figure 3A*). We observed a positive correlation between $Na_V1.9$ current density and membrane potential depolarization (which ranged from 0 mV with no addition of $Na_V1.9$ current, to 9.7 mV with addition of 235 pA/pF Nav1.9 current), and, when fit with an exponential growth equation, the r^2 of the fit was 0.5764. The addition of $Na_V1.9$ current density to iPSC-SNs depolarized their resting membrane potential, theoretically bringing them closer to the voltage threshold for action potential firing.

$f(x,y) = p00 + p10*x + p01*y + p20*x^2 + p11*x*y + p02*y^2$		
Coefficients	Value	95% confidence bounds
p00	-0.4887	(-3.214, 2.237)
p10	0.0159	(-0.01317, 0.04496)
p01	0.05811	(0.02557, 0.09064)
p20	$-3.091*10^{-5}$	(-0.0001129, $5.11*10^{-5}$)
p11	$-7.22*10^{-5}$	(-0.0002453, 0.0001009)
p02	$-8.082*10^{-5}$	(-0.0001426, $-1.908*10^{-5}$)

TABLE 1 – Parameters of the polynomial fit of $Na_V1.8$ and $Na_V1.9$ current density on neuronal membrane potential

Therefore, we sought to quantify whether there was a relationship between $Na_V1.9$ current density and the current stimulus required for action potential firing. iPSC-SNs with $Na_V1.9$ currents by dynamic clamp displayed a significantly reduced threshold to action potential firing (*Figure 3B* left, paired Student's t-test p = 0.0043, n =26). However, there appeared to be no relationship between the amount of $Na_V1.9$ current density and the reduction in current threshold (*Figure 3B*, right).

$f(x,y) = p00 + p10*x + p01*y + p20*x^2 + p11*x*y + p02*y^2$		
Coefficients	Value	95% confidence bounds
p00	-180.8	(-448.4, 86.75)
p10	1.967	(-0.8241, 4.758)
p01	3.708	(0.8919, 6.524)
p20	-0.003327	(-0.01024, 0.003586)
p11	-0.0001459	(-0.01556, 0.01527)
p02	-0.009923	(-0.01862, -0.00123)

TABLE 2 – Parameters of the polynomial fit of $Na_V1.8$ and $Na_V1.9$ current density on repetitive action potential firing

$Na_V1.8$ and $Na_V1.9$ work together to contribute to repetitive firing of DRG neurons

Because human DRG neurons may express both $Na_V1.8$ and $Na_V1.9$, we then investigated the interplay between currents from these two channels on parameters of neuronal excitability. First, we varied $Na_V1.8$ and $Na_V1.9$ current densities and evaluated the depolarization of the resting membrane potential in response to these alterations (*Figure 4A*). When fit with a polynomial with two degrees of freedom for the x variable and two degrees of freedom for the y variable (to avoid overfitting), our model indicated that $Na_V1.9$ currents are predominantly responsible for changing the neuronal membrane potential. The adjusted r^2 of the fit was 0.4147 and coefficient values for the fit are located in *Table 1*. At potentials more negative than -50 mV, the window current created by the overlap of activation and inactivation allows for the depolarizing effect of the $Na_V1.9$ currents on neuronal resting membrane potential,

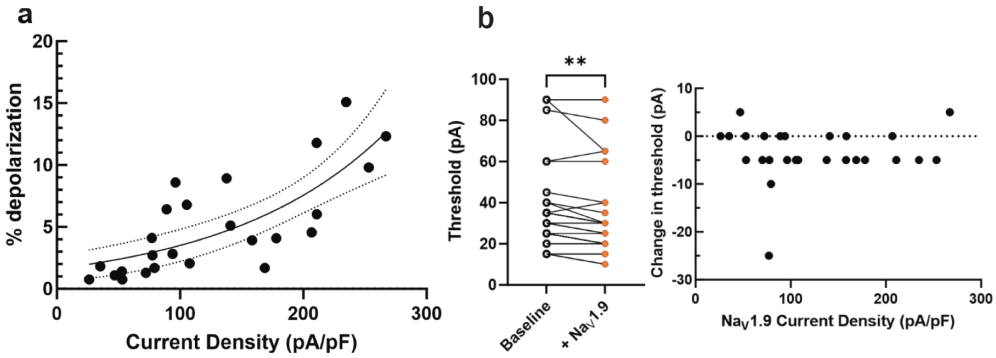

FIGURE 3 – Nav1.9 is responsible for setting the neuronal resting membrane potential and plays a role in setting the threshold to action potential firing. (A) Increasing Nav1.9 current density depolarizes iPSC-SN resting membrane potentials (% depolarization = $1.629*e^{0.007674(\text{current density})}$ with an r^2 of 0.5764. **(B)** Adding Nav1.9 currents to iPSC-SNs results in a statistically significant reduction in threshold to action potential firing (left, paired t-test p = 0.0043). However, there does not appear to be a strong correlation between the levels of Nav1.9 current density and the change in threshold (right).

although the effect observed here may be limited by inactivation as the membrane potential depolarizes further[29]. However, no iPSC-SNs patched in this study had a resting membrane potential more positive than -49.67 mV and the average membrane potential was approximately -57 mV.

We also investigated the effect of dual Nav1.8 and Nav1.9 currents on repetitive firing in human iPSC-SNs (*Figure 4B*). When also fit with a polynomial with two degrees of freedom for the x and y variables, the adjusted r^2 of the fit was 0.3514. Interestingly, the model predicts a peak "zone" of excitability in the interplay between Nav1.8 and Nav1.9; as Nav1.9 current density increases, the ability of a neuron to repetitively fire increases, up to a point, until excitability again begins to dampen—creating an "inverted u-shaped"[57] model for neuronal excitability, which likely reflects reduced availability of Nav1.7 as increased levels of Nav1.9 depolarize the neuronal membrane potential. The coefficient values for the fit can be found in *Table 2*.

Small biophysical changes in Nav1.8 significantly alter excitability of human neurons

Having shown that variations in TTX-R current levels result in significant changes in neuronal excitability, we next investigated whether variations in gating properties also result in appreciable alterations in excitability. The Nav1.8-I1706V small-fiber neuropathy-associated variant displays a hyperpolarized $V_{1/2}$ of activation, approximately 6 mV more hyperpolarized than wild-type, with no change in the voltage-dependence of fast-inactivation [58]. To roughly approximate this mutation, we equally hyperpolarized the activation of our Nav1.8 dynamic clamp model (*Fig 5A*).

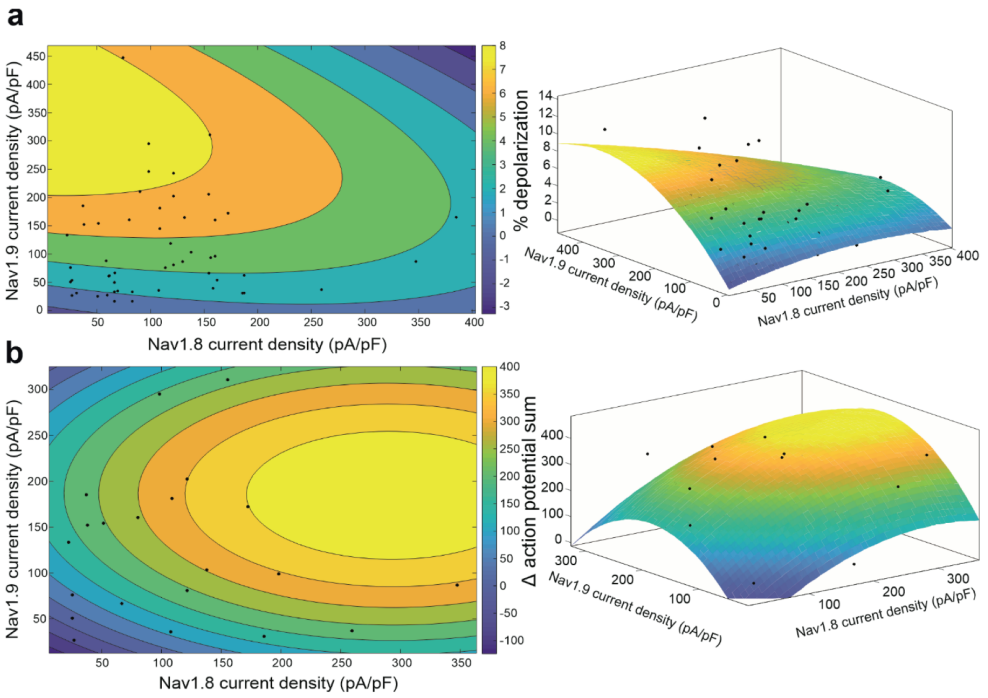

FIGURE 4 – While the resting membrane potential is primarily set by Nav1.9, both Nav1.9 and Nav1.8 play important roles in repetitive firing. (A) The relationship between Nav1.8 and Nav1.9 current densities with the change in iPSC-SN resting membrane potential can be approximated with a 3-dimensional polynomial curve with two degrees of freedom for the x- and y-axes (right, adjusted r^2 = 0.4147). A contour plot (left) of this fit illustrates that Nav1.9 current density has a stronger effect on changing the neuronal resting membrane potential. **(B)** The relationship between Nav1.8 and Nav1.9 current densities with the change in iPSC-SN repetitive firing can be approximated with a 3-dimensional polynomial curve with two degrees of freedom for the x- and y-axes (right, adjusted r^2 = 0.3514). A contour plot of this fit illustrates that both Nav1.8 and Nav1.9 contribute to enhanced repetitive firing.

Rather than tune in arbitrary amounts of Nav1.8 current density, we determined the approximate Nav1.8 current levels expressed in human neurons by voltage-clamping autopsy- derived human DRG neurons. To isolate TTX-R channels from the full complement of ion channels expressed in human DRG neurons, extracellular bath solution contained 1 μM TTX, 20 mM TEA, 0.1 mM $CdCl_2$, and intracellular pipette solution contained 140 mM CsF. Additionally, Nav1.8 was isolated from Nav1.9 by holding DRG neurons at -60 mV, which inactivates the Nav1.9 channels. To improve voltage control, extracellular sodium was reduced to 70 mM (see representative traces in *Figure 5B*). Human Nav1.8 current density was recorded (*Figure 5C*). The average recorded value was doubled, to correct for the reduced sodium bath solution, and tuned into iPSC-SNs via dynamic clamp. Outliers were not excluded given that human DRG neurons represent a heterogeneous population of cells.Nav1.8 current was first tuned into iPSC-SNs as 100% wild-type Nav1.8. In the same neuron, 50% of the Nav1.8 current density was replaced with 50% "Nav1.8-I1706V" current density. First, we

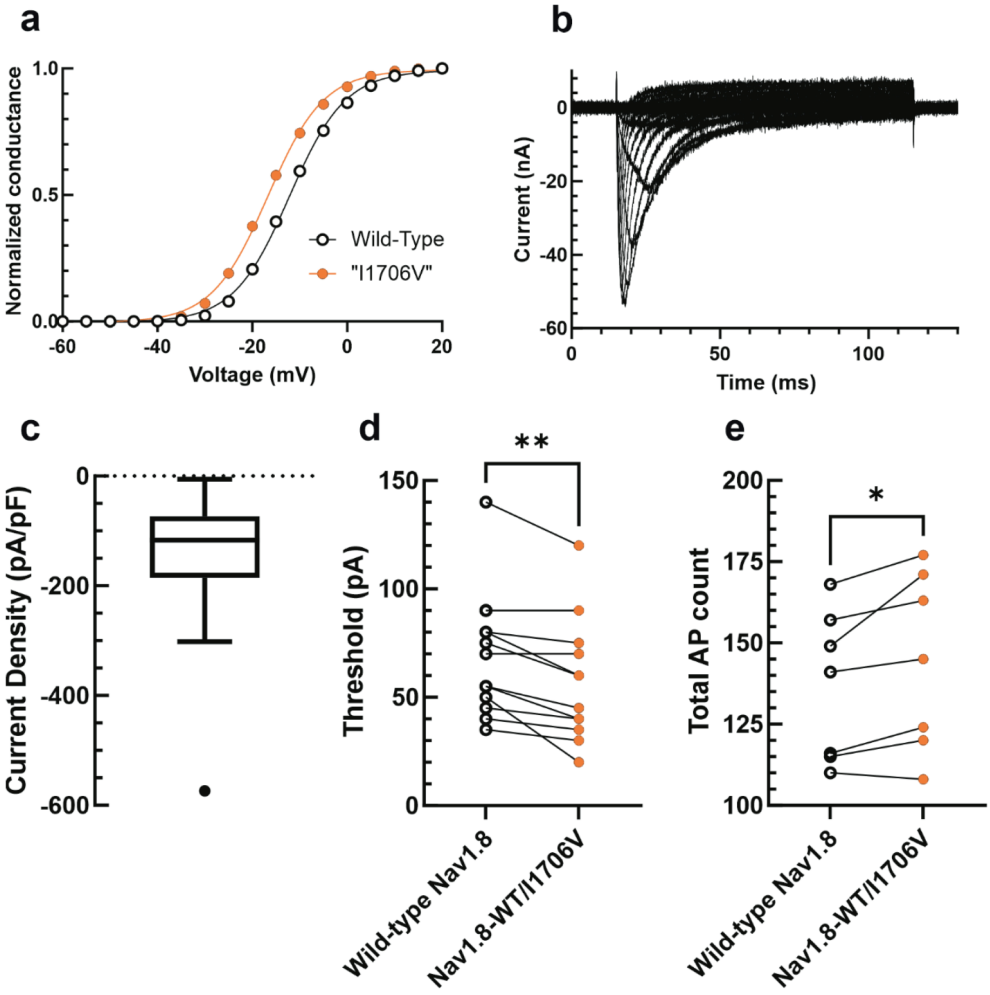

FIGURE 5 – Small biophysical shifts in $Na_V1.8$ gating can substantially alter neuronal excitability. (A) Conductance-voltage relationship between the wild-type $Na_V1.8$ dynamic clamp model and the model with a 4.5 mV hyperpolarized voltage-dependence of activation, approximating the gain-of-function mutation $Na_V1.8$-I1706V. **(B)** Representative traces of $Na_V1.8$ current recorded from human autopsy-derived DRG neurons. **(C)** Box-and-whisker plot showing the $Na_V1.8$ current density recorded from autopsy-derived human DRG neurons in 70 mM NaCl (-143.69 ± 24.54 pA/pF, n = 24). **(D)** Injection of 50% wild-type $Na_V1.8$ current density and 50% "$Na_V1.8$-I1706V" current density resulted in a statistically significant (paired t-test p = 0.0023, n = 13) reduction in current threshold to action potential firing. **(E)** Injection of 50% wild-type $Na_V1.8$ current density and 50% "$Na_V1.8$-I1706V" current density resulted in a statistically significant (paired t-test p = 0.0367, n = 7) enhancement of repetitive action potential firing.

assessed the effect of the $Na_V1.8$ gain-of-function change on threshold to action potential firing (*Figure 5D*). When before-and-after recordings were compared, there was a statistically significant reduction in the action potential threshold (paired t-test

p = 0.0023, n =13).We then evaluated the effect of this hyperpolarization of activation on the ability of iPSC-SNs to repetitively fire action potentials (*Figure 5E*). Following a similar paradigm as above, in which we summed the total action potentials fired by iPSC-SNs after subsequent graded 500 ms depolarizations of increasing stimulus in 25 pA increments, there was a statistically significant increase in action potentials fired with the replacement of 50% $Na_V1.8$ current with the hyperpolarization-shifted variant (paired t-test p = 0.0367, n = 7).

DISCUSSION

Taken together, the studies performed here display the utility of dynamic clamp in iPSC-SNs to probe somatosensory neuronal physiology and investigate the pathophysiology of human disease. We have quantified the contribution of the TTX-R VGSCs, $Na_V1.8$ and $Na_V1.9$, to neuronal physiology in a way that is more precise than pharmacologic approaches and more feasible than attempts at genetic regulation. Furthermore, we have shown that dynamically clamping iPSC-SNs allows for investigation into human pain-related mutations and gain-of-function changes in ion channels.

Most previous studies investigating mutations in various sodium channels have relied on channel transfection and uncontrolled overexpression in a nonhuman cell background—either containing native rodent channels or in a channel-null background. More recent studies utilizing human iPSC-SNs have been unable to probe mutations in $Na_V1.8$ due to the inability to differentiate neurons expressing this channel [49]. Dynamically clamping iPSC-SNs has three advantages that further our ability to research human physiology and disease-relevant pathophysiology. First, dynamic clamp circumvents the problem of inability to express the channel genetically by allowing researchers to create kinetic models that mimic its function with high fidelity. Second, dynamic clamp allows for before-and-after recordings in the same neuron, limiting inter-population heterogeneity between samples used in comparisons. Third, dynamically clamping neurons with precise current inputs can be more physiologically relevant than transfection and overexpression. In this study, we calibrated the amount of $Na_V1.8$ currents we injected when investigating a $Na_V1.8$ gain-of-function mutation to the amount of $Na_V1.8$ currents recorded from human autopsy-derived DRG neurons.

While dynamically clamping iPSC-SNs opens up a new avenue for the further study of human physiology and preclinical pharmacology, the technique is not without limitations. First, kinetic models of ion channels for use in dynamic clamp are only as good as the data used to generate said models. It is imperative that the voltage-clamp recordings used to create the models reflect channel biology as relevantly as possible. For example, the equations defining sodium channel gating voltage-dependences and kinetics should ideally contain information reflecting not only activation and fast-inactivation, but also slow-inactivation. When DRG neurons are held at their resting

membrane potential (approximately -50 to -70 mV), an appreciable amount of slow-inactivation builds up, resulting in reduced channel availability, potentially altering neuronal excitability[59, 60]. In the studies conducted here, the $Na_V1.9$ kinetic model accounted for slow-inactivation, whereas the $Na_V1.8$ model did not, potentially limiting our conclusions. Additionally, another potential limitation of dynamic clamp is that it recapitulates the currents of the ion channels, but not the physical presence of the channel on the membrane. This precludes the binding of channel partners, which are known to play important roles in modulating sodium channels[61, 62] and other ion channels[63], and therefore does not reflect a completely physiological situation.

Having now shown the utility of dynamically clamping iPSC-SNs, future studies should extend this technique to studying pharmacologic blockade of VGSCs. Previous studies have shown that iPSC-SNs derived from patients suffering from inherited erythromelalgia respond strongly to $Na_V1.7$-specific channel blockers, including PF-05089771[35]. However, the results of clinical trials of this $Na_V1.7$ blocker and others have been mixed[64, 65]. One potential reason for this mismatch between preclinical and clinical data is the that the level of blockade possible *in vivo* is less than the pharmacological blockade possible *in vitro* due to limitations in bioavailability and penetration into the central nervous system[27]. Dynamic clamp of iPSC-SNs could enable understanding of the precise degree of channel inhibition necessary to induce relief from pain without resulting in total loss of helpful and informative pain sensation.

REFERENCES

1. Gaskin, D.J. and P. Richard, *The economic costs of pain in the United States.* J Pain, 2012. **13**(8): p. 715-24.
2. Breivik, H., et al., *Survey of chronic pain in Europe: prevalence, impact on daily life, and treatment.* Eur J Pain, 2006. **10**(4): p. 287-333.
3. Kurita, G.P., et al., *The burden of chronic pain: a cross-sectional survey focussing on diseases, immigration, and opioid use.* Pain, 2012. **153**(12): p. 2332-2338.
4. Gunnarsdottir, S., S.E. Ward, and R.C. Serlin, *A population based study of the prevalence of pain in Iceland.* Scand J Pain, 2010. **1**(3): p. 151-157.
5. Raftery, M.N., et al., *Chronic pain in the Republic of Ireland--community prevalence, psychosocial profile and predictors of pain-related disability: results from the Prevalence, Impact and Cost of Chronic Pain (PRIME) study, part 1.* Pain, 2011. **152**(5): p. 1096-1103.
6. Landmark, T., et al., *Chronic pain: One year prevalence and associated characteristics (the HUNT pain study).* Scand J Pain, 2013. **4**(4): p. 182-187.
7. Azevedo, L.F., et al., *Epidemiology of chronic pain: a population-based nationwide study on its prevalence, characteristics and associated disability in Portugal.* J Pain, 2012. **13**(8): p. 773-83.
8. da Costa, B.R., et al., *Effectiveness of non-steroidal anti-inflammatory drugs for the treatment of pain in knee and hip osteoarthritis: a network meta-analysis.* Lancet, 2017. **390**(10090): p. e21-e33.
9. Enthoven, W.T., et al., *Non-steroidal anti-inflammatory drugs for chronic low back pain.* Cochrane Database Syst Rev, 2016. **2**(2): p. CD012087.
10. Vowles, K.E., et al., *Rates of opioid misuse, abuse, and addiction in chronic pain: a systematic review and data synthesis.* Pain, 2015. **156**(4): p. 569-576.
11. Ho, K.Y., et al., *Nonsteroidal anti-inflammatory drugs in chronic pain: implications of new data for clinical practice.* J Pain Res, 2018. **11**: p. 1937-1948.
12. Yu, F.H. and W.A. Catterall, *Overview of the voltage-gated sodium channel family.* Genome Biol, 2003. **4**(3): p. 207.
13. Catterall, W.A., A.L. Goldin, and S.G. Waxman, *International Union of Pharmacology. XLVII. Nomenclature and structure-function relationships of voltage-gated sodium channels.* Pharmacol Rev, 2005. **57**(4): p. 397-409.
14. Bennett, D.L., et al., *The Role of Voltage-Gated Sodium Channels in Pain Signaling.* Physiol Rev, 2019. **99**(2): p. 1079-1151.
15. Haroutounian, S., et al., *Primary afferent input critical for maintaining spontaneous pain in peripheral neuropathy.* Pain, 2014. **155**(7): p. 1272-9.
16. Vaso, A., et al., *Peripheral nervous system origin of phantom limb pain.* Pain, 2014. **155**(7): p. 1384-91.
17. Buch, N.S., et al., *The role of afferent input in postamputation pain: a randomized, double-blind, placebo-controlled crossover study.* Pain, 2019. **160**(7): p. 1622-1633.
18. Yatziv, S.L. and M. Devor, *Suppression of neuropathic pain by selective silencing of DRG ectopia using non-blocking concentrations of lidocaine.* Pain, 2019. **160**(9): p. 2105-2114.
19. Cox, J.J., et al., *An SCN9A channelopathy causes congenital inability to experience pain.* Nature, 2006. **444**(7121): p. 894-898.
20. Ahmad, S., et al., *A stop codon mutation in SCN9A causes lack of pain sensation.* Hum Mol Genet, 2007. **16**(17): p. 2114-21.

21. Goldberg, Y.P., et al., *Loss-of-function mutations in the Nav1.7 gene underlie congenital indifference to pain in multiple human populations.* Clin Genet, 2007. **71**(4): p. 311-9.
22. Yang, Y., et al., *Mutations in SCN9A, encoding a sodium channel alpha subunit, in patients with primary erythermalgia.* J Med Genet, 2004. **41**(3): p. 171-4.
23. Cummins, T.R., S.D. Dib-Hajj, and S.G. Waxman, *Electrophysiological properties of mutant Nav1.7 sodium channels in a painful inherited neuropathy.* J Neurosci, 2004. **24**(38): p. 8232-6.
24. Faber, C.G., et al., *Gain of function Nav1.7 mutations in idiopathic small fiber neuropathy.* Ann Neurol, 2012. **71**(1): p. 26-39.
25. Faber, C.G., et al., *Gain-of-function Nav1.8 mutations in painful neuropathy.* Proc Natl Acad Sci U S A, 2012b. **109**(47): p. 19444-9.
26. Huang, J., et al., *Gain-of-function mutations in sodium channel Na(v)1.9 in painful neuropathy.* Brain, 2014. **137**(Pt 6): p. 1627-42.
27. Alsaloum, M., et al., *Status of peripheral sodium channel blockers for non-addictive pain treatment.* Nature Reviews Neurology, 2020. **16**(12): p. 689-705.
28. Renganathan, M., T.R. Cummins, and S.G. Waxman, *Contribution of Na(v)1.8 sodium channels to action potential electrogenesis in DRG neurons.* J Neurophysiol, 2001. **86**(2): p. 629-40.
29. Herzog, R.I., T.R. Cummins, and S.G. Waxman, *Persistent TTX-resistant Na+ current affects resting potential and response to depolarization in simulated spinal sensory neurons.* J Neurophysiol, 2001. **86**(3): p. 1351-64.
30. Huang, J., et al., *A Novel Gain-of-Function Nav1.9 Mutation in a Child With Episodic Pain.* Front Neurosci, 2019. **13**: p. 918.
31. Dib-Hajj, S.D., *Human pain in a dish: Native DRG neurons and differentiated pluripotent stem cells.* Pain, 2014. **155**(9): p. 1681-1682.
32. Prinz, A.A., L.F. Abbott, and E. Marder, *The dynamic clamp comes of age.* Trends Neurosci, 2004. **27**(4): p. 218-24.
33. Vasylyev, D.V., et al., *Dynamic-clamp analysis of wild-type human Nav1.7 and erythromelalgia mutant channel L858H.* J Neurophysiol, 2014. **111**(7): p. 1429-43.
34. Rostock, C., et al., *Human vs. Mouse Nociceptors – Similarities and Differences.* Neuroscience, 2018. **387**: p. 13-27.
35. Cao, L., et al., *Pharmacological reversal of a pain phenotype in iPSC-derived sensory neurons and patients with inherited erythromelalgia.* Sci Transl Med, 2016. **8**(335): p. 335ra56.
36. Mis, M.A., et al., *Resilience to Pain: A Peripheral Component Identified Using Induced Pluripotent Stem Cells and Dynamic Clamp.* J Neurosci, 2019. **39**(3): p. 382-392.
37. Chambers, S.M., et al., *Combined small-molecule inhibition accelerates developmental timing and converts human pluripotent stem cells into nociceptors.* Nat Biotechnol, 2012. **30**(7): p. 715-20.
38. Young, G.T., et al., *Characterizing human stem cell-derived sensory neurons at the single-cell level reveals their ion channel expression and utility in pain research.* Mol Ther, 2014. **22**(8): p. 1530-1543.
39. MeLean, M.J., P.B. Bennett, and R.M. Thomas, *Subtypes of dorsal root ganglion neurons based on different inward currents as measured by whole-cell voltage clamp.* Mol Cell Biochem, 1988. **80**(1-2): p. 95-107.
40. Cummins, T.R. and S.G. Waxman, *Downregulation of tetrodotoxin-resistant sodium currents and upregulation of a rapidly repriming tetrodotoxin-sensitive sodium current in small spinal sensory neurons after nerve injury.* J Neurosci, 1997. **17**(10): p. 3503-14.

41. Belkouch, M., et al., *Functional up-regulation of Nav1.8 sodium channel in Aδ afferent fibers subjected to chronic peripheral inflammation.* J Neuroinflammation, 2014. **11**: p. 45.
42. Sleeper, A.A., et al., *Changes in expression of two tetrodotoxin-resistant sodium channels and their currents in dorsal root ganglion neurons after sciatic nerve injury but not rhizotomy.* J Neurosci, 2000. **20**(19): p. 7279-89.
43. Tyrrell, L., et al., *Glycosylation alters steady-state inactivation of sodium channel Nav1.9/NaN in dorsal root ganglion neurons and is developmentally regulated.* J Neurosci, 2001. **21**(24): p. 9629-37.
44. Han, C., et al., *Human Na(v)1.8: enhanced persistent and ramp currents contribute to distinct firing properties of human DRG neurons.* J Neurophysiol, 2015. **113**(9): p. 3172-85.
45. Bett, G.C., et al., *Electronic "expression" of the inward rectifier in cardiocytes derived from human-induced pluripotent stem cells.* Heart Rhythm, 2013. **10**(12): p. 1903-10.
46. Ma, D., et al., *Identification of an I(Na)-dependent and I(to)-mediated proarrhythmic mechanism in cardiomyocytes derived from pluripotent stem cells of a Brugada syndrome patient.* Sci Rep, 2018. **8**(1): p. 11246.
47. Chambers, S.M., et al., *Dual-SMAD Inhibition/WNT Activation-Based Methods to Induce Neural Crest and Derivatives from Human Pluripotent Stem Cells.* Methods Mol Biol, 2016. **1307**: p. 329-43.
48. Marmigère, F. and P. Ernfors, *Specification and connectivity of neuronal subtypes in the sensory lineage.* Nat Rev Neurosci, 2007. **8**(2): p. 114-27.
49. Eberhardt, E., et al., *Pattern of Functional TTX-Resistant Sodium Channels Reveals a Developmental Stage of Human iPSC- and ESC-Derived Nociceptors.* Stem Cell Reports, 2015. **5**(3): p. 305-13.
50. Baker, M.D., et al., *GTP-induced tetrodotoxin-resistant Na+ current regulates excitability in mouse and rat small diameter sensory neurones.* J Physiol, 2003. **548**(Pt 2): p. 373-82.
51. Dib-Hajj, S.D., et al., *Rescue of alpha-SNS sodium channel expression in small dorsal root ganglion neurons after axotomy by nerve growth factor in vivo.* J Neurophysiol, 1998. **79**(5): p. 2668-76.
52. Jarecki, B.W., et al., *Paroxysmal extreme pain disorder mutations within the D3/S4-S5 linker of Nav1.7 cause moderate destabilization of fast inactivation.* J Physiol, 2008. **586**(17): p. 4137-53.
53. Klein, J.P., et al., *Patterned electrical activity modulates sodium channel expression in sensory neurons.* J Neurosci Res, 2003. **74**(2): p. 192-8.
54. Akopian, A.N., L. Sivilotti, and J.N. Wood, *A tetrodotoxin-resistant voltage-gated sodium channel expressed by sensory neurons.* Nature, 1996. **379**(6562): p. 257-62.
55. Choi, J.S. and S.G. Waxman, *Physiological interactions between Na(v)1.7 and Na(v)1.8 sodium channels: a computer simulation study.* J Neurophysiol, 2011. **106**(6): p. 3173-84.
56. Elliott, A.A. and J.R. Elliott, *Characterization of TTX-sensitive and TTX-resistant sodium currents in small cells from adult rat dorsal root ganglia.* J Physiol, 1993. **463**: p. 39-56.
57. Huang, J., et al., *Sodium channel NaV1.9 mutations associated with insensitivity to pain dampen neuronal excitability.* Journal of Clinical Investigation, 2017. **127**(7): p. 2805-2814.
58. Huang, J., et al., *Small-Fiber Neuropathy Nav1.8 Mutation Shifts Activation to Hyperpolarized Potentials and Increases Excitability of Dorsal Root Ganglion Neurons.* J Neurosci, 2013. **33**(35): p. 14087-14097.
59. Ulbricht, W., *Sodium channel inactivation: molecular determinants and modulation.* Physiol Rev, 2005. **85**(4): p. 1271-301.

60. Hampl, M., et al., *Sodium channel slow inactivation interferes with open channel block.* Sci Rep, 2016. **6**: p. 25974.
61. Vega, A.V., G. Avila, and G. Matthews, *Interaction between the transcriptional corepressor Sin3B and voltage-gated sodium channels modulates functional channel expression.* Sci Rep, 2013. **3**: p. 2809.
62. Allouis, M., et al., *14-3-3 is a regulator of the cardiac voltage-gated sodium channel Nav1.5.* Circ Res, 2006. **98**(12): p. 1538-46.
63. Straub, C. and S. Tomita, *The regulation of glutamate receptor trafficking and function by TARPs and other transmembrane auxiliary subunits.* Curr Opin Neurobiol, 2012. **22**(3): p. 488-95.
64. McDonnell, A., et al., *Efficacy of the Nav1.7 blocker PF-05089771 in a randomised, placebo-controlled, double-blind clinical study in subjects with painful diabetic peripheral neuropathy.* Pain, 2018. **159**(8): p. 1465-1476.
65. Siebenga, P., et al., *Lack of Detection of the Analgesic Properties of PF-05089771, a Selective Na(v) 1.7 Inhibitor, Using a Battery of Pain Models in Healthy Subjects.* Clin Transl Sci, 2020. **13**(2): p. 318-324.

SUPPLEMENTARY TABLES

Day	Media components + inhibitors	Notes
-1	mTeSR + Ri	Ri = 10 µM Y-27632 ROCK inhibitor
0-1	KSR + LSB	Passage on day 0; LSB = 100 nM LDN-193189, 10 µM SB-431542 KSR = KnockOut Serum Replacement
2-3	KSR + LSB + 3i	3i = 3 µM CHIR99021, 10 µM SU5402, 10 µM DAPT
4-5	KSR:N2 (3:1) + LSB + 3i	KSR + N2 supplement in a 3:1 ratio
6-7	KSR:N2 (1:1) + 3i	KSR + N2 supplement in a 1:1 ratio
8-9	KSR:N2 (1:3) + 3i	KSR + N2 supplement in a 1:3 ratio
10-11	N2 + 3i	After day 12, change medium 2X/week
12-56	N2 + 4GF	4GF = 25 ng/mL BDGN, GDNF, NGF, and NT-3 Passage on day 56

TABLE S1 – iPSC-SN differentiation protocol

Gene	Company	Catalog number	Assay ID
SCN1A	Bio-Rad	100-31225	qHsaCIP0027254
SCN2A	Thermo Fisher	4331182	Hs01109871_m1
SCN3A	Thermo Fisher	4331182	Hs00366913_m1
SCN4A	Bio-Rad	100-31225	qHsaCIP0030523
SCN5A	Thermo Fisher	4331182	Hs00165693_m1
SCN8A	Thermo Fisher	4331182	Hs00274075_m1
SCN9A	Bio-Rad	100-31225	qHsaCIP0027256
SCN10A	Thermo Fisher	4351372	Hs01045146_m1
SCN11A	Bio-Rad	100-31225	qHsaCIP0030516
HPRT1	Bio-Rad	100-31225	qHsaCIP0030549

TABLE S2 – Assay probes for ddPCR of human iPSC-SNs


4

DISCUSSION

Part 4

CHAPTER 6

GENERAL DISCUSSION AND FUTURE PERSPECTIVES

GENERAL DISCUSSION

RETHINKING PAIN MANAGEMENT

The World Health Organization (WHO)'s recommendations for human pain disorders follow the so-called analgesic ladder, which is based on pain severity and persistence, with drug prescriptions spanning from opioids, non-steroidal anti-inflammatory drugs (NSAIDs), tricyclic antidepressants (TCAs) and (selective) serotonin-(norepinephrine) reuptake inhibitors (SSRI/SNRIs), given on a trial-and-error basis [1].

Still, pain management is mostly ineffective and associated with a wide range of adverse effects. First and foremost, chronic pain as a disorder should be redefined to better encompass psychiatric and emotional comorbidities for diagnosis and treatment strategies. In turn, patient stratification needs to focus less on whether the etiology is nociceptive, neuropathic, or central and instead recognize that many patients suffer from widespread pain that cannot be classified as either one or the other. A systemic classification that better covers these limitations has been addressed in the 11th revision of the International Statistical Classification of Diseases and Related Health Problems (ICD-11) [2]. Furthermore, as a large proportion of individuals suffer from a combination of syndromes associated with related or unrelated comorbidities (medical and/or psychiatric disorders), strategizing a pain-focused medical program can sometimes be even more debilitating than pain itself. Emotional comorbidities, notably, have been shown to interfere with the therapeutic efficacy and side effects of pain medications [3]. Possible pharmacokinetic and pharmacodynamic interferences associated with drugs for other medical issues also need to be taken into consideration. The definition of pain was recently revised by the International Association for the Study of Pain (IASP) to better include non-pain related components of chronic pain and now reads as "an unpleasant sensory and emotional experience associated with, or resembling that associated with, actual or potential tissue damage" [4]. Nevertheless, it is critical for adequate pain treatment that comorbidities, concomitant diseases, and the full range of symptoms are systematically considered when drawing a treatment plan. Pain pathophysiological mechanisms are still poorly understood, and with a vast spectrum of etiologies and symptoms, the pharmacological focus should be mechanism-based and patient-specific.

A growing body of literature has underscored genetic markers as probes to aid drug development and guide clinicians' treatment decisions. Specifically, the implementation of pharmacogenomic-guided approaches could help physicians select the appropriate drug and dosing for a particular patient instead of treating a 'disease' or 'symptoms'. But, so far, trial-and-error drug prescription remains the most common form of analgesic management in clinical practices. With patient reports showing this method to be largely unsatisfactory, routine pharmacogenomic testing, already well-validated in clinical trials and used in some medical practices, will likely pave the way towards effective, personalized medicine.

THE ROAD FROM PHARMACOGENOMICS TO PRECISION MEDICINE

At times pain management still requires multiple rounds of medications, which correlate with poor efficacy, adverse effects, and in some cases, worsening of the pain symptoms, the need for precision medicine has never been greater. Pain is a complex biopsychosocial phenomenon of which the location, intensity and duration are highly inter-individually dependent. Several factors influence patient-to-patient pharmacological outcomes, such as their cognitive profile, ethnicity, cultural habits, gender, as well as psychiatric comorbidities [5-9], all of which are imprinted into the final genetic makeup of a patient that can be accessed using pharmacogenomic tools.

Applied pharmacogenomics can guide the development of selective mechanism-based compounds that are tailored to the patient's underlying pathology. In particular, adverse effects from current analgesics are often the result of unspecific binding to proteins that are widely expressed throughout the body. In **chapter 2** and **chapter 3**, we highlight the power of pharmacogenetic strategies in defining the role of select motifs in unknown drug mechanisms. Specifically, the identification of a $Na_V1.7$ variant (W1538R) that provides insensitivity to the anticonvulsant lacosamide [10], in a mutation-specific manner (**chapter 2**), has set the scene for establishing the pivotal interaction between lacosamide and the W1538 residue that promotes its binding to the pore (**chapter 3**). Meanwhile, these studies also support pharmacogenomic-based research for precision medicine in selective ion channel blockers; lacosamide represents the perfect example of the potential for more selective antiepileptic drugs (AEDs) to provide therapeutic relief where conventional non-selective AEDs (ie. carbamazepine, lamotrigine, phenytoin) have failed [11]. Spotlighted for its differential mechanisms of action, lacosamide interaction with the less-conserved voltage-sensing domain (VSD; **chapter 3**) may explain, at least in part, its improved tolerance compared to its counterparts [11]. Nonetheless, as aryl sulfonamide $Na_V1.7$ selective blockers (VSD4-binders) have shown mixed outcomes in clinical trials, the VSD alone might be insufficient to provide true therapeutic benefits [12, 13]. Hence, our findings raise new perspectives on exploiting drugs, targeting both the conserved pore and the VSD of sodium channels to achieve increased selectivity, with fewer undesirable side effects (**chapter 3**). Nevertheless, clinical assessment of voltage-gated sodium channel (VGSC) blockers has been rather disappointing when considering the dramatic effect VGSC loss- and gain-of-function mutations have had on neuronal excitability and human pain phenotypes [14-16]. Importantly, multiple other factors contribute to pain modulation, including bioavailability and penetration into the spinal cord and the central nervous system (CNS), which can impede the potency of analgesics targeting VGSCs. Also, the high protein-binding potential of aryl sulfonamides limits free drug availability and thus may lead to poor target engagement [17].

Future drug development strategies that include population genomics would enable the discovery of new pain modifying therapeutic targets and broaden our horizons on the polygenic contributors of chronic pain and drug interactions. For instance, since potassium channel variants have been found to induce pain resilience in two IEM

patients [18, 19], new evidence has highlighted $K_V7.2$ activator, XEN1101, to show efficacy in treating neuropathic pain [20]. Furthermore, the association between a common haplotype in GTP cyclohydrolase GCH1 (the enzyme responsible for BH4 synthesis) and reduced pain [21, 22] led to a phase II placebo-controlled clinical trial using Sulfasalazine, a BH4 synthetic pathway blocker (clinical trial identifier: NCT01667029), which showed promising results in preclinical studies [21, 23]. Other examples include the discovery of catechol-*O*-methyl transferase (COMT) polymorphisms that act as pain-protective alleles [24], and P2x7 hypofunctional variants that were linked to reduced chronic pain [25]. Building on these discoveries, clinical trials targeting P2x7 were set up but have so far been unsuccessful [23, 26, 27]. The implementation of pharmacogenomics can also bring new prospects to gene therapy. A rapidly growing field, genetic approaches targeting peripheral sodium channels are still at an early developmental stage. Nonetheless, viral delivery of genetic constructs, designed to decrease the expression of pain-related genes, has shown promising outcomes [28]. Furthermore, virus-mediated knockdown of $Na_V1.7$ and $Na_V1.3$ channels in animal models alleviated pain phenotypes [17, 29-31]. With the discovery of genetic variants affecting drug metabolism and efficacy, future therapies might apply precision editing with CRISPR-Cas9 technology to remove deleterious variants in postmitotic neurons and improve treatment outcomes [32]. Nonetheless, with prominent off-target effects and low-efficiency, gene therapy strategies still have a long way to go before specific genetic variants can be dissected out.

Clinical implementation of pharmacogenomics

Compared to the fields of oncology and palliative care [33], available pharmacogenomic literature in chronic pain is scarce and heterogenous, with limited evidence for its implementation in clinical practices [5]. Despite clear advances supporting its benefits, sizeable challenges have slowed down the transition of pharmacogenomic profiling into routine clinical testing. Large-scale, randomized clinical trials with standardized outcome measures are a crucial step towards individualized pharmacological management. Human genome-wide association studies (GWAS) are particularly helpful to personalized treatment strategies as they allow the identification of common disease variants that might confer susceptibility to pain pathogenesis and/or psychiatric comorbidities, as well as altered sensitivity to select treatments across the population [34]. Expanding on our small sample findings (**chapter 2**), large and well-defined cohorts carrying common variants will facilitate the discovery of important variant-drug associations, adding another level to patient stratification [23]. Importantly, for newly identified variants to be validated as predictors of therapeutic effects and/or toxicity of certain compounds, they need to be functionally evaluated first. Notably in the past, the costs, limited access, and long turnaround times of genetic tests, combined with the lack of an integrated decision system in place, inexperience in data interpretation and few prospective studies, have all restricted the clinical integration of pharmacogenomic-guided approaches [35]. Furthermore, no robust genetic predictors of inter-individual variability in drug response have yet been determined, although this is rapidly changing by Whole Exome and Whole Genome

Sequencing strategies. The inclusion of pharmacogenomics into routine medical practices has also been urged by the FDA following compiling evidence that up to 30% of FDA-approved drug response variability and dosing issues are associated to genetic variants [36-39]. In fact, the Clinical Pharmacogenetics Implementation Consortium (CPIC) have included -and regularly update- variant-specific dosing guidelines for several treatments. One of the most prominent examples is the interaction between *CYP2D6* polymorphisms and opioid medications [40]. Nevertheless, with several high-risk drugs still commonly prescribed to pharmaco-sensitive patients, morbidity and mortality rates are not likely to rapidly decline.

Success stories in pharmacogenomic-guided precision analgesia

Numerous studies have reported improved clinical outcomes in chronic pain patients after using a pharmacogenomic-guided approach. Particularly, polymorphisms in the cytochrome P450 (CYP), a major contributor to the metabolism of common pain medications (ie. NSAIDs, Opioids, TCAs, SSRI/SNRIs) [41], have funneled toxicological re-assessment in certain variant carriers that were more susceptible to overdose [42]. As previously inferred, we need to rethink patient stratification and adopt a format based on drug-modulatory genetic variants, or pharmacogenes.

CYP2D6-guided therapeutic management is a great proof-of-concept example of successfully applied pharmacogenomics [43-45]. An extensive list of variants in the opioid-metabolizing *CYP2D6* complex has been linked to altered opioid tolerability and efficacy in human carriers [46-48]. In a non-randomized, open-label, prospective, cluster design clinical trial, chronic pain patients screened for *CYP2D6* variants were treated with opioids following a *CYP2D6*-guided or usual care approach for three months [43]. Patients were classified according to their metabolizing rate, based on their *CYP2D6* genotype, and metabolizers at higher risk of inefficacy or toxicity were prescribed alternative therapy. The patients whose treatment was adjusted due to high-risk *CYP2D6* variant expression showed at least a 30% reduction in pain intensity, which directly correlated with phenotype-based recommendations, whereby poor metabolizers benefitted from this approach, but no difference was observed in normal metabolizers. Furthermore, 24% of the patients in the *CYP2D6*-guided branch showed pain improvement compared to 0% of those treated as usual, highlighting the benefits of using a personalized approach to pharmacotherapy [43]. Applied *CYP2D6*-guided analgesia has also been shown to improve cancer-related pain in an outpatient oncology palliative care setting [45]. In a separate study, *CYP2D6*-based recommendations led to the addition of 70 new medications, removal of 115 and re-dosing of 58. Interestingly, patients who experienced less severe pain benefitted the most from pharmacogenomic-driven therapeutic decisions, while those with the most severe pain were less likely to change pain medication [44]. Such differences may be caused by other unassessed variants and/or additional factors contributing to pharmacotherapy efficacy. In turn, identifying these variants in patients' genomic records allow us to pre-determine their opioid metabolizing rate and predict their individual response to analgesics [49].

Other isoforms, such as *CYP2B6*, *CYPC8*, *CYP2C9*, *CYP2C19*, *CYP2D6*, and *CYP3A4* also interact with some non-opioid treatments [5]. Notably, *CYP3A4* variants have been linked to altered opioid responses [50, 51], while patients carrying mutant CYPC8 and CYP2C9 enzymes report slower NSAID metabolization rates [48, 52]. In 2020, the FDA published a list of scientifically supported pharmacogenetic associations that would likely alter drug metabolism in human carriers [36]. In chronic pain, only three pharmacogenes (ie. *CYP2C9*, *CYP2C19* and *CYP2D6*) qualify for preemptive testing, albeit pharmacogenomic analysis performed prior to prescription, as opposed to reactive testing, performed following adverse effects or lack of efficacy [36, 53]. In the future, as genomic screening becomes more frequent, increasing numbers of drug-modulating genetic variants should be incorporated, which will promote preemptive testing. Altogether, these studies exemplify the positive impact pharmacogenomic-guided therapy can have on pain management in the population if implemented into clinical settings.

Population pharmacogenetic variants

Inter-individual differences in treatment response have been highlighted in groups of patients with the same etiology, down to the same disease-causing variant [10].
In **chapter 2**, we examined the effect of five $Na_V1.7$ variants on lacosamide in HEK293 cells, which we classified as either responsive to lacosamide or non-responsive. In patients, however, the drug response was not as explicit. Differential therapeutic responses were observed in individuals carrying the same mutations, suggesting the presence of additional contributors. Specifically, in mostly responsive I739V carriers, one patient did not respond to lacosamide, while amongst non-responsive L1267V carriers, one rersponded. Diverse response to treatment could arise from altered drug binding or channel interaction only occurring in specific mutant channels. Alternatively, additional genetic variants in the carriers of the same mutation might influence their own response, similarly to protective pain resilience variants in IEM patients [18, 19]. Future studies might consider a more translational *in vitro* model using iPSCs derived from patients carrying the same disease-causing mutation but with opposed drug responses. Functional assessment of patient-specific iPSC-SNs might delineate which variants influence pharmaco-responsiveness and reveal important factors for the tolerability and potency of lacosamide, ultimately increasing the success rates in clinical trials. However, a major pitfall of this approach is that being in unrelated patients, such diverse genetic, environmental, and epigenetic factors might further amplify inter-individual variations.

Proposed approach

With genomic testing becoming increasingly affordable and available, the era of personalized analgesia is on the horizon. Here, we suggest a model that focuses on a preemptive and comprehensive approach, whereby all clinically relevant genes are evaluated as a panel prior to drug prescription. Genomic assessment should include variants that may be associated with drug metabolism, drug targets, and mechanism-

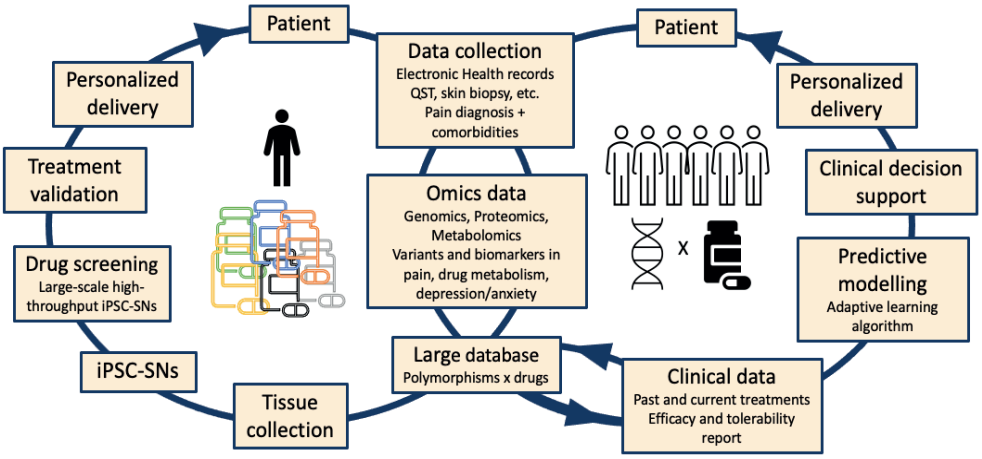

FIGURE 1 – Diagram of the key components for personalized medicine. Two approaches are suggested to advance pharmacogenomics-guided analgesic management. ***(Right)*** **A population to single patient approach that encompasses the cataloging of clinical and omics data. Drug recommendations are made to individual patients following predictive modelling.** ***(Left)*** **Second, a single patient to large in vitro drug testing approach that includes somatic cell collection for high-throughput screening of iPSC-SNs against a large library of compounds. Combined, both approaches thrive from widespread cataloging and classification of drug-modulating variants.**

based targets underlying pain and associated comorbidities, such as depression [36, 54]. Drug-to-drug interactions and concurrent medical conditions can be confounding factors and should ideally be taken into consideration when performing a pharmacogenomic analysis. Routine sequencing and genomic screening must be incorporated in analgesic treatment guidelines. Patients should be classified based on their likelihood to respond to a particular treatment with minimal risk to develop adverse reactions [55, 56].

The first step towards clinical preemptive testing and personalized medicine should follow a population to individual approach. To proceed, population-wide omics data need to be collected, cataloged and cross-tested for treatment reactivity. The most extensive and global method to define susceptibility genes and predictive biomarkers can be achieved through consistent whole-exome sequencing and genome-wide association studies. Identified high risk variants for impaired efficacy and/or adverse drug effects can be classified and stored in a large library. Functional assessment of suspected biomarkers in clinical trials and treatment-effect analysis can then be used to identify the likely responders based on the variants they carry, as exemplified by Greef et al. [10] and in **chapter 2** [55]. Likewise, the response of each patient to multiple treatments and their electronic health records should be integrated into a shared database with their omics portfolio. Combined with artificial intelligence, an individualized treatment algorithm-applied for personalized medicine can be developed, such as Q-learning [57], whereby clinicians can retrieve response charts of patients with the same variants to a range of medications and choose the one most

likely to work with the fewest side effects. As the library enlarges, the likelihood for the adaptive learning algorithm to find matches between genetic variants and diverse drugs will increase, reducing the risk for physicians to prescribe ineffective/toxic treatments (*Figure 1, right*). In order to achieve effective clinical decision support systems, it is critical for health information to be exchanged between institutions and pharmacogenomic testing to be standardized.

Recent advances in the field of stem cell research allow us to suggest a secondary, functionally based approach that does not require direct genomics comparison with unrelated individuals. From a single patient's skin biopsy, fibroblasts can be differentiated into iPSC-SNs and screened against large analgesic compound libraries, enabling personalized drug efficacy prediction and even revise drug interactions (*Figure 1, left*). However, high-throughput screening and production of iPSCs is more costly and requires extensive technical knowledge. Thus, this approach might only be preferred in patients with expensive and critical treatments, such as for cancer, or in therapy-refractory patients.

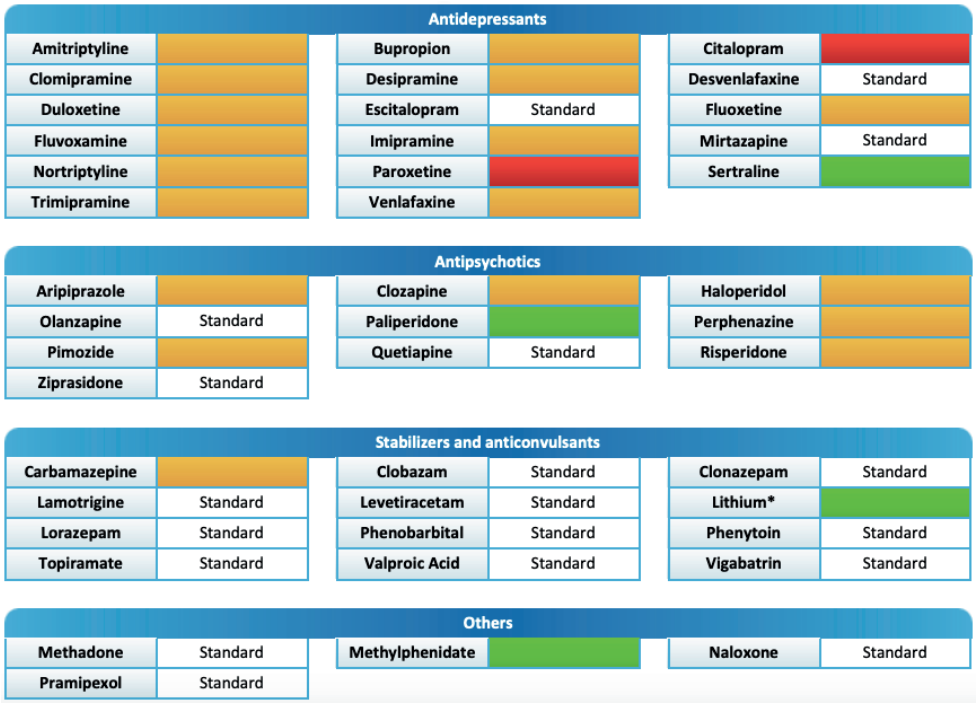

FIGURE 2 – Sample pharmacogenetic test report from Neuropharmagen® color-coded to guide treatment plan decisions. For each drug examined, the result is indicated according to the following code: *(standard)* No genetic variants relevant to treatment have been detected, use treatment as directed. *(green)* Increased likelihood of positive response and/or lower risk of adverse drug reactions. *(yellow)* Need for drug dose monitoring and/or less likelihood of positive response. *(red)* Increased risk of adverse effects.

Pharmacogenetic tests

Commercially available genetic tests have the potential to directly predict the patient's response to a range of analgesics. Notably, Neurofarmagen Analgesia® (AB-Biotics) scans for cytochrome polymorphisms that affect the pharmacokinetics of common analgesics (ie. NSAIDs, TCAs, AEDs, opioids, and SSRI/SNRIs; *Figure 2*). In a recent study, treatment prescription based on Neurofarmagen results correlated with clinical efficacy in two out of three patients suffering from chronic pain [5] and in 50% of patients (n=136) with major depressive disorder [58]. The observed discordance in unresponsive patients may arise from other genetic and epigenetic variants, as well as uncontrolled environmental factors. Furthermore, the test was reported to lack sensitivity and to only suggest moderate efficacy/tolerability. Regular updating of these tests to include more variants as they are discovered will better predict drug response [5]. Furthermore, additional markers for therapeutic efficacy and toxicity should be incorporated to improve sensitivity and distinguish them from one another.

Pharmacokinetic-pharmacodynamic (PK-PD) modelling

Integrating omics to quantitative systems pharmacology modelling has been suggested to support pharmacotherapy predictions [59]. Combining genomics, metabolomics, and proteomics, with pharmacokinetics and model-based predictions of drug exposure, this integrative approach encompasses molecular profiling of polymorphisms in metabolizing enzymes, μ-opioid receptors, endogenous opioids, drug transporters, cytokines, inflammatory markers, endocannabinoids, stress hormones, ion channels, etc. to guide pharmacotherapy. Pharmacokinetic-pharmacodynamic (PK-PD) modeling consists in quantifying the dynamic relationship between drug exposure and drug response [60]. The model generally runs in parallel with a nonlinear mixed effect framework to quantify inter-individual variability [61, 62]. For example, PK-PD modelling has been used to measure sex and age effects on the analgesic response of pregabalin in fibromyalgia patients [63]. Concurrently, metabolomics and proteomics provide the closest biochemical description of the clinical phenotype, and in contrast to genomics, they include environmental factors [64, 65]. Findings from metabolomics and proteomics studies have led to the discovery of novel biomarkers and interacting psychiatric risk factors [66, 67]. For instance, heightened cortisol levels from chronic stress have been linked to pain catastrophizing [59, 68]. In rheumatoid arthritis, high auto-antibody levels have been correlated to disease severity, and thus, could be used as indicators in patients that need more aggressive treatments [69]. Therefore, implementing approaches that include both PK-PD modelling and quantitative metabolomics/proteomics may improve personalized treatment outcomes for multiple components of pain [59].

FUNCTIONAL ASSESSMENT OF POLYMORPHISM – DRUG INTERACTIONS

Functional testing of novel pharmacogenetic variants requires a thorough and time-consuming dissection. Recommended multistep guidelines include: First, structural modeling and proximity assessment that align with known pathogenic or drug-

modulating variants in the 3D folded channel; second, thermodynamic coupling between mutants to verify their energetic association; and third, voltage- and current-clamp analysis of the effect of the compound of interest on the mutant channel biophysical properties and cellular excitability [23]. In **chapter 3**, structural modeling and molecular docking of the $Na_V1.7$ channel predicted residues showing high affinity to lacosamide. Yet, without dynamic modelling, energetic associations between lacosamide and specific regions of the target sodium channel cannot be measured, limiting our interpretation of the $Na_V1.7$-W1538R mutant's impact on lacosamide's functions. Furthermore, this multistep process has been limited to rare monogenic variants, described in small groups of patients and in heterologous cellular models. Hence, to understand the contribution of common polymorphisms and paint a more complete picture of individual pain pathologies, substantial functional assessment in other tissue models is critical.

The development of high-throughput screening has been paramount to facilitating *in vitro* pharmacogenomics studies. Several platforms exist, but the Qube automated electrophysiology platform (Sophion Bioscience) is superior by permitting the simultaneous evaluation of up to 384 compounds. We were able to validate its applicability in **chapter 3**: Transfected HEK293 cells with $Na_V1.7$ or $Na_V1.3$ variants were exposed to diverse compounds, including lacosamide, lidocaine, and aryl sulfonamide selective blockers ICA-121431 and PF-05089771 (unpublished), at different concentrations. Nonetheless, while assessing the modulatory role of different analgesics on mutant channels in heterologous systems is crucial for determining direct drug-channel interaction effects, this method cannot explain inter-individual variability in response to treatment. The approach used in **chapter 2** is generally considered a medium throughput assay to test responsiveness of specific mutations to a drug treatment. As previously mentioned, DNA transfection in HEK293 cells uses an over-expression system that is limited to the sole expression of the channel of interest. Also, as a non-neuronal cell background, many channel partners are missing. Therefore, other patient-specific genetic and epigenetic modulators that may alter drug binding or efficacy cannot be assessed using this system only.

HOW TO OPTIMIZE PHARMACOGENOMICS – GUIDED APPROACHES IN IPSC-SNS?

To provide pain management in a non-'one-size-fit-all' fashion, cellular models should recapitulate the complexity of a patient's pharmacological response, and what better models than the patient's very own cells? Over the past decade, iPSC-SNs have become the ideal platform to study pharmacogenetic interactions, which have yielded personalized treatments in patients otherwise unresponsive to pharmacotherapy [12, 70-72]. The scalability of patient-specific iPSCs has enabled high-throughput drug screening and offers the possibility to assay multiple drugs in one patient or multiple variants susceptible to affect the patient therapeutic response and tolerance to one compound. However, current differentiation protocols have failed to derive mature heterogenous iPSC-SNs, hence closing the gap between human dorsal root ganglions (DRGs) and iPSC-SNs is indispensable before they can fulfill their surrogate purpose.

High-throughput drug screening in mutant iPSC-SNs

Considering the wide spectrum of responsiveness associated with new and old analgesics in neuropathic pain patients, implementing high-throughput screening of alternative drugs would likely yield more effective treatment strategies. Patient-specific iPSC-SNs allows assessment of a library of potential analgesics without requiring the patient to test them themselves. Drug screening in iPSCs-derived systems is well-established, and has proven to be instrumental in facilitating the identification of novel disease-modulating therapeutics [73]. New evidence for positive drug-induced neuronal modulation of iPSCs-SNs has been documented [70], which recapitulated the effect of treating the patient in the clinic. A recent drug screening investigation in amyotrophic lateral sclerosis (ALS) research has demonstrated the ability of a test compound to revert neurite degeneration in motor-like neurons, derived from unrelated patients, carrying different disease-causing versions of the same *TDP-43* gene [74]. Although their results should be carefully interpreted, they support the utilization of the iPSC-derived cell model for drug screening and treatment efficacy assessment, even in unrelated subjects. Finally, a mismatch between the iPSC-SNs and patient's response might indicate drug effects at other anatomical levels, such as spinal or supra-spinal circuits. To test this alternative hypothesis, iPSCs can be differentiated into spinal neurons in future studies.

Drug-induced changes in iPSC excitability might be used to predict the clinical response in future trials as well as extend our knowledge on iPSC-derived cell metabolism in response to drug administration. However, while their high scalability allows for high-throughput drug screening, producing large enough numbers of iPSC-SNs is both challenging and expensive using current protocols. Using partially differentiated, immature iPSC-SNs for in-assay plate maturation has emerged as a novel method to test large library of compounds based on the rationale that growing neurites are more sensitive to toxins than established ones. Cryopreservation of the immature neurons has also been helpful for scaling up numbers before use [75, 76], providing a more robust and cost-effective approach. Nevertheless, the process from fibroblast to iPSCs to immature iPSC-SNs remains the most time-consuming and costly part of the whole procedure. Future prospects might want to focus on developing shorter, less labor-intensive differentiation protocols that produce diverse subclasses of functional iPSC-SNs that contribute to different forms of pain [23].

Direct reprogramming: A cost- and time-effective differentiation strategy

New developments in stem cell research have started to shift away from the traditional -and most extensively used- *in vitro* differentiation strategies that recapitulate the different stages of DRG embryonic development. As such, iPSCs are differentiated into neural progenitors and then into sensory neurons [77]. Instead, direct conversion protocols have emerged, whereby somatic cells can be directly reprogrammed into sensory neurons, bypassing the iPSC stage altogether, and thus, providing a faster, more cost-effective differentiation strategy. Forced expression of lineage-specific

modulators has yielded mixed sensory neuron populations in fewer steps than indirect reprogramming. For instance, Wainger et al. have achieved neuronal differentiation of mouse fibroblasts into neuron characteristic of nociceptors with five key transcription factors: Ascl1, Myt1l, Ngn1, Isl2, and Kfl7 [78]. While the conversion rates only reached a low 14% for neuronal identity, the cells expressed markers for peripherin, NF-200, CGRP, TRMP8 and TRPA1. Electrophysiological assessment further highlighted different combinations of TTX-R slow and persistent sodium currents, consistent with $Na_V1.8$ and $Na_V1.9$' signatures. Additionally, the cells were responsive to noxious agonists, including capsaicin, menthol and mustard oil, emphasizing the functionality of the produced neurons. Last, generated neurons from familial dysautonomia patients using the same protocol showed reduced neurite outgrowth compared to healthy controls, showcasing this study as a proof-of-concept that direct reprogramming can be used to model peripheral neuropathies [78]. However, it remains limited by its low neuronal conversion efficacy and by its reduced capacity to maintain neurons in culture. A possible solution to circumvent that is to expand fibroblasts in culture prior to induction, a consideration for future studies, which is however expensive and more time-consuming, defeating its main purpose [78].

The choice of somatic cell matters

Direct conversion of less commonly used somatic cells has shed a light on the relevance of the cell of origin to derive selective sensory neuron subtypes. For instance, peripheral blood cells and hair follicles have been directly reprogrammed into capsaicin-sensitive peptidergic nociceptors, which traditional protocols have so far failed to produce persistently [79-81]. Importantly, fibroblasts are primed for neural potential, whereby their cell fate is restricted, while blood cells require *de novo* acquisition of neural crest development genes [79, 80], which reduces the risk of differentiation-induced variability [82]. Converted nociceptors were functionally and morphologically at least equivalent to iPSC-SNs. Furthermore, the production from initial reprogramming to mature neurons was over three times faster than the conventional route and yielded high numbers of cells available for high-throughput screening of chemotherapeutic compounds [80]. Taken together, these findings set the stage for using diverse somatic cells for direct conversion into specific sensory neuronal lineages.

Catching the right wave

Neural induction strategies have further explored triggering the signaling cascades responsible for sensory cell fate determination. Sensory neurogenesis occurs in two migratory waves; large diameter neurons, including proprioceptors and mechanoreceptors, are first generated from neurogenin-2 (*NGN2*)$^+$ cells, followed by small and medium diameter nociceptors during the second wave, stimulated by neurogenin-1 (*NGN1*) [83]. Peptidergic and non-peptidergic nociceptors emerge later following alternative expression of *TRKA* and *RUXN1* [83]. Mimicking this phenomenon through *NGN1/NGN2* modulation, and subsequently *RUNX1* and *TRKA*, has been suggested to promote selective differentiation of nociceptor-like cells [84]. Direct reprogramming of human dermal fibroblasts through inducible lentiviral co-

expression of *BRN3A* with *NGN1* or *NGN2* has achieved evenly mixed sensory neuron subtypes, representing all three DRG subgroups, namely proprioceptors, mechanoreceptors, and nociceptors. Obtained neurons were electrophysiologically functional, and responsive to pruritic and noxious agonists and to noxious temperatures. Specifically, forced expression of *BRN3A/NGN1/NGN2* yielded $TRKA^{+}CGRP^{+}$ capsaicin-sensitive and $TRPM8^{+}$-mediated menthol-sensitive thermoreceptors, indicative of peptidergic C-fibers [78, 85]. However, low conversion rates from using fibroblasts, once again, hinders progress towards an iPSC-free model. Past studies have suggested that forced conversion of transcription factors greatly affects differentiation efficiency [86, 87], which may be resolved by using other somatic cell types or by using additional steps. Nevertheless, available direct conversion strategies still provide insufficient functional sodium channel expression, and solutions towards heterogenous nociceptor populations are still limited.

Microenvironmental interactions drive iPSC maturation

The current gap in knowledge on sensory neurogenesis and maturation *in vivo* hinders our ability to model human DRGs using iPSCs *in vitro*. Furthermore, neural induction and differentiation depend on intrinsic cell qualities and the extracellular environment, including cell-to-cell communication and spatial cues, which are missing from traditional *in vitro* protocols and are still poorly understood [88]. The first step towards advancing disease modelling using iPSCs is to identify and/or recreate the critical key components of the human DRG microniche influencing cell fate. Direct access to the native milieu can provide select microenvironmental interactions and help list adequate enrichment strategies to improve sensory neuron differentiation [86]. Additionally, the absence of complex cellular interactions might account for some of the differences in reported drug effects between *in vivo* and *in vitro* recipients [17]. Promoting culture heterogeneity should paint a more complete picture that includes drug metabolism and effect on other cell types.

In **chapter 4**, we transplanted undifferentiated and pre-differentiated iPSCs into rodent DRGs with the hope of inducing their differentiation *in vivo* and *ex vivo*. However, premature termination of the project due to the COVID-19 pandemic prevented long-term iPSC differentiation and behavior assessment at later stages post-graft. Nonetheless, we demonstrated that undifferentiated cells transplanted in the DRG of immunodeficient animals did not allow sensory neuronal differentiation, but instead yielded teratoma development. In fact, the elevated tumorigenic potential of xenotransplanted iPSCs [89], along other transplantation-related concerns, such as cell survival, migration and further differentiation, has restricted their use for disease modelling. Strategies to reduce iPSC-induced tumorigenicity are currently under development. Bee venom, for instance, selectively targets and eliminates undifferentiated, still pluripotent cells [90]. Additionally, modified fibrin gels controlling the delivery of growth factors and small molecules have been able to improve stem cell neurite growth, survival and differentiation post-graft [88]. However, this strategy is still far from optimal; the DRG anatomical location and small

structure make this technique challenging and further offsets its potential benefits. Furthermore, differences between human and rodent DRG microenvironments may confound the composition and protein expression levels of *in vivo* derived iPSC-SNs and may not reflect the phenotype they would have achieved in native human tissues. Post-mortem human DRGs should be compared to the same donor's fibroblasts after they have been differentiated into iPSC-SNs to delineate the true protein expression range and define canonical markers. Nevertheless, other microniche and multi-cellular strategies are consistently emerging to defeat these limitations and provide iPSC-SNs with the nutrients and signaling cascades they require to reach their final mature state.

Linear co-cultures

Because of their ability to recapitulate cell-neuron communication, co-cultures are emerging as a powerful *in vitro* tool [91-96]. Schwann cells (SCs) have been a particularly attractive cell type for sensory neuron co-cultures as they are required for both the maintenance and development of peripheral nerves. Also, myelinated neurons are crucial for pain signaling. Xenogeneic co-cultures of human iPSC-SNs with rat SCs have enabled the production of myelinated fibers with unlimited capacity for remyelination. Electrophysiological characterization of myelinated iPSC-SNs demonstrated characteristic properties to those of functional neurons [97]. In a separate study, co-culture of SCs with iPSC-SNs yielded VGSCs in the nodes of Ranvier and shaker-type potassium channels at the juxtaparanode, which were molecularly and functionally comparable to human DRG neurons [98]. Both protocols provided net improvements over existing methods; however, a clear limitation is the use of non-human SCs. Recently, a protocol for directly induced human SC precursors has been published, which might serve as the missing puzzle piece for generating fully myelinated peripheral neurons [99]. Although nociceptors are only lightly myelinated, if at all, so SCs might not be the best suited cell type for their growth, other co-culture systems exist. Namely, astrocytes, microglia, muscle, and skin cells have improved CNS neuronal differentiation and functions [100-103]. Incorporating alternative cell types, including non-nociceptive and even neuronal cells, may reconstitute the crosstalk between nociceptors and neighboring cells *in vitro*.

3D-Organoids

Human iPSCs can be grown three-dimensionally (3D) to create complex tissue structures that include multiple sensory neuronal populations and supporting glial cells, mimicking *in vivo* conditions and consequently, improving neuronal differentiation [104]. As opposed to 2D-adherent monolayer strategies, such as Chambers' [77], 3D suspension cultures have yielded more diverse cell types that better reflect endogenous neurogenesis [105]. For example, 3D organoids derived from human fibroblasts, virally transduced with ASCl1, Brn3b and Isl11, yielded self-organized and networked heterogenous sensory neuron ganglions, closely resembling DRGs, that showed TTX-R currents and expressed *SCN9A*, *SCN11A*, CGRP and NF200, suggesting nociceptor subtype diversity [106]. Furthermore, 3D structures challenge 2D-related lack of maturity [107, 108], producing mature and diverse cells expressing

higher *SCN10A* levels [104], notably by allowing iPSC-SN aggregates in suspension to be cultured for twice as long [109]. Also, non-adherent 3D cultures better replicate native spatial organization, cellular composition expression patterns, dynamic cell-matrix interactions and organ functions [104], which further allow the assessment of drug tissue penetration [110, 111]. In a model of amyotrophic lateral sclerosis (ALS), organoid cultures adopted a DRG-like structure and produced physiologically functional neuromuscular junctions, along with diverse neuronal, glial, endothelial, and skeletal muscle cellular cohorts [112]. However, 3D models are more laborious and costly, they have a limited high-throughput capacity and hinder microscopy and dynamic readouts [107]. Additionally, limited control over their formation increases the risk of phenotypic variability among organoids of the same patient, which can however be contained by changing scaffolds, somewhat improving uniformity [107, 113]. For instance, 3D cultured iPSC-SNs in fibroblast-populated collagen sponge release significantly more substance P after capsaicin stimulation than 2D models [109]. Adopting a 3D architecture has also been shown to reduce extensive cell death, commonly observed in 2D cultures, due to a deficiency in glial supporting cells and lack of cell-to-cell contact.

Organoids and co-culture

Combining 3D-organoid and co-culture strategies may further bridge the gap towards obtaining mature sensory neurons. In a first-of-a-kind fully human tissue-engineered skin model, human keratinocytes and fibroblasts were derived to form a skin cell network, where iPSC-3D sensory ganglions were co-cultured with iPSC-derived SCs. This protocol allowed neuronal cells to reach higher levels of maturity and to extend neurites long enough to reach epidermal-like layers, promising valuable insights for studying skin-associated pain pathologies [109]. Concomitantly, iPSC-DRG organoids cultured with human intrafusal muscle fibers enabled sensory neurons to contact their required targets and reconstitute the muscle spindle of proprioceptors, which further improved cell survival, expression of mature neuronal genes, and active neurotransmitter trafficking machinery [104].

Bio-architecture constraints

Some of the main challenges of 3D cultures regard iPSC-derived DRG organoids disorganized, sporadic cell growth [107]. By creating a spatial structure that mimics endogenous microarchitectures, iPSCs can differentiate and mature in a controlled and precise manner [114]. For example, microfluidic ‘organ-on-a-chip’ provides a rapid, inexpensive tool for culturing cells in small amounts of fluids, easing drug discovery [111]. In a proof-of-concept study, iPSC-derived brain organoids formed in a microfluidic chamber demonstrated key features of human brain development, including neuronal differentiation and cortical organization [115] Furthermore, the chambers allow cellular compartmentalization; thus, enabling the study of axonal outgrowth, injury or transport, independently from the soma. Also, they permit the co-culture of distinct cell types in a circuit and the testing of different chemical compounds, which would not be possible in other systems [116]. Likewise, 3D

bioprinting has been shown to improve iPSC-SN differentiation and reproducibility. Differentiated cells on printed laden gelatin bioink were responsive to mechanical stress and to a range of chemicals [114].

Pushing forward iPSC-SN functional protein expression *in vitro*

While several strategies have led to heterogenous sensory neuronal populations, none thus far have reliably captured cells with functional expression of $Na_V1.8$ and $Na_V1.9$ channels. In **chapter 5**, we artificially induced $Na_V1.8$ and $Na_V1.9$ currents using dynamic clamp and recapitulated native DRG sodium channel electrophysiology in iPSC-SNs. The contribution of each channel to the cell's current density, action potential overshoot and repetitive firing was measured from human DRG recordings and from injecting varying current levels into iPSC-SNs with dynamic clamp. Building on these findings, we were able to precisely 'inject' the amount of current representative of the two missing channels, allowing us to study, for the first time, the effect of a $Na_V1.8$ mutation in iPSC-SNs. However, in this model, iPSC-SNs do not actually express the physical channel proteins, which precludes pharmacological evaluation of selective blockers or binding partners of $Na_V1.8$ and $Na_V1.9$ channels. Likewise, non-selective channel blockers, such as lacosamide, are known to differentially affect VGSC isoforms [117], thus the total current block recorded will not reflect the drug effect nor its underlying mechanisms on the two 'ghost' channels. Establishing a cellular model that allows functional expression of the full complement of ion channels is necessary to perform pharmacogenomic-guided screening in patient-specific cells. To make this strategy work, we need functionally mature iPSCs that reflect the contribution of $Na_V1.8$ and $Na_V1.9$ channels to action potentials and cellular excitability.

It's all about timing

The duration and timing of exposure to selected transcription factors and molecules have been recurrently shown to play a crucial role in the development and maturation of iPSCs [86]. One strategy worth considering is extended passaging [118]. This method has been shown to reduce differentiation-induced variability, and to improve both neural conversion and 3D formation. Koehler et al. adapted an embryonic stem cell neural induction protocol, whereby common deficits of iPSCs, such as delayed neural conversion and difficulties forming neurospheres or embryoid bodies, was corrected by prolongating the expansion of an iPSC clone. Although more time-consuming, after 20 passages, cells formed larger embryoid bodies and expressed neural markers sooner, late passage iPSC-SNs showed greater excitability and larger sodium currents, suggesting enhanced maturation [118]. However, no information regarding ion channel expression levels, specific currents or sensory neuron subtypes was specified in the study, and the utility of this approach remains to be investigated.

Transgene expression of lineage-specific transcription factors in iPSCs

Expanding on the applicability of forced induction of sensory neurogenesis in somatic cells *in vitro*, iPSCs have also been transduced to express regulatory transcription factors. Virally induced exogenous expression of *NGN2* in migrating iPSC-NPCs

resulted in a high percentage of sensory neurons with diverse phenotypes [119]. Current-clamp electrophysiology confirmed the presence of both TTX-S and TTX-R channels. However, low levels of expression of *SCN9A*, *SCN10A*, and *TRKA* suggest that their protocol does not produce high numbers of nociceptors, and that other channels, such $Na_V1.1$ and $Na_V1.6$, that are abundant in proprioceptors and mechanoreceptors, are likely contributing to most of the TTX-S sodium current recorded [119]. Interestingly, the authors reported $Na_V1.8$ immunoreactivity, which may however be attributed to Aβ low-threshold mechanoreceptors (Aβ-LTMR) [119, 120]. Selective Aβ-LTMR identity was reproduced in a separate study, where viral *NGN2*, combined with retinoic acid and neurotrophic factors, produced TTX-S neurons conducting rapidly adapting currents from mechanical stimuli. These findings underscore the capacity of NGN2 to preferably induce mechanoreceptors and suggest that overexpressing *NGN1* instead may specialize cells to more nociceptor-like populations [87]. However, no differences in capsaicin or menthol sensitivity were described in converted sensory neurons from somatic cells expressing either *NGN1* or *NGN2* alone [85]. Also, it has been argued that successful conversion requires *BRN3A* induction, as neurons expressing *NGN2* alone more closely resemble CNS pyramidal neurons than sensory neurons [86]. The contrasted results may be explained by using viral induction [87, 119] over gene engineering [86], and highlight the magnitude of protocol changes can have on cellular phenotypes.

Stable transgene expression of *NGN2* and *BRN3A* generated uniform cultures of cold-mechanoreceptors sensitive to both 4°C and menthol stimuli, while resistant to capsaicin and heat [86]. Interestingly, cell fate determination was time-dependent, whereby briefly induced (24h) cells acquired a phenotype and gene expression profile consistent with LTMR, while those that underwent long exposure (14 days) corresponded to cold-mechanoreceptors, suggesting that extending *NGN2/BRN2A* transgene activation overrides the LTMR transcription and result in PIEZO2+/TRPM8+ neurons [86]. While the obtained cells lacked a nociceptive identity and the expression of many genes involved in pain and itch, including *SCN10A* and *SCN11A*, the aforementioned studies provide important insights on alternative strategies to promote sensory neuron selective subtype differentiation and emphasize the importance of timing and duration of developmental signals to manipulate cell fate determination. With the same goal to improve differentiation, other ways to induce reprogramming are currently in development, such as microRNAs, which behave in synergy with neurogenesis factors to convert fibroblasts into functioning neurons [121, 122].

Tracking and segregating neuronal subtypes

Imaging of human iPSCs can provide new avenues to monitor cell distribution, differentiation, proliferation, and survival both *in vitro* and *in vivo*. Notably, genetic knock-in of fluorescent and epitope tag proteins, where the protein of interest transduces a fluorescent marker, can give us insights on *in vivo* cellular behaviors and patterns of expression [123]. Also, future studies might consider using Ca^{2+} reporter

lines to assess iPSC activity in the DRG *in vivo* [124]. Concomitantly, the generation of sensory neuron reporter cell lines may further enable the identification of specific subtypes and exploration of their electrogenic profile *in vitro* [78]. While heterogenous cultures provide the opportunity to test new analgesic compounds on different cell types, a concurrent drawback lays in the incapacity to identify and isolate cell groups of interest for functional assessment. Immunopanning, an antibody-based purification technique, allows the segregation of selective subtypes from a large pool of neurons, by precoating dishes with specific cell-surface antibodies (eg. anti-TRKA) to which cells of interest (eg. nociceptors) can bind [125].

CONCUSIONS

The burden of large and heterogeneous patient populations, together with technical and financial considerations have long limited the clinical implementation of pharmacogenomic testing. Despite these concerns, a range of variants and susceptible genes are supported by clinical evidence and dosing guidelines for the management of chronic pain, progressively abandoning the conceptual one-size-fits-all idea. Nevertheless, with a major focus on toxicity, from higher numbers of CYP variants involved in the metabolism of common analgesics, increasing our focus instead on novel more selective analgesics, such as VGSC inhibitors, might improve pharmacogenomic analysis using predictors of therapeutic efficacy.

Future innovations in both the fields of pharmacogenomics and iPSC models will revolutionize the way we think about therapy development that really treats the patient. The implementation of routine pharmacogenomic testing could lead to variant classification globally, of common polymorphisms and gene variants beyond pain pathologies, promoting fast and effective diagnoses and treatments with the right effect at the right dose. Rapid technology advances raise new possibilities for iPSC modelling, promising but still far from perfect. Combined efforts are still needed to circumvent the limitations of this system. The optimization of high-throughput pharmacogenomic-guided screening in patient-specific cellular models could significantly improve research in almost any disease of genetic origin or in patients carrying susceptibility genes, which encompasses most disorders. To overcome inter-individual variability and find more widely applicable treatment solutions, it is critical to catalog patient and corresponding iPSC-derived data in libraries. Although pain is not exclusively dependent on genomics but on many other factors, which cannot always be studied in iPSCs nor anticipate complex drug response, it is highly desirable to center our efforts on building a database that can assist clinicians' decisions in prescribing individualized treatments. In turn, this will also allow the standardization of pharmacotherapy. Likewise, the field should aim for consistent and validated protocols to reduce inter-lab variability and efforts of replication.

REFERENCES

1. Smith, D.M., et al., *Clinical application of pharmacogenetics in pain management.* Per Med, 2018. **15**(2): p. 117-126.
2. Scholz, J., et al., *The IASP classification of chronic pain for ICD-11: chronic neuropathic pain.* Pain, 2019. **160**(1): p. 53-59.
3. Sheng, J., et al., *The link between depression and chronic pain: neural mechanisms in the brain.* Neural plasticity, 2017.
4. Raja, S.N., et al., *The revised International Association for the Study of Pain definition of pain: concepts, challenges, and compromises.* Pain, 2020. **161**(9): p. 1976-1982.
5. Panella, L., et al., *Pharmacogenetic Testing in Acute and Chronic Pain: A Preliminary Study.* Medicina (Kaunas), 2019. **55**(5).
6. Bates, M.S., T.W. Edwards, and K.O. Anderson, *Ethnocultural influences on variation in chronic pain perception.* Pain, 1993. **52**(1): p. 101-112.
7. Diatchenko, L., et al., *Genetic basis for individual variations in pain perception and the development of a chronic pain condition.* Hum Mol Genet, 2005. **14**(1): p. 135-43.
8. Marazziti, D., et al., *Pain and psychiatry: a critical analysis and pharmacological review.* Clin Pract Epidemiol Ment Health, 2006. **2**: p. 31.
9. Poloni, N., et al., *[Recovery style, symptoms and psychosocial functioning in psychotic patients: a preliminary study].* Riv Psichiatr, 2013. **48**(5): p. 386-92.
10. de Greef, B.T.A., et al., *Lacosamide in patients with Nav1.7 mutations-related small fibre neuropathy: a randomized controlled trial.* Brain, 2019. **142**(2): p. 263-275.
11. Kim, D.W., H.K. Kim, and E.K. Bae, *Switching from traditional sodium channel blockers to lacosamide in patients with epilepsy.* Seizure, 2019. **65**: p. 172-175.
12. McDonnell, A., et al., *Efficacy of the Nav1.7 blocker PF-05089771 in a randomised, placebo-controlled, double-blind clinical study in subjects with painful diabetic peripheral neuropathy.* Pain, 2018. **159**(8): p. 1465-1476.
13. Siebenga, P., et al., *Lack of Detection of the Analgesic Properties of PF-05089771, a Selective Nav 1.7 Inhibitor, Using a Battery of Pain Models in Healthy Subjects.* Clin Transl Sci, 2020. **13**(2): p. 318-324.
14. Faber, C.G., et al., *Gain of function Nanu1.7 mutations in idiopathic small fiber neuropathy.* Ann Neurol, 2012. **71**(1): p. 26-39.
15. Faber, C.G., et al., *Gain-of-function Nav1.8 mutations in painful neuropathy.* Proc Natl Acad Sci U S A, 2012. **109**(47): p. 19444-9.
16. Huang, J., et al., *Gain-of-function mutations in sodium channel Na(v)1.9 in painful neuropathy.* Brain, 2014. **137**(Pt 6): p. 1627-42.
17. Alsaloum, M., et al., *Status of peripheral sodium channel blockers for non-addictive pain treatment.* Nat Rev Neurol, 2020. **16**(12): p. 689-705.
18. Yuan, J.H., et al., *KCNQ variants and pain modulation: a missense variant in Kv7.3 contributes to pain resilience.* Brain Commun, 2021. **3**(3): p. fcab212.
19. Mis, M.A., et al., *Resilience to Pain: A Peripheral Component Identified Using Induced Pluripotent Stem Cells and Dynamic Clamp.* J Neurosci, 2019. **39**(3): p. 382-392.
20. Bialer, M., et al., *Progress report on new antiepileptic drugs: A summary of the Fourteenth Eilat Conference on New Antiepileptic Drugs and Devices (EILAT XIV). I. Drugs in preclinical and early clinical development.* Epilepsia, 2018. **59**(10): p. 1811-1841.
21. Latremoliere, A. and M. Costigan, *Combining Human and Rodent Genetics to Identify New Analgesics.* Neurosci Bull, 2018. **34**(1): p. 143-155.
22. Tegeder, I., et al., *GTP cyclohydrolase and tetrahydrobiopterin regulate pain sensitivity and persistence.* Nat Med, 2006. **12**(11): p. 1269-77.
23. Yang, Y., et al., *NaV1.7 as a Pharmacogenomic Target for Pain: Moving Toward Precision Medicine.* Trends Pharmacol Sci, 2018. **39**(3): p. 258-275.

24. Meloto, C.B., et al., *COMT gene locus: new functional variants.* Pain, 2015. **156**(10): p. 2072-2083.
25. Sorge, R.E., et al., *Genetically determined P2X7 receptor pore formation regulates variability in chronic pain sensitivity.* Nat Med, 2012. **18**(4): p. 595-9.
26. Ali, Z., et al., *Pharmacokinetic and pharmacodynamic profiling of a P2X7 receptor allosteric modulator GSK1482160 in healthy human subjects.* Br J Clin Pharmacol, 2013. **75**(1): p. 197-207.
27. Stock, T.C., et al., *Efficacy and safety of CE-224,535, an antagonist of P2X7 receptor, in treatment of patients with rheumatoid arthritis inadequately controlled by methotrexate.* J Rheumatol, 2012. **39**(4): p. 720-7.
28. Vega-Loza, A., et al., *Gene therapies to reduce chronic pain: are we there yet?* 2020, Future Medicine. p. 209-212.
29. Yeomans, D.C., et al., *Decrease in inflammatory hyperalgesia by herpes vector-mediated knockdown of Nav1.7 sodium channels in primary afferents.* Hum Gene Ther, 2005. **16**(2): p. 271-7.
30. Samad, O.A., et al., *Virus-mediated shRNA knockdown of Na(v)1.3 in rat dorsal root ganglion attenuates nerve injury-induced neuropathic pain.* Mol Ther, 2013. **21**(1): p. 49-56.
31. Tan, A.M., et al., *Virus-Mediated Knockdown of Nav1.3 in Dorsal Root Ganglia of STZ-Induced Diabetic Rats Alleviates Tactile Allodynia.* Mol Med, 2015. **21**: p. 544-52.
32. Uddin, F., C.M. Rudin, and T. Sen, *CRISPR Gene Therapy: Applications, Limitations, and Implications for the Future.* Front Oncol, 2020. **10**: p. 1387.
33. Kummar, S., et al., *Application of molecular profiling in clinical trials for advanced metastatic cancers.* J Natl Cancer Inst, 2015. **107**(4).
34. Motsinger-Reif, A.A., et al., *Genome-wide association studies in pharmacogenomics: successes and lessons.* Pharmacogenet Genomics, 2013. **23**(8): p. 383-94.
35. Ko, T.M., et al., *Pharmacogenomics for personalized pain medicine.* Acta Anaesthesiol Taiwan, 2016. **54**(1): p. 24-30.
36. Fredrikson, K.M. and T. Fasolino, *Pharmacogenetic testing: Clinical integration and application for chronic pain management.* Nurse Pract, 2021. **46**(4): p. 12-19.
37. Zhou, Y., M. Ingelman-Sundberg, and V.M. Lauschke, *Worldwide Distribution of Cytochrome P450 Alleles: A Meta-analysis of Population-scale Sequencing Projects.* Clin Pharmacol Ther, 2017. **102**(4): p. 688-700.
38. Relling, M.V. and W.E. Evans, *Pharmacogenomics in the clinic.* Nature, 2015. **526**(7573): p. 343-50.
39. Dunnenberger, H.M., et al., *Preemptive clinical pharmacogenetics implementation: current programs in five US medical centers.* Annu Rev Pharmacol Toxicol, 2015. **55**: p. 89-106.
40. Crews, K.R., et al., *Clinical Pharmacogenetics Implementation Consortium guidelines for cytochrome P450 2D6 genotype and codeine therapy: 2014 update.* Clin Pharmacol Ther, 2014. **95**(4): p. 376-82.
41. Knezevic, N.N., et al., *The Role of Genetic Polymorphisms in Chronic Pain Patients.* Int J Mol Sci, 2018. **19**(6).
42. Johansson, I. and M. Ingelman-Sundberg, *Genetic polymorphism and toxicology--with emphasis on cytochrome p450.* Toxicol Sci, 2011. **120**(1): p. 1-13.
43. Smith, D.M., et al., *CYP2D6-guided opioid therapy improves pain control in CYP2D6 intermediate and poor metabolizers: a pragmatic clinical trial.* Genet Med, 2019. **21**(8): p. 1842-1850.
44. Loh, F.H., et al., *Pharmacogenomic Testing and Patient Perception Inform Pain Pharmacotherapy.* J Pers Med, 2021. **11**(11).
45. Patel, J.N., et al., *Pilot study of multi-gene pharmacogenetic testing for pain management in oncology palliative medicine.* Pharmacogenomics, 2021. **22**(12): p. 737-748.
46. Stamer, U.M., et al., *Impact of CYP2D6 genotype on postoperative tramadol analgesia.* Pain, 2003. **105**(1-2): p. 231-8.

47. Stamer, U.M. and F. Stuber, *Codeine and tramadol analgesic efficacy and respiratory effects are influenced by CYP2D6 genotype.* Anaesthesia, 2007. **62**(12): p. 1294-5; author reply 1295-6.
48. Stamer, U.M., L. Zhang, and F. Stuber, *Personalized therapy in pain management: where do we stand?* Pharmacogenomics, 2010. **11**(6): p. 843-64.
49. Leandro-Garcia, L.J., et al., *Determination of CYP2D6 gene copy number by multiplex polymerase chain reaction analysis.* Anal Biochem, 2009. **389**(1): p. 74-6.
50. Zhang, W., et al., *Influence of CYP3A5*3 polymorphism and interaction between CYP3A5*3 and CYP3A4*1G polymorphisms on post-operative fentanyl analgesia in Chinese patients undergoing gynaecological surgery.* Eur J Anaesthesiol, 2011. **28**(4): p. 245-50.
51. Xu, Y., et al., *[Human pregnane X receptor-mediated transcriptional regulation of CYP3A4 by extracts of 7 traditional Chinese medicines].* Zhongguo Zhong Yao Za Zhi, 2011. **36**(11): p. 1524-7.
52. Ablin, J.N. and D. Buskila, *Personalized treatment of pain.* Curr Rheumatol Rep, 2013. **15**(1): p. 298.
53. Packiasabapathy, S., N. Horn, and S. Sadhasivam, *Genetics of perioperative pain management.* Curr Opin Anaesthesiol, 2018. **31**(6): p. 749-755.
54. Ting, S. and S. Schug, *The pharmacogenomics of pain management: prospects for personalized medicine.* J Pain Res, 2016. **9**: p. 49-56.
55. Finnerup, N.B., R. Kuner, and T.S. Jensen, *Neuropathic Pain: From Mechanisms to Treatment.* Physiol Rev, 2021. **101**(1): p. 259-301.
56. Smith, S.M., et al., *The Potential Role of Sensory Testing, Skin Biopsy, and Functional Brain Imaging as Biomarkers in Chronic Pain Clinical Trials: IMMPACT Considerations.* J Pain, 2017. **18**(7): p. 757-777.
57. Krakow, E.F., et al., *Tools for the Precision Medicine Era: How to Develop Highly Personalized Treatment Recommendations From Cohort and Registry Data Using Q-Learning.* Am J Epidemiol, 2017. **186**(2): p. 160-172.
58. Perez, V., et al., *Efficacy of prospective pharmacogenetic testing in the treatment of major depressive disorder: results of a randomized, double-blind clinical trial.* BMC Psychiatry, 2017. **17**(1): p. 250.
59. Goulooze, S.C., et al., *Towards personalized treatment of pain using a quantitative systems pharmacology approach.* Eur J Pharm Sci, 2017. **109S**: p. S32-S38.
60. Breimer, D.D. and M. Danhof, *Relevance of the application of pharmacokinetic-pharmacodynamic modelling concepts in drug development. The "wooden shoe' paradigm.* Clin Pharmacokinet, 1997. **32**(4): p. 259-67.
61. Komatsu, T., et al., *Population pharmacokinetics of oxycodone in patients with cancer-related pain.* J Pain Palliat Care Pharmacother, 2012. **26**(3): p. 220-5.
62. Krekels, E.H., et al., *Evidence-based morphine dosing for postoperative neonates and infants.* Clin Pharmacokinet, 2014. **53**(6): p. 553-63.
63. Byon, W., et al., *Exposure-response analyses of the effects of pregabalin in patients with fibromyalgia using daily pain scores and patient global impression of change.* J Clin Pharmacol, 2010. **50**(7): p. 803-15.
64. Mogil, J.S., *Pain genetics: past, present and future.* Trends Genet, 2012. **28**(6): p. 258-66.
65. Backryd, E., *Pain in the Blood? Envisioning Mechanism-Based Diagnoses and Biomarkers in Clinical Pain Medicine.* Diagnostics (Basel), 2015. **5**(1): p. 84-95.
66. Beger, R.D., et al., *Metabolomics enables precision medicine: "A White Paper, Community Perspective".* Metabolomics, 2016. **12**(10): p. 149.
67. Kohler, I., et al., *Integrating clinical metabolomics-based biomarker discovery and clinical pharmacology to enable precision medicine.* Eur J Pharm Sci, 2017. **109S**: p. S15-S21.
68. Quartana, P.J., et al., *Pain catastrophizing and salivary cortisol responses to laboratory pain testing in temporomandibular disorder and healthy participants.* J Pain, 2010. **11**(2): p. 186-94.

69. Mc Ardle, A., et al., *Early biomarkers of joint damage in rheumatoid and psoriatic arthritis.* Arthritis Res Ther, 2015. **17**: p. 141.
70. Namer, B., et al., *Pain relief in a neuropathy patient by lacosamide: Proof of principle of clinical translation from patient-specific iPS cell-derived nociceptors.* EBioMedicine, 2019. **39**: p. 401-408.
71. Cao, L., et al., *Pharmacological reversal of a pain phenotype in iPSC-derived sensory neurons and patients with inherited erythromelalgia.* Sci Transl Med, 2016. **8**(335): p. 335ra56.
72. Capurro, A., et al., *Nav1. 7 gating in human iPSC derived sensory neurons: an experimental and computational study.* bioRxiv, 2020.
73. Elitt, M.S., L. Barbar, and P.J. Tesar, *Drug screening for human genetic diseases using iPSC models.* Hum Mol Genet, 2018. **27**(R2): p. R89-R98.
74. Egawa, N., et al., *Drug screening for ALS using patient-specific induced pluripotent stem cells.* Sci Transl Med, 2012. **4**(145): p. 145ra104.
75. Stacey, P., et al., *Plate-Based Phenotypic Screening for Pain Using Human iPSC-Derived Sensory Neurons.* SLAS Discov, 2018. **23**(6): p. 585-596.
76. Hoelting, L., et al., *Stem Cell-Derived Immature Human Dorsal Root Ganglia Neurons to Identify Peripheral Neurotoxicants.* Stem Cells Transl Med, 2016. **5**(4): p. 476-87.
77. Chambers, S.M., et al., *Combined small-molecule inhibition accelerates developmental timing and converts human pluripotent stem cells into nociceptors.* Nat Biotechnol, 2012. **30**(7): p. 715-20.
78. Wainger, B.J., et al., *Modeling pain in vitro using nociceptor neurons reprogrammed from fibroblasts.* Nat Neurosci, 2015. **18**(1): p. 17-24.
79. Lee, J.H., et al., *Single Transcription Factor Conversion of Human Blood Fate to NPCs with CNS and PNS Developmental Capacity.* Cell Rep, 2015. **11**(9): p. 1367-76.
80. Vojnits, K., et al., *Chemotherapy-Induced Neuropathy and Drug Discovery Platform Using Human Sensory Neurons Converted Directly from Adult Peripheral Blood.* Stem Cells Transl Med, 2019. **8**(11): p. 1180-1191.
81. Wilson, R., et al., *Human peptidergic nociceptive sensory neurons generated from human epidermal neural crest stem cells (hEPI-NCSC).* PLoS One, 2018. **13**(6): p. e0199996.
82. Schwartzentruber, J., et al., *Molecular and functional variation in iPSC-derived sensory neurons.* Nat Genet, 2018. **50**(1): p. 54-61.
83. Marmigere, F. and P. Ernfors, *Specification and connectivity of neuronal subtypes in the sensory lineage.* Nat Rev Neurosci, 2007. **8**(2): p. 114-27.
84. Boisvert, E.M., et al., *The Specification and Maturation of Nociceptive Neurons from Human Embryonic Stem Cells.* Sci Rep, 2015. **5**: p. 16821.
85. Blanchard, J.W., et al., *Selective conversion of fibroblasts into peripheral sensory neurons.* Nat Neurosci, 2015. **18**(1): p. 25-35.
86. Nickolls, A.R., et al., *Transcriptional Programming of Human Mechanosensory Neuron Subtypes from Pluripotent Stem Cells.* Cell Rep, 2020. **30**(3): p. 932-946 e7.
87. Schrenk-Siemens, K., et al., *PIEZO2 is required for mechanotransduction in human stem cell-derived touch receptors.* Nat Neurosci, 2015. **18**(1): p. 10-6.
88. Iyer, N.R., T.S. Wilems, and S.E. Sakiyama-Elbert, *Stem cells for spinal cord injury: Strategies to inform differentiation and transplantation.* Biotechnol Bioeng, 2017. **114**(2): p. 245-259.
89. Fu, W., et al., *Residual undifferentiated cells during differentiation of induced pluripotent stem cells in vitro and in vivo.* Stem Cells Dev, 2012. **21**(4): p. 521-9.
90. Kim, A., et al., *Elimination of Teratogenic Human Induced Pluripotent Stem Cells by Bee Venom via Calcium-Calpain Pathway.* Int J Mol Sci, 2020. **21**(9).
91. Sadler, K.E., F. Moehring, and C.L. Stucky, *Keratinocytes contribute to normal cold and heat sensation.* Elife, 2020. **9**.
92. Hahn, J.M., et al., *Identification of Merkel cells associated with neurons in engineered skin substitutes after grafting to full thickness wounds.* PLoS One, 2019. **14**(3): p. e0213325.

93. Abdo, H., et al., *Specialized cutaneous Schwann cells initiate pain sensation.* Science, 2019. **365**(6454): p. 695-699.
94. Svaren, J., et al., *Schwann cell transcript biomarkers for hereditary neuropathy skin biopsies.* Ann Neurol, 2019. **85**(6): p. 887-898.
95. Talagas, M., et al., *Lifting the veil on the keratinocyte contribution to cutaneous nociception.* Protein Cell, 2020. **11**(4): p. 239-250.
96. Talagas, M., et al., *Intra-epidermal nerve endings progress within keratinocyte cytoplasmic tunnels in normal human skin.* Exp Dermatol, 2020. **29**(4): p. 387-392.
97. Cai, S., et al., *Human Induced Pluripotent Cell-Derived Sensory Neurons for Fate Commitment of Bone Marrow-Derived Schwann Cells: Implications for Remyelination Therapy.* Stem Cells Transl Med, 2017. **6**(2): p. 369-381.
98. Clark, A.J., et al., *Co-cultures with stem cell-derived human sensory neurons reveal regulators of peripheral myelination.* Brain, 2017. **140**(4): p. 898-913.
99. Kim, H.S., et al., *Directly induced human Schwann cell precursors as a valuable source of Schwann cells.* Stem Cell Res Ther, 2020. **11**(1): p. 257.
100. Schutte, S.C., F. Kadakia, and S. Davidson, *Skin-Nerve Co-Culture Systems for Disease Modeling and Drug Discovery.* Tissue Eng Part C Methods, 2021. **27**(2): p. 89-99.
101. Canfield, S.G., et al., *An isogenic neurovascular unit model comprised of human induced pluripotent stem cell-derived brain microvascular endothelial cells, pericytes, astrocytes, and neurons.* Fluids Barriers CNS, 2019. **16**(1): p. 25.
102. Haenseler, W., et al., *A Highly Efficient Human Pluripotent Stem Cell Microglia Model Displays a Neuronal-Co-culture-Specific Expression Profile and Inflammatory Response.* Stem Cell Reports, 2017. **8**(6): p. 1727-1742.
103. di Domenico, A., et al., *Patient-Specific iPSC-Derived Astrocytes Contribute to Non-Cell-Autonomous Neurodegeneration in Parkinson's Disease.* Stem Cell Reports, 2019. **12**(2): p. 213-229.
104. Mazzara, P.G., et al., *Frataxin gene editing rescues Friedreich's ataxia pathology in dorsal root ganglia organoid-derived sensory neurons.* Nat Commun, 2020. **11**(1): p. 4178.
105. Chiaradia, I. and M.A. Lancaster, *Brain organoids for the study of human neurobiology at the interface of in vitro and in vivo.* Nat Neurosci, 2020. **23**(12): p. 1496-1508.
106. Xiao, D., et al., *Generation of self-organized sensory ganglion organoids and retinal ganglion cells from fibroblasts.* Sci Adv, 2020. **6**(22): p. eaaz5858.
107. Wiegand, C. and I. Banerjee, *Recent advances in the applications of iPSC technology.* Curr Opin Biotechnol, 2019. **60**: p. 250-258.
108. Lee, G., et al., *Modelling pathogenesis and treatment of familial dysautonomia using patient-specific iPSCs.* Nature, 2009. **461**(7262): p. 402-6.
109. Muller, Q., et al., *Development of an innervated tissue-engineered skin with human sensory neurons and Schwann cells differentiated from iPS cells.* Acta Biomater, 2018. **82**: p. 93-101.
110. Kapalczynska, M., et al., *2D and 3D cell cultures - a comparison of different types of cancer cell cultures.* Arch Med Sci, 2018. **14**(4): p. 910-919.
111. Mofazzal Jahromi, M.A., et al., *Microfluidic Brain-on-a-Chip: Perspectives for Mimicking Neural System Disorders.* Mol Neurobiol, 2019. **56**(12): p. 8489-8512.
112. Pereira, J.D., et al., *Human sensorimotor organoids derived from healthy and amyotrophic lateral sclerosis stem cells form neuromuscular junctions.* Nat Commun, 2021. **12**(1): p. 4744.
113. Candiello, J., et al., *3D heterogeneous islet organoid generation from human embryonic stem cells using a novel engineered hydrogel platform.* Biomaterials, 2018. **177**: p. 27-39.
114. Hirano, M., et al., *3D bioprinted human iPSC-derived somatosensory constructs with functional and highly purified sensory neuron networks.* Biofabrication, 2021. **13**(3).
115. Wang, Y., et al., *Engineering stem cell-derived 3D brain organoids in a perfusable organ-on-a-chip system.* RSC advances, 2018. **8**(3): p. 1677-1685.
116. Fantuzzo, J.A., et al., *Compartmentalized Devices as Tools for Investigation of Human Brain Network Dynamics.* Dev Dyn, 2019. **248**(1): p. 65-77.

117. Sheets, P.L., et al., *Differential block of sensory neuronal voltage-gated sodium channels by lacosamide [(2R)-2-(acetylamino)-N-benzyl-3-methoxypropanamide], lidocaine, and carbamazepine.* J Pharmacol Exp Ther, 2008. **326**(1): p. 89-99.
118. Koehler, K.R., et al., *Extended passaging increases the efficiency of neural differentiation from induced pluripotent stem cells.* BMC Neurosci, 2011. **12**: p. 82.
119. Hulme, A.J., et al., *Molecular and Functional Characterization of Neurogenin-2 Induced Human Sensory Neurons.* Front Cell Neurosci, 2020. **14**: p. 600895.
120. Shields, S.D., et al., *Nav1. 8 expression is not restricted to nociceptors in mouse peripheral nervous system.* PAIN®, 2012. **153**(10): p. 2017-2030.
121. Yoo, A.S., et al., *MicroRNA-mediated conversion of human fibroblasts to neurons.* Nature, 2011. **476**(7359): p. 228-31.
122. Ambasudhan, R., et al., *Direct reprogramming of adult human fibroblasts to functional neurons under defined conditions.* Cell Stem Cell, 2011. **9**(2): p. 113-8.
123. Luo, Y., et al., *Stable enhanced green fluorescent protein expression after differentiation and transplantation of reporter human induced pluripotent stem cells generated by AAVS1 transcription activator-like effector nucleases.* Stem Cells Transl Med, 2014. **3**(7): p. 821-35.
124. Viventi, S., et al., *In vivo survival and differentiation of Friedreich ataxia iPSC-derived sensory neurons transplanted in the adult dorsal root ganglia.* Stem Cells Transl Med, 2021. **10**(8): p. 1157-1169.
125. Saito-Diaz, K., et al., *Derivation of Peripheral Nociceptive, Mechanoreceptive, and Proprioceptive Sensory Neurons from the same Culture of Human Pluripotent Stem Cells.* Stem Cell Reports, 2021. **16**(3): p. 446-457.

CHAPTER 7

SIGNIFICANCE STATEMENT

CLINICAL AND SCIENTFIC IMPACT

Chronic pain affects nearly 1 in 4 individuals worldwide [1-3], and despite its global spread, treatments for this condition are still largely ineffective and carry serious side effects [4, 5]. Recent drug developments have focused on inhibitors of voltage-gated sodium channels (VGSC), which, when dysfunctional, are associated with several human pain syndromes [6-8]. Different classes of VGSC blockers have emerged, including anticonvulsants, local anesthetics, and isoform-selective blockers. Lacosamide, an anticonvulsant and emerging candidate for treating pain [9], has shown variable efficacy in patients with $Na_V1.7$-related small fiber neuropathy (SFN) [10]. To date, the peripheral mechanisms underlying lacosamide treatment response modulation are still poorly understood. With limited number of individuals responsive to available medications, unraveling the contributing factors interfering with pain targets and drug modulation is highly warranted. In **chapter 2**, we recapitulated inter-individual variations in lacosamide response in patients with $Na_V1.7$ mutations. Our results support the utilization of a pre-clinical biophysical assessment of specific mutations to select compounds to predict individualized patient response. Furthermore, our -and similar- findings can be extrapolated back to the clinic for patients genotyped with already-assessed $Na_V1.7$ mutations, allowing clinicians to anticipate their response to, in this case, lacosamide. We also linked specific genetic mutations to distinct pharmacological phenotypes in different SFN patients, which can be incorporated in future studies to develop better-suited treatment strategies. Epilepsy research has taught us important lessons on the extrapolation of genomic data for pharmacotherapy, by titrating dosages based on $Na_V1.7$ splicing variants [11]. A comparable, easy-to-use pharmacogenomic-based model is proposed here for pain, which can as well be implemented to study a wide range of mutations and drugs, whereby the biophysical signature correlating to a positive drug response can guide treatment.

Understanding the mechanisms of action of analgesics, such as lacosamide and its isoform-selectivity, is critical to make informed decisions when treating specific patients and could aid future drug developments. Lacosamide has been shown to exert its effects in an unconventional manner compared to traditional pore-blocker sodium channel inhibitors [12-16]. Solving its mechanistic basis can further explain inter-individual variability in efficacy and tolerability in treated patients [10]. **Chapter 3** provides a description of a working model of lacosamide and reports a novel binding region in $Na_V1.7$, in the voltage-sensing domain 4 (VSD4), which, alongside an intact local anesthetic site within the channel's pore, is required for lacosamide to exert its therapeutic functions. The role of the VSD4 seems to be determinant to lacosamide-isoform specificity at clinically-achievable concentrations. By unraveling the interaction between lacosamide and the VSD4, **chapter 3** sheds a light on possible implications in other sodium channelopathies, where other VGSC isoforms are affected, for example in patients with VGSC-related epilepsy or cardiac disease. By establishing the binding properties of lacosamide, we can make better predictions on drug efficacy and tolerability in patients. Our findings also highlight the pivotal role the

VSD play in initiating and maintaining lacosamide functions at therapeutic concentrations, which may be relevant in patients with mutations located in the VSD. Specifically, our results show that in cells expressing the W1538R variant, the mutation-related lacosamide block can be overcome by increasing dosage. Therefore, genomic evaluation of neuropathic pain patients, whereby specific genetic variants in $Na_V1.7$ are detected, can be used as a dosing guideline.

Modeling genetic diseases is a tedious task, as there is a constant need for further developing cellular systems mimicking those in physiological conditions. The use of patient-specific cells can extend our understanding of pain pathophysiological mechanisms [17-20] and drug response [17, 21, 22]. In **chapter 4**, we initiated the development of a dorsal root ganglion (DRG)-targeted *in vivo* and *ex vivo* differentiation method, as a model of "humanized" cells, to offer a more translational approach, which could potentially help increase the success rates in clinical trials. While we did not succeed in forcing iPSC differentiation *in vivo* yet, successful optimization of our iPSC methods could inform us on iPSC patterns of migration, speed of differentiation and body absorption. Furthermore, this may allow drug screening in iPSCs, which will in turn extend our knowledge on iPSC-derived cells metabolism in response to drug exposure, and further delineate the responsiveness of alternative variants to different VGSC-blocking treatments. Furthermore, our results were educational on inter-species physiological interactions and on iPSC behaviors and parameters that affect DRG teratoma development. Our study provided substantial data on the differentiation and migration properties of undifferentiated cells in the rat DRG and its potential for tumorigenicity, as well as its influence on non-transplanted adjacent organs and overall physiological functions. Although beyond the scope of this thesis, these findings can serve as a basis for stem cell therapy in the DRG on how to avoid cell graft rejection and tumor formation, which can have major implications for advances in regenerative medicine. Furthermore, our model provides important insights to the study of iPSCs that are transplanted into a specific organ and can be used to propel research efforts in other pain-related or unrelated diseases.

Besides concerns associated with iPSC immaturity, the lack of functional expression of the $Na_V1.8$ and $Na_V1.9$ sodium channels in iPSC-derived sensory neurons (iPSC-SN) still represent a prominent caveat to the study of painful sodium channelopathies in iPSC models [18, 23]. These two channels are particularly important to pain signaling as they contribute to a large portion of the sodium current transmission and cellular excitability [24, 25]; therefore, without their physiological input, the recorded current is corrupted and not representative of the patient's cells true electrophysiological properties. In **chapter 5**, we described for the first time the relationship and contribution of human $Na_V1.8$ and $Na_V1.9$ channels to human neuronal excitability as pain correlates. Furthermore, not only were we able to produce $Na_V1.8$ and $Na_V1.9$ currents, but we also developed a brand-new model allowing the study of $Na_V1.8$ and $Na_V1.9$ mutations in iPSC-SNs via dynamic clamp, which was never possible before. Moreover, this technique can be used to introduce several mutations simultaneously,

in the same patient-specific cells, covering a wider range of genetic variants and possible interactions. In turn, patients who carry genetic variants in the two channels can be evaluated in the future. Additionally, the overall cellular excitability of patient iPSC-SNs with $Na_V1.7$ mutations might be restored to similar levels that would have been recorded in the donor's neurons, and thus, aid find better fitted treatments. Our ability to modulate $Na_V1.8$ and $Na_V1.9$ via dynamic clamp may further guide future therapeutic considerations in drug development and clinical trial dosing. Specifically, dynamic clamp of iPSC-SNs might bridge the gap in knowledge regarding the precise degree of channel inhibition needed to induce therapeutic relief without total loss of pain sensation [26, 27].

Taken together, the findings from this thesis have set the stage for using pharmacogenomic-guided tools in patient-specific iPSC-SNs to solve pain mismanagement while providing novel strategies to implement personalized therapy in pain research.

REFERENCES

1. Reid, K.J., et al., *Epidemiology of chronic non-cancer pain in Europe: narrative review of prevalence, pain treatments and pain impact.* Curr Med Res Opin, 2011. **27**(2): p. 449-62.
2. Kennedy, J., et al., *Prevalence of persistent pain in the U.S. adult population: new data from the 2010 national health interview survey.* J Pain, 2014. **15**(10): p. 979-84.
3. McCarberg, B.H. and R. Billington, *Consequences of neuropathic pain: quality-of-life issues and associated costs.* Am J Manag Care, 2006. **12**(9 Suppl): p. S263-8.
4. Nishikawa, N. and M. Nomoto, *Management of neuropathic pain.* J Gen Fam Med, 2017. **18**(2): p. 56-60.
5. Finnerup, N.B., et al., *Pharmacotherapy for neuropathic pain in adults: a systematic review and meta-analysis.* Lancet Neurol, 2015. **14**(2): p. 162-73.
6. Bennett, D.L., et al., *The Role of Voltage-Gated Sodium Channels in Pain Signaling.* Physiol Rev, 2019. **99**(2): p. 1079-1151.
7. Dib-Hajj, S.D. and S.G. Waxman, *Sodium Channels in Human Pain Disorders: Genetics and Pharmacogenomics.* Annu Rev Neurosci, 2019.
8. Dib-Hajj, S.D., et al., *The Na(V)1.7 sodium channel: from molecule to man.* Nat Rev Neurosci, 2013. **14**(1): p. 49-62.
9. Carona, A., et al., *Pharmacology of lacosamide: From its molecular mechanisms and pharmacokinetics to future therapeutic applications.* Life Sci, 2021. **275**: p. 119342.
10. de Greef, B.T.A., et al., *Lacosamide in patients with Nav1.7 mutations-related small fibre neuropathy: a randomized controlled trial.* Brain, 2019. **142**(2): p. 263-275.
11. Raymond, C.K., et al., *Expression of alternatively spliced sodium channel alpha-subunit genes. Unique splicing patterns are observed in dorsal root ganglia.* J Biol Chem, 2004. **279**(44): p. 46234-41.
12. Errington, A.C., et al., *The investigational anticonvulsant lacosamide selectively enhances slow inactivation of voltage-gated sodium channels.* Mol Pharmacol, 2008. **73**(1): p. 157-69.
13. Niespodziany, I., et al., *Comparative study of lacosamide and classical sodium channel blocking antiepileptic drugs on sodium channel slow inactivation.* J Neurosci Res, 2013. **91**(3): p. 436-43.

14. Sheets, P.L., et al., *Differential block of sensory neuronal voltage-gated sodium channels by lacosamide [(2R)-2-(acetylamino)-N-benzyl-3-methoxypropanamide], lidocaine, and carbamazepine.* J Pharmacol Exp Ther, 2008. **326**(1): p. 89-99.
15. Wang, Y., et al., *Development and characterization of novel derivatives of the antiepileptic drug lacosamide that exhibit far greater enhancement in slow inactivation of voltage-gated sodium channels.* ACS Chem Neurosci, 2011. **2**(2): p. 90-106.
16. Rogawski, M.A., et al., *Current understanding of the mechanism of action of the antiepileptic drug lacosamide.* Epilepsy Res, 2015. **110**: p. 189-205.
17. Cao, L., et al., *Pharmacological reversal of a pain phenotype in iPSC-derived sensory neurons and patients with inherited erythromelalgia.* Sci Transl Med, 2016. **8**(335): p. 335ra56.
18. Meents, J.E., et al., *The role of Nav1.7 in human nociceptors: insights from human induced pluripotent stem cell-derived sensory neurons of erythromelalgia patients.* Pain, 2019. **160**(6): p. 1327-1341.
19. Mis, M.A., et al., *Resilience to Pain: A Peripheral Component Identified Using Induced Pluripotent Stem Cells and Dynamic Clamp.* J Neurosci, 2019. **39**(3): p. 382-392.
20. Yuan, J.H., et al., *KCNQ variants and pain modulation: a missense variant in Kv7.3 contributes to pain resilience.* Brain Commun, 2021. **3**(3): p. fcab212.
21. Capurro, A., et al., *Nav1. 7 gating in human iPSC derived sensory neurons: an experimental and computational study.* bioRxiv, 2020.
22. Namer, B., et al., *Pain relief in a neuropathy patient by lacosamide: Proof of principle of clinical translation from patient-specific iPS cell-derived nociceptors.* EBioMedicine, 2019. **39**: p. 401-408.
23. Eberhardt, E., et al., *Pattern of Functional TTX-Resistant Sodium Channels Reveals a Developmental Stage of Human iPSC- and ESC-Derived Nociceptors.* Stem Cell Reports, 2015. **5**(3): p. 305-13.
24. Herzog, R.I., T.R. Cummins, and S.G. Waxman, *Persistent TTX-resistant Na+ current affects resting potential and response to depolarization in simulated spinal sensory neurons.* J Neurophysiol, 2001. **86**(3): p. 1351-64.
25. Renganathan, M., T.R. Cummins, and S.G. Waxman, *Contribution of Na(v)1.8 sodium channels to action potential electrogenesis in DRG neurons.* J Neurophysiol, 2001. **86**(2): p. 629-40.
26. McDonnell, A., et al., *Efficacy of the Nav1.7 blocker PF-05089771 in a randomised, placebo-controlled, double-blind clinical study in subjects with painful diabetic peripheral neuropathy.* Pain, 2018. **159**(8): p. 1465-1476.
27. Siebenga, P., et al., *Lack of Detection of the Analgesic Properties of PF-05089771, a Selective Na(v) 1.7 Inhibitor, Using a Battery of Pain Models in Healthy Subjects.* Clin Transl Sci, 2020. **13**(2): p. 318-324.

APPENDIX

Summary

Abbreviations

Curriculum Vitae

List of publications

Acknowledgements

SUMMARY

Neuropathic pain represents a major health burden, affecting 6.9% to 10% of the global population. The clinical, economical, and psycho-emotional burden of neuropathic pain underlines the urgency to find novel, effective treatment options. Patients consistently report lack of efficacy from available treatments and severe adverse effects, yielding to years of trial-and-error therapies that result in insignificant improvements. With no analgesic development in over a decade, there is a considerable need to focus on personalized and precision medicine. For example, patients can react differently to commonly used analgesics, like lacosamide, requiring a personalized approach to decide upfront who will benefit from the treatment and who will not. Therefore, the first aim of the work presented in this thesis was to delineate the involvement of specific residues in the pharmacology of lacosamide, and the effect of associated mutations in patients' responsiveness, as a template for using pharmacogenomic-based approaches to treat human pain disorders. Since current cell and animal models are often poor surrogates for studying human pathologies and mechanisms, studies using these models may not provide an accurate answer. Even in humanized systems, such as patient-derived induced-pluripotent stem cell (iPSC) models, our ability to develop a personalized strategy is affected by culture and differentiation-induced variability. Therefore, developing better models and tools to study pain pathologies is critical for advancing pharmacogenomics and precision medicine research. My second aim was to develop alternative iPSC systems that express critical proteins and better mimic human DRGs to study neuropathic pain-associated sodium channel mutations. My final aim was to shed light on iPSC behaviors in transplanted DRGs, which remain unexplored. Chapter 1 provides a general introduction of neuropathic pain and the involvement of sodium channels in its etiology. This chapter also discusses available treatment options and the latest advances in pharmacogenomics to provide individualized therapeutic strategies. Also, this chapter touches upon the use of patient-derived iPSCs for pain pathology and pharmacology research. Despite clear developments in using iPSC-derived sensory neurons, substantial limitations exist, including the lack of functional expression of the full range of sodium channels, slowing down advances in human DRG modeling. To overcome these challenges, we developed innovative solutions that will pave the way for patient-specific iPSC-based pharmacotherapy.

In chapter 2, we extended on the clinical findings that lacosamide, which blocks sodium channels in a use-dependent manner, attenuates pain in some patients with $Na_v1.7$ mutations; however, only a subgroup of these patients responded to the drug. Here, we used voltage-clamp recordings to evaluate the effects of lacosamide on five $Na_v1.7$ variants from patients who were mostly responsive (I739V, W719C) or non-responsive (I228M, L1267V, W1538R) to treatment. We showed that, at the clinically-achievable concentration of 30 μM, lacosamide acts as a potent sodium channel inhibitor of $Na_v1.7$ variants carried by responsive patients via a hyperpolarizing shift of voltage-dependence

of both fast- and slow-inactivation and enhancement of use-dependent inhibition. By contrast, the effects of lacosamide on slow-inactivation and use-dependence in $Na_V1.7$ variants from non-responsive patients were less robust. Importantly, we found that lacosamide selectively enhances fast-inactivation only in variants from responders. Taken together, these findings begin to unravel biophysical underpinnings that contribute to responsiveness to lacosamide in patients with small fiber neuropathy carrying select $Na_V1.7$ variants.

Building on our findings that the $Na_V1.7$-W1538R mutation completely abolishes $Na_V1.7$ inhibition by clinically-achievable concentrations of lacosamide, using molecular docking, we showed in **chapter 3** that W1538 and pore residues are high affinity binding sites for lacosamide. We also used voltage-clamp recordings to demonstrate that lacosamide requires an intact local anesthetic binding site to inhibit $Na_V1.7$ channels. Additionally, we demonstrated that the W1538R mutation does not abrogate local anesthetic lidocaine-induced blockade, but it does confer sensitivity to the $Na_V1.3$-selective aryl-sulfonamide blocker ICA-121431. Furthermore, we demonstrated that the naturally occurring arginine in $Na_V1.3$ ($Na_V1.3$-R1560), which corresponds to $Na_V1.7$-W1538R, is not sufficient to explain the resistance of $Na_V1.3$ to clinically-relevant concentrations of lacosamide, suggesting that the contribution of W1538 to lacosamide inhibitory effects is isoform-specific. We concluded that both the W1538 residue and an intact local anesthetic site are required for lacosamide's block of $Na_V1.7$ at a clinically-achievable concentration.

The translation of our findings is however hindered by using an overexpression heterologous system, as transient expression of $Na_V1.7$ channel variants in HEK293 cells only provide a partial view of the underlying pathology described in patients. Patient-derived iPSCs offer the opportunity to study patient-specific pathophysiological mechanisms and treatment response *in vitro*. Nevertheless, reprogramming and differentiation protocols to obtain nociceptors have mostly yielded immature, homogenous cell populations. In **chapter 4**, we developed an iPSC model based on the influence of microenvironmental interactions to induce cellular differentiation and provide cells with the full spatiotemporal context and nutrients needed for acquiring a mature phenotype. Specifically, we grafted undifferentiated iPSCs and pre-differentiated iPSCs inro neural precursor cells into adult rat DRG *in vivo* and into the excavated ganglions of neonatal rats for *ex vivo* differentiation. We reported poor cell survival and differentiation in both models, which lacked immunoreactivity to canonical neuronal markers, indicative of their unsuccessful differentiation and maturation. Last, we showed that xeno-transplanted undifferentiated iPSCs maintain an elevated proliferative potential and induce tumorigenesis. Ultimately, further differentiation is necessary to improve their surrogacy as human neurons.

An alternative way to bridge the gap between human DRGs and iPSC-derived sensory neurons (iPSC-SN) lacking $Na_V1.8$ and $Na_V1.9$ expression is to artificially induce it. In **chapter 5**, we utilized dynamic clamp electrophysiology to precisely tune in varying levels

of $Na_V1.8$ and $Na_V1.9$ currents into iPSC-SNs, allowing us to quantify how graded changes in these currents affect different parameters of neuronal excitability and electrogenesis. We quantified the direct relationships between $Na_V1.8$ current density and action potential half-width, overshoot, and repetitive firing, and $Na_V1.9$ current density effect on neuronal membrane potential. Furthermore, we examined the simultaneous interplay between $Na_V1.8$ and $Na_V1.9$ on neuronal excitability. By altering $Na_V1.8$ gating properties, we were able to render human iPSC-SNs hyperexcitable, in a first-of-its-kind investigation of a gain-of-function $Na_V1.8$ mutation in a human neuronal background.

Chapter 6 provides a general overview of the research chapters and discusses future advances in the fields of pharmacogenomics and stem cell research. Specifically, our findings related to lacosamide mode of action and the influence of select genetic variants in $Na_V1.7$ sodium channels on lacosamide effects in neuropathic pain patients set the stage for the application of pharmacogenomic-guided research and medical care. Furthermore, optimization and appropriate utilization of iPSC-derived systems, for example using microenvironmental interactions or dynamic clamp current induction, at a large scale, can have a global influence on the clinical implementation of individualized approaches to treatment. Chapter 7 describes the scientific and clinical impact I believe my research will have.

JULIE I.R. LABAU

BIO

Passionate about science, exploration and social justice, Julie approaches global issues through an interdisciplinary lens, using photography and science communication. From a young age, Julie has showed great interest for science and for understanding how the world worked. It started with finding bones and rocks to study trepanation and continued with chronic pain research. She also advocates for gender minorities in STEMM and climate justice as a mentor and organizer. Her prime goals lay in improving the quality of life of people afflicted by disease and raising awareness on health disparities globally. Julie is also an aspiring explorer, and documentary photographer, with a passion for adventure. She hopes to combine her research and communication skills to tell stories that can help shape a better future.

EDUCATION

Yale University, USA / **Maastricht University,** Netherlands (2018 - now)
Joint – PhD candidate in Neuroscience, Genetics and Pharmacology

Maastricht University, Maastricht, Netherlands (2015 - 2017)
MSc, Research Master in Cognitive and Clinical Neuroscience. Specialization: Fundamental Neuroscience

University of Greenwich, Chatham, United Kingdom (2012 - 2014)
BSc, Biological Sciences, First Class Honours. Second & Final year Undergraduate years

University Paul Sabatier, Toulouse, France (2011 - 2012)
First Year Undergraduate Life Sciences

AWARDS & FELLOWSHIPS

Marie-Sklowdoska Curie Actions (MSCA) Fellowship for the European Innovative

WORK EXPERIENCE

Yale University School of Medicine, Centre for Neuroscience and Regeneration Research (CNRR), New Haven, USA (2017 - 2021)
Postgraduate Associate/PhD candidate

Ospedale San Rafaele (OSR), Milan, Italy (May – Jul. 2019)
Research intern – DNA sequencing and genotyping

DI.V.A.L Toscana Srl / Universita di Firenze, Florence, Italy (Apr. - May 2019)
Research intern – drug toxicity and live surgery

Maastricht University, Toxicogenomics, Maastricht, Netherlands (Apr. – Jul. 2018; May - Dec. 2021)
Research Intern/PhD candidate – Molecular genetics and zebrafish work

Institute for Molecular Bioscience, University of Queensland, Brisbane, Australia (2016 - 2017)
MSc Research; Thesis "Characterisation of caveolin-1 in nociception and sensory neuron functions"

Training Network (ITN): PAIN-Net Project (2017 - 2021)

The Royal Society of Biology Award for Best Performing Student in Biosciences, University of Greenwich (2014)

VOLUNTEERING

Sunrise New Haven Actions Lead (2019 - 2021) Organizer for the Sunrise National Movement in the New Haven hub, a youth-led climate justice movement

Women In Science at Yale (WISAY) Executive Board Leader (2019 - 2021) Career development, networking, and support for Yale gender minorities in STEM

Chair of the MSCA Pain-Net group (2017 - 2021) Organization and coordination of meetings and activities within the consortium

Domestic Violence App development with ***BrightAct*** Application to protect victims of domestic abuse (Apr. - Aug. 2021) European Hackathon winner

University of Greenwich, Chatham, United Kingdom (2013- 2014) BSc Research ; Thesis "The role of the gene CG8403 in the development of the nervous system in *Drosophila melanogaster"*

LEADERSHIP & COMMUNICATION

Homeward Bound Leadership Program HB7
Homeward Bound Projects (2022 - now) – Global leadership initiative and network of women in STEM

Yale STEM Outreach Programs, New Haven, CT, USA (2020 - 2021),
Speaker:
- Pathways to Science Summer Scholars *Program enrichment session,*
- *Open Labs - Science Cafe Talk*
- *Science in the News*

TEACHING & MENTORING

Wyzant, Blabla EdTech, Preply, worldwide (2022 – now)
Biology, ESL and French educator

New York Academy of Sciences, New York City, USA (2019 - 2021)
Mentor and science expert for middle and high school students,
Programs:
- *1000 Girls, 1000 Futures*
- *Junior Academy of Science*

Chengdu Normal University, Chengdu, China (Feb. - Jul. 2015)
English teacher as a foreign language

Equifun 66, ADAV, Telligo, France (2012 - 2016)
Science tutor and leader in summer camps for children and teenagers

LIST OF PUBLICATIONS

RESEARCH ARTICLES

Alsaloum, M., **Labau, J.I.R**, Liu, S., Effraim, P., and Waxman, S.G., 2022. Stem cell-derived sensory neurons modelling inherited erythromelalgia: normalization of excitability. *Brain*, awac031

Labau, J.I.R, Alsaloum, M., Estacion, M., Tanaka, B., Dib-Hajj, F.B., Lauria, G., Smeets, H.J., Faber, C.G., Dib-Hajj, S. and Waxman, S.G., 2021. Lacosamide Inhibition of NaV1. 7 Channels Depends on its Interaction With the Voltage Sensor Domain and the Channel Pore. *Frontiers in Pharmacology, 1-17*

Alsaloum, M., **Labau, J.I.R**, Liu, S., Estacion, M., Zhao, P., Dib-Hajj, F. and Waxman, S.G., 2021. Contributions of NaV1. 8 and NaV1. 9 to excitability in human induced pluripotent stem-cell derived somatosensory neurons. *Scientific reports*, *11*(1), pp.1-14.

Alsaloum, M., **Labau, J.I.R**, Sosniak, D., Zhao, P., Almomani, R., Gerrits, M., Hoeijmakers, J.G., Lauria, G., Faber, C.G., Waxman, S.G. and Dib-Hajj, S., 2021. A novel gain-of-function sodium channel β2 subunit mutation in idiopathic small fiber neuropathy. *Journal of Neurophysiology*, *126*(3), pp.827-839.

Labau, J.I.R., Estacion, M., Tanaka, B.S., de Greef, B.T., Hoeijmakers, J.G., Geerts, M., Gerrits, M.M., Smeets, H.J., Faber, C.G., Merkies, I.S. and Lauria, G., 2020. Differential effect of lacosamide on Nav1. 7 variants from responsive and non-responsive patients with small fibre neuropathy. *Brain*, *143*(3), pp.771-782.

SCIENTIFIC REVIEWS - *in preparation*

Labau, J.I.R. Andelic, M., Lauria, G. Dib-Hajj, S. Recent advances in human induced-pluripotent stem cell model strategies for neuropathic pain. *Neuroscience Letters*

CONFERENCE ABSTRACTS AND PRESENTATIONS

- **PAIN-Net Annual Meeting, online – 2020**
  Presenter, project finalization

- **Society for Neuroscience (SFN) Conference, Chicago (USA) – 2019**
  Abstract and Poster Presentation **Labau, et al**, 2020. Differential effect of lacosamide on Nav1. 7 variants from responsive and non-responsive patients with small fibre neuropathy.

- **PAIN-Net Annual Meeting, Strasbourg, France – 2019**
  Presenter, updates on project advances over the past year

- **PAIN-Net Annual Meeting, Maastricht, Netherlands – 2018**
  Presenter, project introduction

ACKNOWLEDGEMENTS

My journey towards completing my PhD has been long and strenuous, and started as far back as high school, when I decided to take the Science route to pursue a career as a biologist. Each day, along the way, my family has remained by my side, both mentally and financially. They have supported me through the many moments of doubts, existential crises, and burnouts. They have supported me through my constant life of travels around the world, allowing me to chase my dreams and build my confidence, while putting aside their own fears and desolation. I will always be grateful for them.

Papa, Maman, Je vous remercie de m'avoir toujours soutenue, et tenu la main, même dans les moments durs. J'ai toujours su que quoiqu'il arrive, je ne me retrouverai jamais seule. Je n'y serais pas arrivée sans vous, en tous cas, pas aussi loin. Merci pour tout.

To my grandparents, who unfortunately will not get to read (even if they could read English) this thesis, I also want to thank for always believing in me. *À Maïou et Tata Suzanne, sachez que lors de l'écriture de cette thèse, je vous trouvais toujours dans mes pensées. Merci pour m'avoir soutenue et pour avoir toujours cru en moi.*

To my dearest friends that I have met in so many places, and who have always been there for me, in the good and the bad days, I want to thank you for helping me grow as an individual, for helping me find clarity in the darkness and through my constant states of confusion. Thank you for the laughs, the stories *-past and future-*, and for being exactly who you are.

I want to thank my partner in crime for his love and the humongous amount of support he has provided, in particular, while crossing the finishing line. You have shown me I can do so much more than I thought I was capable of, thank you.

I also want to express my deepest gratitude to a few people that this thesis would not have been possible without. First, I want to thank **Dr. Irina Vetter** for her mentoring during my research in Australia. Being a part of her lab not only forged the path that led me to where I am today, but she has also inspired me to become a strong STEM leader. I will always have an incredible appreciation and admiration of her as a scientist, mentor and leader. I, of course, want to thank my PhD supervisors, **Dr. Sulayman Dib-Hajj**, **Prof. dr. Stephen Waxman**, **Prof. dr. Bert Smeets** and **Prof. dr. Karin Faber**. In particular, I want to thank Sulayman and Steve for giving me the opportunity to conduct groundbreaking, exciting research in their lab, and for their mentorship. Likewise, I want to thank the **Pain-Net consortium** for bringing together this passionate group of young researchers, which with your support, will make considerable changes to the field. To the ESRs, thank you for making this journey so wholesome.

I want to thank my fellow Yale lab-mates, you have been like a second family away from home. Special thanks to **Dr.** (still weird to write) **Matt Alsaloum,** for being such a

wonderful colleague and friend over the past four years. Thank you for the trips to the VA store, the games late in lab, and most of all, for keeping me somewhat sane. **Dr. Brian Tanaka** and **Dr. Mark Estacion**, thank you for your mentorship and for consistently saving me from my 'possessed' rig. **Dr. Peng Zhao** and **Jennifer Carrara,** thank you for your technical support and friendship, the iPSC project could have never come to life without you, and even though it had to be terminated early, this boat would have longed sank if it weren't for you.

There are so many of you I would like to thank that naming each and every one of you would probably take more pages than the thesis itself... Nevertheless, I do want to thank every single person who has helped me be where I am today, be that by your friendship, mentorship or simply by being a part of my life. Thank you.

ABBREVIATIONS

AAVS1	Adeno-associated virus integration site 1
AED	Anti-epileptic drug
ALS	Amyotrophic lateral sclerosis
BDNF	Brain-derived neurotrophic factor
CAG	Chicken β-actin globin
CBZ	Carbamazepine
CIP	Congenital insensitivity to pain
CIPN	Chemotherapy-induced peripheral neuropathy
CNS	Central nervous system
COMT	Catechol-O-methyl transferase
CPIC	Clinical Pharmacogenetics Implementation Consortium
CRMP2	Collapsin response mediator protein 2
CYP	Cytochrome P450
DPN	Diabetic peripheral neuropathy
DRG	Dorsal root ganglion
ECM	Extracellular matrix
FRDA	Friedreich's Ataxia
GFAP	Glial fibrillary acidic protein
GFP	Green fluorescent protein
GoF	Gain-of-function
GWAS	Genome-wide association studies
HEK293	Human embryonic kidney cells
hNu	Human nucleus
HSAN	Hereditary sensory & autonomic neuropathy
IACUC	Institutional Animal Care and Use Committee
IASP	International Association for the Study of Pain
IEM	Inherited erythromelalgia
iPSC	Induced pluripotent stem cells
iPSC-NPCs	iPSC-derived neural precursor cells
iPSC-SNs	iPSC-derived sensory neurons

KO	Knock-out
LA	Local anesthetic
LCM	Lacosamide
LDC	Lidocaine
LENSS	Lacosamide Efficacy-N-Safety in SFN
LoF	Loss-of-function
LTMR	Low-threshold mechanoreceptors
NB	Neurobasal
NPC	Neural progenitor cells
NGF	Nerve growth factor
NeuPSIG	Neuropathic Pain Special Interest group
NSC	Neural stem cell
NGN	Neurogenin
NSAIDs	Non-steroidal anti-inflammatory drugs
NT	Neurotrophin
PBS	Phosphate buffered saline
PDL/LAM	Poly-D-lysine/laminin
PEPD	Paroxysmal extreme pain disorder
PFA	Paraformaldehyde
PI-NRS	Pain intensity numerical rating scale
PK-PD	Pharmacokinetic-pharmacodynamic
PM	Pore module
PNS	Peripheral nervous system
SC	Schwann cells
SCN9A	Sodium voltage-gated channel alpha subunit 9
SD	Sprague-Dawley
SFN	Small fiber neuropathy
SN	Sensory neuron
SNRI	Serotonin-norepinephrine reuptake inhibitors
SSRI	Selective serotonin reuptake inhibitors
TALEN	Transcription activator-like effector nuclease
TCA	Tricyclic antidepressants

TN	Trigeminal neuralgia
TTX	Tetrodotoxin
VGSC	Voltage-gated sodium channels
VSD	Voltage-sensing domain
WES	Whole-exome sequencing
WHO	World Health Organization
WT	Wild type
YFP	Yellow fluorescence protein